TECHNISCHE UNIVERSITÄT MÜNCHEN

TUM Campus Straubing für Biotechnologie und Nachhaltigkeit

Effect of exopolysaccharide structures and their modification on their rheological properties

Moritz Michael Richard Gansbiller

Vollständiger Abdruck der von der promotionsführenden Einrichtung TUM Campus Straubing für Biotechnologie und Nachhaltigkeit der Technischen Universität München zur Erlangung des akademischen Grades eines

Doktors der Naturwissenschaften (Dr. rer. nat.)

genehmigten Dissertation.

Vorsitzender: Prof. Dr. Rubén Dario Costa Riquelme

Prüfer der Dissertation: 1. Prof. Dr. Volker Sieber

     2. Prof. Dr.-Ing. Jochen Schmid

Die Dissertation wurde am 03.05.2021 bei der Technischen Universität München eingereicht und durch die promotionsführende Einrichtung TUM Campus Straubing für Biotechnologie und Nachhaltigkeit am 17.07.2021 angenommen.

Again, I would like to thank the whole CBR Team. Thank you for the "meetings" the birthday parties at the lakes, the barbecues, the techno parties, the Freibierfeste, the Asia Fridays, the cakes, the movies, the Feuerzangenbowles, and all the memorable years I had in this unique group of people.

My sincerest gratitude to my family, my parents and my sister, my grandfather my grandmothers for supporting me and all of my decisions. My interest as a child in everything slimy turned out to be a big foreshadowing to all of this.

To my wife Sophia for all the support along this time, for sharing my enthusiasm, supporting my decisions (before or afterwards), and keeping my spirit up all the time.

Although you always claim you do not understand, what I am doing, this is for you:

Abstract

Understanding the correlation of structural properties with rheological behavior is key to identify novel or to develop targeted modified exopolysaccharides (EPS) for specific applications. Many studies describe the rheological properties of EPS regarding their chemical structures and super-structures but are almost exclusively carried out for one individual EPS. This work aims to identify more systematic structure-function relationships, by rheological characterization of different groups of EPS, with either solely minor natural structural differences or targeted structural modifications by genetically engineering their production organisms Based on that approach, the rheological properties are connected to the structural differences. The first group of investigated EPS comprised the sphingans, which have high structural similarities with minor differences in the main- and side-chain composition. The rheological properties were evaluated regarding these structural differences using mechanical models to describe the viscoelastic behavior, which aided to observe minor differences by varying the parameters or even the describing models themselves. Expanding these studies towards interaction with surfactants gave insights on intramolecular interactions as well as application-related properties. As a second EPS, xanthan, one of the most relevant industrial polysaccharides was modified regarding its acetylation and pyruvylation pattern by genetic engineering of the organism *Xanthomonas campestris* which gave further insights on the effect of these functional groups and their position regarding the rheological properties in connection to the effects on the molecular structure of the modified xanthan variants. Finally, a not completely structurally elucidated EPS, paenan, a naturally produced mixture of three different EPS from *Paenibacillus polymyxa* was investigated. By genetic modification of the producing strain, the single EPS structures as well as their combinations were obtained. Supported by the insights of the first two studies, their rheological properties were linked to possible intra-and intermolecular interactions based on their molecular structures and substituents. In addition, an artificially modify xanthan should be designed by *in-vivo* introducing crotonyl-residues on the terminal mannose of the sidechain, to replace the natural acetyl residues. Via the double bond of the crotonyl-residue, UV-inducible crosslinking of this novel xanthan variant was aimed. For the engineering of the substrate specificity of the native acetyltransferase, GumG from acetyl-CoA towards crotonyl-CoA, a plasmid-based expression system was established to express modified GumG-variants. First results based on an alanine scan of highly conserved amino acids could be achieved via bioinformatic analysis of *de-novo* models and sequence alignments. By that, a putative catalytic center was identified, which can be targeted in further approaches. In addition, a plasmid-based system to increase the intracellular crotonyl-CoA levels comprising the genes *phaA* and *phaB* form *Cupriavidus necator* and the R-specific crotonase encoding *crt* from *Clostridium acetobutylicum* was designed. Furthermore, highly sensitive HPLC-MS analytics was established for the quantification of intracellular CoA-esters in *X. campestris* to analyze the functionality of the pathway. While a direct analysis of crotonyl-CoA was not realized, differences in acetyl-CoA levels were observed, and shifts in the levels of 3-hydrxybutyryl-CoA could also be used to perform further pathway engineering. Since the biotechnologically crotonylated xanthan could not be realized, a chemically crotonylation of xanthan was performed to obtain first insights on the targeted product, which already showed promising properties based on first rheological evaluations. The results of this work and the established biomolecular and analytical tools encourage further studies towards novel modifications of EPS for a broader field of applications.

Table of contents

1 Introduction

1.1 Polysaccharides

Polysaccharides are biological macromolecules made up by a defined sequence of diverse mon-osaccharides such as pentoses, hexoses and uronic acids. Their structures are highly defined and conserved amongst the producing cellular organisms and by that, they play important functional roles in the corresponding species. In general, polysaccharides can be classified into three major groups according to their biological function: structural, storage and extracellular polysaccharides (Dumitriu, 2004). They can be further divided by their occurrence in the biological domains into eukaryotic (e.g. plants, fungi, algae), archaic and bacterial polysaccharides (Phillips, 2016; Poli, Di Donato, Abbamondi, & Nicolaus, 2011). Amongst eukaryotic polysaccharides, the structural polysaccharides cellulose and alginates as well as starch, a storage polysaccharide are the most known representatives and are of commercial interest as food additives or for pharmaceutical and many other applications. Another very prominent class of polysaccharides for industrial applica-tions are bacterial polysaccharides, especially exopolysaccharides, which are secreted to the en-vironment.

1.2 Bacterial polysaccharides

Bacterial polysaccharides, like polysaccharides in general, are commonly divided in three groups: storage polysaccharides, capsular polysaccharides (CPS) and extracellular polysaccharides (EPS). In nature EPS play a crucial role in cell adhesion, protection from environmental factors and cell-cell communication. Like their eukaryotic counterparts, bacterial polysaccharides, espe-cially EPS are of great interest for various (industrial) applications. Furthermore, unlike eukaryotic polysaccharides, bacterial (exo-) polysaccharides offer the advantage of regionally- and season-ally independent, controlled production processes and represent probably the most abundant re-newable resource on this planet with both natural and industrial production rates unchallenged by any other resource (Dumitriu, 2004). Their large spectrum of properties, which makes them so interesting for a wide variety of applications stems from their structural variety based on their pro-duction organisms.

1.3 Structure function relationship of polysaccharides

The most important physicochemical properties of exopolysaccharides are their viscoelastic prop-erties, which describe their rheological behavior as aqueous solutions, ranging from viscoelastic fluids to elastic gel structures. These diverse properties make them effective additives of industrial interest like thickeners, stabilizers, or gelling agents for various applications. These properties are closely related to their chemical structure, based on the monomer composition, the type of linkage of these monosaccharides, as well as existing branched or unbranched polysaccharide chains

and the resulting superstructures and their interactions. The substitutions of these (side-) chains, which may contain various ester-bonds with acetic acid, pyruvic acid, succinic acid, glyceric acid or sulfuric acid further expands this structural diversity and heavily impact the rheological properties of the corresponding EPS. Studying these structure function relationships of bacterial polysaccharide enables the targeted design of modified EPS, either by post production, chemical or enzymatic modifications or by direct modification of the production organism by means of *in-vivo* genetic engineering. Two interesting polysaccharides to study these relations and modifications are xanthan, a branched exopolysaccharide produced by *Xanthomonas campestris*, and the sphingans, a group of polysaccharides produced by various *Sphingomonas* species, which share a common backbone structure with various degrees of branching or acyl ester groups. Xanthan, as a branched EPS has two possible positions of acetylation as well as one possible pyruvylation position, resulting in a total of 8 different combinations of acylation patterns. Analyzing defined variants with specific decoration patterns in context of their resulting rheological properties is a crucial step in understanding structure function relationships of EPS. The sphingan group of EPS on the other hand allows studies of how different branching-structures on identical or highly similar polysaccharide structures influence the rheological properties as well as intermolecular interactions. In terms of the relationship of (microbial) exopolysaccharides and their rheological properties, up to now, investigations are mostly done on a per-polysaccharide basis, often only describing a limited set of properties from a single polysaccharide (M Tako, 1992; Masakuni Tako, 1992, 1993, 1994; Masakuni Tako & Tamaki, 2005). Part of the aim of this work was therefore to describe the rheological properties of two known exopolysaccharide (groups) in relation to their known structural aspects, compile the results and extend them to the rheological properties of unknown polysaccharides, to achieve a heuristic approach to a structure function relationship of exopolysaccharides.

1.4 Investigated groups of polysaccharides for their structure function-relationship

1.4.1 Xanthan

Xanthan is a heteropolysaccharide produced by the Gram-negative Gammaproteobacterium *Xanthomonas campestris* (*pv. campestris*) and was first described in 1961 as polysaccharide B-1459, based on the production organism *X. campestris* NRRL B-1459 (Jeanes, Pittsley, & Senti, 1961). Since then, various studies have been carried out to elucidate its structure, characteristics, and biosynthesis pathway. Overall, it took until 1975, 14 years after the discovery of xanthan, for the final structure to be resolved, and a minor update followed another 18 years later in 1993. (Jansson, Kenne, & Lindberg, 1975; Stankowski, Mueller, & Zeller, 1993).

1.4.1.1 Structure and biosynthesis of xanthan

Xanthan is produced via the so called Wzx/Wzy-dependent pathway and consists of a cellulose like backbone (D-Glc$p$-ß-(1→4)-D-Glc$p$) with a ß-D-Man$p$-(1→4)-ß-D-GlcA-(1→2)-α-D-Man$p$ (1→3)-linked to every second Glc$p$ of the backbone. The terminal ß-D-Man$p$ is either 6-O-acety-lated or forms a ketal with pyruvic acid at position C4 and C6 (Jansson et al., 1975). It took another 18 years to discover, that the terminal mannose can be also O-acetylated (Stankowski et al., 1993). The genes for the biosynthesis of xanthan are arranged in a 16-kb cluster, the so-called *gum*-operon, composed of genes *gumB-gumN,* responsible for the assembly of the repeating unit from activated sugars in the form of sugar nucleotides as well as their acetylation and pyruvylation with Ac-CoA and phosphoenol pyruvate (PEP), while the function of the protein encoded by *gumN* The supply of the sugar-nucleotide precursors is governed by several proteins such as glucoki-nase (GK), phosphoglucose isomerase (PGI), UDP-glucose pyrophosphorylase (UDPG-PP), UDP-glucose dehydrogenase (UDPG-DH) as well as the genes *xanA* and *xanB*, which are in-volved in the GDP-mannose biosynthesis. The assembly of the pentasaccharide repeating unit is initiated by GumD, which transfers a glucose monomer to a polyprenol (PP) lipid anchor in form of UDP-glucose, followed by the sequential addition of a second glucose unit by the action of GumM. The branching mannose is attached via the GumH protein in form of GDP-mannose, fol-lowed by glucuronic acid attachment via GumK activity with UDP-glucuronic acid as substrate. The terminal mannose of the side chain is assembled by the action of the GumI protein, which also use GDP-mannose as substrate. The thus assembled pentasaccharide repeating unit is then decorated with acetyl esters, on the inner and outer mannose by action of the GumF and GumG protein respectively. Both of these proteins use Ac-CoA as substrate. In addition, the outer man-nose can be pyruvylated via the formation of a pyruvate ketal by the action of GumL using phos-phoenol-pyruvate (PEP) as substrate (Becker, Katzen, Pühler, & Ielpi, 1998). Polymerization and export are governed by a Wzx/Wzy dependent pathway. In detail, the assembled pentasaccharide unit is flipped from the inner membrane to the periplasm by GumJ (Wzx), polymerized via GumE (Wzy) and exported by the polymer co-polymerase protein (PCP) GumC and outer membrane polysaccharide export protein (OPX) GumB (Schmid, Sieber, & Rehm, 2015) (Table 1).

1.4.1.2 Production, properties, and applications of xanthan

After its discovery in 1961, substantial commercial production of xanthan followed in 1964 under the brand name Kelzan® by the American nature-based hydrocolloid producer CP Kelco (Kelco, 2008). Xanthan was approved for the use in food products by the FDA in 1969 (Stephen, 1995). It is regulated worldwide by national and international authorities, e.g. under E-number 415 by the FDA and EFSA. (Blekas, 2016; EFSA Panel on Food Additives Nutrient Sources added to Food, 2017). Due to its broad worldwide approval and outstanding properties as rheological enhancer even at low concentrations, xanthan can be found in a vast number of products ranging from food, cosmetics, pharmaceuticals to oil drilling applications (Petri, 2015; R Sharma, C Dhuldhoya, U

Merchant, & C Merchant, 2006). Applied concentrations range from 0.05 - 3.0 %, depending on the desired function, for example as emulsifying, stabilizing, foaming or gelling agent (Palaniraj & Jayaraman, 2011). The popularity of this product has led to ever growing markets and in 2018, approximately 165,000 metric tons of xanthan have been sold worldwide, of which about 80 % are for food & beverage and oil-drilling applications (Misailidis & Petrides, 2020). The predicted market growth within the next decade estimates annual growth rates between 5-6 %. In 2019, global market was distributed globally with about ⅖ of xanthan being produced in the Asian pacific region, ⅓ in the European region, about ¼ in North America and the rest being distributed between South America and the middle east & Africa.
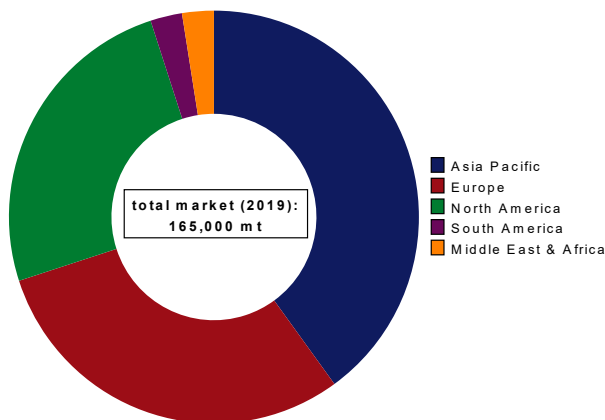
Figure 1. Approximate regional xanthan market share in 2019.

Modified to: https://www.transparencymarketresearch.com/xanthan-gum-market.html

Production at this scale requires robust and economical processes, to ensure a consistent product which meets the required qualities and quantities. Today's xanthan production is usually carried out by batch or (semi-) continuous fermentations in stirred tank reactors, using sucrose, glucose (syrup) or liquefied starch as substrate, while more inexpensive substrates like whey, sugarcane molasses and other carbon-rich raw extracts may be used for non-food applications (Palaniraj & Jayaraman, 2011; Wilson, Sahm, Stahmann, & Koffas, 2019). The typical unit processes include inoculation of a preculture from a lyophilized production strain, followed by the setup of an inoculum fermenter, from which the main production fermenter is started. Production processes range from up to 96 h for batch fermentations to multiple stages of these batch fermentations, where the most part of the fermentation volume is drained, and the remaining broth is supplemented with fresh media over multiple cycles (Garcıa-Ochoa, Santos, Casas, & Gomez, 2000; Palaniraj & Jayaraman, 2011). Production media are mainly complex media consisting of 2-4 % (w/v) carbon source, nitrogen source in form of ammonium or nitrate salts or complex organic nitrogen sources like corn steep liquor (Wilson et al., 2019). Other processes describe incorporation of L-glutamic acid produced primarily for monosodium glutamate (MSG) production into the xanthan production medium as carbon-and nitrogen-source (Rosales-Calderon & Arantes, 2019). Other essential

factors for xanthan production are phosphate and magnesium salts, which are often provided as potassium phosphate and magnesium chloride and micronutrients such as boric acid, zinc, iron and calcium and potassium salts. Diverse optimization studies show optimal production rates at pH 7.0 at temperatures from 25 - 30 °C (Amanullah, Satti, & Nienow, 1998; Esgalhado, Roseiro, & Collaço, 1995; Psomas, Liakopoulou-Kyriakides, & Kyriakidis, 2007). Regulation of pH is necessary, as the formation of organic acids decrease during xanthan production, causing the pH to drop to 5.5 -5.0, which significantly decreases productivity. On an industrial scale, pH is typically regulated at 7.0 with potassium or sodium hydroxide and production temperatures are 28-30 °C.

Another key factor towards a high productivity is the sufficient aeration, reported values range from 0.3 - 1 (v/v), requiring a specific power input of around 1 kW m^{-3} (García-Ochoa et al., 2000; Palaniraj & Jayaraman, 2011). The need for high aeration combined with the viscosity of the fermentation broth requires stirring powers of up to 400 kW for industrial production vessels (Misailidis & Petrides, 2020; Palaniraj & Jayaraman, 2011). Vessel geometry is the last key point in industrial xanthan production, and a high stirrer-diameter-ratio is required for sufficient agitation, requiring large reactor heights at industrial scale. (Misailidis & Petrides, 2020). Although energy cost at this scale is not negligible, resource costs are relatively low and the largest cost factor for food-grade xanthan production are downstream processing steps, making up to 50 % of total cost (Palaniraj & Jayaraman, 2011). These steps typically include pasteurization, cell removal, precipitation, followed by drying and milling. Precipitation is usually carried out using isopropanol, which is recycled by distillation. Depending on the required quality, further washing- and precipitation steps are applied before drying, which drastically increase the cost of food-grade xanthan compared to more crude products for technical applications.

1.4.2   Sphingans

Sphingans are a group of heteropolysaccharides produced by *Sphingomonas spp,*, a family of Gammaproteobacteria, which have a highly conserved backbone structure and differ by the absence or presence of a saccharide side chain as well as in its composition and pattern of O-acetylation (Pollock, 2005).

1.4.3   Structure and biosynthesis of sphingans

The backbone structure of sphingans typically consists of a linear →4)-α-L-Rha*p*-(1→3)-β-D-Glc*p*-(1→4)β-D-GlcA (1→4)-β-D-Glc*p*(1→ tetrasaccharide. Next to some variances in the backbone, e.g. α-L-Man*p* instead of α-L-Rha*p* for Sphingans S-88 and S-198 or 2-dexoy-GlcA instead of GlcA in sphingans I-886 and S-7, their main differences stem primarily from various sidechain structures, consisting of ß or α-D-Glc*p*, α-L-Rha*p* and/or α-L-Man*p*, resulting in a total of six different side-chain variants amongst the different described sphingans (Pollock, 2005). Another factor of their variability are different acylations with acetic acid- and glyceric acid groups in the main chain (Pollock, 2005). Like xanthan, the biosynthesis of sphingans follows the Wzx/Wzy-

dependent pathway. The biosynthesis of the sphingans gellan, welan, diutan, S-88 and S-7 has been investigated so far, and the genes involved in the pentasaccharide assembly, decoration and export, commonly named *spn* and have been individually named for certain groups of sphingans: *gel* for gellan, *wel* for welan and *dps* for diutan, *sps* for S-88 (Coleman, Patel, & Harding, 2008; Schmid, Sperl, & Sieber, 2014; Yamazaki, Thorne, Mikolajczak, Armentrout, & Pollock, 1996). The assembly of the tetrasaccharide repeating unit is governed by genes *spnBKLQ*. Based on functional and sequence-based analyses *spnB* was identified to encode the initiating glycosyl-isoprenylphosphate-transferase in all described sphingan biosynthesis pathways. SpnB uses UDP-glucose as substrate and a C55-isoprenylphosphate anchor as acceptor. By that, SpnB has the same function as GumD in the xanthan-biosynthesis. The glycosyltransferases SpnKLQ sequentially assemble the remaining trisaccharide, analogous to the tetrasaccharide assembled by GumMHKI in *Xanthomonas*. Beyond the assembly of the main chain, unlike the biosynthesis of xanthan, the biosynthesis of the sphingan repeating units has not been completely clarified yet, however some putative genes responsible for the synthesis of the branching chains have been identified and later termed *urf* (for unknown reading frame) 31, 31.4 and 34 (Schmid et al., 2014). Polymerization and export are not completely clarified as well, however, a Wzx/Wzy-dependent pathway, where genes *spnS, spnG* and *spnC, spnE* have been identified as a Wzx-like flippase, a Wzy-like polymerase and two PCP-family proteins, respectively (Table 1).

1.4.3.1 Production, properties, and applications of sphingans

Currently, only the sphingans gellan (S-60), diutan (S-657) and welan (S-130) are commercialized, while rhamsan (S-194) has previously been mentioned for the use in agricultural and coating applications (Kang & Pettitt, 1993), it cannot be found under the portfolio of any of the commercial sphingan producers. Gellan is the only member of the sphingan family which is approved for the use in food, cosmetics and pharmaceutical products under the E-number 418. It can be applied as highly acylated gellan as viscosity enhancing and stabilizing agent, or as deacylated, or low acylated gellan as a gelling agent (Sworn, 2009; Valli & Clark, 2009). Welan and diutan are primarily used in the construction & building, oil-drilling, mining and agriculture sector as suspension, viscosity enhancing and stabilization agents. In March 2019, a collaboration of CP Kelco with Lubrizol was announced, and shortly after, diutan was found as Kelco-Care™ as active ingredient for cosmetic products (Cebrian et al., 2019; Kelco, 2019), making diutan the second sphingan used in the cosmetic sector: For both welan and diutan no official approval for food application or according E-number exist excluding their application in food or pharmaceutical products. Like xanthan, sphingans are typically produced in batch fermentations over 60-70 h using inexpensive carbon sources like corn syrup or sucrose and ammonium nitrate and hydrolyzed soy protein as nitrogen source as well as dipotassium sulfate, magnesium sulfate and trace elements, including magnesium molybdate, zinc (II) chloride, copper (II) chloride, cobalt(III) chloride, boric acid, manganese chloride and ferrous sulfate (Kaur, Bera, Panesar, Kumar, & Kennedy, 2014; Pollock,

2005). Optimal production temperatures are between 28-35 °C and like for xanthan production, the optimal pH is 7.0 (Kaur et al., 2014; Li et al., 2016). Unlike xanthan production pH regulation is not necessary at high dipotassium phosphate levels and initial pH set to 7-7.5, which leads to a pH shift to around 6.5 caused by the consumption of ammonium, followed by an increase to 6.5 caused by nitrate consumption. After nitrogen depletion, the pH will drop again due to the formation of organic acids during polysaccharide production (Pollock, 2005). Controlled pH processes, however, show increased product titers, making pH control essential for an efficient industrial process (Li et al., 2016).

1.4.4   Paenan

First described by Rütering et al. (Rütering, Schmid, Rühmann, Schilling, & Sieber, 2016), the heteropolysaccharide produced by *Paenibacillus polymyxa* DSM 356, later named *paenan* (Rütering et al., 2017), is the third polysaccharide selected for this study. It is a non-commercial polysaccharide, however its unique rheological properties and good compatibility with surfactants make it both an interesting candidate for both basic research and commercial applications (Rütering et al., 2018).

1.4.4.1   Biosynthesis and structure of paenan

Based on the carbon source, *P. polymyxa* produces levan, a poly-fructose polysaccharide produced by the extracellular levansucrase SacB, whose reaction is driven by the cleavage of the ß-$(1 \rightarrow 2)$ glycosidic bond of sucrose, resulting in an α-D-glucose at the beginning of each polysaccharide chain. While the biosynthesis of the produced heteropolysaccharide, paenan is yet to be completely elucidated, it has been described following the Wzx/Wzy-dependent pathway and is independent of the used carbon source. A 34,238 bp cluster containing 28 genes involved in the biosynthesis have been identified and first studies of deletion variants showed impact on the monomer composition and rheological properties of the resulting EPS-variants (Rütering et al., 2017). Further studies on the structural elucidation of paenan strongly indicated that paenan is not one heteropolysaccharide, but in fact a mixture of three different heteropolysaccharides, Paenan I, II & III, whose production ratio can be precisely governed by targeted gene deletions. All three polysaccharides are branched and have glucose as the initial Monomer of the repeating unit, which is linked to a PP-lipid anchor by PepC for paenan I, PepQ for paenan II and PepC or PepQ in case of paenan III. The main chain of paenan I consists of a glucose monomer followed by a mannose and a galactose, which has a branching sidechain consisting of a glucose and galactose residue. The terminal galactose of the sidechain is decorated with a pyruvate ketal by the ketalase EpsO. While the function of the ketalase EpsO and the initial transferase PepC have been clarified, the function of the further described involved glycosyltransferases PepD and PepF is yet to be fully elucidated. Paenan II consists of a fucose attached to the initial glucose, followed by a glucuronic acid, forming the main chain of the polysaccharide. From the fucose a branching mannose is

described (Schilling, Klau, Aachmann, et al., 2022). The glycosyltransferases involved in the bio-synthesis of paenan II are PepT, PepU and PepV, the precise role of each transferase is yet to be unveiled. The main chain of the third polysaccharide, paenan III, is postulated to consist of a mannose attached to the initial glucose, which is followed by a glucuronic acid. Two branching points with a glucose sidechain attached to the mannose of the main chain as well as a mannose attached to the glucuronic acid of the main chain have been described(Schilling, Klau, Rühmann, et al., 2022). PepC or PepQ might take the role of the initial transferase and the further involved glycosyltransferases are PepI, PepJ, PepK and PepL. Like for paenan I and paenan II, their precise role is yet to be elucidated.
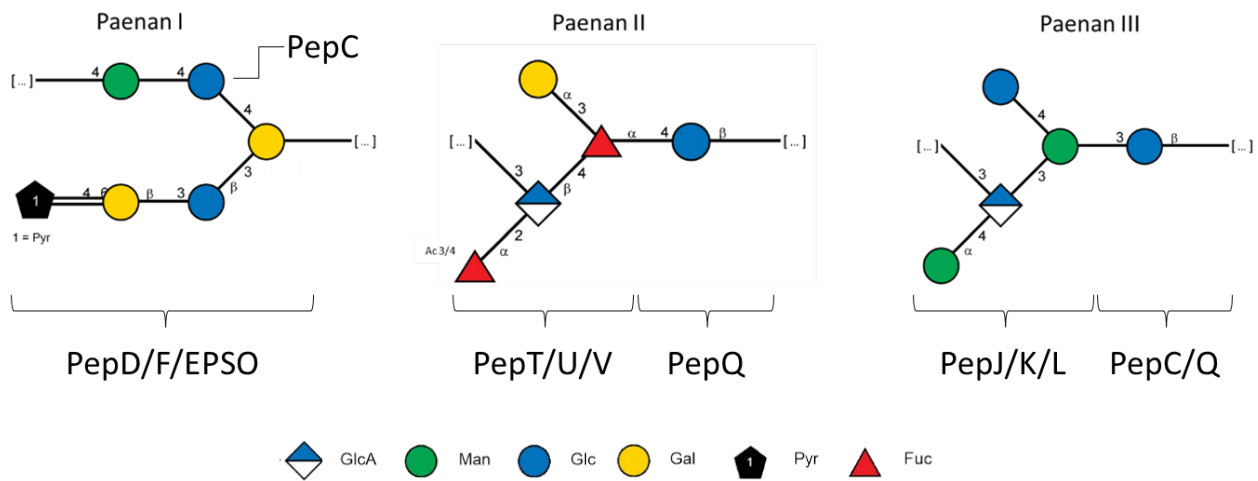
Figure 2. Structure of the heteropolysaccharides paenan I-III produced by *P. polymyxa* DSM 365

Structure of the heteropolysaccharides paenan I-III produced by *P. polymyxa* DSM 365, assembled by the glycosyltransferases PepC/D/F/Q/T/U/V/I/J/K/L; epsO: pyruvyltransferase forming the ketal for paenan I. Blue circle: Glc; green circle: Man, yellow circle: Gal; black pentagon: pyruvate; blue diamond: GlcA, red triangle: Fuc.

1.4.4.2 Production, properties, and possible application of paenan

Lab scale productions of wt paenan have been carried out in scales up to 30 L, with a medium containing glucose and glycerol source as well as different vitamins and trace elements. In fed-batch productions up to 6.7 g L^{-1} have been achieved using glycerol as carbon source and peptone as nitrogen source (Rütering et al., 2016). While the production of wt paenan is dependent of the carbon source, as levan is primarily produced when sucrose is used as carbon source, the inactivation of the levansucrase by deletion of the *sacB* gene, which has been previously described eliminates this limitation. Given its outstanding rheological properties and great compatibility with other rheology determining agents like surfactants (Rütering et al., 2018) make this polysaccharide an interesting candidate for various applications, especially in the cosmetic and personal care product sector. The fact that the polymer ratio can be altered by design via genetic engineering

and therefore tailoring its properties to required fields of application is an advantage of this polysaccharide.

Table 1. Overview of structure, biosynthesis, and industrial applications of the investigated groups of EPS

EPS (group)	Structure	Glycosyl-transferases	Export Proteins	Industrial relevance	Applications
Xanthan		main chain: GumDM; side chain: GumHKI	GumBCEJ	high	Thickener, stabilizer in dressings, sauces or toothpaste, oil drilling
Sphingans Gellan Welan S-88 Diutan		mainchain: SpnBKLQ; side chain: ?	SpnECGS	medium	Gelling agent, thickener (Gellan) Oil drilling, concrete Viscosifier, thickener, oil drilling (Welan/Diutan) cosmetics (Diutan)
Paenan I II III		Paenan I: PepCDE*; Paenan II: PepQTUV*; Paenan III: PepC/QIJKL*	?	n.A.	-

16

1.5 Modification of polysaccharides

Despite their diversity, the physicochemical properties of polysaccharides sometimes do not sufficiently meet demands for industrial applications or do not fulfill the properties of petrochemical products, to fully render them a viable, sustainable alternative. To tackle this problem, polysaccharides can be modified in various ways to achieve improved or even completely altered properties, to tailor them to their desired applications. These modifications reach from simple chemical, or less harsh, enzymatic post production modifications to *in-vivo* modifications made by engineering the production organism, eliminating the need of post-production modifications entirely.

1.5.1 Post productional modification

Post-production modifications describe the treatment of polysaccharides after production and purification and can either be carried out chemically, physically, or enzymatically. While enzymatic modifications allow milder conditions, the limitation of enzymatically accessibility of polysaccharide modifications make chemical modifications more widespread, as they are also less expensive and easily scalable.

1.5.1.1 Chemical modification

Chemical modification of polysaccharides is a widespread method to modify their properties as these methods are quite simple and inexpensive. One of the most well-known chemically modified polysaccharide is cellulose and the processes creating nitrocellulose, celluloid or cellulose acetate have been applied in industrial scales for over a century (Cumpstey, 2013). Further polysaccharides which are chemically modified include amylose, inulin, curdlan, dextran, xylan, pullulan, guar gum, alginates, pectins, chitosan and chitin (Cumpstey, 2013). These modifications include etherification, and esterification of OH-groups, oxidation, alkylation and acylation of amines and many other modifications (Cumpstey, 2013). A common chemical treatment of microbial EPS is deacylation, which is also applied to xanthan and some sphingans, especially gellan, in industrial scale (Bajaj, Survase, Saudagar, & Singhal, 2007; Pinto, Furlan, & Vendruscolo, 2011). The chemical modification of polysaccharides represents an inexpensive way of modification and the possible range of acyl donor exceeds their natural substituents. However, site specific modifications require more complicated, multi-step reaction setups and the overall harsh reaction conditions at high temperatures and the use of chemicals like bases may lead to depolymerization or even affect the physicochemical properties by altering the polysaccharides tertiary structures compared to the native variant (Bejenariu, Popa, Picton, & Le Cerf, 2010; E. R. Morris, Gothard, Hember, Manning, & Robinson, 1996). A recent study demonstrated the possibility of acetylation of xanthan in the ionic liquid 1-Butyl-3-methyl-imidazolium-chloride (BMIMCl) and acetic anhydride as acyl donor, reaching DS values of about 50 %, meaning every other OH group of the xanthan repeating unit was acetylated, leading to high thermal stabilities of the polysaccharide derivate. But in this study

as well, high temperatures (100 °C) were necessary to achieve high degree of substitution (DS) values. However, recently ionic liquids have been identified as a good solvent for enzymatically catalyzed reactions, which are also applied for polysaccharide modification.

1.5.1.2   Enzymatic modification

Enzymatic modifications present an alternative to the chemical treatments of polysaccharides due to higher selectivity and mild reaction conditions, preventing undesired alterations of the polymers native structure. Regioselectivity of enzymes is another advantage to chemical modification, and it has been shown, that regioselective acylation of polysaccharides is possible, for example with *Candida antarctica* Lipase B (CALB) and vinyl esters or acid anhydrides as donors (Cumpstey, 2013; Ding et al., 2017). However, in aqueous solutions due to the excess of water, the reaction equilibrium is on the side of de-acetylation, resulting in very low degrees of substitution, thus requiring solvents, which are both suitable for solubilizing or suspending the polysaccharides as well as for the enzymes to be active. For this, multiple studies have been carried out using nonpolar solvents in combination with surfactants or nanoparticles to improve accessibility of the insoluble polysaccharides. Other studies describe esterification by using polar solvents like dimethyl sulfoxide (DMSO), dimethyl formamide (DMF) for acylation of starch using lipases and acetonitrile for production of cellulose acetate with immobilized CALB. Another possible group of solvents are ionic liquids. They not only increase solubility of polysaccharides (Cumpstey, 2013), resulting in a better accessibility of enzymatic reactions, but also proofed to be a good solvent for enzymatic reactions (Ranganathan, Zeitlhofer, & Sieber, 2017). The use of ionic liquids instead of water also has the benefit of shifting the reaction equilibrium towards the esterification reaction, allowing for higher degrees of substitution. While the esterification of most polysaccharides can be achieved with lipases like CALB, which also allows for a certain regioselectivity, more specific modifications require elaborate screenings for polysaccharide modifying enzymes. Until now, a number of polysaccharide specific enzymes have been identified, for example for gellan and xanthan (W. Hashimoto et al., 1996; W. Hashimoto, Sato, Kimura, & Murata, 1998; Kennedy & Sutherland, 1994; Marijn M Kool, 2014; Sutherland & Kennedy, 1996). While the identified gellan lyases are not relevant for industrial modifications of the polysaccharide, a couple of characterized esterases active on acetylated xylans (Razeq et al., 2018) as well as two esterases, AXE3 produced by *Myceliophtora thermophila C1* and YesY from *Bacillus subtilis* strain 168 with specific activity on the inner and outer acetylated mannose of xanthan are possible candidates for mild and site-specific modifications of polysaccharide acetylation patterns (Marijn M Kool, 2014). Furthermore, xanthan lyases with specific activity on the cleavage of the outer mannose from *Bacillus sp. GL1* and *Paenibacillus alginolyticus XL-1* have been described (Wataru Hashimoto, Nankai, Mikami, & Murata, 2003), which have been characterized to be specifically active on pyruvate mannose residues, but more recent studies also show activity on non-pyruvylated mannose residues (Marijn M Kool, 2014).

1.5.2 *In-vivo* modification

While the previously described methods allow for various, non-natural modification of polysaccharides, they are, in case of chemical modifications relatively unspecific and require harsh treatment conditions or, in the case of enzymatic modifications are still quite limited in terms of available enzymes and large-scale approaches. The biggest downside of both methods is, however, the further treatment of already purified polysaccharides, resulting in a second purification process after modification. One way to circumvent these additional processing steps and produce modified polysaccharides in their most natural way is the *in-vivo* modification. While this type of polysaccharide modification is most elegant and can be carried out by established production processes, it requires detailed knowledge of the genes involved in the biosynthesis pathway. For xanthan, investigations of the biosynthesis pathways began in the early 1980s with the identification of the assembly order of the repeating unit by *in-vitro* experiments (L. Ielpi, R. Couso, & M. Dankert, 1981; L. Ielpi, R. O. Couso, & M. A. Dankert, 1981) and the genes involved in the synthesis were identified by the end of the decade (Coplin & Cook, 1990). Identification of the genes and modification alongside the first characterization of the created xanthan-variants went hand in hand (Hassler & Doherty, 1990), opening the possibility to create variants tailored to desired properties. Following studies investigated the effect of the deletion mutations on the plant virulence of *X. campestris*, linking the structure and properties of xanthan to its natural role (Katzen et al., 1998). Besides xanthan, the largely identified biosynthesis pathways of the sphingans also make them a promising group of microbial EPS for *in-vivo* modification. While genetic engineering of the sphingan-producers mostly focus on increasing overall yield and facilitating downstream production, patents hold by sphingan-producing companies also describe methods like the production of deacetylated variants by genetically engineered strains (Schmid et al., 2014). Most recently, several genes involved in the biosynthesis of *paenan* were identified, their function hypothesized and some of them were successfully modified using a CRISPR/Cas9 system (Rütering et al., 2017). The resulting variants showed altered monomer compositions and differences in degree of pyruvylation. The pyruvate-free variant showed significantly altered rheological properties, from a gel-forming EPS with high solution viscosity to a low viscosity viscoelastic fluid. This shows that the modification of microbial EPS via genetic engineering does not have to be limited to fully clarified pathways and furthermore even helps unraveling biosynthetic pathways. Outside microbial EPS, successful *in-vivo* modification of plant cell-wall polysaccharide galactomannan has been shown by creating a transgenic guar species with increased α-galactosidase activity. The resulting galactomannans, which are naturally composed of a β-1→4 linked D-mannose backbone, with variable branching α-1→6 linked galactose substituents, showed significantly decreased degrees of substitution, making it the first *in-vivo* modified plant polysaccharide (Joersbo, Marcussen, & Brunstedt, 2001). Given the large number of enzymes active on cell-wall polysaccharides (Fry, 1995) and current advances of genetic engineering by the introduction of CRISPR/Cas9, in-*vivo* modification of plant polysaccharides seems viable and promising, however, to date there is no known industrial relevance of *in-vivo* modified plant polysaccharides.

1.6 Rheology of polysaccharides

1.6.1 Rheological parameters

Rheology is the study of viscoelastic materials and can describe everything from ideally viscous to ideally elastic materials. In solution, polysaccharides form viscous to viscoelastic systems and therefore, viscosity and viscoelasticity are the two terms which are commonly used for the characterization of polysaccharide solutions.

The viscosity of a fluid can be regarded as the resistance to flow. It can be best described by the two-plate model, where the fluid is sheared between one stationary and one moving plate with an area A and a gap width h in a one-dimensional direction, by a force F, causing the plate to move for a distance x with the velocity u of the moving plate. The deformation of the fluid is then defined as

$$\gamma = \frac{dx}{dh} \left[\frac{m}{m}\right]; [\ ] \tag{1}$$

and the resulting shear rate as

$$\dot{\gamma} = \frac{dv}{dh} \cdot \left[\frac{ms^{-1}}{m}\right]; [s^{-1}] \tag{2}$$

The required force F to move the upper plate with area A at velocity v, results in the shear stress

$$\tau = \frac{F}{A} \cdot \left[\frac{N}{m^2}\right]; [Pa] \tag{3}$$

The (dynamic) viscosity is then defined as

$$\eta = \frac{\tau}{\dot{\gamma}} \cdot \left[\frac{Pa}{s^{-1}}\right]; [Pa\ s^{-1}] \text{ (Newton's law)} \tag{4}$$

It thereby states the required (change of) shear stress for a resulting (change of) the shear rate.

Depending on the nature of the fluid, the required change of shear stress for an increase of the shear rate is either constant (Newtonian fluid) or variable (non-Newtonian fluid), where the required change of shear stress either decreases (shear thinning) or increases (shear thickening) with increasing shear rates.

For the determination of viscoelasticity, the fluid is sheared between two parallel plates with area A and a deformation γ_A at a given amplitude of shear stress τ_A and frequency f in a sine wave.

The resulting complex shear modulus G* is then given by:

$$G^* = \frac{\tau_A}{\gamma_A} \left[\frac{Pa}{\frac{m}{m}} \right]; [Pa] \tag{5}$$

Depending on the viscoelastic properties of the fluid, the resulting response sine wave (of the resulting deformation for a given shear stress and vice versa), is phase shifted from the preset sine wave (shear stress or deformation with a phase angle δ. From the complex notation of G*, storage modulus G' and loss modulus G'' can be determined:

$$G' = \frac{\tau_A}{\gamma_A} * cos\delta \left[\frac{Pa}{\frac{m}{m}} \right]; [Pa] \tag{6}$$

$$G'' = \frac{\tau_A}{\gamma_A} * sin\delta \left[\frac{Pa}{\frac{m}{m}} \right]; [Pa] \tag{7}$$

The real part, storage modulus G' [Pa] represents the elastic portion and the imaginary part, loss modulus G'' [Pa] the viscous portion of the fluid. The phase angle δ can be expressed as the loss factor tanδ:

$$tan\delta = \frac{G''}{G'} \left[\frac{Pa}{Pa} \right]; [\,] \tag{8}$$

For ideally elastic materials, the value of tanδ is 0, as the viscous portion G'' is 0, while for ideally viscous materials tanδ is not defined, as the elastic portion G' is 0. In the latter case tanδ is often given to approach infinity.

1.6.2   Rheological properties of polysaccharides

In aqueous solutions starting at concentrations of 0.1 % (w/v) or below, most polysaccharides show viscous and viscoelastic properties caused to the interactions of the high molecular weight chains. Except for some polysaccharides like starch, which exhibits shear thickening properties, most EPS have shear thinning properties. This effect is caused by the interactions of the polysaccharide chains at low shear rates, with a break-up and parallel orientation of the molecules at increasing shear rates. When all polymer molecules are perfectly arranged in parallel, this will lead to a Newtonian plateau (at infinitely high shear rates). While these shear thinning properties apply to almost every group of polysaccharides, with starch as the only known exception as shear thickening polysaccharide, they can be further subdivided into gel-forming and non-gel-forming polysaccharides. The viscoelastic properties of non-gel forming are determined by weak entanglement interactions between the molecules and usually exhibit predominantly liquid-like behavior at low concentrations. Gel forming polysaccharides exhibit predominantly (visco-)elastic behavior, even at low concentrations. The formation of these gel-like structures is often caused by cation-mediated polymer-polymer interactions (c.f. alginates, deacetylated gellan, hyaluronan) of charged, unbranched polysaccharides. This leads to strong, and, depending on the polysaccharide

concentration, brittle gel structures. For branched, charged polysaccharides like xanthan and sphingans, however the viscoelastic properties show much weaker gel strengths compared to linear polysaccharides.

As polysaccharides are industrially applied as stabilizers, thickeners or gelling agents, their rheological properties are of utmost importance for evaluating their quality, performance, and aptitude for the desired applications. For most industrial products, the general flow behavior and gelling properties are the most important parameters for product evaluation. However, industrial regulations concerning the rheological properties are far below the possible evaluation methods.

The viscosity, for example, can be evaluated by a power-law fit of the flow curve.

$$\tau = K\dot{\gamma}^n \tag{9}$$

With the flow consistency index K [Pa s^n] and the flow behavior index n [ ]. A higher value of K represents overall higher viscosity, while values of n <1 (for shear thinning materials) indicate the shear rate dependency of the viscosity. Here smaller values represent higher dependency on the shear rate. Gel strength or viscoelasticity can be evaluated by oscillatory shear tests, where a tan δ < 1 represents predominant elastic behavior and smaller values of tan δ represent higher brittleness of the gel. On the other hand, tan δ > 1 shows predominant fluid behavior, with no gel characteristics. From an amplitude sweep, with either increasing shear stress or deformation, the basic viscoelastic properties can be determined. The first is linear-viscoelastic (LVE)-region, a deformation region, where the sample can re-deform to its initial state before the next measuring point. Secondly, the flow point, in case of predominant elastic behavior within the LVE region, which is defined as the shear stress or strain amplitude, at which the G' and G''-curves intersect. Both moduli are also dependent on the frequency of oscillation. With the frequency sweep, long term behavior like storage can be predicted with low frequencies in the range of 10^{-2} Hz, while high frequencies (10^1-10^2 Hz) allow for the short-term behavior, e.g. processing of the sample. Another important characterization method is temperature stability, where values of G' and G'' under constant shear stress (or strain) and oscillatory frequency can be determined over a wide range of temperatures to predict the heat stability of the viscoelastic properties. Finally, the (ir-)reversibility of the degradation of the network structure formed by the polymers under high shear, can be assessed by the thixotropy test, where the sample exposed to high shear after oscillatory test within the LVE and the regeneration of G' and G'' are evaluated over time under oscillation within the LVE region. While most of these tests assess the overall quality of the EPS solution, it enables the creation of a heuristic for the determination of the rheological properties in regard to the physical structures or alterations of the polysaccharides, in order to establish a structure function relationship. These insights allow for a systematic approach to predict structures of unknown polysaccharides based on their monomeric composition and their rheological properties as well as establish and tailor polysaccharides to their applications.

1.7 Scope of this work

The scope of this work consists of two major parts.

The first part is the elucidation of the structure function relationship of microbial exopolysaccharides. Linking their structural differences, either of natural origin or introduced by genetic modification of the producing strains, to their rheological properties in order to gain insight, whether there is a common heuristic for predicting rheological properties of polysaccharides by investigating their structures and monomer compositions as well as predicting necessary modifications, either *in-vivo* or *in-vitro* to create polysaccharides with required performances. For this, three types of polysaccharides have been studied in different ways to gain insight into the structure function relationship:

1) Sphingans, a group of highly structurally similar polysaccharides with main differences in the sidechain composition. Here the focus was the evaluation of these very minute differences on the rheological properties.
2) Paenan, whose unique composition of individual polysaccharides allows for targeted modification of the ratios by genome editing of the producing strain. This allowed an investigation of the natural interactions between individual polysaccharides on the effect on the rheological properties.
3) Xanthan, whose structure is highly clarified and has a unique decoration pattern of two acetyl- and one pyruvyl-residue, where the targeted modification of these residues by genetic modification of the production strain *X. campestris* LMG 8031. This work should give detailed insight on the effect of the decoration of exopolysaccharides on the structural changes and therefore their rheological properties.

The second part is the *in-vivo* modification of the exopolysaccharide xanthan in terms of an un-natural decoration with a crotonyl residue, to create a cross-linkable polysaccharide, which may be produced by established fermentation processes. For this modification, an *in-vivo* crotonyla-tion of xanthan was targeted for the introduction of a double bond to allow for native crosslinkability without the addition of further crosslinking agents by crosslinking via (UV-)light. The substrate, crotonyl-CoA should be enriched within the target organism by metabolic engineering, while the acceptance of the substrate by an acyltransferase was aimed to be achieved by the modification of one the acetyltransferases involved the xanthan biosynthesis. The scope of this part is split into following subsections:

1) Modification of a selected acetyl-CoA acetyltransferase from *X. campestris* and its modifi-cation towards the substrate crotonyl-CoA
2) Increasing the intracellular crotonyl-CoA levels in *X. campestris* and the establishment of analytical methods for the quantification of CoA levels in *X. campestris*
3) Creation of a synthetical analogue of the targeted xanthan-variant by means of chemical modification

2 Materials

2.1 Chemicals

The chemicals used in this work and their suppliers are listed in Table 2.

Table 2. Overview of the chemicals used in this work

Chemical	Supplier	Catalogue number
1-Phenyl-3-methyl-5-pyrazolon	Sigma-Aldrich	M70800
Acetic acid	Carl Roth	6755.1
Acetic acid (glacial) 100 %	Merck	100066
Acetonitrile LC-MS grade	VWR	83.040.320
Agar-Agar Kobe I	Carl Roth	5210.2
Agarose	Serva Electrophoresis	11406
Ammonia 32 %	Carl Roth	P093.1
Ammoniumformate	Sigma-Aldrich	17843
Antifoam B, 10% emulsion	VWR	BAKR8390.0500
Boric acid	Sigma-Aldrich	B7901
Calcium choloride dihydrate	Carl Roth	5239.1
Cobalt(II) chloride hexahydrate	Alfa Aesar	A16346
Coenzyme A, lithium salt	Sigma-Aldrich	C3019-10MG
Copper(II) sulfate pentahydrate	Fisher Scientific	
Crotonly-coenzyme A, trilithium salt	Sigma-Aldrich	28007-5MG
DA-64 (N-(Carboxymethylaminocarbonyl)-4,4'-bis(dimethylamino)diphenylamine sodium salt)	FUJIFILM Wako Chemicals	043-22351
D(+)-Glucose monohydrate	Carl Roth	6887.5
Dimethyl sulfoxide	Carl Roth	4720.1
DNA Stain Clear G	Serva Electrophoresis	39804.02
D(+)-Sucrose	Carl Roth	4621.2
Formic acid	Sigma-Aldrich	56.302
Gentamicin sulfate	Carl Roth	0233.2
Glycerol 98 %	Carl Roth	7530.4
Glycerol, 99.5 % p.a.	Carl Roth	3783.2
Hydrochloric acid, 37 %	Carl Roth	4625.1
Iron(II) sulfate heptahydrate	Sigma-Aldrich	31236
Isopropanol HPLC grade	Sigma-Aldrich	7343.1
Isopropanol, technical	VWR	20.922.466
Kanamycin A sulfate	Carl Roth	T832.3

Lithium nitrate	VWR	13405.30
Magnesium sulfate heptahydrate	Carl Roth	8283.2
Manganese(II) chloride tetrahydrate	Sigma-Aldrich	63535-50G-F
Methanol LC-MS grade	VWR	83.638.320
Paraffin oil, low viscosity	Carl Roth	9190
Phenol red	Alfa Aesar	B21710
Potassium chloride	Carl Roth	6781.1
Orthophosphoric acid, 85 %	Carl Roth	9079.3
Potassium dihydrogen phosphate	Carl Roth	P749.3
Pullulan	PSS	PSS-dpul
Rubidium chloride	Carl Roth	4471.1
Sodium Chloride	Carl Roth	P029.3
Sodium hydroxide	Carl Roth	6771.2
Sodium molybdate dihydrate	Carl Roth	M1651
Sodium tartrate dihydrate	Carl Roth	0254.1
Sulfuric acid, 96 %	Carl Roth	4623.4
Trans-crotonic acid anhydride	Sigma-Aldrich	94128
Trifluoracetic acid	Sigma-Aldrich	T6508
Tryptone/Peptone	Carl Roth	8952.5
Vitamin solution RPMI 1640 100x	Sigma-Aldrich	R7256
Xanthan, 4.5 MDa	Sigma-Aldrich	42663-100MG
Yeast extract	Carl Roth	2363.4
Zinc chloride	Merck	1.08816.0250
Trans-crotonic acid	Alfa Aesar	A15765
Sodium pyruvate	Sigma-Aldrich	P2256

2.2 Enzymes and kits

All enzymes and enzyme buffers used in this work are shown in Table 3. Overview of the enzymes and buffers used in this workTable 3.The kits used in this work are listed in Table 4.

Table 3. Overview of the enzymes and buffers used in this work

Enzymes and buffers	Supplier
Accuzyme™ Mix	Bioline
CIP alkaline phosphatase	New England Biolabs
Glucose oxidase	Sigma-Aldrich
GoTaq® G2 Polymerase	Promega
Horseradish peroxidase	
Phusion® High-Fidelity DNA-polymerase & Phusion® HF buffer	New England Biolabs
Restriction endonucleases & NEB cutsmart® buffer	New England Biolabs
T4 polynucleotide-kinase	New England Biolabs
T4-DNA ligase & T4-DNA ligase buffer	New England Biolabs
T7-DNA ligase & T7 DNA ligase buffer	New England Biolabs
Taq polymerase with Thermopol® buffer	New England Biolabs

Table 4. Overview of the Kits used in this work

Kit	Supplier
DNeasy® UltraClean Microbial Kit	Qiagen
GeneJET™ Plasmid Miniprep Kit	Thermo Fischer Scientific Inc.,
NucleoSpin® Gel and PCR Clean-up Kit	Macherey-Nagel GmbH & Co. KG GmbH & Co. KG

2.3 Devices

Autoclave Varioklav 135S	Thermo Fischer Scientific Inc.
Chromatography	
UltiMate 3000 RS LC System	Thermo Fischer Scientific Inc.
Degasser SRD 3400	Thermo Fischer Scientific Inc.
Pump HPG 2400 RS	Thermo Fischer Scientific Inc.
Autosampler WPS 3000 TRS	Thermo Fischer Scientific Inc.
Column oven TCC 3000 RS	Thermo Fischer Scientific Inc.
Diode-array-detector 3000 RS	Thermo Fischer Scientific Inc.
RI detector Shodex RI-101	Showa Denko K.K.
SECurity GPC System	
SECcurity SLD7000 MALLS	Polymer Standard Service GmbH
SECcurity GPC1260 RI	Polymer Standard Service GmbH
Columns	
YMC Triart C-18	YMC Europe GmbH
Rezex ROA-Organic Acid H+	Phenomenex Ltd.Germany
Nucleodur C18 Gravity	Macherey-Nagel GmbH & Co. KG
Suprema 10.000 Å	Polymer Standard Services GmbH
Suprema 100 Å	Polymer Standard Services GmbH
Mass Spectrometry	
Bruker HCT	Bruker Daltonics GmbH
Crossflow filtration	
Sarto®Jet	Sartorius AG
Hydrosart® Casette 100 kD	Sartorius AG
Bioreactors	
DASGIP 8x parallel reactor system	DASGIP GmbH
Biostat Bplus 2L	Sartorius AG
Gel electrophoresis	
Mini-Sub Cell GT System	Bio-Rad Laboratories GmbH
Dark Reader® transillumina	Clare Chemical Research Inc.
Gel iX Imager	Intas Science Imaging Instruments GmbH
Freezer -20 °C	Liebherr-Hausgeräte GmbH
Freezer -80 °C Forma 906 -86°C ULT	Thermo Fischer Scientific Inc.
Microliter syringe, 25 µL	Hamilton AG
Thermomixer Tmix	Analytik Jena AG

Incubators

Constant climate chamber KBF 240 5.1/C   BINDER GmbH

Incubator Function Line B12   Thermo Fischer Scientific Inc., Haeraeus

Heating oven Function Line T12   Thermo Fischer Scientific Inc., Haeraeus

Incubator shaker

HAT Minitron   Infors AG

MaxQ 2000   Thermo Fischer Scientific Inc.

TiMix 5 control   Edmund Bühler GmbH

KS 4000ic control   IKA®-Werke GmbH & CO. KG

Vacuum Concentrator

SpeedVac Plus SC210A   Savant Instruments Pvt. Ltd.

Refrigerated Vapor Trap RVT100   Thermo Fischer Scientific Inc.

Magnetic stirrer

MR 3001 K   Heidolph Instruments GmbH & Co.KG

     VWR International GmbH

VMS-C7   Thermo Fischer Scientific Inc.

Variomag Telesystem

Pipets

Transferpette S Set,0.1-10,000 µl   BRAND GmbH & Co. KG

Transferpette S electronic 10-200 µl   BRAND GmbH & Co. KG

Transferpette S-8   BRAND GmbH & Co. KG

Transferpette S-12   BRAND GmbH & Co. KG

HandyStep electronic   BRAND GmbH & Co. KG

Research pro 8x 1200 µL   Eppendorf AG

Microwave MH 25 ED   ECG

pH-meter and electrodes

FiveGoTM   Mettler-Toledo GmbH

FiveEasyTM   Mettler-Toledo GmbH

InLab® Expert Pro pH 0-14 ; 0-100 °C   Mettler-Toledo GmbH

InLab® Micro Pro pH 0-14 ; 0-100 °C   Mettler-Toledo GmbH

PCR-cycler

MJ MiniTM Personal Thermo Cycler   Bio-Rad Laboratories GmbH

MyCycler™ Thermal Cycler   Bio-Rad Laboratories GmbH

Rheometer

Physica MCR 300   Anton Paar GmbH

Measuring system CP 50-1   Anton Paar GmbH

Temperature control element TEK 150P   Anton Paar GmbH

Pure Water Systems

PURELAB Classic	ELGA LabWater
Milli-Q	Merck KgaA

Mixer mill MM400	Retsch GmbH
Vacuum drying chamber VD 53	BINDER GmbH
Biological Safety Cabinet MSC-Advantage	Thermo Fischer Scientific Inc.

UV-Vis spectrophotmeter

Multiskan Spectrum	Thermo Fischer Scientific Inc.
Varioscan	Thermo Fischer Scientific Inc.
Infinite 200 pro	Tecan Group Ltd.
Nanophotometer P-class	Implen
Ultrospec 10	Amersham Biosciences

Vacuum pump PC 2004 VARIO	VACUUBRAND GmbH & Co. KG
Vortex Genie 2	Scientific Industries Inc.
Cell disruptors Genie™ Disruptor Model Digital	Scientific Industries Inc.

Lab balances

Pioneer®	Ohaus Europe GmbH
TE6101	Sartorius AG
TE1502S	Sartorius AG

Water bath ED-33	JULABO Labortechnik GmbH

Centrifuges

Sorvall RC 6+	Thermo Fischer Scientific Inc.
Sorvall Lynx 6000	Thermo Fischer Scientific Inc.
Fresco 21	Heraeus
Pico 17	Heraeus
Rotana 460R	Hettich Lab Technology
Galaxy MiniStar	VWR International

Rotors

Sorvall RC 6+

F9S4x1000y	Thermo Fischer Scientific Inc.
F10S6x500y	Thermo Fischer Scientific Inc.
SS34	Thermo Fischer Scientific Inc.

Sorvall Lynx 6000

BIOFlex HC Rotor	Thermo Fischer Scientific Inc.
Fiberlite F9-6x1000 LEX	Thermo Fischer Scientific Inc.
A27-8x50	Thermo Fischer Scientific Inc.

MicroPulser Electroporator	Bio-Rad Laboratories Inc.
Nicolet™ 380 FT-IR	Thermo Fischer Scientific Inc.

2.4 Software

Local applications

Bruker DataAnalysis	Bruker Daltonics GmbH
Bruker QuantAnalysis	Bruker Daltonics GmbH
ChemBioDraw Ultra 14.0	Perkin Elmer Informatics
Chromeleon 6.80	Thermo Fisher Scientific, Dionex
DASware control	DASGIP GmbH
Module Operator Service Program 3.0	Sartorius AG
Microsoft Office 365 ProPlus	MICROSOFT Corporation
PSS WinGPC Unichrom 8.1	Polymer Standard Services GmbH
Rheoplus/32 V3.61	Anton Paar GmbH
SkanIt 2.4.3	Thermo Fischer Scientific Inc.
SnapGene® 2.3.2	GSL Biotech LLC
GraphPad Prism7	GraphPad Software, Inc.
MATLAB R2017a	The MathWorks, Inc.

Server based applications

BLAST	National Center for Biotechnology Information
	https://blast.ncbi.nlm.nih.gov/Blast.cgi
Braunschweig Enzyme Database	Technische Universität Braunschweig,
	https://www.brenda-enzymes.info/
Robetta	University of Washington
	http://robetta.bakerlab.org/
Benchling	Benchling Inc.
	https://www.benchling.com/
KEGG Pathway Database	Kanehisa Laboratories
	https://www.genome.jp/kegg/

2.5 Antibiotics and media

All media and solutions were prepared with ultrapure water from PURELAB classic or Milli-Q devices. Heat stable solutions were sterilized at 121 °C for 20 minutes at 2 bar. Non-heat stable solutions were filtered through a 0.2 μm sterile filter. For media consisting of multiple solutions, each solution was sterilized separately. For solid media 1.5 % (w/v) Agar-Agar was added prior to autoclaving. Antibiotics were prepared as 1000 x stock solutions, sterile filtered and stored at -20 °C. For Selective media, antibiotics were added to cooled down media after autoclaving. All media and solutions were stored at room temperature unless otherwise specified.

2.6 Cultivation media

LB medium

Tryptone/peptone 10 g L^{-1}; yeast extract 5 g L^{-1}, NaCl 10 g L^{-1}

SOB medium

Trypton/peptone 20 g L^{-1}, yeast extract 5 g L^{-1}, NaCl 0.5 g L^{-1}, KCl 0.2 g L^{-1}, 100 mM $MgCl_2$ solution 100 mL L^{-1} (autoclaved separately)

SOC medium

SOB medium with 20 mM Glucose

MM1 P100 (EPS) medium

Tryptone/peptone 5 g L^{-1}, KH_2PO_4 1.67 g L^{-1}, $MgSO_4 \cdot 7\ H_2O$ 1.33 g L^{-1}, $CaCl_2 \cdot 2\ H_2O$ 0.05 g L^{-1}, Glucose monohydrate 33 g L^{-1}, trace element solution 1 mL L^{-1}, vitamin solution RPMI 1640 2 mL L^{-1}

Tryptone/peptone with $MgSO_4$ were prepared and autoclaved as one solution, all other solutions were prepared and autoclaved separately. Vitamin and trace element solutions were added through a 0.22 μm sterile syringe filter to the cooled down medium.

Trace element solution, 1000 x

$MnCl_2 \cdot 4\ H_2O$ 1.8 g L^{-1}, $FeSO_4 \cdot 7\ H_2O$ 2.5 g L^{-1}, boric acid 0.258 g L^{-1}, $CuSO_4 \cdot 5\ H_2O$ 0.031 g L^{-1}, $ZnCl_2$ 0.021 g L^{-1}, $CoCl_2 \cdot 6\ H_2O$ 0.075 g L^{-1}; Na_2MoO_4 0.023 g L^{-1}, sodium tartrate $\cdot 2\ H_2O$ 2.1 g L^{-1}

2.7 Bacterial strains

The used and created bacterial strains are shown in Table 5.

Table 5. Bacterial strains used and created in this work

Strain	Genotype	Source
E. coli NEB Turbo	F' *proA+B+ lacIq* Δ (lacZ) M15*/fhuA2* Δ(*lac*-proAB) *glnV gal* R(*zgb*-210::Tn10)TetS *endA*1 *thi*-1 Δ(*hsdSmcrB*)5	NEB
E. coli DH5α	F- *endA1 glnV44 thi-1 recA1 relA1 gyrA96 deoR nupG* Φ80d*lacZ*ΔM15 Δ(*lacZYA-argF*)U169, hsdR17(*rKmK+*), λ–	Life Technologies
E. coli BL21(DE3)	F- *ompT gal dcm hsdSB*(*rB- mB-*) λ(DE3)	Novagen (Merck)
E. coli (ATCC®47055™)-S17.1	*recA pro hsdR* RP42Tc::MuKm::Tn7	ATCC
Xanthomonas campestris LMG 8031	wildtype	BCCM/LMG Bacteria Collection
Xanthomonas campestris LMG 8031 Δ*gumD*	*gumD-*	This work
Xanthomonas campestris LMG 8031 Δ*gumF*	*gumF-*	This work
Xanthomonas campestris LMG 8031 Δ*gumFG*	*gumFG-*	This work
Xanthomonas campestris LMG 8031 Δ*gumFGL*	*gumFGL-*	This work
Xanthomonas campestris LMG 8031 Δ*gumFL*	*gumFL-*	This work
Xanthomonas campestris LMG 8031 Δ*gumG*	*gumG-*	This work

Xanthomonas cam-pestris LMG 8031 *ΔgumGL*		*gumFGL*-, pSRKGm-*gumF*, GentaR	This work
Xanthomonas cam-pestris LMG 8031 *ΔgumK*		*gumK*-	This work
Xanthomonas cam-pestris LMG 8031 *ΔgumL*		*gumL*-	This work

2.8 Plasmids

The plasmids used and created in this work are shown in Table 6

Table 6. Plasmids used and created in this work

Plasmid	Size (bp)	Description	Source
pSRKKm	5773	*kan^R*, broad host expression plas-mid, lac-operon	
pSRKGm	5739	*gm^R*, broad host expression plas-mid, lac-operon	
pK19mobsacB	5722	*kan^R*, integrative plasmid; oriV, Ec oriT, sacB	
pK19Gm	5803	pK19mobsacB*Δkan^R::gm^R*	This work
pGAGm	5375	pSRKGm Δ*lacZα,* replacement of MCS with *BamHI* restriction site	This work
pGAKm	5409	pSRKKm Δ*lacZα,* replacement of MCS with *BamHI* restriction site	This work
pHExXan	3114	pGAGm Δ*mob* Δ*lacI*, replace-ment of lac-promoter with *gum*-promoter from *Xcc* LMG 8031	This work
pK19Gm-dgumD	6833	Gm^R, pK19Gm with fused homol-ogy regions up- and downstream of *gumD,* cloned with XbaI and HindIII	This work
pK19Gm-dgumF	6748	Gm^R, pK19Gm with fused homol-ogy regions up- and downstream of *gumF,* cloned with XbaI and NheI	This work
pK19Gm-dgumFG	6893	Gm^R, pK19Gm with fused homol-ogy regions up- and downstream	This work

		of *gumFG,* cloned with XbaI and BamHI	
pK19Gm-dgumG	6911	Gm^R, pK19Gm with fused homology regions up- and downstream of *gumG,* cloned with XbaI and BamHI	This work
pK19Gm-dgumL	6929	Gm^R, pK19Gm with fused homology regions up- and downstream of *gumL,* cloned with XbaI and BamHI	This work
pK19Gm-dgumK	6824	Gm^R, pK19Gm with fused homology regions up- and downstream of *gumK,* cloned with XbaI and HindIII	This work
pSRKGm-gumD	6831	Gm^R pSRKGm with *gumD* gene, cloned with NdeI and NheI	This work
pSRKGm-gumF	6466	Gm^R pSRKGm with *gumF* gene, cloned with Gibson Assembly	This work
pSRKGm-gumG	6442	Gm^R pSRKGm with *gumG* gene, cloned with Gibson Assembly	This work
pSRKGm-gumG-R21A	6442	Gm^R, pSRKGm with *gumG* with AA mutation at position 21 from arginine to alanine	This work
pSRKGm-gumG-D26A	6442	Gm^R, pSRKGm with *gumG* with AA mutation at position 26 from aspartic acid to alanine	This work
pSRKGm-gumG-H40A	6442	Gm^R, pSRKGm with *gumG* with AA mutation at position 40 from histidine to alanine	This work
pSRKGm-gumG-H56A	6442	Gm^R, pSRKGm with *gumG* with AA mutation at position 56 from histidine to alanine	This work
pSRKGm-gumG-K29A	6442	Gm^R, pSRKGm with *gumG* with AA mutation at position 29 from lysine to alanine	This work
pSRKGm-gumG-T290A	6442	Gm^R, pSRKGm with *gumG* with AA mutation at position 290 from threonine to alanine	This work

pSRKGm-gumG-T297A	6442	Gm^R, pSRKGm with *gumG* with AA mutation at position 297 from threonine to alanine	This work
pSRKGm-gumG-F60A	6442	Gm^R, pSRKGm with *gumG* with AA mutation at position 60 from phenylalanine to alanine	This work
pSRKGm-gumG-F61A	6442	Gm^R, pSRKGm with *gumG* with AA mutation at position 61 from phenylalanine to alanine	This work
pSRKGm-gumG-V18A	6442	Gm^R, pSRKGm with *gumG* with AA mutation at position 18 from valine to alanine	This work
pSRKGm-gumG-L63A	6442	Gm^R, pSRKGm with *gumG* with AA mutation at position 63 from leucine to alanine	This work
pSRKGm-gumG-F60AF61A	6442	Gm^R, pSRKGm with *gumG* with AA mutation at position 60 and 61 from phenylalanine to alanine	This work
pSRKGm-gumG-T87A	6442	Gm^R, pSRKGm with *gumG* with AA mutation at position 87 from threonine to alanine	This work
pSRKGm-gumG-L84A	6442	Gm^R, pSRKGm with *gumG* with AA mutation at position 84 from leucine to alanine	This work
pSRKGm-gumG-S16A	6442	Gm^R, pSRKGm with *gumG* with AA mutation at position from serine to alanine	This work
pHExXan-gumD	4565	Gm^R, pHExXan with *gumD* gene	This work
pHExXan-GumG	4181	Gm^R, pHExXan with *gumG* gene	This work
pHExXan-gumG-R21A	6442	Gm^R, pHExXan with *gumG* with AA mutation at position 21 from arginine to alanine	This work
pHExXan-gumG-D26A	6442	Gm^R, pHExXan with *gumG* with AA mutation at position 26 from aspartic acid to alanine	This work
pHExXan-gumG-H40A	6442	Gm^R, pHExXan with *gumG* with AA mutation at position 40 from histidine to alanine	This work

pHExXan-gumG-H56A	6442	Gm^R, pHExXan with *gumG* with AA mutation at position 56 from histidine to alanine	This work
pHExXan-gumG-K29A	6442	Gm^R, pHExXan with *gumG* with AA mutation at position 29 from lysine to alanine	This work
pHExXan-gumG-T290A	6442	Gm^R, pHExXan with *gumG* with AA mutation at position 290 from threonine to alanine	This work
pHExXan-gumG-T297A	6442	Gm^R, pHExXan with *gumG* with AA mutation at position 297 from threonine to alanine	This work
pHExXan-gumG-F60A	6442	Gm^R, pHExXan with *gumG* with AA mutation at position 60 from phenylalanine to alanine	This work
pHExXan-gumG-F61A	6442	Gm^R, pHExXan with *gumG* with AA mutation at position 61 from phenylalanine to alanine	This work
pHExXan-gumG-V18A	6442	Gm^R, pHExXan with *gumG* with AA mutation at position 18 from valine to alanine	This work
pHExXan-gumG-L63A	6442	Gm^R, pHExXan with *gumG* with AA mutation at position 63 from leucine to alanine	This work
pHExXan-gumG-F60AF61A	6442	Gm^R, pHExXan with *gumG* with AA mutation at position 60 and 61 from phenylalanine to alanine	This work
pHExXan-gumG-T87A	6442	Gm^R, pHExXan with *gumG* with AA mutation at position 87 from threonine to alanine	This work
pHExXan-gumG-L84A	6442	Gm^R, pHExXan with *gumG* with AA mutation at position 84 from leucine to alanine	This work
pHExXan-gumG-S16A	6442	Gm^R, pHExXan with *gumG* with AA mutation at position from serine to alanine	This work

pCRTGm	8174	Gm^R, pSRKGm with *phaA*, *phaB* genes from *Cupriavidus necator* and *crt* gene from *Clostridium acetobutylicum*, cloned with Gibson Assembly	This work
pCRTKm	8218	Kan^R, pSRKGm with *phaA*, *phaB* genes from *Cupriavidus necator* and *crt* gene from *Clostridium acetobutylicum*, cloned with Gibson Assembly	This work

2.9 Oligodesoxyribonucleotides

Oligodesoxyribonucleotides (oligonucleotides) used for PCR and sequencing are shown in Table 7. Oligonucleotides were synthesized by biomers.net GmbH and Eurofins Genomics Germany GmbH. Inserted restriction sites are underlined, inserted mutations are shown in bold.

Table 7. Overview of the used oligonucleotides

Name	Length (bases)	Sequence 5'-3'
27_fw	20	AGAGTTTGATCMTGGCTCAG
1525_r	17	AAGGAGGTGWTCCARCC
gumD_flu_fw_XbaI	30	CCG<u>TCTAGA</u>GCAGCATCCGC-TACAACATGC
gumD_fld_rev_HindIII	28	CC<u>AAGCTT</u>ACCAGATCGCCATAA-GCCGA
pBBR1_oriV_fw	38	TTGAC-GGGGTCTCCATGGCGGCGGCCAC-CGGCTGGCTC
pBBR1_oriV_rev	37	TTGACGGGGTCTCCAGAGCCTAC-CGGCGCGGCAGCGT
Cas9_check_fw	22	CCTTTAGTTGAGGCCGCATACC
Cas9_check_rev	22	CTTAATCATATGCGCTAAGGCC
oriV_check_fw	22	GAAGTCCAGCGCCAGAAACAG
oriV_check_rev	21	CTGCGTGGCCATGCTTATCTC
pSRK_Seq1	18	CGCATTTCGCCCTATATC
gumD_gDNA_check_fw	20	ATCAGGAGCAGCTGCTCAAC
gumD_gDNA_check_rev	20	TCCAGAACCCTTCTGCACTC
gumFG_check_fw	20	CATGATTGTGGCATCCGACG
gumFG_check_rev	20	TGCCCTGCATACTTCTCCAC

gumFG_fld_fw_OE	40	ATACGGTGACAGGGGCATCG-CAGAATCATCAGTCGATGTG
gumFG_fld_rev_BamHI	32	TATA-TA<u>GGATCC</u>CGAACAGATCGCCGTCATTC
gumFG_flu_fw_XbaI	32	TATATA<u>TCTAGA</u>GCCGTTATTGAAAC-GGATGG
gumFG_flu_rev_OE	40	CACATCGACTGATGAT-TCTGCGATGCCCCTGTCACCGTAT
gumK_check_fw	20	CATCGCCTGCATTTTTGTTG
gumK_check_rev	20	CTGCTGATGACAAATTCCGC
gumK_fld_fw_OE	40	CCGCATGAAGGGAGATATGCGAG-GAGGCGCTTTTTTGATG
gumK_fld_rev_HindIII	32	TATATA<u>AAGCTT</u>TGTACTTCTCAAC-CGGCTCG
gumK_flu_fw_XbaI	33	TATATA<u>TCTAGA</u>CTGGTCTGGATCGG-CAAGATC
gumK_flu_rev_OE	41	GATCAAAAAAGCGCCTCCTCGCATA-TCTCCCTTCATGCGGG
gumL_check_fw	20	ACGTCTTCCATGTAGGTCAC
gumL_check_rev	20	CGGAGAGAAAATCCAGCAAG
gumL_fld_fw_OE	40	GTTTGAAGGAGGATCCCTGTAAC-GACAATGCATGGCCAGC
gumL_fld_rev_HindIII	31	TATATA<u>AAGCTT</u>GTTGCCGAAGGCCAC-CAAC
gumL_flu_fw_XbaI	32	TATATA<u>TCTAGA</u>G-TATGCCGAAGGCATCCATG
gumL_flu_rev_OE	40	GCTGGCCATGCATT-GTCGTTACAGGGATCCTCCTTCAAAC
pK19_gum_check_fw	20	CCCAGGCTTTACACTTTATG
pK19_gum_check_rev	20	CGATTAAGTTGGGTAACGCC
pSRK_MCS_Seq_rev	19	AATACGCAAACCGCCTCTC
pSRK_Seq_2_rev	21	AAATTGATGGGGCAAGGCCGC
pSRK_Seq_ab_GmR_fw	21	AGATTACGGTGACGATCCCG
pSRK_MCS_Seq_fw	17	ATTCCGGGCATGGAACC
gumD_fw_NdeI	32	TATATA<u>CATATG</u>CTTTTGGCAGACTT-GAGTAG
gumD_rev_NheI	32	TATATA<u>GCTAGC</u>TCAGTAC-GCGGTCTTCTGTC
oriV_Seq_fw	20	GACAAGCTGATGGACAGGCT

oriV_Seq_rev	20	GTGGCCATGCTTATCTCCAT
gumF_fld_fw_OE	38	ATACGGTGACAGGGGCATCGATGAC-GACGGCTGCGATC
gumF_fld_rev_NheI	32	TATATA<u>GCTAGC</u>CAACCAGCAAACTG-CAGACC
gumF_flu_rev_OE	38	GATCG-CAGCCGTCGTCATCGATGCCCCTGTCA CCGTAT
gumG_fld_fw_OE	40	CCTCAACTGTCGCG-GAGCGCCAGAATCATCAGTCGATGTG
gumG_flu_fw_XbaI	32	TATATA<u>TCTAGA</u>ATT-GTTCTGGGGCCTGGATG
gumG_flu_rev_OE	39	CACATCGACTGATGAT-TCTGGCGCTCCGCGACAGTTGAG
gumF_gDNA_check_rev	20	GCAGCACATCCAGTGCAAAC
gumG_gDNA_check_fw	20	GGCTGTCGCAGTTGTTCTC
gumDfld_rev_HindIII	28	CC<u>AAGCTT</u>ACCAGATCGCCATAA-GCCGA
GmR_mob_fw_new	34	TTCCTGGGGTCTCACGCTGCCAC-TCATCGCAGTC
pSRK_check_fw	20	TGCTTCCGGCTCGTATGTTG
pSRK_check_rev	20	TTAACGACCCTGCCCTGAAC
BB_phaABcrt_fw	36	AATAGATAGG<u>GCTAGC</u>AATTCGAAA-GCAAATTCGAC
BB_phaABcrt_rev	39	GTCAGTCATTT-GCTGTTTCCTGTGTGAAATT-GTTATCCG
crt_GA_fw	50	GCTGAA-TATAGGAGGCCTCATGGAACTAAACAA TGTCATCCTTGAAAAGG
crt_GA_rev	48	GAATT<u>GCTAGC</u>CCTATCTATTTTTGAA-GCCTTCAATTTTTCTTTTCTC
phaAB_GA_fw	34	GAAACAGCAAATGACTGACGTT-GTCATCGTATCC
phaAB_GA_rev	41	GTTCCATGAGGCCTCCTA-TATTCAGCCCATATGCAGGCCGC
pSRK_BamHI_fw	33	TATATAT<u>GGATCC</u>AATTCGAAA-GCAAATTCGAC
pSRK_BamHI_rev	31	TATA-TA<u>GGATCC</u>TGCTGTTTCCTGTGTGAAA

gumF_GA_fw	37	CACACAGGAAACAGCAGGTGAATAC-GGTGACAGGGGC
gumF_GA_rev	40	TCGAATTTGCTTTCGAATT-GTCATGCCGACACCGGACGTG
gumG_GA_fw	33	CACACAGGAAACAGCAGATGACGAC-GGCTGCGA
gumG_GA_rev	50	TCGAATTTGCTTTCGAATTGTCACTT-GCGTTTCAATCCCAACATCCAGGG
gumL_GA_fw	36	CACACAGGAAACAGCAGATGGCCAAC-GCTTTACTGC
gumL_GA_rev	45	TCGAATTTGCTTTCGAATTGTCAC-CACAAATCGTAAGGGAACGCA
gum-prom_fw_EcoRI	33	TATATA<u>GAATTC</u>CGTGTTGTGCCTT-GCGATGTG
gum-prom_rev_BamHI	31	TATATA<u>GGATCC</u>GAGCAGAG-CAGAGCCAGGC
pHEXXAN_GmR_fw	22	CAATTTACCGAACAACTCCGCG
pHEXXAN_oriV_rev	20	ATATGTGGACGATGGCCGCG
gumD_pHExXan_fw	45	AGCCTGGCTCTGCTCTGCTCGATGCTTTTGGCAGACTTGAGTAGC
gumD_pHExXan_rev	42	TCGAATTTGCTTTCGAATTGTCAGTAC-GCGGTCTTCTGTCCG
pCRT_2.0_fw	54	CAAGGCCTCAGCCTGGCTCTGCTCTGCTCGATGACTGACGTTGTCATCG-TATCC
pCRT_2.0_rev	70	GACGACCGGGTCGAATTT-GCTTTCGAATTGCTATCTATTTTTGAA-GCCTTCAATTTTTCTTTTCTCTATG
gumG_pHExXan_fw	40	GCCTGGCTCTGCTCTGCTCGATGAC-GACGGCTGCGATCAC
pHExXan_BB_fw	24	CAATTCGAAAGCAAATTCGACCCG
pHExXan_BB_rev	20	CGAGCAGAGCAGAGCCAGGC
GumG_F_F60A	41	GTGCCTCTG**GCC**TTCGTTCTTTCCGGCTGGGTCGGTGAACG
GumG_R_F60A	45	CCGGAAAGAAC-GAA**GGC**CAGAGGCACATGGAAGCTG-TAGGCAAAC
GumG_F_F61A	41	GTGCCTCTGTTT-**GC**CGTTCTTTCCGGCTGGGTCGGTGAACG

GumG_R_F61A	45	CCGGAAAGAACG**G-C**AAACAGAGGCACATGGAAGCTG-TAGGCAAAC
GumG_F_V18A	40	CGCCTCAACTG**C**CGCG-GAGCGCGACTGGCAGATCGACGTG
GumG_R_V18A	45	CGCTCCGCG**G**CAGTT-GAGGCGATTGTGTCGACGCGACC
GumG_F_L63A	42	GTTTTTCGTT-**GCC**TCCGGCTGGGTCGGTGAAC-GCTTCGGGCG
GumG_R_L63A	43	GACCCAGCCGGA**GGC**AAC-GAAAAACAGAGGCACATGGAAGCTG
GumG_F_T87A	41	GCTTGCGCGC**GCC**CTGCTGAT-TCCCTACGTCAGCTTTTTTC
GumG_R_T87A	38	GAATCAGCAG**GGC**GCGCGCAA-GCTTTCCCACCGTCTTC
GumG_F_L84A	42	GTGGGAAAG**GCC**GCGCGCAC-GCTGCTGATTCCCTACGTCAGC
GumG_R_L84A	41	CAGCGTGCGCGCAAG**GGC**TCCCAC-CGTCTTCCGGCCAAATG
GumG_F_V67A	38	CTTTCCGGCTGGG**C**CGGTGAAC-GCTTCGGGCGTCGTGC
GumG_R_V67A	45	GAAGCGTTCACCG**G**CCCAGCCGGAAA-GAACGAAAAACAGAGGCAC
GumG_F_S16A	45	CACAATCGCC**GCC**ACTGTCGCG-GAGCGCGACTGGCAGATCGACG
GumG_R_S16A	41	CCGCGACAG-T**GGC**GGCGATTGTGTCGACGCGAC-CGGCAGTG
GumG_F60AF61A_fw	40	CATGTGCCTCTG**GCCGC**CGTTCTTTCC GGCTGGGTCGGTG
GumG_F60AF61A_rev	45	CCAGCCGGAAAGAAC-G**GCGGC**CAGAGGCACATGGAAGCTG-TAGGC
pSRKKm_Seq_KmR_rev	20	GGGAATCTCAAAGCGCGTTG
pSRKKm_Seq_lacl_rev	20	CCTGGTCATCCAGCGGATAG
GumG_F_D26A	38	CTGG-CAGATCG**C**CGTGGCCAAGGCTCTT-GCGATCATTC

GumG_R_D26A	31	GGCCACG**G**CGATCTGCCAG- TCGCGCTCCGCG
GumG_F_R21A	42	CTGTCGC**G**GAGGCGGACTGG- CAGATCGACGTGGCCAAGGCTC
GumG_R_R21A	31	CTGCCAGTC**CGC**CTCCGCGACAGTT- GAGGCGATTGTGTCG
gumprom_fw	21	CGTGTTGTGCCTTGCGATGTG
gumprom_rev	20	CGAGCAGAGCAGAGCCAGGC

2.10 DNA-markers

DNA molecular size ladder (New England BioLabs; Cat. no.: N3200L, Ipswich, MA, USA)
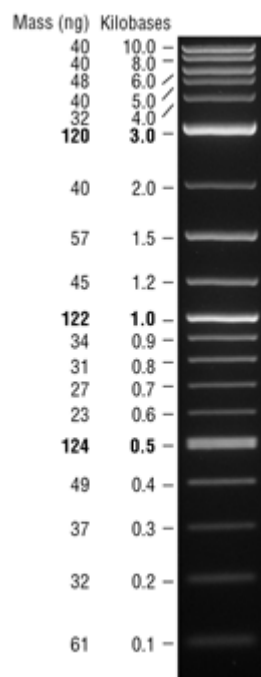

Figure 3. 1 kb Plus DNA Ladder on a 1 % agarose gel.

The shown masses per band (left column) are in respect to a total ladder mass of 5 µg. The right column shows the size of each respective band in kbp.

3 Methods

3.1 Microbiological methods

3.1.1 Sterilization of instrumentation

Instruments and media were autoclaved at 121 °C, 20 min at 2 bar prior to use. Non-heat sterile solutions were filtered through 0.22 µm syringe or disc filter using vacuum. Glassware was sterilized at 200 °C for 3 hours.

3.1.2 Determination of optical density of cell suspensions

For the determination of the optical density (OD_{600}) 1 ml of cell suspensions were measured in a semi-micro cuvette (VWR cuvettes PS semi-micro) at 600 nm (Photometer Ultrospec 10, Amersham Biosciences). Cell suspensions were diluted to be measured within the linear range of the photometer (Absorbance 0.1-0.8).

3.1.3 Cultivation and storage of *E. coli* and *X. campestris* strains

Unless otherwise specified, *E. coli* strains were cultivated at 37 °C at 150 rpm, *X. campestris* were cultivated at 30 °C at 170 rpm. For cultivation media described in 2.6 were used, for strains carrying plasmids, respective antibiotics were added. For double selection media, half the concentration of each antibiotic was used. For plasmid isolation and creation of competent cells, media were inoculated with single colonies from agar-plates. *E. coli* was grown over night at 37 °C, *X. campestris* for 24-48 h at 30 °C. For short time storage strains were kept on 4 °C on agar plates. For long time storage 600 µl of cell suspension was mixed with 600 µl sterile 60 % (w/v) glycerol solution and stored at -80 °C.

3.1.4 Cultivation of *X. campestris* for xanthan production in shaking flasks

For xanthan production in shaking flasks, 50 ml MM1 P100 were inoculated 1:50 from a 10 ml preculture, inoculated with single colonies. Main cultures were incubated in 250 ml aerobic screw-cap baffled shaking flasks (DWK Life Sciences GmbH) at 170 rpm, 30 °C for 72 h. For strains carrying plasmids with inducible promoters, 1 mM IPTG was added after 8 h, when cells reached an OD_{600} of 1. After 72 h cells were centrifuged (Sorvall Lynx 6000, A27-8 x 50 rotor, 87,000 x g, 15 min, 25 °C). The supernatant was used for downstream processing.

3.1.5 Cultivation of *X. campestris* for xanthan production in bioreactors

For the controlled production of xanthan, *X. campestris* strains were cultivated in Sartorius Bplus 2L-Bioreactors and DASGIP parallel bioreactors. All Bioreactors were equipped with probes for the detection of pH, dissolved oxygen, temperature and foam. For aeration a ring-sparger was

used. For stirring two 6-blade Rushton impellers were used. For sampling and inoculation sampling tubes with a sterile sampling valve was used. After sampling, the tubes were flushed with 20 ml air through a sterile 0.22 µm syringe filter.

For the production in 2L bioreactors, a total volume of 1450 ml MM1 P100 medium was inoculated with up to 50 ml preculture to an OD_{600} of 0.1. Production was carried out over 48 h at pH 6.8 (controlled with 7 % H_3PO_4 and 2 M NaOH) and 30 % dissolved oxygen (DO) at 30 °C. DO was regulated by a regulating cascade of increasing stirrer rpm from 300-600 rpm with subsequent increase of air flow from 0.3-1.5 L min^{-1}. Foam formation was regulated using an antifoam probe and a 1% (v/v) antifoam B solution.

For the production in DASGIP Bioreactors, a total volume of 600 ml was inoculated with up to 20 ml preculture to an OD_{600} of 0.1. Production was carried out over 48 h at pH 6.8 (controlled with 7 % H_3PO_4 and 2 M NaOH) and 30% DO at 30 °C. DO was regulated by a regulating cascade of increasing stirrer rpm from 200-600 rpm with subsequent increase of air flow from 6-8 L h^{-1}. Foam formation was regulated using an antifoam probe and a 1% (v/v) antifoam B solution.

3.1.6   Creation of chemically competent *E. coli* cells

For the creation of chemically competent *E. coli* cells, TFB I and TFB II buffers were prepared. TFB I buffer was prepared freshly on the day of preparing competent cells. TFB I buffer (30 mM KOAc, 100 mM RbCl, 10 mM $CaCl_2$·2 H_2O, 50 mM $MnCl_2$·4 H_2O, 15 % (v/v) glycerol) was adjusted to pH 5.8, filtered through a 0.22 µm syringe filter and cooled on ice. TFB II buffer (10 mM MOPS, 75 mM $CaCl_2$·2 H_2O, 10 mM RbCl, 15 % (v/v) glycerol) was adjusted to pH 6.5 with KOH, filtered through a 0.22 µm syringe filter and stored at 4 °C until use.

From a single colony a 5 ml preculture was inoculated in a culture tube and incubated over night at 37 °C and 300 rpm. From the preculture, 100 mL LB containing 20 mM $MgSO_4$ was inoculated 1:100 in a shaking flask and grown to OD_{600} 0.4-0.6 at 37 °C and 150 rpm. The culture was centrifuged (800 x g,10 min, 4 °C) and the pellet was subsequently kept on ice for all further steps. The cells were resuspended in 40 ml freshly prepared, cold TFB I Buffer, incubated on ice for 5 min and subsequently centrifuged (800 x g, 10 min, 4 °C). The supernatant was decanted, the pellet resuspended in 8 mL cold TFB II buffer and incubated on ice for 60 min. 100 µl aliquots were prepared in 1.5 mL reaction tubes in a pre-cooled steel tube rack, stored previously at -20 °C, subsequently frozen in liquid nitrogen and stored at -80 °C.

3.1.7   Transformation of chemically competent *E. coli* cells

For the transformation of chemically competent *E. coli*, up to 20 µl of DNA solution was pipetted to 100 µl competent cells thawed on ice and further incubated for 30 min on ice. The cells were heat shocked at 42 °C for 45 seconds and put back on ice for 5 min. Subsequently 1 mL SOC

medium was added and cells were incubated at 37 °C for 1 h under shaking at 150 rpm. After incubation cells were centrifuged (4,000 x g, 1 min, 25 °C), resuspended in the remaining 100 µl of SOC medium and plated out on selective LB agar using sterile glass beads.

3.1.8 Preparation of electrocompetent *X. campestris* cells

Preparation of electrocompetent cells was adapted from *Wang et al.*(Wang, Zheng, & Liang, 2016). In a 100 mL baffled shaking flask10 mL LB medium were inoculated from a single colony from a MM1 P100 agar plate and incubated 24 h at 30 °C at 170 rpm. In a 250 ml aerobic screwcap baffled shaking flask, 50 mL LB medium were inoculated with the preculture to OD_{600} 0.1 and incubated at 30 °C and 170 rpm. At OD_{600} 0.8-1.0 the culture was centrifuged (8,000 x g, 5 min, 20 °C), resuspended in 25 mL sterile 250 mM sucrose solution and centrifuged (12,000 x g, 2 min). Resuspension and centrifugation were repeated two more times. Cells were finally resuspended in 2 mL 250 mM sucrose solution and 100 µl aliquots were created in 1.5 mL reaction tubes and stored at -80 °C.

3.1.9 Transformation of electrocompetent *X. campestris* cells

To 100 µl suspensions of competent *X. campestris* cells, thawed at room temperature, up to 10 µl salt free DNA solution was added. The solution was transferred to an electroporation cuvette (Gene Pulser/MicroPulser Electroporation Cuvettes, 0.1 cm gap, Bio-Rad Laboratories, Inc.) and electroporated at 18 kV cm^{-1}, with a typical pulse time of 5 milliseconds. 1 mL of SOC was added and carefully mixed with the cell suspension by pipetting. The suspension was transferred into a fresh 1.5 mL reaction tube and incubated at 30 °C, 170 rpm for 1.5-2 h. After incubation the suspension was centrifuged (4,000 x g, 1 min, 20 °C), after decanting the supernatant, the cells were resuspended in the remaining 100 µl and plated out using glass beads.

3.2 Molecular biological methods

3.2.1 Isolation and purification of plasmid DNA from *E. coli*

For the isolation of plasmid DNA from *E. coli*, the *GeneJET™ Plasmid Miniprep Kit (Thermo Fischer Scientific, Fermentas)* was used with 2-4 mL of a 5 mL overnight culture. The isolation was done according to the manufacturers protocol. For elution of DNA 50 µl ultrapure H_2O heated up to 70 °C was used. Purified plasmid DNA was stored at -20 °C.

3.2.2 Isolation and purification of genomic DNA

For the isolation of genomic DNA (gDNA) the *DNeasy® UltraClean Microbial Kit* (Qiagen) was used. All steps were carried out according to the manufacturers protocol. Purified gDNA was stored at -20 °C.

3.2.3 Quantification of purified DNA

Purified DNA was quantified photometrically with a Nanophotometer P-class, using 1-3 µl of purified DNA-solution. DNA was quantified by the absorption maximum at 260 nm, with a calculated concentration of 50 µg mL^{-1} cm^{-1} for double stranded DNA. Purity was calculated by the A_{260}/A_{230}–ratio, with expected values above 2.0 for purified DNA.

3.2.4 Agarose gel electrophoresis

For agarose gel electrophoresis of DNA, 1 % agarose gels containing SYBR Safe DNA Gel Stain (Thermo Fisher Scientific) were used. Electrophoresis was carried out at 130 V for 20 min. 1 kb Plus DNA Ladder (NEB) was used as size standard. For analytical gel electrophoresis, the Gels were documented on a UV table with the Gel iX Imager, for preparative gel electrophoresis, DNA-bands were cut out on a Dark Reader® transillumina blue light table and DNA was subsequently purified from the gel fragments with the NucleoSpin® Gel and PCR Clean-up Kit according to the manufacturers protocol. DNA was eluted in two steps with 15 µl H$_2$O at 70 °C each.

3.2.5 Cloning methods

3.2.5.1 Restriction digest and ligation of DNA fragments

Up to 3 µg of DNA was incubated with 10-20 U of each restriction enzyme in the respective restriction enzyme buffer and incubated at 37 °C for up to 60 min. Digested plasmid DNA was separated with gel electrophoresis and purified from gel fragments. Digested amplified DNA was purified directly from the reaction mixture using the NucleoSpin® Gel and PCR Clean-up Kit. For ligation of DNA fragment, 100 ng of plasmid DNA was mixed with a 3:1 molar excess of insert DNA and incubated with T4 DNA ligase in T4 DNA ligase buffer at room temperature for 10-20 min. Alternatively, ligation was carried out at 4 °C over night. After heat inactivation at 65 °C for 10 min, 10 µl of the reaction mixture was used for transformation of chemically competent *E. coli*.

3.2.5.2 Gibson Assembly

For Gibson Assembly,100 ng of plasmid DNA with a 1:1 to 3:1 excess of insert DNA with 20-40 bp complementary overhangs to the plasmid DNA was mixed with Gibson Assembly Mix in a 1:1 ratio and incubated at 50 °C for 60 min. After cooling on ice, up to 10 µl of the reaction was used for the transformation of chemically competent *E. coli*.

3.2.5.3 Golden Gate cloning

Fragments were amplified using primers for the introduction of TypeIIS restriction enzyme recognition sites for creation of complementary overhangs. Amplified and purified fragments were mixed equimolar (total volume of 6 µl) in a reaction mix containing 0.75 µl TypeIIS restriction enzyme, 0.25 µl T7 ligase,1 µl cutsmart buffer, 1 µl 10 mM ATP, 1 µl 10 mM DTT and incubated in a thermocycler, with a temperature program of 20 cycles of 37 °C for 5 min and 20 °C for 5 min. The reaction was stopped at 80 °C, 20 min, 1.5 µl ATP-dependent exonuclease (Plasmidsafe, Biozym Scientific GmbH), 1.5 µl Plasmidsafe buffer, 1.5 µl 10 mM ATP and 0.5 µl H_2O were added and incubated 37 °C for 30 min. The reaction was stopped at 70 °C, 30 min. After cooling on ice, up to 10 µl of the reaction was used for the transformation of chemically competent *E. coli*.

3.2.6 Polymerase chain reaction (PCR)

3.2.6.1 Colony PCR for *E. coli*

For *E. coli* colony PCR (cPCR), single colonies were picked from solid medium and directly suspended in 10 µl PCR master mix containing *Taq* Polymerase, *Thermopol* buffer, dNTPs, forward and reverse Primers. The suspended cells were incubated at 95 °C for ten minutes in the PCR master mix for cell lysis. The DNA was amplified in 30 cycles, according to the Polymerase suppliers protocol using the respective annealing temperatures for each primer set with an extension time of 60 s per 1 kbp. For gel electrophoresis, 10 µl of PCR reaction mix was mixed with 2 µl of 5x blue loading dye and applied to the gel.

3.2.6.2 Colony PCR for *X. campestris*

For *X. campestris* cPCR, single colonies were picked from solid medium, resuspended in 20 µl ultrapure H_2O and incubated at 98 °C for 10 minutes for cell lysis. The suspension was subsequently centrifuged (2,000 x g, 10 s, MiniStar, VWR). 1 µl of the supernatant was mixed with 9 µl of PCR master mix containing *GoTaq* Polymerase, *GoTaq Green* buffer, dNTPs, forward and reverse primers. The DNA was amplified in 35 cycles, according to the polymerase specific protocol using the respective annealing temperatures for each primer set with an extension time of 60 s

per 1 kbp. As *GoTaq Green* buffer is pre-stained, the PCR reaction mixture was applied directly to the gel for gel electrophoresis.

3.2.6.3 Overlap extension PCR

For overlap extension PCR, two amplified DNA fragments with complementary regions of 20-40 bp were mixed in an equimolar ratio and amplified using a PCR master mix containing *Phusion* polymerase, *Phusion* HF buffer, dNTPs as well as the outer forward primer of fragment one and the outer reverse primer for fragment 2. The fragments were annealed and amplified in 25-30 cycles using the Polymerase specific protocol using the respective annealing temperatures of the outer primers with an extension time of 30 s per 1 kbp.

3.2.7 Sequencing of DNA

DNA sequencing was done via Sanger-sequencing by Eurofins Genomics GmbH. The purified DNA was mixed with the respective primer according to the supplier's specifications. The sequencing results were analyzed by sequence alignment using SnapGene® version 2.3.2.

3.3 Analytical methods

3.3.1 Size exclusion chromatography

For size exclusion chromatography (SEC) exopolysaccharides were dissolved in 0.1 M $LiNO_3$ at 1 g L^{-1}. Solutions were centrifuged (21,000 x g, 1 min, 20 °C) and supernatants were used for analysis. For separation a combination one 100 Å and two 10,000 Å suprema columns were used at 50 °C at a flow rate of 1 ml min^{-1} with 0.1 M $LiNO_3$ as mobile phase. As detectors a 7-angle MALS- and RI detector were used. The molecular weight was determined by relative quantification with pullulan standards ranging from 342-2.35·10^6 Da.

3.3.2 Analysis of acetic acid, crotonic acid and pyruvic acid content

For determination of the degree of acylation, 10 g L^{-1} EPS were hydrolyzed in 250 mM H_2SO_4 at 90 °C for 16 h. After hydrolysis samples were cooled down and centrifuged (21,000 x g, 2 min, 20 °C), supernatant was filtered through a 0.22 µm PVDF syringe filter and used for HPLC analysis. Samples were separated using a Rezex™ ROA-H^+ at 70 °C with a flow rate of 0.5 mL min^{-1} with 2.5 mM H_2SO_4 as mobile phase. 0.44 g L^{-1} pyruvic acid, 1.05 g L^{-1} acetic acid and 0.12 g L^{-1} crotonic acid in 0.25 mM H_2SO_4 were used as standards.

3.3.3   Analysis of intracellular CoA and CoA-esters of *X. campestris*

50 mL *X. campestris* cultures were grown in baffled shaking flasks and 10 mL were centrifuged (4,000 x g, 10 min, 4°C) at mid-exponential phase (OD_{600} 2-4.5). The cell pellet was kept on ice and resuspended in 2 mL of an acetonitrile, methanol and water mixture (40:40:20), cooled to -20 °C for metabolite quenching and extraction. 300 µl aliquots in 1.5 mL reaction tubes and solvent was evaporated in a vacuum concentrator at 65 °C for 1 h. Dried samples were dissolved in 300 µl ultrapure water and filtered through a 0.22 µm polyvinylidene fluoride (PVDF) filter for HPLC-MS/MS analysis. For spiking, 10µl of CoA or CoA-esters, with a final concentration of 1-5 µM were added either before or after evaporation of the acetonitrile-methanol-water-mixture. Samples were kept at 10 °C in the autosampler. HPLC-MS/MS was carried out with a YMC-Triart C18 column at 50 °C and a flow rate of 0.6 mL min^{-1}. Mobile phase A was 26.5 ammonium formate, pH 6.5, adjusted with 3.2 % ammonia. Mobile phase B was Acetonitrile. The gradient was set as follows: 0-2 min 0 % B; 2-7 min 0-50 % B, linear gradient; 7-9 min 50 % B; 9-13 min 0 % B.

3.3.4   Determination of monomer composition

Determination of the monomer composition was performed by the 1-phenyl-3-methyl-5-pyrazo-lone-high throughput method (HT-PMP) (B. Rühmann, Schmid, & Sieber, 2014).For this a 0.1 % xanthan-solution was prepared by dissolving the powder in ultrapure water under stirring (250 rpm, room temperature). Samples were subsequently hydrolyzed by adding 20 µl of 4 M trifluo-racetic acid (TFA) to 20 µl in a 96-well PCR plate, sealing with a rubber lid and sealing the plate in a custom-made metal device. Hydrolysis was carried out at 121 °C over 90 min in a sand bath. After hydrolysis, the samples were neutralized by the addition of 3.2 % NH4OH. The required volume was previously determined using 2 M TFA and phenol red as indicator. Derivatization was done by the addition of 75 µl PMP-master mix to 25 µl of neutralized hydrolysate and incubation at 70 °C for 100 min in a thermal cycler. After derivatization 20 µl of the sample were mixed with 130 µl of 26-fold diluted 0.5 M acetic acid, mixed using the metal device and subsequently filtered through a 0.2 µm Filter plate (1000 g, 5 min, 20 °C). The 96-well microtiter plate was subsequently sealed with a silicone cap mat and placed in the autosampler for HPLC-MS/MS measurements.

3.4 Processing of exopolysaccharides

Fermentation broths were 1:10 diluted and centrifuged (15,000 x g, 20 min, 25 °C) to separate cells. The supernatant was desalted and concentrated using cross flow filtration with a molecular weight cut-off of 100 kDa. The filtered supernatant was precipitated in 2-fold excess of isopropa-nol. Precipitated Exopolysaccharide was dried in a vacuum oven at 40 °C for 24 h and milled in a ball mill for 30 s at 30 Hz. Dried EPS powder was used for further processing.

3.5 Crotonylation of xanthan

1.3 ml (22.3 mmol) trans-crotonic acid anhydride containing 1.4 % (v/v) H_2SO_4 was heated up to 60 °C in a 25 ml round bottom flask. 500 mg (0.61 mmol) acetyl- and pyruvyl free xanthan, produced by *Xcc* Δ*gumFGL*, were added. Xanthan was suspended by stirring with a magnetic stirrer at 250 rpm. The reaction was carried out over 16 h at 60 °C and then cooled to room temperature and washed 5 times with 45 ml of ultrapure water by mixing in a 50 mL tube on a rocking shaker for 60 min and subsequent centrifugation (4,000 x g, 5 min, 20 °C). Water soluble fractions were precipitated from each washing step with 2 volumes of isopropanol, the water insoluble fraction was collected after the final centrifugation step. All samples were dried in a vacuum oven at 40 °C for 24-48 h. All samples were analyzed for their degree of crotonylation according to 3.3.2.

3.6 Rheological methods

3.6.1 Setup and sample preparation

Rheological measurements were carried out with a MCR 300 modular compact rheometer (Anton Paar GmbH, Graz, Austria), equipped with a CP-50-1 cone-and-plate measuring geometry (diameter 50 mm, cone angle 1 °, truncation 50 μm) and a peltier controlled TEK 150-P bottom plate. All measurements were carried out at 20 °C, unless otherwise stated. Samples were dissolved in ultrapure water and stirred at 50 °C for at least 24 h. After dissolving, samples were centrifuged at 1,000 x *g* for 5 min to remove remaining air bubbles. To ensure the resting state of the samples, they were stored at 4 °C for at least 12 h prior to measurements and to ensure temperature uniformity for the measurements and avoid pre-shear induced effects, samples were incubated for 5 min at the measuring temperature after application on the rheometer.

3.6.2 Viscosity curves

The determination of viscosity curves was carried out at a logarithmically increasing shear rate of 10^{-3}–10^{3} s^{-1} by measuring four data points per decade with a decreasing measuring time of 100–5 s per data point.

3.6.3 Amplitude sweeps

Amplitude sweeps were performed at logarithmically increasing shear stress amplitude of 10^{-1}-10^{2} Pa at a frequency of 1 Hz.

3.6.4 Frequency sweeps

Frequency sweeps were carried out in the linear viscoelastic region (LVE) at a logarithmically increasing frequency of 10^{-2}–10^{2} Hz.

3.6.5 Temperature sweeps

Temperature sweeps were preformed within LVE at the frequency of 1 Hz. A discrete temperature ramp from 20 °C to 75 °C with a heating rate of 4 °C min^{-1} was applied. To prevent evaporation, the edge of the sample was covered with a low viscosity paraffin oil.

3.6.6 Thixotropy

The thixotropic behavior of the sample was evaluated by a 3-stage oscillatory shear. During the first stage, the sample was measured within the previously determined LVE region followed by the high oscillatory shear of 10^{2} Pa and 1 Hz. Then, the recovery of the structure was measured over 10 min within the LVE region.

3.6.7 Creep tests

For creep and creep-recovery tests, the shear stress was abruptly increased from 0 Pa to the shear stress value within the LVE region (≤ 1 Pa) and subsequently held at that value for 300 s. Exact shear stress values were 0.5 Pa for welan, diutan and S-88 and 0.8 Pa for gellan. During that time, the strain of the sample was continuously measured. Subsequently, the shear stress abruptly decreased to 0 Pa, and the reversal of the strain was measured until the strain curve reached a plateau value.

4 Results

4.1 Influence of the structural difference of EPS on the rheological properties in EPS-surfactant mixtures

In this study, the rheological properties of four sphingans, diutan, gellan, welan and S-88 in respect to pure solutions as well as in mixtures with four different surfactants were carried out. The study was driven both by the heuristic approach of small structural differences of EPS with a common backbone structure to describe their impact on the rheological behavior as well as their interactions with defined surfactants, as well as the application-based aspect of the general rheological properties of EPS-surfactant mixtures, as EPS might be applied as rheological thickeners in cosmetic and personal care products. As the rheological properties might only have minute differences and the vast amount generated data is often tedious to describe, the essential rheological behavior of the systems has been modeled with mathematical models, like the generalized Maxwell model for frequency sweeps and the Burgers model for creep- and creep recovery, in order reduce data and create a model- and parameter-based comparison. This study revealed the impact of the different side-chain composition of the sphingans on the masking of anionic charges in the main chain and the impact on these effects on their interactions with differently charged surfactants. This work helped understanding the effect on the side-chain composition on the interactions of polysaccharide chains with each other as well as other compounds and gave further insights into findings from previous studies of EPS surfactant systems, like the described paenan-surfactant systems (Rütering et al., 2018).

Moritz Gansbiller was involved with the conceptualization, methodology, validation, formal analysis, investigation, data curation, writing and visualization of the original draft.

Jochen Schmid was involved in the conceptualization, methodology, validation, visualization, reviewing and editing the original draft as well as supervision, resource provision and project administration.

Volker Sieber was involved in conceptualization and supervision, reviewing and editing the original draft as well as resource provision, project administration and funding acquisition.

Rheology of sphingans in EPS–surfactant systems

Moritz Gansbiller[a], Jochen Schmid[a,b], Volker Sieber[a,c,d,e,*]

[a] *Chair of Chemistry of Biogenic Resources, Technical University of Munich, Campus for Biotechnology and Sustainability, Schulgasse 16, 94315, Straubing, Germany*
[b] *Norwegian University of Science and Technology, Department of Biotechnology and Food Science, Sem Sælands vei 6-8, 7491, Trondheim, Norway*
[c] *Fraunhofer IGB, Straubing Branch BioCat, Schulgasse 23, 94315, Straubing, Germany*
[d] *TUM Catalysis Research Center, Ernst-Otto-Fischer-Straße 1, 85748, Garching, Germany*
[e] *The University of Queensland, School of Chemistry and Molecular Biosciences, 68 Copper Road, St. Lucia, 4072, Australia*

ABSTRACT

A model-based rheological characterization of four sphingans in combination with four prominent surfactants of cosmetic formulations of cationic, anionic, zwitterionic and neutral headgroup characteristics was performed. The impact of the surfactants on the rheological properties, based on changes in the mechanical models was evaluated in respect to the closely related structural differences of the polysaccharides, to give an insight on the structure-function relationship of these interactions. The side chains of the sphingans Welan, Diutan and S-88 seem to be involved in the masking of the anionic charge of the polysaccharide backbone, making them highly compatible even with cationic surfactants. The effect of a disaccharide side chain of Diutan also impacts its intermolecular interactions opposed to Welan and S-88, resulting in different surfactant interactions as well as temperature stability. The lack of a side chain in Gellan leads to large incompatibilities with zwitterionic and cationic surfactants due to high polysaccharide-surfactant interactions.

1. Introduction

A diverse group of commercial and not yet commercial microbial exopolysaccharides (EPS) is characterized by unique viscoelastic properties, which create a wide line-up for formulations in the industrial sector for food, cosmetic, and pharmaceutical applications (Bais, Trevisan, Lapasin, Partal, & Gallegos, 2005; Freitas, Alves, & Reis, 2014; Kaur, Bera, Panesar, Kumar, & Kennedy, 2014; Semenzato, Costantini, & Baratto, 2014). Microbial exopolysaccharides as bio-based rheological modifiers offer many advantages (e.g., biodegradability, low energy demand, emission costs, as well as seasonal and regional independency) to replace fossil- or plant-based products, which still dominate this sector, while bio-based alternatives currently account for only up to 13 % of total chemicals produced (in Germany) (Biddy, Scarlata, & Kinchin, 2016; Corolleur, Level, Matt, & Perez, 2020; Ögmundarson, Herrgård, Forster, Hauschild, & Fantke, 2020; Aranoff et al., 2008). However, the high energy cost and emission of fossil-based chemical production in combination with increasing socio-economic demands (e.g., awareness of climate change and sustainability) require ever growing numbers of bio-based alternatives. Regarding EPS as bio-based alternatives, up to now, only a limited number is commercialized to be applied in various industries, especially in the cosmetic sector (de Melo Pereiraa et al., 2019; Fiume et al., 2016; Freitas

et al., 2014). These EPS, which are based on well-established production processes and product titers, dominate the market even if they are not perfectly suited for the targeted application (Moscovici, 2015; Shukla, Mehta, Parmar, Pandya, & Saraf, 2019). Therefore, the discovery and characterization of EPS producing species with superior rheological properties is of highest interest for the development of novel bio-based solutions to extend the existing portfolio (Rühmann, Schmid, & Sieber, 2015; Rütering et al., 2018). In cosmetic formulations, surfactants are core components and require studies on the interaction or incompatibility of EPS–surfactant mixtures as well as on the effect on rheological properties to measure the final product quality and applicability. Several EPS–surfactant mixtures have already been characterized (Bain et al., 2010; Bais et al., 2005; Bonnaud, Weiss, & McClements, 2010; Dickinson, Goller, & Wedlock, 1993; Fijan, Šostar-Turk, & Lapasin, 2007; Goddard, 1994, 2002; Goddard & Hannan, 1976; Hansson & Lindman, 1996; Manca, Lapasin, Partal, & Gallegos, 2001; Piculell, Egermayer, & Sjöström, 2003; Rütering et al., 2018) for individual EPS for specific fields of application. In this study, we compare the poorly characterized sphingan S-88 with three commercial sphingans (i.e., Welan, Diutan, and Gellan). Welan, Diutan, and Gellan have been previously extensively characterized (Kaur et al., 2014; Pollock, 2005; Tako et al., 2016; Xu, Gong, Dong, & Li, 2015); however, there are almost no data on the rheological characterization of S-88.

* Corresponding author at: Chair of Chemistry of Biogenic Resources, Technical University of Munich, Schulgasse 16, 94315, Straubing, Germany.
E-mail addresses: m.gansbiller@tum.de (M. Gansbiller), jochen.schmid@ntnu.no (J. Schmid), sieber@tum.de (V. Sieber).

Fig. 1. Chemical structures of the four different sphingans analyzed in this study. The constituents include glucopyranose (*Glcp*), glucuronic acid (*GlcA*), manno-pyranose (*Manp*), and rhamnopyranose (*Rhap*). Possible acetyl (*O-Ac*) and/or glyceryl (*O-Gl*) groups are shown at position 2 and/or 6 of the second glucose in the repeating unit of Gellan, Welan, and Diutan. The putative acetylation of S-88 at the second glucose at an unknown position is indicated by the? symbol.

The sphingan family is a closely related group of EPS in terms of their chemical structures, which only differ in side chain, backbone monosaccharides, and decorations. Interestingly, these slight differences result in distinct rheological properties and, thus, can serve as a perfect starting point for the in-depth structure–function analysis. Fig. 1 shows the detailed structures of Gellan, Welan, Diutan, and sphingan S-88, based on their main components glucopyranose (Glcp), mannopyranose (Manp), rhamnopyranose (Rhap), and glucuronic acid (GlcA) and have almost the same backbone structure, consisting of a →4)α-L-Rhap-(1→3)ß-D-Glcp-(1→4)ß-D-GlcA-(1→4)-ß-D-Glcp(1→ backbone, while S-88 slightly differs and has L-Rhap or L-Manp at the end of the repeating unit. Gellan is a linear polymer without branching sugar units; Welan has either L-Rhap or L-Manp α-(1→3) linked to the first glucose of the backbone; Diutan has a L-Rhap(1→4)-α-Rhap-dimer α-(1→3) attached to the first glucose monomer of the repeating unit, and S-88 has L-Rhap α-(1→3) linked to the first glucose of the backbone (Pollock, 2005; Schmid, Sperl, & Sieber, 2014).

While native Gellan has O-acetyl and O-glyceryl groups attached at C2 and C6 of the second glucose in the backbone, two commercial Gellan variants exist [i.e., high acyl Gellan (Gellan HA) and low acyl Gellan (Gellan LA)] with the latter showing a high degree of deacetylation, which is caused by alkaline treatment after microbial production. The degree of acetylation considerably affects the gel strength; low acyl Gellan forms the strongest and most brittle gels upon the addition of cations (Bajaj, Survase, Saudagar, & Singhal, 2007). Both Diutan and

Welan are acetylated at the C2 position of the second glucose in the backbone, while Diutan is also acetylated at the C6 position. Thus far, it has not been completely clarified yet whether S-88 is acetylated (Schmid et al., 2014; Tako & Tamaki, 2005). The decoration of microbial EPS with acetyl or pyruvyl groups considerably affects the rheological properties, as has been recently reported by a multitude of studies for Xanthan (Callet, Milas, & Rinaudo, 1987; Gansbiller, Schmid, & Sieber, 2019; Hassler & Doherty, 1990; Tako & Nakamura, 1984; Wu et al., 2019). Owing to similar chemical structures, with only minor and highly specific differences, the sphingan family provides a unique possibility to link rheological properties with structural information. Thus, more insights into the structure–function relationship of microbial EPS and surfactant systems can be obtained, and mathematic models for the prediction of these relationships can be applied. Therefore, the rheological characterization of EPS–surfactant mixtures of selected sphingans with four surfactants [i.e., cocamidopropyl betaine (CAPB), sodium laureth sulfate (SLES), cetyltrimethylammonium chloride (CTAC), and lauryl glucoside Plantacare (PC), representing cationic, anionic, zwitterionic, and uncharged surfactant headgroups, respectively] were chosen for this study, as they are often used in cosmetic products (Pedro & Walters, 2019). Plantacare has the unique position, that it is not only produced from 100 % renewable resources, but its aqueous solutions also exhibits Newtonian flow behavior with considerably high viscosity (Rütering et al., 2018). A comparison of the models or model parameters of the systems is used to quickly identify

2

changes in the rheological properties and to allow a faster comparison between the systems to establish a detailed structure–function relationship of sphingans and their impact on the interaction with surfactants.

2. Materials and methods

2.1. EPS and EPS–surfactant sample preparation

Diutan (KELCO-CRETE® DG Line), low acyl Gellan (KELCOGEL® F), and Xanthan (KELTROL® CG-SFT) were provided by CP Kelco (Atlanta, GA, USA). Welan (COLLSTAB W-100) was provided by COLLTEC GmbH (Bielefeld, Germany).

SLES, Texapon NSO) and lauryl glucoside (PC, Plantacare 1200 UP) were purchased from BASF (Ludwigshafen). Cocamidopropyl betaine (CAPB, TEGO Betaine F 50) and cetrimonium chloride (CTAC, VARIS-OFT 300;) were provided by Evonik Industries (Essen). Sphingan S-88 was produced by fermentation in a 2-L Biostat® Bplus fermenter (Sartorius AG, Göttingen, Germany) equipped with a 6-blade stirrer and the total volume of 1.2 L. The fermentation was carried out for 48 h with a controlled pH of 6.8 and pO_2 with 30 % saturation. The medium used was MM1 P100, as described by Rütering et al., which contained 30 g L^{-1} glucose (Rütering, Schmid, Rühmann, Schilling, & Sieber, 2016). The highly viscous fermentation broth was adequately diluted (1:4) with ultrapure water and centrifuged for 20 min at 17,700×g at 20 °C to remove the biomass. EPS was precipitated by slowly pouring the supernatant into two volumes of 2-propanol while stirring at 170 rpm with an overhead stirrer (Heidolph Instruments GmbH & Co. KG, Schwabach, Germany). Then, harvested EPS was dried at 45 °C overnight in a VDL 53 vacuum drying oven (Binder, Tuttlingen, Germany) and milled for 20 s at 30 Hz in a ball mill MM400 (Retsch, Haan, Germany). For the concentration series of various EPS (0.1–1.0 g L^{-1} in 0.1 g L^{-1} increments), different amounts of EPS powder were dissolved in 50 mL of ultrapure water at 50 °C for 12 h using a magnetic stirrer at 250 rpm in 250-mL Erlenmeyer flasks. Subsequently, 1 mL of a 25 % (w/w) NaCl solution was added to produce the final NaCl concentration of 0.5 % or 85 mM. The pH was adjusted to 5.5 ± 0.1 with NaOH or HCl. The adjustment of NaCl was done due to the concentration of salts caused by the addition of the individual surfactants, making the systems more comparable. The adjustment of pH was done to further enhance comparability and the pH of 5.5 was chosen as it is often set in cosmetic and personal care products. Then, air bubbles were removed by centrifugation (1,000×g, 5 min at room temperature). All EPS-samples were stored at 4 °C overnight before the measurements. EPS–surfactant mixtures were prepared by mixing EPS and surfactant solutions with double the final concentration in a 1:1 ratio with subsequent stirring at 250 rpm at 50 °C for 12 h. The pH was adjusted to 5.5 with NaOH or HCl and air bubbles were removed by centrifugation (1,000×g, 5 min at room temperature), and the samples were stored at 4 °C for 12 h before the measurements.

2.2. Molecular weight determination

A total of 0.1 % (w/v) of untreated EPS-powder was dissolved in 0.1 M $LiNO_3$ at 50 °C for 12 h under stirring (250 rpm). Treated samples [0.5 % (w/v), 85 mM NaCl, pH 5.5] were diluted to the concentration of 0.1 % (w/v), and no further treatment was applied prior to the measurements. The determination of molecular weight was carried out via size-exclusion chromatography (SECcurity GPC System, PSS Polymer Standards Service GmbH, Germany) with a SECcurity GPC1260 RI-detector and a SECcurity SLD7000 7-angle light-scattering detector. Separation was achieved with a Suprema 100-Å column, coupled with two Suprema 10,000-Å columns, and a Suprema pre-column at 50 °C using 0.1 M $LiNO_3$ as eluent at the flow rate of 1 mL/min. A total of 100 μL of sample was injected for analysis.

2.3. Monomer composition

The determination of the monomer composition was achieved by the modified 1-phenyl-3-methyl-5-pyrazolone (PMP) method at high-throughput (HT-PMP), as described by Rühmann et al. (Rühmann, Schmid, & Sieber, 2014). Specifically, a 0.1 % solution was prepared by dissolving the powder in ultrapure water under stirring with a magnetic stirrer (250 rpm) at room temperature. By adding up the recoveries of monomers, the total recovery can be calculated to give an estimate of the EPS purity.

2.4. Fourier-Transformation Infrared (FTIR) spectroscopy

FTIR spectroscopy was carried out on a Nicolet™ 380 (*Thermo Fisher Scientific Inc.*). 10 mg of EPS powder were mixed with 400 mg KBr and pressed to a pellet using an *Atlas™ Manual Hydraulic press* (*Specac Inc*) and *Atlas Evacuable Pellet Dies*, 13 mm diameter. Pellets were pressed under a weight of 7 t for 2 min. IR spectra were measured at wavenumbers 4,000-400 cm^{-1} against a blank pellet of pure KBr.

2.5. Rheological measurements

Rheological measurements were carried out with a stress-controlled MCR300 rotational rheometer (Anton Paar GmbH, Austria) equipped with a CP 50-1 cone-and-plate measuring system, 50 mm diameter, 1° cone angle, 50 μm cone truncation (Anton Paar GmbH, Austria), and a Peltier controlled TEK 150 P temperature unit (Anton Paar GmbH, Austria). Standard measurements were carried out at 20 °C, and all samples were incubated in the measuring system at 20 °C for 5 min prior to the measurement. All measurements were carried out in triplicates.

2.5.1. Viscosity curves

The determination of viscosity curves was carried out at a logarithmically increasing shear rate of 10^{-3}–10^3 s^{-1} by measuring four data points per decade with a decreasing measuring time of 100–5 s per data point.

2.5.2. Amplitude sweeps

Amplitude sweeps were performed at logarithmically increasing shear stress amplitude of 10^{-1}–10^2 Pa with a frequency of 1 Hz.

2.5.3. Frequency sweeps

Frequency sweeps were carried out in the linear viscoelastic region (LVE) at a logarithmically increasing frequency of 10^{-2}–10^2 Hz.

2.5.4. Temperature sweeps

Temperature sweeps were preformed within LVE at the frequency of 1 Hz. A discrete temperature ramp from 20 °C to 75 °C with a heating rate of 4 °C min^{-1} was applied. To prevent evaporation, the edge of the sample was covered with a low viscosity paraffin oil.

2.5.5. Thixotropy

The thixotropic behavior of the sample was evaluated by a 3-stage oscillatory shear. During the first stage, the sample was measured within the previously determined LVE region followed by the high oscillatory shear of 10^2 Pa and 1 Hz. Then, the recovery of the structure was measured over 10 min within the LVE region.

2.5.6. Creep tests

For creep and creep-recovery tests, the shear stress was abruptly increased from 0 Pa to the shear stress value within the LVE region (≤ 1 Pa) and subsequently held at that value for 300 s. Exact shear stress values were 0.5 Pa for Welan, Diutan and S-88 and 0.8 Pa for Gellan. During that time, the strain of the sample was continuously measured. Subsequently, the shear stress abruptly decreased to 0 Pa, and the

reversal of the strain was measured until the strain curve reached a plateau value.

2.6. Modeling of rheological data

The modeling of rheological data was carried out using MATLAB. The models were applied by implementing the respective model equations and subsequently fitted to the experimental data using the least squares method. The best fit was determined based on the most reliable R^2-value.

2.6.1. Model and model equations for frequency sweeps

To model a frequency test, a generalized Maxwell model was applied. The number of individual Maxwell elements was typically in the range of 3–4 elements. Within the model, storage modulus G', loss modulus G'', and the absolute value of the complex viscosity was fitted using Eqs. (1)–(3), respectively.

$$G'(\omega) = \sum_{l=1}^{n} \frac{G_l \omega^2 \lambda_l^2}{1 + \omega^2 \lambda_l^2} \qquad (1)$$

$$G''(\omega) = \sum_{l=1}^{n} \frac{G_l \omega \lambda_l}{1 + \omega^2 \lambda_l} \qquad (2)$$

$$|\eta^*| = \frac{\sqrt{G'(\omega)^2 + G''(\omega)^2}}{\omega} \qquad (3)$$

G'(ω) [Pa]: storage modulus
G''(ω) [Pa]: loss modulus
G_l [Pa]: modulus of resilience of the ith Maxwell element
λ_l [s]: relaxation time of the ith Maxwell element
ω [rad s^{-1}]: angular frequency
|η*| [Pa·s]: absolute value of the complex viscosity

2.6.2. Model and model equations for creep tests

To model the creep test, a six-parameter Burgers model was applied. In this model, the same parameters are chosen for both creep and creep-recovery phases using Eq. (4) for the creep phase and Eq. (5) for the creep-recovery phase

$$\gamma(t) = \frac{\tau_0}{G_0} + \left(\frac{\tau_0}{G_0}\right)^{-\frac{G_1}{\eta_1}t} + \left(\frac{\tau_0}{G_2}\right)^{-\frac{G_2}{\eta_2}t} + \frac{\tau_0}{\eta_0}t \qquad (4)$$

$$\gamma(t) = \gamma_{max} - \left(\frac{\tau_0}{G_0} + \left(\frac{\tau_0}{G_0}\right)^{-\frac{G_1}{\eta_1}t} + \left(\frac{\tau_0}{G_2}\right)^{-\frac{G_2}{\eta_2}t}\right) \qquad (5)$$

τ_0 [Pa]: applied shear stress
γ []: strain
γ_{max} []: maximum strain during the creep phase
G_0 [Pa]: modulus of the ith spring element
η_{0i} [Pa·s]: modulus of the ith damper element
t [s]: time

3. Results and discussion

3.1. Characterization of sphingans

Commercial low acyl Gellan, Welan, Diutan, sphingan S-88 produced for this work were evaluated in terms of their monomer composition and molecular weight distribution. In addition, the absence or presence of acetate on the polymers was estimated by FTIR spectroscopy. The theoretical distribution and the monomer distribution from the monomer analysis as well as the presence of acetate indicated by FTIR spectra are shown in Table S1. Rha was chosen as a highly stable reference for calculating the ratio, because the remaining Glc–GlcA dimers (which could not be quantified) and the degradation of GlcA during hydrolysis led to lower recoveries of these monomers. The IR

spectra (Fig. S3) of Diutan (a), Welan (b), and S-88 (c) showed clear peaks at 1725–1737 cm^{-1}; this is a typical region for the C—O stretching vibration of carbonyl esters, which indicated the acetylation of polysaccharides. While the peak was most prominent in Welan (Fig. S3 b), it was also clearly observed in S-88 (Fig. S3 d). However, Gellan (Fig. S3 c) did not show a distinct peak in this area, which indicated that polysaccharide was completely deacetylated. The quantification of monomer composition is shown in Fig. S4, detailed elution diagrams of the individual monomer derivates is shown in Figs. S5–S8. The determined monomer distribution for Gellan correlated well with the theoretical values. The lower recovery of GlcA can be attributed to the general degradation of uronic acids during hydrolysis (Rühmann et al., 2015). The determined values for Welan also confirmed the theoretical values, which indicated an equal distribution of L-Rha and L-Man in the sidechain. The lower ratios of Glc and GlcA were attributed to the remaining Glc–GlcA dimers (owing to their stability) and to the degradation of GlcA to the higher amount of Rha in polysaccharide because the Rha:Man ratio perfectly fits the theoretical values. However, Diutan and S-88 showed considerably higher values of Glc compared to theoretical values, which indicated the presence of lower amounts of rhamnose in polysaccharide. For S-88, the ratio of rhamnose to mannose matched exactly the theoretical value, which indicated a 50:50 distribution of rhamnose and mannose in the backbone and rhamnose as sidechain of every repeating unit in S-88. Because this polysaccharide was produced by fermentation and a crude downstream processing, residual glucose in the media was responsible for the higher values. Because concentrations were set on a viscosity basis compared to 0.7 % Xanthan, a lower EPS purity would not affect the results. Molecular weight distributions showed M_w of 7.35×10^5 Da for Gellan and 3.46×10^7 Da, 2.67×10^7 Da, and 4.28×10^7 Da for Diutan, Welan, and S-88, respectively. There are two possible reasons for the lower molecular weight of Gellan. The first reason is that chemical treatment leads to partial degradation owing to its chemical deacetylation. The other reason could be due to the decreased viscosity of the 0.1 % Gellan solution compared to those of other sphingans, which leads to an elution shift during SEC, because the applied method was relatively comparable to Pullulan–Standards. Absolute quantification can clarify this question; however, absolute quantification could not be achieved with the setup used in this study.

3.2. Rheological properties and modeling of sphingans

Rotational shear behavior and reference concentrations
To better compare sphingans between each other and with their respective surfactant systems, they were compared to a 0.7 % (w/w) Xanthan solution with an NaCl concentration of 0.5 % at pH 5.5, which represents the salt content and pH-value caused by mixing with the surfactant solutions. The concentration of sphingans to fit the viscosity curve of 0.7 % Xanthan was 0.6 % for Gellan, 0.5 % for Welan and Diutan, and 1.1 % for S-88 (Fig. 2). All sphingans at the respective concentration showed a shear thinning behavior that is comparable to that of Xanthan at 0.7 %, while the behavior of Welan and Diutan was very similar and fit the behavior of Xanthan in the entire range. The flow behavior of S-88 indicated a very weak zero-viscosity plateau, and Gellan appeared to have a transitional region from an emerging viscosity plateau to another shear thinning region between 1 s^{-1} and 100 s^{-1}. The rotational shear behavior of the sphingans generally conformed with the previous reported values. Previously reported viscosities are 0.6 Pas for S-88 at 20 °C at a concentration of 0.8 % and a shear rate of 9.5 s^{-1} (Tako & Tamaki, 2005), our results showed a viscosity of 0.57 Pas at a shear rate of 13.3 s^{-1} and 0.85 Pas at 8.25 s^{-1}. Reported values for Welan range from viscosities of 1.77 – 8.51 Pas at concentrations from 0.1 to 0.175 % solutions at a shear rate of 0.2 s^{-1} (Xu, Xu, Liu, Chen, & Gong, 2013) and 1.1 Pas at 10 Pas for 0.1 % and 0.175 % concentrations at 0.01 s^{-1} (Xu, Dong, Gong, Sun, & Li, 2015). These values are higher than the results obtained in this study, showing
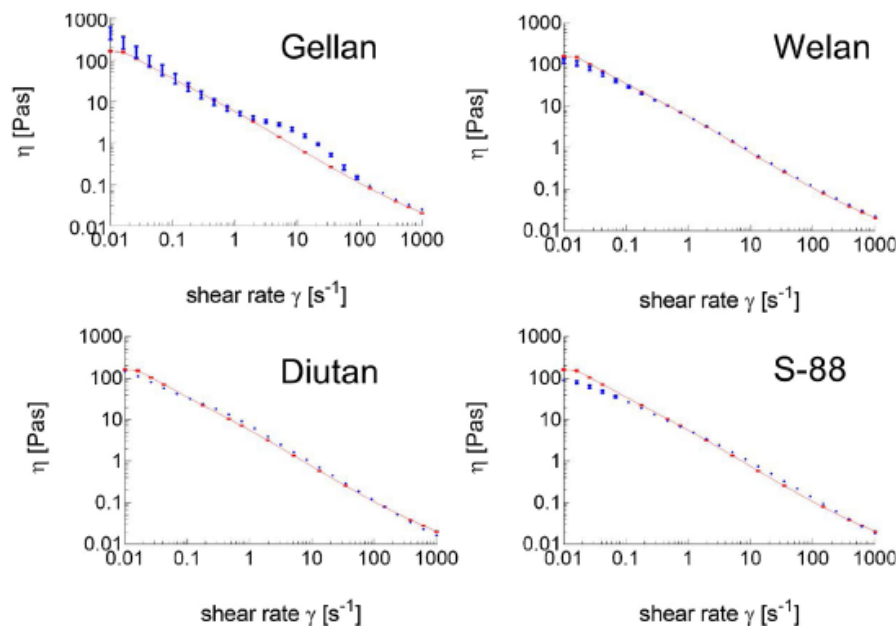
4

Fig. 2. Viscosity curves of (a) Gellan 0.6 %, (b) Welan 0.5 %, (c) Diutan 0.5 %, and (d) S-88 1.1 %, compared to that of a 0.7 % Xanthan solution (red line). All samples were set to a NaCl concentration of 0.5 % and pH 5.5 to allow better comparability to the surfactant mixtures. The small red and blue lines indicate the standard deviation of triplicates. (For interpretation of the references to colour in this figure legend, the reader is referred to the web version of this article).

viscosities of 0.32 Pas for the 0.1 % solution and 2.26 Pas for the 0.2 % solution at 0.2 s^{-1}. At lower shear rate of 0.01 s^{-1} viscosities were also lower with 0.5 Pas and 7.7 Pas for the respective Welan solutions. The same phenomenon was seen for Diutan gum with a viscosity of 3.2 Pas and 16.5 Pas at a shear rate of 0.02 s^{-1} for concentrations of 0.1 % and 0.2 % opposed to reported values of 5 Pas and 11.5 Pas for 0.1 % and 0.175 % Diutan solutions (Xu, Gong et al., 2015). As the rheological behavior of sphingans is rather independent from the pH (Tako & Kiriaki, 1990), these minor discrepancies might be explained by lack of cations in the solutions from the reported works in contrast to the relative high cation concentrations used in this work, which have a decreasing effect on viscosities for the non-gelling sphingans Welan, Diutan and S-88 (Xu, Dong et al., 2015; Xu, Gong et al., 2015). The viscosity of Gellan on the other hand with a viscosity of 3 Pas at a shear rate of 0.01 s^{-1} and 0.1 % concentration was much higher than other reported values of 0.012 Pas at the same shear rate and concentrations. Here the addition of cations has an increasing effect on the viscosity due to the cation mediated gel formation (Sharma & Bhattacharya, 2015; Tako et al., 2016; Xu, Dong et al., 2015). The emergent plateau observed for Gellan was also observed in previous works (Rütering et al., 2018; Xu, Dong et al., 2015) in the same shear rate region, even at very low concentrations of 0.1 % and below. The flow curves (shear stress plotted against shear rate) show a distinct profile of shear banding phenomenon, however as this effect also occurs at very low concentrations and in the absence of cations, which prevents gelling, the cause of this effect cannot be caused by the flow behavior of a broken gel structure resulting in these shear bands. Clarifying this effect is of great interest for future studies, as this is often observed but no explanation has been stated yet.

3.2.1. Oscillatory shear behavior and modeling

For the determination of the linear viscoelastic region of sphingans, an amplitude sweep was performed. An aberration of storage modulus

(G') or loss modulus (G'') greater than 5% from the plateau value was defined as the yield stress, this value also defines the end of the linear viscoelastic region. The pour point is defined at the intersection of G' and G'', when the sample loses its gel-like character and begins to show a fluid-like behavior. The gel strength was defined as the plateau value of G', while a low damping factor represents a stronger gel character and vice versa. Gel strength and damping factor as well as yield stress and pour point are summarized in Table 1.

A direct comparison of the data with literature values is difficult as they are highly dependent on polymer and salt concentrations. However the general viscoelastic properties were comparable with reported values and the temperature dependency of their viscoelastic properties confirm previous results (Tako & Kiriaki, 1990; Tako, Sakae, & Nakamura, 1989; Xu, Gong et al., 2015). The recovery from mechanically (thixotropy tests, Fig. 3) and thermally (temperature sweeps, Fig. 6) induced changes of the viscoelastic properties was tested; and except for Gellan, all samples showed the complete reversibility of mechanical and temperature-induced changes. Furthermore, the viscoelastic structures of Welan (Fig. 6a), S-88 (Fig. 6b), and Diutan (Fig. 6c), were stable across the investigated temperature range from 20 °C to 75 °C. The irreversible destruction of the gel structure of Gellan is attributed to its brittle gel structure (Rütering et al., 2018). This result is caused by cation-mediated interactions of the molecules (Morris, Gothard, Hember, Manning, & Robinson, 1996; Tako et al., 2016),

Table 1
Summary of the general viscoelastic properties of sphingans.

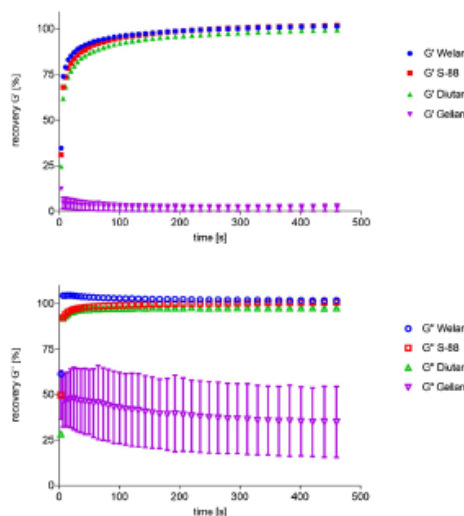| EPS	Gellan	Welan	Diutan	S-88
Storage modulus (G') [Pa]	368.30	11.00	20.60	12.50
Damping factor (tan δ)	0.11	0.36	0.23	0.40
Yield point [Pa]	1.13	2.88	1.13	2.56
Flow point [Pa]	4.50	9.10	11.25	11.50

59

Fig. 3. Recovery of storage modulus G' (filled symbols) and loss modulus G' (empty symbols) over time after high strain.

while the sidechains and acetylation of Welan, Diutan, and S-88 hinder these strong cation-mediated interactions (Tako et al., 2016). The weak, yet highly reversible, viscoelastic structure of these sphingans can be attributed to weaker molecular interactions, as entanglements of un-ordered molecule structures.

Frequency sweeps, which were carried out between 10^{-2} Hz and 10^2 Hz, were modeled with different empirical or mechanical models. For Gellan, the power law was used to describe the parallel trend of G' and G" across the investigated frequency range that was typical for a strong gel structure. The mechanical-based general Maxwell model with three Maxwell elements was applied for Welan and S-88 (Fig. S10 b & d), while Diutan could be best described by a Maxwell model consisting of four Maxwell elements (Fig. S10 c) (Table 2). The description by a 3-elements Maxwell model resulted in a poor fit for Diutan. These models represent an entangled polymer structure in these solutions. The power

law model for Gellan results in a very good fit ($R^2 = 0.9995$) (Fig. S10 a), due to the true gel structure of Gellan, and the parameters can predict the long and short-term behavior of the gel; but, this model does not yield a mechanical interpretation of the system. However, the mechanical models of Welan, S-88, and Diutan yield the parameters of spring (G_i) and dashpot elements ($\eta_{0,i}$), which differ by approximately an order of magnitude within the model and result in a typical loga-rithmic relaxation time (λ_i) spectrum (Fig. S11). Welan, Diutan, and S-88 showed relaxation times of different Maxwell elements between 10^{-2} s and 10^2 s. Given the fast recovery of the structure after high mechanical strain, the first two short relaxation times represent the polymer structure recovery up to 80 % of the initial value within sec-onds, while the longer relaxation times represent the slow recovery from 80 % to 100 %, which requires several minutes.

To further investigate the relaxation time spectra of Welan, Diutan, and S-88, a creep test and modeling with the six-parameter Burgers model was performed. Experimental and model data are given in Fig. S12.

The modeling of creep tests with the six-parameters Burgers model resulted in good fits ($R^2 = 0.972$–0.985). The parameters from the fit are shown in Table 3. Compared to the Maxwell model, where the system is represented by parallel Maxwell elements, the Burgers model represents a sequential dashpot (η_0) and a spring (G_0) combined with two Maxwell elements consisting of a parallel arrangement of springs (G_1, G_2) and dashpots (η_1, η_2); therefore, the mechanical representation is slightly different.

However, the combination of the parameters also leads to the re-laxation time spectrum (λ_{1-3}, Fig. S13), which also separates each ele-ment by approximately an order of magnitude, and the relaxation times were comparable to those from the Maxwell model of the frequency-dependent behavior. By correlating data from structural recovery after mechanical strain (Fig. 3) with the parameters from the Burgers model, it is also evident that very short relaxation times govern the structural relaxation or recovery of up to 80 % within seconds, while longer re-laxation times govern residual relaxation processes within minutes. However, these events only make up approximately 20 % of the total structural recovery. In addition, creep-recovery tests showed that elastic re-deformation of the samples accounted for only approximately 50 %, depending on the polymer, over the investigated timespan; this observation indicated the occurrence of even slower processes with much higher relaxation times. Therefore, the modeling of this behavior with more elements, would result in an extended relaxation time spectrum; however, the proportional contribution of additional re-laxation times to the overall relaxation process will be negligible. However, the addition of another parameter to the model would allow to determine whether this plateau is reached within minutes, hours, or even days and, therefore, would allow to predict the long-term behavior of the sample.

3.3. Sphingan–surfactant systems

Compatible sphingan–surfactant systems consisting of one of the

Table 2
Model and model parameters describing frequency sweeps of sphingans.

EPS	Model/parameter						R^2
	Power law						
	k [Pa^n]			n []			
Gellan	61.195			0.061			0.9995
	General Maxwell model (3 elements)						
	G_i [Pa]			η_{0i} [Pas]			
	1	2	3	1	2	3	
Welan	2.63	5.35	10.42	321.18	19.56	1.02	0.9903
S-88	2.92	8.04	15.61	210.27	20.59	1.05	0.9901
	General Maxwell model (4 elements)						R^2
	G_i [Pa]				η_{0i} [Pas]		
	1	2	3	4	1	2	3	4	
Diutan	7.54	3.74	9.41	8.75	722.19	108.60	1.05	0.59	0.9984

Table 3
Model parameters for the six-parameter Burgers model for the creep- and creep-recovery tests of Welan, S-88, and Diutan.

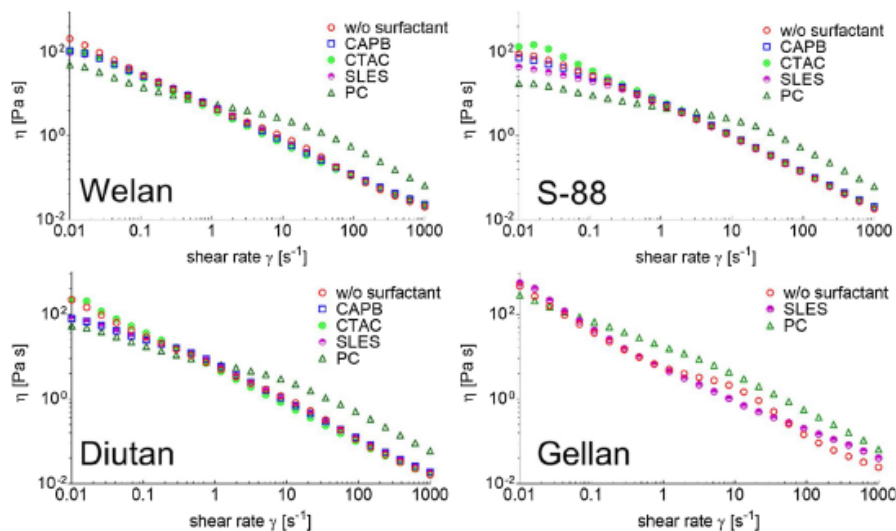| EPS	Model/parameter						R^2
	Burgers model (six parameter)						
	G_0 [Pa]	G_1 [Pa]	G_2 [Pa]	η_0 [Pas]	η_1 [Pas]	η_2 [Pas]	
Welan	16.44	4.26	5.30	620.56	36.23	640.48	0.9816
S-88	9.60	5.08	3.08	208.05	33.34	199.81	0.9724
Diutan	9.09	5.49	2.40	375.10	28.01	200.52	0.9848

6

Fig. 4. Viscosity curves of EPS surfactant mixtures.
Welan 0.5 % (w/w), S-88 1.1 % (w/w), Diutan 0.5 % (w/w), and Gellan 0.6 % (w/w) without a surfactant and in 5% (active matter) CAPB, PC, SLES, and CTAC respectively at pH 5.5 and 20 °C.

four sphingans Welan, Diutan, S-88, and Gellan and one of the four model surfactants SLES, CTAC, CAPB, and PC were characterized with the same rheological methods and modeling as pure sphingans. The mixing of Gellan with CTAC or CAPB led to immiscible precipitation most likely owing to the incompatibility of anionic groups of the surfactants and the exposed $-COO^-$ group of the glucuronic acid of Gellan. Even when masking the charge of these groups by the addition of counterions in the form of NaCl or $CaCl_2$ before mixing, the respective surfactants did not resolve this issue. Hence, these two EPS–surfactant systems were not characterized.

The flow curves (Fig. 4) of the respective EPS–surfactant mixtures were similar to those of EPS without a surfactant, which indicated that EPS had a predominant role in the viscosity and shear thinning behavior of the mixture. All EPS except for Gellan in combination with PC showed the onset of a viscosity plateau between $0.1\ s^{-1}$ and $10\ s^{-1}$ followed by an overall increased viscosity compared to that of pure Gellan. This can be explained by the Newtonian high viscosity flow behavior of PC. Within the intermediate shear rates, the Newtonian flow properties of PC become more evident when the total viscosity of the system approaches the shear rate-independent viscosity of the 5% solution of PC. At higher shear rates, the viscosity of PC adds to the shear thinning of EPS, which results in an overall higher viscosity. The lower viscosity of EPS–PC mixtures can be explained by the formation of surfactant superstructures, which hinder the intermolecular interactions of EPS strands or by the formation of EPS–surfactant structures. Both theories will be discussed later in detail. The behavior of Gellan–surfactant systems was slightly different because EPS alone showed an onset of a Newtonian plateau at moderate shear rates ($1-10\ s^{-1}$), which disappeared upon the addition of SLES; the addition of PC led to an overall increased viscosity, except for very low shear rates, which is comparable to the phenomena observed for other sphingans at high shear rates.

The modeling of frequency sweeps (Fig. S14) of different systems showed considerable changes in the models used to describe the rheological behavior. The formulation of Gellan with SLES and PC can be best described using the Maxwell model, which consists of three elements rather than the power law used to describe pure Gellan, which

could not be modeled appropriately with the Maxwell model (Fig. S10 a). This change of the model shows the loss of a true gel structure seen in Gellan alone and a structure that is more comparable to the entangled polymer network, as seen in the pure solutions of Welan, Diutan and S-88. While some EPS–surfactant mixtures can still be sufficiently described with the 3-element Maxwell model, the addition of a fourth element leads to better fit in most cases. The parameters of the fits are shown in Table S2; the calculated relaxation time spectra are shown in Fig. 5). The introduction of a fourth Maxwell element results in the introduction of a fourth relaxation time, which was approximately an order of magnitude smaller than the lowest relaxation time of pure EPS. This represents a faster initial relaxation when EPS is mixed with surfactants, which may be attributed to the Newtonian properties of the surfactants. However, S-88 in the mixture with surfactants, except for CAPB, could still be described with a three element Maxwell model; however, the overall relaxation times of individual elements typically decreased compared to those of EPS without surfactants.

Creep- and creep-recovery tests of EPS–surfactant mixtures showed a higher initial strain at the same shear stress applied to pure EPS solutions, which exhibited a softer, less elastic gel character. While the incompatibility of Gellan and CTAC or CAPB did not allow the characterization, the mixtures of Gellan with anionic SLES or uncharged PC allowed to measure creep- and creep-recovery. However, it was not possible to describe it with the 6-parameter Burgers model. A possible explanation is the still dominant elastic behavior of the mixture caused by the gel structure of Gellan. The modeling of creep- and creep-recovery tests of the sphingan–surfactant systems with Diutan, Welan, and S-88 did not lead to the introduction of new parameters owing to the fixed mechanical layout of the model. However, changes in the model parameter (relaxation time) of each element were evident between pure EPS and the EPS–surfactant mixtures. For both S-88 and Diutan, an increase in the second relaxation time (λ_1) was evident; however, for Welan, the changes were especially evident in the first relaxation time (λ_0). The different relaxation times calculated from the model parameters (Table S3) are given in Table 4.

The relatively small changes in the mechanical modelling of the rheological data of the sphingans Welan, Diutan and S-88 in
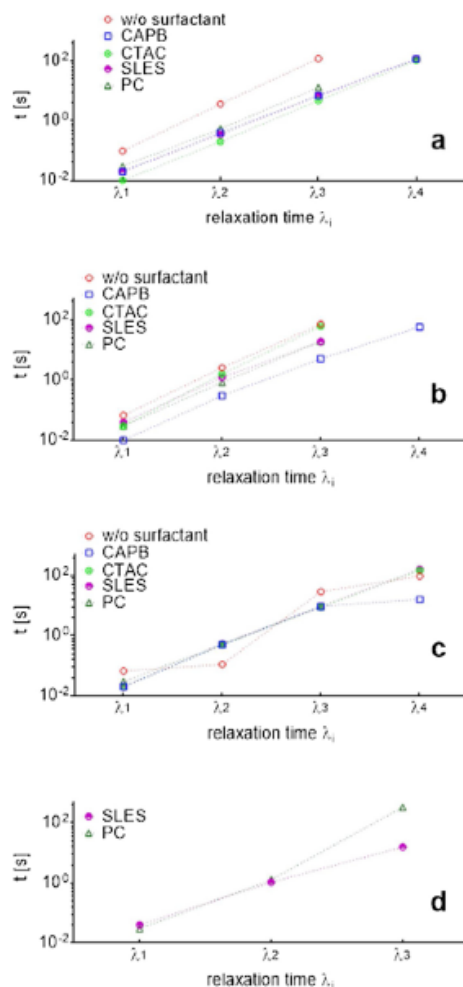
Fig. 5. Changes in the relaxation time spectra of the Maxwell model of the frequency sweep for (a) Welan, (b) S-88, (c) Diutan, and (d) Gellan.

Table 4
Relaxation times of the Burgers model of sphingans and sphingan–surfactant mixtures.

Sphingan	Relaxation time	Surfactants				
		No surfactant	CAPB	CTAC	SLES	PC
Welan	λ_0 [s]	21	36	38	41	9
	λ_1 [s]	6.6	5.1	5.4	5.4	4.9
	λ_2 [s]	65	83	87	83	42
S-88	λ_0 [s]	41	13	28	0.7	1.3
	λ_1 [s]	5.1	5.4	11	228	1.3
	λ_2 [s]	84	59	253	33	0.0006
Diutan	λ_0 [s]	38	28	48	24	43
	λ_1 [s]	8.5 s	369	33	8.5	258
	λ_2 [s]	121	34	49	98	29

combination with CTAC, CAPB and SLES, show that the inter- and intramolecular interactions of the sphingans still dominate the rheological behavior. Comparing the mixtures containing the cationic CTAC with the other surfactant-mixtures do not suggest stronger interactions of the cationic head group with the anionic GlcA in the polysaccharide backbone of Welan, Diutan and S-88. Such interactions, which lead to a ball-and-chain structure caused by the interaction of positively charged micelles with the anionic polysaccharide chains (Bonnaud et al., 2010). This effect might be explained by a masking of the glucuronic acid, which in this case may have three different origins: the masking of the charge by cations in the solution, the protonation of GlcA and the masking due to steric hindrance by the sidechain. The low pKs value of GlcA, suggests it is still charged at the pH of 5.5, therefore eliminating the masking by protonation. Considering the rheological data of the pure sphingans especially Gellan, shows that the ionic strength is high enough to cause cation mediated gel formation, therefore the concentrations of cations in the surfactant mixtures could be still sufficient to mask the negative charges. However, the incompatibility of Gellan with both cationic CTAC and zwitterionic CAPB suggest strong interactions of the positive charges in the head groups in the absence of a side chain, leading to precipitation of these complexes (Goddard & Hannan, 1976; Goddard, Phillips, & Hannan, 1975). This strongly suggests the masking of the charge by the side chains of Welan, Diutan and S-88, which leads to a higher surfactant compatibility. The introduction of a lower relaxation time however suggests a weaker network characteristic, which can be explained by the incorporation of micelles in the polymer network, hindering interactions of polysaccharide chains. This is especially evident in Gellan, where gel character is significantly decreased when mixed with SLES or PC, where larger surfactant structures can hinder cation mediated intermolecular interactions, thereby hindering gel formation. Especially PC had a large impact on the rheological behavior, causing significantly decreased gel strength for Gellan and now predominant liquid character for Welan, Diutan and S-88. This can be explained by formation of rod-like micelles formed by PC (Platz et al., 1995). Interestingly here the effect seems to be more pronounced for the branched sphingans. Comparing the data of the models, Diutan is least affected by the addition of surfactants. As Diutan has a disaccharide side, while Welan and S-88 only possess a monosaccharide side-chain, the association of the polysaccharide molecules may be stronger compared to Welan and S-88, where the monosaccharide side chain hinders strong intermolecular interactions, as described for the structurally similar Rhamsan (Tako et al., 2016). These stronger intermolecular interactions explain why the rheological properties of Diutan are less affected by surfactants. Interestingly, the cationic CTAC is incompatible with the branched polysaccharide Xanthan, as reported by a previous study (Rütering et al., 2018). Whether this incompatibility is due to the anionic charge density or distribution of Xanthan or rather its structural conformation will further improve our understanding these polysaccharide-surfactant interactions. Studies of interactions with modified Xanthan variants created in previous works (Gansbiller et al., 2019), combined with further structural analyses could further elucidate polysaccharide-surfactant interactions.

3.4. Effect of EPS–surfactant mixtures on temperature stability

Fig. 6 shows the temperature sweeps from 20 °C to 75 °C with subsequent cooling to 20 °C within the determined LVE region. For Welan, Diutan, and S-88, only a slight (temperature reversible) decrease in the (weak) gel strength was observed; Gellan showed a strong onset of loss of gel properties at 40 °C, with a complete and irreversible loss of its gel character at 55 °C. An increase in G" at that temperature indicated dissipated energy owing to internal friction within the gel structure, which was possibly due to the combination of temperature-induced changes of viscoelastic properties and mechanical strain of the structure. For Diutan, a slight increase in G" was also observable
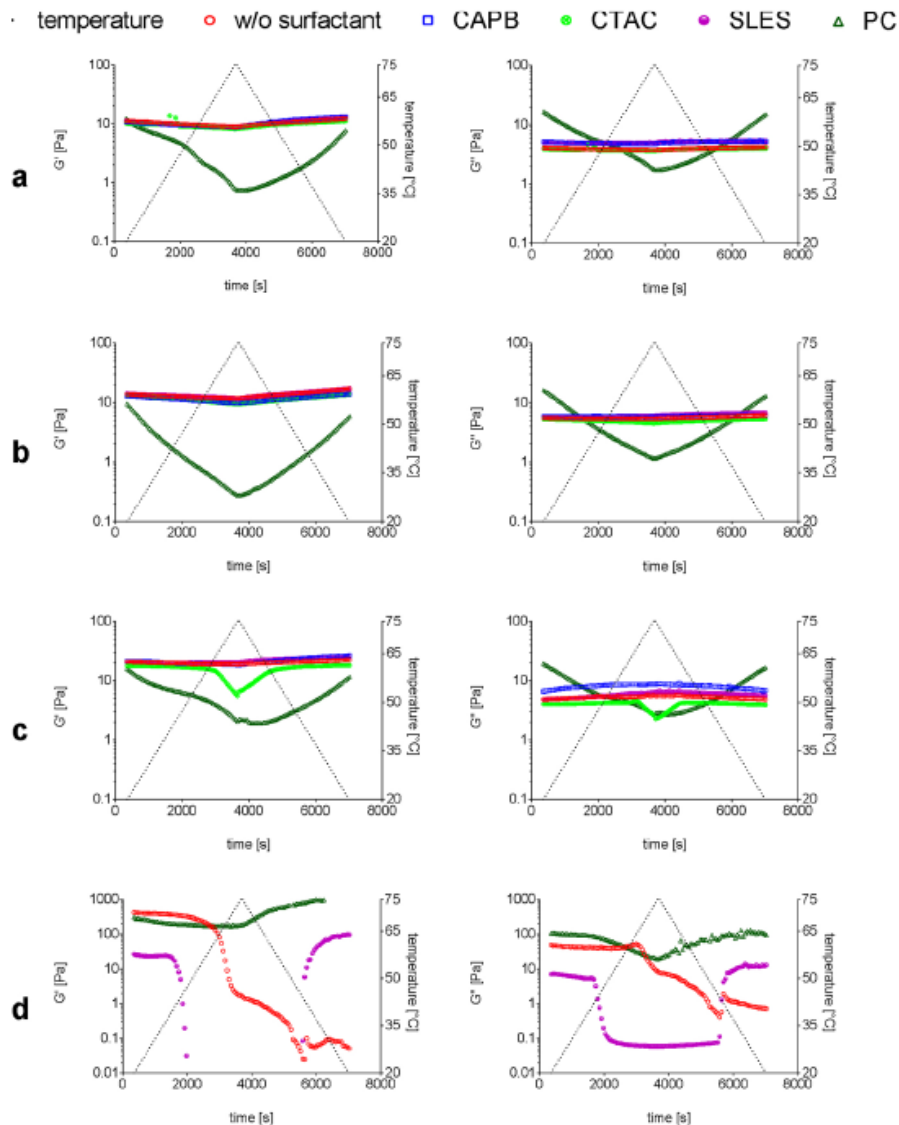
8

Fig. 6. Temperature sweeps of (a) Welan, (b) S-88, (c) Diutan, and (d) Gellan. Storage modulus G' and loss modulus G" are shown individually for better overview.

compared to Welan and S-88, which indicated a stronger physical interaction of polymer strands. As previously described, the addition of surfactants decreased the overall gel strength, while PC led to the complete loss of the predominate elastic character for Welan, Diutan, and S-88 with a strong influence of temperature on the structure and viscosity. Among all non-gelling sphingans, Diutan in the mixture with cationic CTAC showed a reversible loss of its viscoelastic properties starting at 50 °C with a complete loss of at 75 °C. While Diutan alone has a higher temperature stability than Welan and S-88, due to the disaccharide side chain (Tako, 1992), addition of the cationic CTAC lead to a destabilization at high temperature. This might be due to an increased mobility of the side chain at high temperatures, reducing the

shielding of the anionic $-COO^-$ group of GlcA, allowing the cationic surfactant to interact with the polysaccharide backbone. Another explanation is based on a proposed helical structure, where the side chain protrudes into the helix (Xu, Gong et al., 2015). This structure might be affected by the cationic head group of CTAC at high temperatures. However, to elucidate the cause of this behavior, further studies are necessary. The mixtures of Gellan with uncharged PC and anionic SLES exhibited the most interesting properties because the mixtures possessed reduced gel strength compared to Gellan alone, due to increased interactions with the surfactants, and was overall comparable to other sphingans without surfactants. While the mixture of Gellan and PC exhibited a low temperature dependency of its rheological properties,

9

Gellan/SLES showed a complete loss of its viscoelastic properties between 30 °C and 40 °C, which was completely reversible.

4. Conclusion

We were able to describe the rheological properties of three commercial sphingans (Gellan, Welan, and Diutan) and self-prepared sphingan S-88 using a (mechanical) model-based description of the frequency sweep and creep- and creep-recovery tests. While the frequency sweeps of non-gel-forming sphingans Welan, Diutan, and S-88 could be described with a generalized Maxwell model with 3–4 elements, gel-forming Gellan was best described by the power law model, which did not provide a mechanical interpretation. Likewise, a 6-parameter Burgers model was applied to Welan, Diutan, and S-88 but could not be applied to Gellan owing to its brittle gel properties. The differences in the models used to describe Diutan and structurally closely related Welan and S-88 were similar; however, there were slight differences in the rheological properties. Although not quantitatively, the acetylation of sphingan S-88 was confirmed in this study, which provided a consistency in the rheological properties of Welan, Diutan, and S-88 with respect to their structural similarity. The prepared mixtures of sphingans with four surfactants (each representing a different group based on the head charge) were subsequently evaluated, and the comparison based on the changes in models and model parameters was established. The branched Sphingans Welan, Diutan, and S-88 showed higher surfactant compatibilities than the linear Gellan, which is most likely due to the masking of the negative charge of GlcA by the sidechains. The viscoelastic properties of Diutan were least affected by the addition of surfactants. These differences were very minute but became evident by the comparison of the models and model parameters. These different effects of the surfactants could be explained by the presence of a disaccharide side chain in Diutan opposed to the monomeric side chain of Welan and S-88. While the monomeric side chains hinder stronger intermolecular interactions in Welan and S-88, the orientation of the disaccharide side chain of Diutan, allows stronger intermolecular interactions. The same disaccharide sidechain might also explain the different influence of temperature in mixture with cationic surfactants. However, the precise mechanism has yet to be completely clarified. The incompatibility of Gellan with cationic and zwitterionic surfactants was attributed to the lack of a side chain, causing strong interactions of these surfactants with the polysaccharide, causing precipitation. In combination with SLES and PC, Gellan showed drastically reduced gel strength, and in case of SLES drastically decreased temperature stability, indicating stronger interactions with the surfactants due to the lack of side chains. The uncharged lauryl glucoside PC had the highest impact on the rheological properties of all four sphingans. This is most likely due to the formation of large micelle structures of the surfactant, hindering overall intermolecular interactions of the polysaccharides.

CRediT authorship contribution statement

Moritz Gansbiller: Conceptualization, Methodology, Software, Validation, Formal analysis, Investigation, Data curation, Writing - original draft, Visualization. **Jochen Schmid:** Conceptualization, Methodology, Validation, Writing - review & editing, Visualization, Supervision, Resources, Project administration. **Volker Sieber:** Writing - review & editing, Project administration, Resources, Funding acquisition.

Acknowledgements

Appendix A. Supplementary data

Supplementary material related to this article can be found, in the online version, at doi:https://doi.org/10.1016/j.carbpol.2020.116778.

References

Aranoff, S. L., D.R.P, Okun, D. T., Lane, C. R., Williamson, I. A., & Pinkert, D. A. (2008). In U. S. I. T. Commission (Ed.). *Industrial biotechnology: Development and adoption by the U.S. Chemical and biofuel industries.*

Bain, C. D., Claesson, P. M., Langevin, D., Meszaros, R., Nylander, T., Stubenrauch, C., ... von Klitzing, R. (2010). Complexes of surfactants with oppositely charged polymers at surfaces and in bulk. *Advances in Colloid and Interface Science, 155*(1–2), 32–49.

Bais, D., Trevisan, A., Lapasin, R., Partal, P., & Gallegos, C. (2005). Rheological characterization of polysaccharide–surfactant matrices for cosmetic O/W emulsions. *Journal of Colloid and Interface Science, 290*(2), 546–556.

Bajaj, I. B., Survase, S. A., Saudagar, P. S., & Singhal, R. S. (2007). Gellan gum: Fermentative production, downstream processing and applications. *Food Technology and Biotechnology, 45*(4), 341–354.

Biddy, M. J., Scarlata, C., & Kinchin, C. (2016). *Chemicals from biomass: A market assessment of bioproducts with near-term potential.* Golden, CO (United States): National Renewable Energy Lab. (NREL).

Bonnaud, M., Weiss, J., & McClements, D. J. (2010). Interaction of a food-grade cationic surfactant (Lauric arginate) with food-grade biopolymers (pectin, carrageenan, xanthan, alginate, dextran, and chitosan). *Journal of Agricultural and Food Chemistry, 58*(17), 9770–9777.

Callet, F., Milas, M., & Rinaudo, M. (1987). Influence of acetyl and pyruvate contents on rheological properties of xanthan in dilute solution. *International Journal of Biological Macromolecules, 9*(5), 291–293.

Corolleur, F., Level, A., Matt, M., & Perez, S. (2020). Innovation potentials triggered by glycoscience research. *Carbohydrate Polymers*Article 115833.

de Melo Pereiraa, G. V., Karp, S. G., Letti, L. A., Pagnoncelli, M. G., Finco, A. M., Machado, M. R., & Soccol, C. R. (2019). Bioactive polysaccharides produced by microorganisms: Production and applications. *A handbook on high value fermentation products, volume 2: Human welfare*231.

Dickinson, E., Goller, M. I., & Wedlock, D. J. (1993). Creaming and rheology of emulsions containing polysaccharide and non-ionic or anionic surfactants. *Colloids and Surfaces A: Physicochemical and Engineering Aspects, 75,* 195–201.

Fijan, R., Šostar-Turk, S., & Lapasin, R. (2007). Rheological study of interactions between non-ionic surfactants and polysaccharide thickeners used in textile printing. *Carbohydrate Polymers, 68*(4), 708–717.

Fiume, M. M., Heldreth, B., Bergfeld, W. F., Belsito, D. V., Hill, R. A., Klaassen, C. D., ... Slaga, T. J. (2016). Safety assessment of microbial polysaccharide gums as used in cosmetics. *International Journal of Toxicology, 35*(1_suppl), 5S–49S.

Freitas, F., Alves, V., & Reis, M. M. (2014). Bacterial polysaccharides: Production and applications in cosmetic industry. In K. G. Ramawat, & J.-M. Mérillon (Eds.). *Polysaccharides* (pp. 1–24). Springer International Publishing.

Gansbiller, M., Schmid, J., & Sieber, V. (2019). In-depth rheological characterization of genetically modified xanthan-variants. *Carbohydrate Polymers, 213,* 236–246.

Goddard, E. D. (1994). Polymer/surfactant interaction – Its relevance to detergent systems. *Journal of the American Oil Chemists Society, 71*(1).

Goddard, E. D. (2002). Polymer/surfactant interaction: Interfacial aspects. *Journal of Colloid and Interface Science, 256*(1), 228–235.

Goddard, E. D., & Hannan, R. B. (1976). Papers presented at the 49th national colloid symposium, Clarkson cationic polymer/anionic surfactant interactions. *Journal of Colloid and Interface Science, 55*(1), 73–79.

Goddard, E. D., Phillips, T., & Hannan, R. (1975). Water soluble polymersurfactant interaction—Part 1. *Journal of the Society of Cosmetic Chemists, 26,* 461–475.

Hansson, P., & Lindman, B. (1996). Surfactant-polymer interactions. *Current Opinion in Colloid & Interface Science, 1*(5), 604–613.

Hassler, R. A., & Doherty, D. H. (1990). Genetic engineering of polysaccharide structure: Production of variants of xanthan gum in Xanthomonas campestris. *Biotechnology Progress, 6*(3), 182–187.

Kaur, V., Bera, M. B., Panesar, P. S., Kumar, H., & Kennedy, J. F. (2014). Welan gum: Microbial production, characterization, and applications. *International Journal of Biological Macromolecules, 65,* 454–461.

Manca, S., Lapasin, R., Partal, P., & Gallegos, C. (2001). Influence of surfactant addition on the rheological properties of aqueous Welan matrices. *Rheologica Acta, 40*(2), 128–134.

Morris, E. R., Gothard, M. G. E., Hember, M. W. N., Manning, C. E., & Robinson, G. (1996). Gellan Gum: Structures, Properties and Functions International Workshop on Gellan and Related PolysaccharidesConformational and rheological transitions of welan, rhamsan and acylated gellan. *Carbohydrate Polymers, 30*(2), 165–175.

Moscovici, M. (2015). Present and future medical applications of microbial exopolysaccharides. *Frontiers in Microbiology, 6*(1012).

Ögmundarson, Ó., Herrgård, M. J., Forster, J., Hauschild, M. Z., & Fantke, P. (2020). Addressing environmental sustainability of biochemicals. *Nature Sustainability, 3,* 167–174.

Pedro, R., & Walters, K. A. (2019). Surfactants in cosmetic products. *Cosmetic Formulation: Principles and Practice,* 129.

Piculell, L., Egermayer, M., & Sjöström, J. (2003). Rheology of mixed solutions of an associating polymer with a surfactant. Why are different surfactants different? *Langmuir, 19*(9), 3643–3649.

Platz, G., Poelike, J., Thunig, C., Hofmann, R., Nickel, D., & von Rybinski, W. (1995). Phase behavior, lyotropic phases, and flow properties of alkyl glycosides in aqueous solution. *Langmuir, 11*(11), 4250–4255.

Pollock, T. J. (2005). *Sphingan group of exopolysaccharides (EPS). Biopolymers online.* Wiley-VCH Verlag GmbH & Co. KGaA.

Rühmann, B., Schmid, J., & Sieber, V. (2014). Fast carbohydrate analysis via liquid chromatography coupled with ultra violet and electrospray ionization ion trap detection in 96-well format. *Journal of Chromatography A, 1350*, 44–50.

Rühmann, B., Schmid, J., & Sieber, V. (2015). High throughput exopolysaccharide screening platform: From strain cultivation to monosaccharide composition and carbohydrate fingerprinting in one day. *Carbohydrate Polymers, 122*, 212–220.

Rütering, M., Schmid, J., Gansbiller, M., Braun, A., Kleinen, J., Schilling, M., & Sieber, V. (2018). Rheological characterization of the exopolysaccharide Paenan in surfactant systems. *Carbohydrate Polymers, 181*, 719–726.

Rütering, M., Schmid, J., Rühmann, B., Schilling, M., & Sieber, V. (2016). Controlled production of polysaccharides–exploiting nutrient supply for levan and hetero-polysaccharide formation in Paenibacillus sp. *Carbohydrate Polymers, 148*, 326–334.

Schmid, J., Sperl, N., & Sieber, V. (2014). A comparison of genes involved in sphingan biosynthesis brought up to date. *Applied Microbiology and Biotechnology, 98*(18), 7719–7733.

Semenzato, A., Costantini, A., & Baratto, G. (2014). Green polymers in personal care products: Rheological properties of tamarind seed polysaccharide. *Cosmetics, 2*(1), 1–10.

Sharma, S., & Bhattacharya, S. (2015). Flow behaviour of gellan sol with selected cations. *Journal of Food Science and Technology, 52*(2), 1233–1237.

Shukla, A., Mehta, K., Parmar, J., Pandya, J., & Saraf, M. (2019). Depicting the exemplary knowledge of microbial exopolysaccharides in a nutshell. *European Polymer Journal, 119*, 298–310.

Tako, M. (1992). *Molecular-origin for thermal-stability of Welan and Rhamsan gum. ABSTRACTS OF PAPERS OF THE AMERICAN CHEMICAL SOCIETY (Vol. 204, pp. 38-CARB). NW, WASHINGTON, DC: AMER CHEMICAL SOC 1155 16TH ST20036.*

Tako, M., & Kiriaki, M. (1990). Rheological properties of Welan gum in aqueous-media. *Agricultural and Biological Chemistry, 54*(12), 3079–3084.

Tako, M., & Nakamura, S. (1984). Rheological properties of deacetylated xanthan in aqueous media. *Agricultural and Biological Chemistry, 48*(12), 2987–2993.

Tako, M., & Tamaki, H. (2005). Molecular origin for the thermal stability of S-88 gum produced by Pseudomonas ATCC 31554. *Polymer Journal, 37*(7), 498–505.

Tako, M., Sakae, A., & Nakamura, S. (1989). Rheological properties of gellan gum in aqueous media. *Agricultural and Biological Chemistry, 53*(3), 771–776.

Tako, M., Yogi, T., Uechi, K., Onaga, M., Tamaki, Y., & Uechi, S. (2016). Structure-function relationship of a gellan family of polysaccharide, S-198 gum, produced by Alcaligenes atcc31853. *Advances in Biological Chemistry, 6*(03), 55.

Wu, M., Qu, J., Tian, X., Zhao, X., Shen, Y., Shi, Z., ... Ma, T. (2019). Tailor-made polysaccharides containing uniformly distributed repeating units based on the xanthan gum skeleton. *International Journal of Biological Macromolecules, 131*, 646–653.

Xu, L., Xu, G., Liu, T., Chen, Y., & Gong, H. (2013). The comparison of rheological properties of aqueous welan gum and xanthan gum solutions. *Carbohydrate Polymers, 92*(1), 516–522.

Xu, L., Dong, M., Gong, H., Sun, M., & Li, Y. (2015). Effects of inorganic cations on the rheology of aqueous welan, xanthan, gellan solutions and their mixtures. *Carbohydrate Polymers, 121*, 147–154.

Xu, L., Gong, H., Dong, M., & Li, Y. (2015). Rheological properties and thickening mechanism of aqueous diutan gum solution: Effects of temperature and salts. *Carbohydrate Polymers, 132*, 620–629.

11

4.2 Influence of polymer-polymer-interactions on the rheological properties of paenan

As seen by the previous study, even small differences the composition of the sidechain composition of exopolysaccharides have major influence on their rheological properties. These effects can be explained by different intra-and intermolecular interactions of the polymer chains due to the differences in their composition. While several of these effects have already been clarified and can lead to a heuristic of a structure function relationship in some polysaccharides, it still needs to be proven for unstudied polysaccharides. In the following study, a novel polysaccharide, or rather group of polysaccharides, paenan was studied for its rheological properties in respect to different polysaccharide compositions. *Paenibacillus polymyxa* shows the unique characteristic of producing three individual types of polysaccharides, which can be altered by the targeted deletion of Glycosyltransferases. In this study, every single paenan polymer as well as all of their possible combinations could be produced in this way and were characterized for their rheological properties. The rheological behavior of paenan was found to be dependent of the interactions between the different polymer types of paenan rather than the interactions of the same polymer types with each other, indicating the formation of helices composed of heterologous polymer strains. While the previous studies of structure function relationships, including the ones in this work helped to understand the cause and effect, the interactions of different paenan polymers are in strong contrast to the ones described for other polysaccharides like the sphingans or xanthan, and give new insights on the structure function relationship of polysaccharides. In detail, it was concluded, that like for xanthan, the pyruvylation of the terminal galactose of paenan I plays a crucial role in polymer-polymer-interactions, causing high viscosity and gel strength to the polymer-solutions. Unlike xanthan, the rheological data of the individual paenan types I-III, however, suggest a helix-formation between at least two different paenan variants, paenan I and III, while the interaction of paenan II leads to higher temperature stability of the rheological properties.

Design and planning of this study were performed by Christoph Schilling in collaboration with Moritz Gansbiller, Volker Sieber and Jochen Schmid. Strain construction, EPS production by fermentation and carbohydrate analysis were performed by Christoph Schilling. Rheological measurements were performed by Christoph Schilling. Rheological evaluation and modeling were performed by Moritz Gansbiller. Potential applications were evaluated by Christoph Schilling. All authors contributed to content and language of the manuscripts and provided scientific or technical advice.

Rheological characterization of artificial paenan compositions produced by *Paenibacillus polymyxa* DSM 365

Christoph Schilling[‡], Moritz Gansbiller[‡], Broder Rühmann, Volker Sieber
& Jochen Schmid

Prepared manuscript

(2022)

[‡]: authors contributed equally

Abstract

Microbial exopolysaccharides (EPS) constitute a sustainable alternative to petroleum-based rheological modifiers. Recent studies revealed that the heteroexopolysaccharide produced by *Paenibacillus polymyxa* is composed of three distinct biopolymers termed paenan I, II and III. Using CRISPR-Cas9 mediated knock-out variants of glycosyltransferases, defined polysaccharide compositions were produced and rheologically characterized in detail. The high viscosity and gel-like character of the wildtype polymer is proposed to originate from the non-covalent interaction between a pyruvate residue of paenan I and the glucuronic acid found in the backbone of paenan III. Paenan II conveys thermostable properties to the EPS mixture. Opposed to the wildtype polymer mixture, knock-out variants demonstrated significantly altered rheological behavior. Using the structure-function relationship determined in this study, tailor-made paenan variants might be utilized in a wide range of applications including thickening agents, coatings or high value biomedical materials.

Introduction

Carbohydrate polymers represent a highly diverse class of functional polysaccharides found in all domains of life (Sutherland, 1972). Intracellular polysaccharides may function as energy storage (e.g. glycogen) or play a central role as integral parts of cellular structures (e.g. lipopolysaccharides, starch, cellulose etc.). Contrary, extracellular polysaccharides (EPS) cover numerous tasks as natural adhesives, barriers against abiotic stress factors such as desiccation and antibiotics or as protection against extreme environmental conditions (Danese, Pratt, & Kolter, 2000; Ophir & Gutnick, 1994; Poli, Anzelmo, & Nicolaus, 2010). Owing to their complex and diverse structures, a sheer endless variety of physicochemical properties can be derived from different EPS variants and compositions (Moradali & Rehm, 2020). Consequently, various polysaccharides have found commercial success as bulk products in food, feed and technical applications as well as in high-value niches in cosmetics and pharmaceutical industry (Freitas, Alves, & Reis, 2011; Jang, Zhang, Chon, & Choi, 2015; Kaur, Bera, Panesar, Kumar, & Kennedy, 2014; Kumar, Rao, & Han, 2018).

The global market of biopolymers is still dominated by plant and algae derived polysaccharides such as starch, alginates or carrageenans (Williams & Phillips, 2016). However, bacterial EPS variants from *Xanthomonas campestris*, different sphingans or hyaluronic acid produced by *Streptococcus* spp. have found commercial success in bulk products as well as in high-value niche applications (Bajaj, Survase, Saudagar, & Singhal, 2007; Becker, Katzen, Pühler, & Ielpi, 1998; Burdick & Prestwich, 2011). The main advantage of bacterial polysaccharides over their plant and algae derived counterparts is the ability to produce these polymers by large scale fermentation processes in bioreactors under controlled conditions, making them independent of seasonal or geopolitical influences. Furthermore, ongoing research in the development of new genetic tools allowed the targeted modification of polymer structures to generate EPS variants with new physicochemical properties or enhance production via metabolic engineering (Hassler & Doherty,

1990; Schilling, Badri, Sieber, Koffas, & Schmid, 2020; Wu et al., 2019).

Paenibacillus polymyxa is a Gram-positive, spore-forming soil bacterium that has attracted increasing interest as a production platform for an arsenal of different antibiotics (Grady, MacDonald, Liu, Richman, & Yuan, 2016), 2,3-butanediol of extremely high enantiomeric purity (De Mas, Jansen, & Tsao, 1988; Schilling, Ciccone, Sieber, & Schmid, 2020) as well as for an heteroexopolysaccharide termed paenan with outstanding material properties in surfactant systems (Rütering et al., 2018). There have been multiple publications focusing on the rheology of heteroexopolysaccharides produced by *P. polymyxa* (Kahng, Lim, Yun, & Seo, 2001; Madden, Dea, & Steer, 1986; Ninomiya & Kizaki, 1969; Raza, Makeen, Wang, Xu, & Qirong, 2011). Even though monomer analysis typically identified glucose, mannose, galactose and sometimes fucose and pyruvate to be part of the EPS, the available rheological data can be hardly compared as these studies differ with respect to the strains as experimental setups for polymer production and rheological characterization. Even more important, recent advances in the elucidation of the genetics of Paenibacilli and the underlying polymer structure revealed that the heteroexopolysaccharide "paenan" is in fact composed of three polysaccharides with distinct substructures, which are simultaneously produced by *P. polymyxa* (Rütering et al., 2018, Schilling et al., 2021a, 2021b). The biosynthesis of the heteroexopolysaccharides from *P. polymyxa* DSM 365 following the Wzx/Wzy pathway is encoded in a 35 kb gene cluster, encoding eleven glycosyltransferases, two Wzx flippases and two Wzy polymerases as well as multiple genes associated to regulatory functions and precursor synthesis (Rütering et al., 2017). A secondary cluster encoding the pyruvyltransferase EpsO, another putative flippase and two additional glycosyltransferases correspond to the biosynthesis of paenan I. Using a combinatorial approach in performing CRISPR-Cas9 mediated gene deletions of the paenan cluster in *P. polymyxa*, it was possible to isolate the individual polymers and elucidate their structures (Fig. 1). Furthermore, by this approach, distinct glycosyltransferases were attributed to the biosynthesis of individual polymers establishing a structure-function relationship (Schilling et al., 2022a, 2022b).
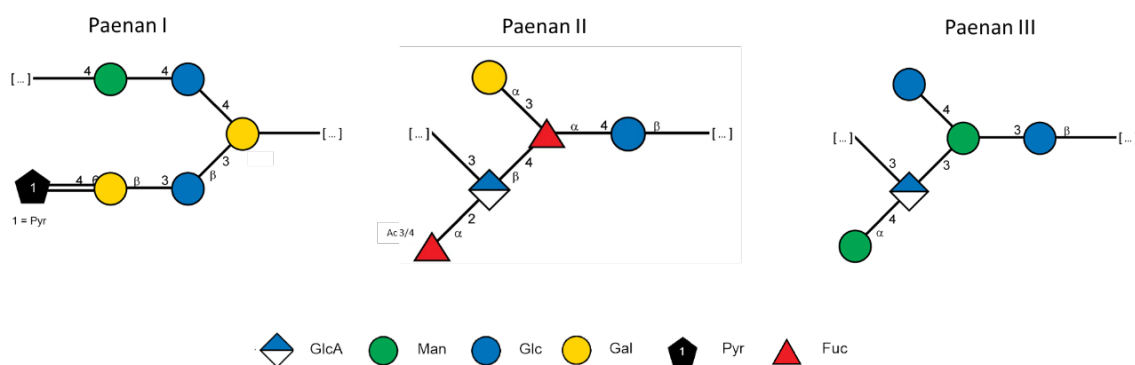
Fig. 1: Overview of the three heteroexopolysaccharides produced by *P. polymyxa* DSM 365. The repeating units of paenan I and paenan III are postulated structures based on current carbohydrate analysis and require further verification by NMR. Figure adapted from (Schilling et al., 2022a, 2022b).

For the first time, this study focuses on the in-depth rheological characterization of defined paenan

compositions. Leveraging CRISPR-Cas9 mediated combinatorial knock-out strains, defined polysaccharide compositions were produced in their natural ratio. The rheological behavior of each polymer is characterized individually and in combination with other paenan variants and will elude how the EPS variants interact with each other, resulting in highly different physicochemical properties.

Materials and Methods

Strains and media

P. polymyxa DSM 365 was acquired from the German Collection of Microorganisms and Cell Culture (DSMZ, Germany). Combinatorial knock-out variants were obtained as previously described (Schilling, Rühmann, et al., 2022a). Strains used in this study are listed in Table S1. All medium components were obtained from Carl Roth GmbH (Germany) if not indicated differently. All strains were stored in 30 % glycerol at -80 °C. Prior to cultivation, strains were streaked on LB agar plates and grown at 30 °C for 24 h.

Fermentation medium contained 30 g L^{-1} glucose, 0.05 g L^{-1} $CaCl_2$ x 2 H_2O, 5 g L^{-1} tryptone, 1.33 g L^{-1} $MgSO_4$ x 7 H_2O, 1.67 g L^{-1} KH_2PO_4, 2 mL L^{-1} RPMI 1640 vitamins solution (Merck, Germany) and 1 mL L^{-1} trace elements solution (2.5 g L^{-1} $FeSO_4$, 2.1 g L^{-1} $C_4H_4O_6Na_2$ x 2 H_2O, 1.8 g L^{-1} $MnCl_2$ x 4 H_2O, 0.258 g L^{-1} H_3BO_3, 0.031 g L^{-1} $CuSO_4$ x 5 H_2O, 0.023 g L^{-1} $NaMoO_4$ x 2 H_2O, 0.075 g L^{-1} $CoCl_2$ x 7 H_2O, 0.021 g L^{-1} $ZnCl_2$). Preculture medium was prepared equal to the fermentation medium except of a reduced glucose concentration of 10 g L^{-1} and additional 20 g L^{-1} MOPS buffered to pH 7.

Fermentative EPS production.

Fermentative production of EPS was performed in 2 L Sartorius Biostat B plus bioreactor systems (Sartorius, Germany) with a working volume of 1 L equipped with two 6-blade Rushton impellers over 28 h at a controlled pH of 6.8 and pO_2 saturation of 30 %. Batch cultivations were started with an initial OD_{600} of 0.1 by inoculation with an appropriate volume of preculture. After fermentation, biomass was separated by centrifugation (15,000 x g, 20 °C, 20 min) followed by cross-flow filtration of the supernatant using 100 kDa filtration cassette (Hydrosart, Sartorius AG, Germany). Highly viscous EPS variants were diluted 1:10 with ddH_2O prior to centrifugation. Concentrated supernatant was afterwards slowly poured into two volumes of isopropanol. Precipitated EPS was then collected and dried overnight in a VDL53 vacuum oven at 40 °C (Binder, Germany). Dry weight of the obtained EPS was determined gravimetrically, before milling to a fine powder in a ball mill at 30 Hz for 1 min (Mixer Mill MM400, Retsch GmbH, Germany).

Carbohydrate fingerprinting

Monomer compositions of all EPS variants were analyzed by the 1-phenyl-3-methyl-5-pyrazolone-high throughput method (HT-PMP) (Rühmann, Schmid, & Sieber, 2014). In short, 0.1 % EPS solutions were hydrolyzed in a 96-well plate, sealed with a silicone mat and further covered by a custom-made metal device with 2 M trifluoroacetic acid (90 min, 121 °C). Samples were neutralized with 3.2 % NH_4OH. 75 µL of PMP master mix (0.1 M methanolic PMP:0.4 % ammonium hydroxide 2:1) were added to 25 µL of neutralized

hydrolysate and incubated at 70 °C for 100 min in a thermal cycler. 20 µL of derivatized samples were mixed with 25 µL 0.5 M acetic acid and 125 µL ddH$_2$O and filtered with a 0.2 µm filter plate (1,000 x g, 2 min) followed by HPLC-UV-MS using a Ultimate 3000 RS HPLC system (Dionex, USA). Separation was performed on a reverse phase column (Gravity C18, 100 x 2 mm, 1.8 µm particle size, Macherey-Nagel, USA) set to 50 °C. Gradient elution was performed using a mobile phase A (5 mM ammonium acetate adjusted to pH 5.6 with 15 % acetonitrile) and mobile phase B (100 % acetonitrile) with a constant pump rate of 0.6 mL min^{-1}.

Enzymatic assays for glucose and pyruvate quantification

Glucose and pyruvate concentrations of obtained EPS samples were determined enzymatically before and after hydrolysis to deduct residual contaminations from the fermentation medium as previously described (Rühmann, Schmid, & Sieber, 2016).

Molecular weight

The molecular weight of polymer variants was determined via size exclusion chromatography using an Agilent 1260 Infinity system (Agilent Technologies, Germany) equipped with a refractive index detector (SECcurity GPC1260) and a SECcurity SLD7000 seven-angle static light scattering detector (PSS Polymer Standards Service, Germany). For this, 0.5 g L^{-1} of each variant was reconstituted in 0.1 M LiNO$_3$ and 100 µL sample were injected to the system in 30 min intervals and analyzed using a TSKgel SuperMP(PW)-H guard column and two consecutive TSKGel SuperMultipore PW-H columns (6.0 mm ID x 15 cm, TOSOH Bioscience, Germany) kept at 50 °C. As an eluent 0.1 M LiNO$_3$ was used at a constant flow rate of 0.3 mL min^{-1}. Absolut molecular weight was determined via light scatter and polymer concentration and further cross-validated using a 12 point-pullulan standard (384 Da – 2.35 MDa) and a 4.5 MDa xanthan reference.

Rheological analysis

For rheological analysis, 1 % (w/w) solutions of each polymer were prepared in ddH$_2$O and 0.5% NaCl (85 mM) respectively. Conductivity of each solution was measured using an LF413T-ID electrode (Schott instruments, Germany) to determine residual salt concentrations of the fermentation broth (Table S2). Rheological measurements were conducted using a MCR 300 stress controlled rotational rheometer (Anton Paar, Austria) equipped with a CP 50-1 cone-plate measuring system (50 mm diameter, 1° cone angle, 50 µm cone truncation). All measurements, except temperature sweeps, were carried out at 20°C controlled by a TEK 150P temperature unit. After applying of the solution to the rheometer, all samples were incubated at 20 °C for 5 minutes before beginning the measurements. All experiments were performed in technical triplicates.

Viscosity curves

Viscosity curves were measured using a logarithmically increased shear rate from 10^{-3} to 10^3 s^{-1} by measuring 3 data points per decade with decreasing measuring time of 100 – 5 s per data point.

Amplitude sweeps

Amplitude sweeps were measured using a logarithmically increasing shear stress amplitude from 10^{-1} to 10^3 Pa with a frequency of 1 Hz.

Frequency sweeps

Frequency sweeps were carried out within the linear viscoelastic range (LVE) at a logarithmically increasing frequency from 10^{-2} to 10 Hz.

Temperature sweeps

Temperature sweeps were performed within the LVE at a frequency of 1 Hz applying a temperature ramp from 20 to 75 °C with a heating rate of 4 °C min^{-1}. The edge of the cone-plate measuring system was covered with low viscosity paraffin oil (Carl Roth, Germany) to prevent evaporation.

Thixotropy test

Thixotropic behavior was evaluated by a three-stage oscillatory shear sequence. In the first stage, samples were subjected to shear stress within the LVE region followed by a high oscillatory shear of 10^3 Pa for 30 s. The structural recovery was then measured over 10 min within the LVE.

Results and discussion

Polymer characterization

In a first step, the EPS of *P. polymyxa* DSM 365 and combinatorial knock-out mutants were produced in bioreactor scale. During downstream processing, the fermentation supernatant was desalted via cross-flow filtration to enable uniform characterization of the rheological behavior. Due to the anionic character of all paenan variants, a residual conductivity between 0.7-1.0 mS cm^{-1} was determined for all 1 % polymer solutions (Table S2). In order to verify the presence of individual paenan polymers, the carbohydrate fingerprint was determined for each variant (Fig. 2). For paenan I, a monomer ratio of 2:1:2:1 (Glc:Man:Gal:Pyr) was expected, while for paenan II an equimolar ratio of 1:1:1:2 (Glc:Gal:GlcA:Fuc) and for paenan III, 2:2:1 (Glc:Man:GlcA) were anticipated. Due to the high susceptibility of uronic acids towards degradation during chemical hydrolysis, GlcA was severely underestimated for all polysaccharide compositions containing the uronic acid (Rodén, Baker, Cifonelli, & Mathews, 1972). In addition to the monomer composition, previously identified key dimers detected via MS/MS analysis were used to assign combinatorial knock-out variants to each paenan variant (Schilling et al., 2022b). By assigning the presence of pyruvate ketals to paenan I, a GlcA-Fuc dimer to paenan II and a GlcA-Man dimer to paenan III, the polymer composition of each knock-out variant was determined, while still retaining the natural polysaccharide distribution in those variants. Henceforward, each EPS variant is named by the present paenan variants, rather than the gene deletions leading to the respective phenotype.

	wt	ΔepsO	ΔpepUL	ΔpepFJ	ΔpepQF	ΔpepLJ	ΔpepF	ΔpepQTUV
Gal$^{4,6\,Pyr}$ m/z 581	x		x			x		x
GlcA-Fuc m/z 671	x	x		x		x	x	
GlcA-Man m/z 687	x	x			x		x	x
Paenan	I+II+III	I+II+III *	I	II	III	I+II	II+III	I+III
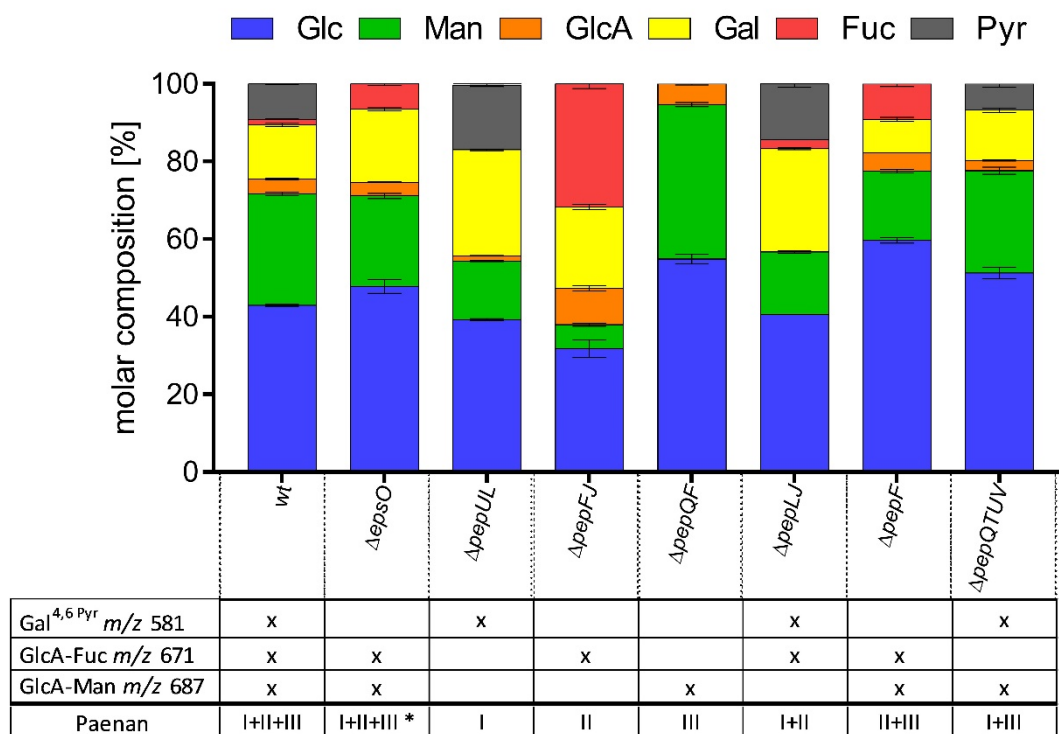
Fig. 2: Carbohydrate fingerprints of EPS obtained from *P. polymyxa* DSM 365 and mutant variants were analyzed via the HT-PMP method. Based on the obtained monomer ratios and the detection of specific dimers in MS analysis, polymer compositions were assigned to the presence of distinct paenan variants (I-III). * The *ΔepsO* variant demonstrated a similar monomer composition as the wildtype polymer, however, neither pyruvate nor the respective ketal were detected anymore.

The molecular weight of each variant was determined by size-exclusion chromatography (Table 1). Despite the presence of three distinct polymers in the wildtype EPS, no clear separation of individual paenan variants was possible (Figure S1). Analysis of individual paenan variants revealed a similar molecular weight distribution for paenan I and paenan III. Only paenan II seems to be significantly smaller with a size of $5.5 \cdot 10^5$ Da. Considering the low proportion of paenan II in the wildtype polymer, this might explain why previous attempts to analyse the heteroexopolysaccharide of *P. polymyxa* DSM 365 were not able to distinguish between multiple paenan variants (Madden et al., 1986; Rütering et al., 2017). Interestingly, while the depyruvylated polymer also showed a minor peak at approximately $3.0 \cdot 10^6$ Da, the main molar mass was detected at a considerable larger size of $8.8 \cdot 10^6$ Da compared to all other paenan variants. In comparison to the production of xanthan, for which side chains are irregularly decorated by acetyl- or pyruvyl residues, all repeating units of paenan I seem to be modified with a pyruvate ketal (Callet, Milas, & Rinaudo, 1987; Sandford et al., 1977). Consequently, the loss of this decoration in the *ΔepsO* knock-out variant might affect chain length control in *P. polymyxa,* resulting in an increased molecular weight and different rheological behavior. Alternatively, pyruvylation can also affect the hydrodynamic radius of the polymer and consequently influence SEC-MALS analysis (Baumgartner, Pavli, & Kristl, 2008; Smolka &

Belmonte, 2006).

Table 1: Calculated Mw of paenan variants obtained by GPC analysis using 0.5 % EPS solutions in 0.1 M LiNO3.

Paenan variant	Molecular weight
I & II & III	$2.6 \cdot 10^6$ Da
I & II & III depyruvylated	$8.8 \cdot 10^6$ Da
I	$5.8 \cdot 10^6$ Da
II	$5.5 \cdot 10^5$ Da
III	$3.9 \cdot 10^6$ Da
I & II	$2.8 \cdot 10^6$ Da
I & III	$2.8 \cdot 10^6$ Da
II & III	$2.7 \cdot 10^6$ Da
Xanthan reference	$4.5 \cdot 10^6$ Da

Rheological characteristics

Flow behavior of paenan-variants
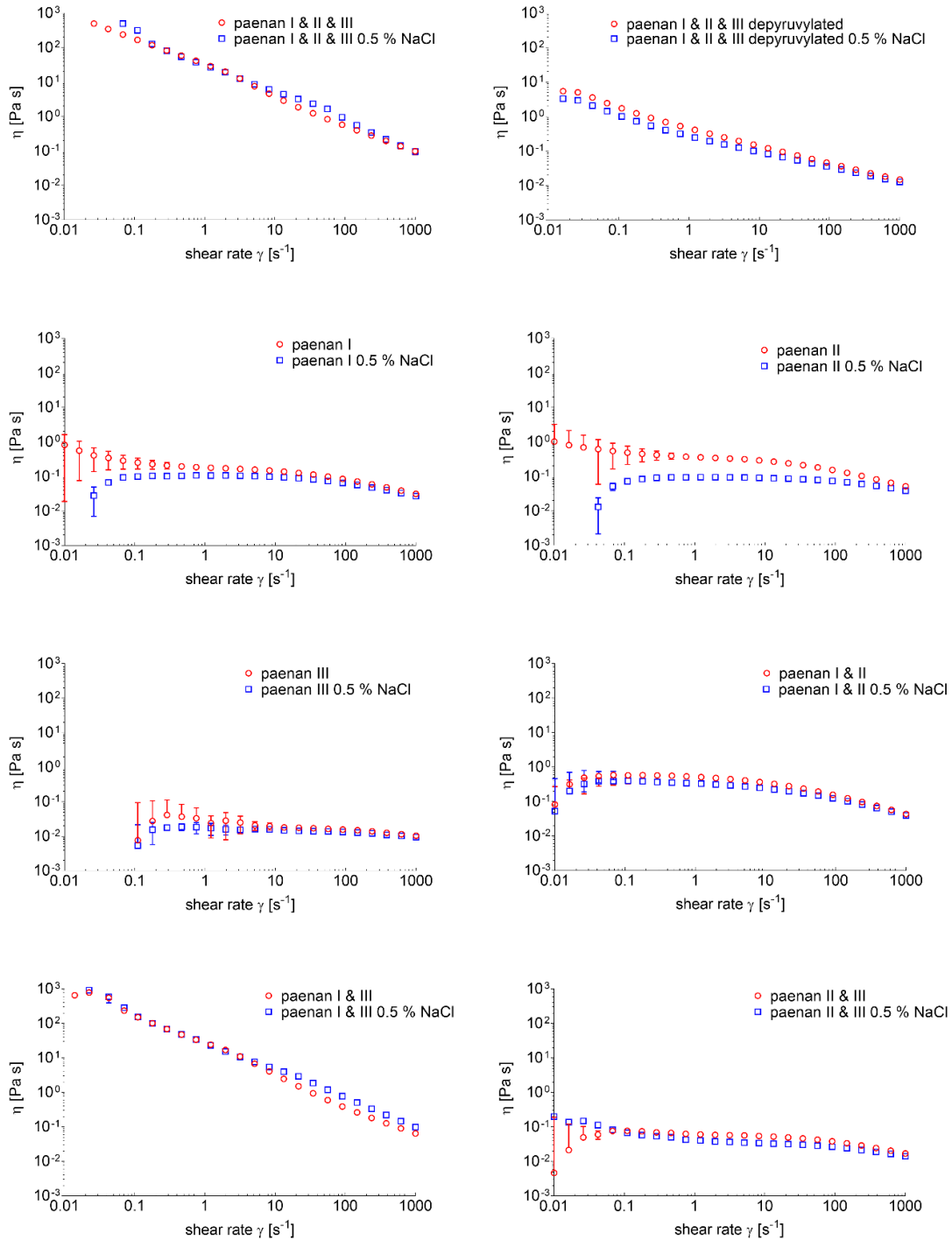
Fig. 3: Viscosity curves of paenan variants measured at logarithmically increasing shear rates from 0.01 to 1000 s^{-1} with a cone-and-plate geometry at 20 °C with (blue squares □) and without (red circles ○) the addition of 0.5 % NaCl. All measurements were carried out in triplicates, error bars show the standard deviation.

Investigations of the flow behavior showed a general shear thinning behavior of all paenan variants (Fig. 3). The highest viscosities and highest shear thinning behavior was observed for paenan wt (I & II & III) with the addition of NaCl, followed by paenan wt without monovalent cations. All individual variants of paenan I-III did not show significantly high viscosities and almost Newtonian flow behavior in the interme-diated shear rate regions. Only the paenan wt as well as paenan I & III showed strictly power-law shear thinning behavior and high viscosities, which increased in the presence of 0.5 % NaCl. Upon depyruvylation of paenan wt, the viscosity drastically decreased and the addition of NaCl now had the adverse effect, comparable to the depyruvylation of xanthan (Gansbiller, Schmid, & Sieber, 2019). For xanthan, the effect is due to lower cation mediated intermolecular interactions between individual polymer molecules. The data of the different paenan polymers suggest a similar effect between the paenan I and paenan III mole-cules. The combination of paenan I & III showed almost the same properties as the combination of paenan I & II & III, underlining the interaction between paenan I and III as the main origin of the high viscosity of the polymers. This interaction may be explained by the cation mediated interaction of the terminal py-ruvate residue of paenan I with the negative charge of the glucuronic acid in the backbone of paenan III. Interestingly, both combinations of paenan I & II and paenan II & III did not result in the behavior of the wildtype. Consequently, the glucuronic acid in the backbone of paenan II did not seem to interact with the pyruvyl residue of paenan I as seen by the low viscosity of this combination. This is particularly interesting, as the single side chain of paenan II would suggest higher accessibility of the charge in paenan II compared to the two side-chains of paenan III, linked to the glucuronic acid and the adjacent mannose (Fig. 1). There are two explanations for the interactions of the individual molecules. First, the formation of individual homohelices of paenan I & II & III molecules respectively and a subsequent interaction of these helices. Second, the formation of heterohelices of paenan I & II & III. Investigation of the individual polymers pro-vides evidence for the latter. The formation of homohelices would also suggest strong interactions be-tween the ones of paenan I alone, if, as suggested the pyruvylated side chain was protruding outwards, like in xanthan. On the other hand, an inwards-protruding side chain, if paenan I was forming homohelices, would result in a similar structure as it is described for diutan gum (Xu, Gong, Dong, & Li, 2015) and might also be the reason for decreased viscosity. As opposed to diutan gum, the main chain does not carry a negative charge due to the lack of an uronic acid in the backbone of paenan I. In all cases, differences in the helical arrangements of paenan II and paenan III could explain the strong interactions of paenan I & III but not between paenan I & II as well as between paenan II & III, giving rise to further investigations of the secondary and tertiary polymer structures.

A detailed investigation of the individual polymer variants and the combination of paenan II & III showed multiple shear thinning regions, indicated by up to three different K and n values of the power law fits of the individual sections (Table 2). This phenomenon was evident for paenan I and paenan II individually as well as for combinations of paenan I & II and paenan I & III. However, for paenan III, paenan I & III or the wildtype composition, only a single shear thinning region was observed. In case of paenan I & II, the New-tonian region is more pronounced in the presence of NaCl, which could be the reason of the slight onset

of a Newtonian region in paenan wt and paenan I & III in the presence of NaCl. Consequently, this effect might be attributed to paenan I and paenan II respectively, which was previously discussed to be caused by shear-banding (Gansbiller, Schmid, & Sieber, 2020; Rütering et al., 2018).

Table 2: Model parameters (K, n) of the power law fits of the different paenan combinations with and without the addition of 0.5 % NaCl. If multiple sections were fitted individually, K and n values of the individual section are shown in ascending order of the corresponding shear rate-region.

Paenan variant	Solution	K	n
wt (I & II & III)	aq.	29.02	0.152
	0.5 % NaCl	34.38	0.171
wt (I & II & III) depyruvylated	aq.	0.47	0.485
	0.5 % NaCl	0.29	0.534
I & II	aq.	0.01	0.830
	0.5 % NaCl	0.01	0.850
I & III	aq.	24.80	0.114
	0.5 % NaCl	27.41	0.203
II & III	aq.	0.06 /0.16	0.924/0.679
	0.5 % NaCl	0.03/0.05/0.10	0.677/0.890/0.718
I	aq.	0.05/0.18/0.52	0.390/0.898/0.597
	0.5 % NaCl	0.11/0.255	1*/0.685
II	aq.	0.20/0.37/1.24	0.649/0.895/0.542
	0.5 % NaCl	0.10/0.26	0.978/0.73
III	aq.	0.03	0.86
	0.5 % NaCl	0.02	0.917

*indicating Newtonian flow behavior

Viscoelastic properties

The basic viscoelastic properties determined by the amplitude sweep (Figure S2-3) are shown in Table 3. Paenan wt (I & II & III) displayed a soft and elastic gel-like behavior with a yield point of 9.1 Pa (32 % strain) and a flow point of 51.1 Pa (550 % strain) with a damping factor of 0.3 within the LVE. The addition of 0.5 % NaCl resulted in an increased yield and flow point of 32.3 Pa and 90.8 Pa respectively, corresponding to a strain of 82 % and 590 %. Damping factor of 0.1 and the distinct G'' peak following the LVE indicates a stronger but more brittle gel character. Frequency sweeps (Figure S4) also revealed a viscoelastic fluid like behavior of G' and G'' for paenan I & II & III with predominant elastic behavior throughout the investigated frequency range, which shifted more towards a gel-like behavior upon the addition of NaCl with lower frequency dependency of both G' and G''. Both, with and without addition of NaCl, no crossover point was evident at low frequencies, indicating long term stability of the network.

This gel character is most likely caused by the cation mediated interactions between the pyruvyl residues of paenan I and the -COO⁻ group of the glucuronic acid of paenan III. Further proof for this was provided by the depyruvylation of paenan I & II & III, which resulted in a complete loss of the viscoelastic properties. Furthermore, all individual paenan polymers as well as the mixtures of paenan I & II and paenan II & III showed predominant fluid properties, with Maxwell-like behavior (Figure S4-5). Interestingly, except for paenan II in the presence of NaCl, no Maxwell-fluid-typical crossover point at higher frequencies could be observed and data suggested an onsetting decrease of G' at higher frequencies, resulting in fluid behavior at both low and high frequencies. This was especially evident for paenan I and paenan III.

The high viscosity and the pronounced intermolecular network resulting in a gel-like character make this polymer variant an interesting compound as a rheological thickening agent. Similar to other microbial polysaccharides, potential applications as rheology modifiers in food and beverages but also technical applications such as oil drilling seem promising (Schmid, Sieber, & Rehm, 2015). Compared to those polysaccharides, viscosifying effects are highly increased, suggesting that lower EPS concentrations are required to obtain similar results. Furthermore, the structurally related polysaccharide from *P. polymyxa* 2H2 has recently demonstrated excellent compatibility with commonly used surfactants such as lauryl sulfate or cocamidopropyl betaine, which are typically used cosmetics and daily care products (Rütering et al., 2018). Consequently, we propose the utilization of the wildtype EPS composition of *P. polymyxa* DSM 365, containing paenan I & II & III as a sustainable thickening agent for variable applications that could replace commercially available petroleum-based acrylic compounds (Kim, Song, Lee, & Park, 2003; Tafuro, Costantini, Baratto, Busata, & Semenzato, 2019).

Table 3: Viscoelastic properties of the paenan polymer variants. n.d.: not determined if measurement was not possible

Paenan variant	Solution	G' [Pa] (LVE)	tanδ (LVE)	Yield point [Pa]	Flow point [Pa]
wt (I & II & III)	aq.	28.5	0.3	9.1	51.1
	0.5 % NaCl	45.5	0.1	32.3	90.8
wt (I & II & III) depyruvylated	aq.	0.71	1.0	n.d.	n.d.
	0.5 % NaCl	n.d.	1.0	n.d.	n.d.
I	aq.	0.15	5.1	n.d.	n.d.
	0.5 % NaCl	0.10	6.7	n.d.	n.d.
II	aq.	0.60	3.0	n.d.	n.d.
	0.5 % NaCl	n.d.	n.d.	n.d.	n.d.
III	aq.	n.d.	n.d.	n.d.	n.d.
	0.5 % NaCl	n.d.	n.d.	n.d.	n.d.
I & II	aq.	0.78	2.6	n.d.	n.d.
	0.5 % NaCl	0.40	3.6	n.d.	n.d.
I & III	aq.	13.9	0.25	11	40
	0.5 % NaCl	35.8	0.1	18	79
II & III	aq.	n.d.	n.d.	n.d.	n.d.
	0.5 % NaCl	n.d.	n.d.	n.d.	n.d.

The paenan I & III mixture showed gel-like properties very similar to the ones of paenan I & II & III, indicating that the interaction is mainly between paenan I and paenan III. However, compared to paenan I & II & III, paenan I & III showed lower gel-strength with yield points at 11 Pa and 18 Pa with and without the presence of 0.5 % NaCl, and a less pronounced G'' peak at the end of the LVE region in the presence of NaCl. This indicates weaker interactions of these polymers. Investigations of the amplitude sweeps of the

individual polymers showed that paenan I and II both show viscoelastic fluid like behavior, while paenan III only shows strictly liquid behavior. Without the formation of gel-like networks, the addition of NaCl resulted in a decrease of both G' and G'', while paenan I exhibited higher salt stability compared to paenan II. This also becomes evident in the mixture of paenan I & II, where the effect of NaCl is more comparable to paenan I than paenan II. These effects point toward an interaction between paenan I and II, which might be responsible for the increased gel strength in paenan I & II & III compared to paenan I & III. As both paenan II and paenan III have a glucuronic acid in the backbone, the strong interaction of paenan I & III suggests a better accessibility of the glucuronic acid of paenan III compared to the one of paenan II. Contrarily, interactions between paenan II and paenan III might lead to a different structural arrangement of these polymers, resulting in better accessibility of the glucuronic acid in paenan II and therefore to increased interactions between paenan I & II in the wt polymer mixture.

In contrast to the native polysaccharide composition containing paenan I & II & III, deletion of individual polymers resulted in significantly altered viscoelastic properties. While the combination of paenan I & III still demonstrated a pronounced intermolecular network resulting in a gel like character, individual biopolymers demonstrated fluid like behavior, which still form films when dried. Consequently, significantly different applications to the wildtype EPS composition arise. On the one hand, bulk application for the formation of edible films and packaging materials similar to pullulan seem practical (Diab, Biliaderis, Gerasopoulos, & Sfakiotakis, 2001). On the other hand, high value biomedical applications as coating materials in pharmaceutical controlled drug release systems should be further investigated (Miao, Wang, Zeng, Liu, & Chen, 2018). For other charged polysaccharides such as hyaluronic acid and alginates, the chemical modification of the functional groups improved targeting of specific cell types allowing effective drug delivery systems (Bhattacharya et al., 2017; Pawar & Edgar, 2012). Furthermore, polysaccharides produced by other strains of *P. polymyxa* have demonstrated anti-oxidant activities, which might further enhance pharmacological applications (Liu et al., 2010; Raza et al., 2011).

Temperature stability and thixotropic properties
Temperature sweeps showed high temperature dependency of the viscoelastic properties of paenan I & II & III both with and without the addition of NaCl (Figure S6-7). The viscoelastic properties of paenan I & III showed even higher temperature dependency, which could be reduced by the addition of NaCl. While the native polysaccharide composition containing all three paenan variants retained a weak gel character up to 75 °C in the presence of NaCl, deletion of paenan II resulted in a loss of temperature stability. This suggests a stabilizing effect of paenan II regarding to temperature stability of the polymer network, which is also evident by the high temperature stability of paenan II compared to paenan I & III. For paenan II, an increase of G' and G'' could be observed during the heating ramp, which was further pronounced by the addition of NaCl. This effect is similar to the one seen in the undecorated xanthan variant previously described (Gansbiller et al., 2019) and might also be explained by structural rearrangements of the single polymer. However, these effects did not occur in any other combination of paenan II with other paenan

polymers, suggesting a different arrangement of the individual polymers in mixture, which underlines the previously described differences between paenan I & II & III and paenan I & III in regards to their viscoelastic properties.

Table 4: Temperature stability of different paenan variants. n.d.: not determined if measurement was not possible within the LVE range

Paenan Variant	Solution	G' at 20°C	G' at 75°C	relative Gel strength at 75°C [%]	tanδ at 75°C
wt (I & II & III)	aq.	29.43	1.15	3.91	1.49
	0.5 % NaCl	51.97	5.01	9.65	0.83
wt (I & II & III) depyruvylated	aq.	0.40	0.00	0.15	n.d.
	0.5 % NaCl	0.18	0.00	0.13	n.d.
I	aq.	0.17	0.01	6.19	22.29
	0.5 % NaCl	0.07	0.00	0.00	n.d.
II	aq.	0.269	n.d.	n.d.	n.d.
	0.5 % NaCl	n.d.	n.d.	n.d.	n.d.
III	aq.	0.139	n.d.	n.d.	n.d.
	0.5 % NaCl	0.139	n.d.	n.d.	n.d.
I & II	aq.	0.31	0.01	4.20	28.02
	0.5 % NaCl	0.08	0.00	0.00	n.d.
I & III	aq.	12.20	0.00	0.00	n.d.
	0.5 % NaCl	35.03	0.07	0.20	35.90
II & III	aq.	0.78	0.20	26.05	1.25
	0.5 % NaCl	0.78	0.12	15.71	1.23

Furthermore, thixotropic properties were determined by a three stage oscillatory shear stress test (Table S3). While structural recovery was observed for all combinatorial variants of paenan, only 86.8 % of the initial gel strength was measured after three minutes with a non-destructive shear stress for the wildtype EPS mixture. This further underlines a pronounced intermolecular network, which takes more time to recover and coordinate non-covalent interactions between individual polymers. Similar effects of a retarded structural recovery were observed for polysaccharide composition containing paenan I & III, consolidating the hypothesis that the gel-like character mainly originates from the interaction between the pyruvate of

paenan I and the glucuronic acid residue of paenan III. Contrarily, for all other knock-out variants, immediate structural recovery resulting in the initial gel strength was observed. Consequently, distinct variants might be applicable as binders that convey thixotropic behavior typically used for varnishes and coatings with divergent rheological profiles.

Conclusion

In this study, we have characterized the rheological behavior of the heteroexopolysaccharides produced by *P. polymyxa* DSM 365, using CRISPR-Cas9 mediated knock-outs of glycosyltransferases. Viscoelastic properties of individual paenan variants and combinations thereof were analyzed in detail. While the wildtype EPS composition demonstrated high viscosity and a gel-like behavior, knock-out variants showed significantly altered physicochemical properties depending on the present individual polysaccharides. Consequently, distinct polysaccharide compositions might be utilized for a wide range of applications such as thickening agents or coating materials. We propose specific intra- but also intermolecular network formations that seem to be highly affected by the presence of distinct pyruvyl- and glucuronic acid residues. Additional analytical approaches such as atomic force microscopy might be necessary to further investigate the precise interaction of individual biopolymers and putative secondary and tertiary structures.

Acknowledgements

References

Bajaj, I., Survase, S., Saudagar, P., & Singhal, R. (2007). Gellan Gum: Fermentative Production, Downstream Processing and Applications. Food Technology and Biotechnology, 45.

Baumgartner, S., Pavli, M., & Kristl, J. (2008). Effect of calcium ions on the gelling and drug release characteristics of xanthan matrix tablets. European Journal of Pharmaceutics and Biopharmaceutics, 69(2), 698–707.

Becker, A., Katzen, F., Pühler, A., & Ielpi, L. (1998). Xanthan gum biosynthesis and application: A biochemical /genetic perspective. Applied Microbiology and Biotechnology, 50(2), 145–152.

Bhattacharya, D. S., Svechkarev, D., Souchek, J. J., Hill, T. K., Taylor, M. A., Natarajan, A., & Mohs, A. M. (2017). Impact of structurally modifying hyaluronic acid on CD44 interaction. J. Mater. Chem. B, 5(41), 8183–8192.

Burdick, J. A., & Prestwich, G. D. (2011). Hyaluronic Acid Hydrogels for Biomedical Applications. Advanced Materials, 23(12), H41–H56.

Callet, F., Milas, M., & Rinaudo, M. (1987). Influence of acetyl and pyruvate contents on rheological properties of xanthan in dilute solution. International Journal of Biological Macromolecules, 9(5), 291–293.

Danese, P. N., Pratt, L. A., & Kolter, R. (2000). Exopolysaccharide Production Is Required for Development

of *Escherichia coli* K-12 Biofilm Architecture. Journal of Bacteriology, 182(12), 3593–3596.

De Mas, C., Jansen, N. B., & Tsao, G. T. (1988). Production of optically active 2,3-butanediol by *Bacillus polymyxa*. Biotechnology and Bioengineering, 31(4), 366–377.

Diab, T., Biliaderis, C. G., Gerasopoulos, D., & Sfakiotakis, E. (2001). Physicochemical properties and application of pullulan edible films and coatings in fruit preservation. Journal of the Science of Food and Agriculture, 81(10), 988–1000.

Freitas, F., Alves, V. D., & Reis, M. A. M. (2011). Advances in bacterial exopolysaccharides: From production to biotechnological applications. Trends in Biotechnology, 29(8), 388–398.

Gansbiller, M., Schmid, J., & Sieber, V. (2019). In-depth rheological characterization of genetically modified xanthan-variants. Carbohydrate Polymers, 213, 236–246.

Gansbiller, M., Schmid, J., & Sieber, V. (2020). Rheology of sphingans in EPS–surfactant systems. Carbohydrate Polymers, 248, 116778.

Grady, E. N., MacDonald, J., Liu, L., Richman, A., & Yuan, Z.-C. (2016). Current knowledge and perspectives of *Paenibacillus*: A review. Microbial Cell Factories, 15(1), 203.

Hassler, R. A., & Doherty, D. H. (1990). Genetic engineering of polysaccharide structure: Production of variants of xanthan gum in *Xanthomonas campestris*. Biotechnology Progress, 6(3), 182–187.

Jang, H. Y., Zhang, K., Chon, B. H., & Choi, H. J. (2015). Enhanced oil recovery performance and viscosity characteristics of polysaccharide xanthan gum solution. Journal of Industrial and Engineering Chemistry, 21, 741–745.

Kahng, G.-G., Lim, S.-H., Yun, H.-D., & Seo, W.-T. (2001). Production of extracellular polysaccharide, EPS WN9, from *Paenibacillus* sp. WN9 KCTC 8951P and its usefulness as a cement mortar admixture. Biotechnology and Bioprocess Engineering, 6(2), 112–116.

Kaur, V., Bera, M. B., Panesar, P. S., Kumar, H., & Kennedy, J. F. (2014). Welan gum: Microbial production, characterization, and applications. International Journal of Biological Macromolecules, 65, 454–461.

Kim, J.-Y., Song, J.-Y., Lee, E.-J., & Park, S.-K. (2003). Rheological properties and microstructures of Carbopol gel network system. Colloid & Polymer Science, 281(7), 614–623.

Kumar, A., Rao, K. M., & Han, S. S. (2018). Application of xanthan gum as polysaccharide in tissue engineering: A review. Carbohydrate Polymers, 180, 128–144.

Liu, J., Luo, J., Ye, H., Sun, Y., Lu, Z., & Zeng, X. (2010). In vitro and in vivo antioxidant activity of exopolysaccharides from endophytic bacterium *Paenibacillus polymyxa* EJS-3. Carbohydrate Polymers, 82(4), 1278–1283.

Madden, J. K., Dea, I. C. M., & Steer, D. C. (1986). Structural and rheological properties of the extracellular polysaccharides from *Bacillus polymyxa*. Carbohydrate Polymers, 6(1), 51–73.

Miao, T., Wang, J., Zeng, Y., Liu, G., & Chen, X. (2018). Polysaccharide-Based Controlled Release Systems for Therapeutics Delivery and Tissue Engineering: From Bench to Bedside. Advanced Science, 5(4), 1700513.

Moradali, M. F., & Rehm, B. H. A. (2020). Bacterial biopolymers: From pathogenesis to advanced materials. Nature Reviews Microbiology. Retrieved February 18, 2020, from http://www.nature.com/articles/s41579-019-0313-3

Ninomiya, E., & Kizaki, T. (1969). Bacterial polysaccharide from *Bacillus polymyxa* No. 271. Die Angewandte Makromolekulare Chemie, 6(1), 179–185.

Ophir, T., & Gutnick, D. L. (1994). A Role for Exopolysaccharides in the Protection of Microorganisms from Desiccation. Applied and Environmental Microbiology, 60(2), 740.

Pawar, S. N., & Edgar, K. J. (2012). Alginate derivatization: A review of chemistry, properties and applications. Biomaterials, 33(11), 3279–3305.

Poli, A., Anzelmo, G., & Nicolaus, B. (2010). Bacterial Exopolysaccharides from Extreme Marine Habitats: Production, Characterization and Biological Activities. Marine Drugs, 8(6), 1779–1802.

Raza, W., Makeen, K., Wang, Y., Xu, Y., & Qirong, S. (2011). Optimization, purification, characterization and antioxidant activity of an extracellular polysaccharide produced by *Paenibacillus polymyxa* SQR-21.

Bioresource Technology, 102(10), 6095–6103.

Rodén, L., Baker, J. R., Cifonelli, J., & Mathews, M. B. (1972). [7] Isolation and characterization of connective tissue polysaccharides. Methods in Enzymology (Vol. 28, pp. 73–140). Elsevier. Retrieved April 3, 2020, from https://linkinghub.elsevier.com/retrieve/pii/0076687972280090

Rühmann, B., Schmid, J., & Sieber, V. (2014). Fast carbohydrate analysis via liquid chromatography coupled with ultra violet and electrospray ionization ion trap detection in 96-well format. Journal of Chromatography A, 1350, 44–50.

Rühmann, B., Schmid, J., & Sieber, V. (2016). Automated Modular High Throughput Exopolysaccharide Screening Platform Coupled with Highly Sensitive Carbohydrate Fingerprint Analysis. Journal of Visualized Experiments, (110), 53249.

Rütering, M., Cress, B. F., Schilling, M., Rühmann, B., Koffas, M. A. G., Sieber, V., & Schmid, J. (2017). Tailor-made exopolysaccharides—CRISPR-Cas9 mediated genome editing in *Paenibacillus polymyxa*. Synthetic Biology, 2(1). Retrieved July 1, 2019, from http://academic.oup.com/synbio/article/doi/10.1093/synbio/ysx007/4772606

Rütering, M., Schmid, J., Gansbiller, M., Braun, A., Kleinen, J., Schilling, M., & Sieber, V. (2018). Rheological characterization of the exopolysaccharide Paenan in surfactant systems. Carbohydrate Polymers, 181, 719–726.

Sandford, P. A., Pittsley, J. E., Knutson, C. A., Watson, P. R., Cadmus, M. C., & Jeanes, A. (1977). Variation in Xanthomonas campestris NRRL B-1459: Characterization of Xanthan Products of Differing Pyruvic Acid Content. In Paul A. Sandford & A. Laskin (Eds.), Extracellular Microbial Polysaccharides, ACS Symposium Series (Vol. 45, pp. 192–210). WASHINGTON, D. C.: AMERICAN CHEMICAL SOCIETY. Retrieved October 13, 2020, from https://pubs.acs.org/doi/abs/10.1021/bk-1977-0045.ch015

Schilling, C., Badri, A., Sieber, V., Koffas, M., & Schmid, J. (2020). Metabolic engineering for production of functional polysaccharides. Current Opinion in Biotechnology, 66, 44–51.

Schilling, C., Ciccone, R., Sieber, V., & Schmid, J. (2020). Engineering of the 2,3-butanediol pathway of *Paenibacillus polymyxa* DSM 365. Metabolic Engineering, 61, 381–388.

Schilling, C., Klau, L.J., Rühmann, B., Aachmann, F.L., Schmid, J., & Sieber, V. (2022a). Structural elucidation of the fucose containing exopolysaccharide from *Paenibacillus polymyxa* DSM 365. Carbohydrate Polymers, 278

Schilling, C., Klau, L.J., Rühmann, B., Aachmann, F.L., Schmid, J., & Sieber, V. (2022b). CRISPR-Cas9 driven structural elucidation of the heteroexopolysaccharides from *Paenibacillus polymyxa* DSM 365. Prepared Manuscript.

Schmid, J., Sieber, V., & Rehm, B. (2015). Bacterial exopolysaccharides: Biosynthesis pathways and engineering strategies. Frontiers in Microbiology, 6. Retrieved July 1, 2019, from http://www.frontiersin.org/Microbiotechnology%2c_Ecotoxicology_and_Bioremediation/10.3389/fmicb.2015.00496/abstract

Smolka, L. B., & Belmonte, A. (2006). Charge screening effects on filament dynamics in xanthan gum solutions. Journal of Non-Newtonian Fluid Mechanics, 137(1–3), 103–109.

Sutherland, I. W. (1972). Bacterial Exopolysaccharides. Advances in Microbial Physiology (Vol. 8, pp. 143–213). Elsevier. Retrieved October 12, 2020, from https://linkinghub.elsevier.com/retrieve/pii/S0065291108601903

Tafuro, G., Costantini, A., Baratto, G., Busata, L., & Semenzato, A. (2019). Rheological and Textural Characterization of Acrylic Polymer Water Dispersions for Cosmetic Use. Industrial & Engineering Chemistry Research, 58(51), 23549–23558.

Williams, P. A., & Phillips, G. O. (Eds.). (2016). Gums and stabilisers for the food industry 18: Hydrocolloid functionality for affordable and sustainable global food solutions. Special publication / Royal Society of Chemistry. Presented at the Gums and Stabilisers for the Food Industry Conference, Cambridge, UK: Royal Society of Chemistry.

Wu, M., Qu, J., Tian, X., Zhao, X., Shen, Y., Shi, Z., Chen, P., et al. (2019). Tailor-made polysaccharides

containing uniformly distributed repeating units based on the xanthan gum skeleton. International Journal of Biological Macromolecules, 131, 646–653.

Xu, L., Gong, H., Dong, M., & Li, Y. (2015). Rheological properties and thickening mechanism of aqueous diutan gum solution: Effects of temperature and salts. Carbohydrate Polymers, 132, 620–629.

4.3 Influence of acetylation and pyruvylation patterns on the rheological properties of xanthan

In this study, seven xanthan variants with unique acetylation and pyruvylation patterns have been created by genetic modification of the producing strain *X. campestris* LMG 8031. Their rheological properties were evaluated in comparison to the wildtype and their specific acetylation and pyruvylation pattern. Additionally, the impact of cations in form of sodium chloride and calcium chloride were evaluated to gain insight into the decoration patterns on the masking of charges within the polymer sidechain and relate these interactions with the rheological properties. The study revealed that the high viscosity behavior of xanthan is linked to the degree of the ordered helical structure, with higher degree of unordered structures leading to higher viscosities. The overall viscoelastic or gel-like behavior is governed by the degree of pyruvylation, which increases cation mediated interactions between the different side chains. Due to the precisely created acetylation patterns of the inner and outer mannose of the xanthan-sidechain individually by deleting the respective transferases by gene editing, it allowed to pinpoint the precise effect of each acetyl residue on the rheological properties and linking it to the structural properties. It was concluded that pyruvate plays a role in destabilizing the sidechain orientation while acetyl residues seem to stabilize it, leading to lower and higher degrees of ordered structure, resp., which in term governs the rheological properties. Furthermore, the acetylation of the inner mannose seems to be most important for this stabilization and also plays an essential role in the polymer's temperature stability. Another important conclusion drawn from this study, was that the deletion of the individual acetyl- and pyruvyl-transferases and plasmid-based expression did not affect the productivity for xanthan, which is important for the creation of novel xanthan variants, which are the main goal in the second part of this work.

Moritz Gansbiller was involved with the conceptualization, methodology, validation, formal analysis, investigation, data curation, writing and visualization of the original draft.

Jochen Schmid was involved in the conceptualization, methodology, validation, visualization, reviewing and editing the original draft as well as supervision, resource provision and project administration and funding acquisition.

Volker Sieber was involved in conceptualization, supervision, methodology, validation, reviewing and editing the original draft as well as resource provision, project administration and funding acquisition.

Contents lists available at ScienceDirect

Carbohydrate Polymers

journal homepage: www.elsevier.com/locate/carbpol

In-depth rheological characterization of genetically modified xanthan-variants

Moritz Gansbiller[a], Jochen Schmid[a,b], Volker Sieber[a,c,d,e,*]

[a] Chair of Chemistry of Biogenic Resources, Technical University of Munich, Campus for Biotechnology and Sustainability, Schulgasse 16, 94315, Straubing, Germany
[b] Chair of Bioprocess Engineering, Technical University of Munich, Campus for Biotechnology and Sustainability, Schulgasse 16, 94315, Straubing, Germany
[c] Fraunhofer IGB, Straubing Branch BioCat, Schulgasse 23, 94315, Straubing, Germany
[d] TUM Catalysis Research Center, Ernst-Otto-Fischer-Straße 1, 85748, Garching, Germany
[e] The University of Queensland, School of Chemistry and Molecular Biosciences, 68 Copper Road, St. Lucia, 4072, Australia

ARTICLE INFO

ABSTRACT

Xanthan is an extensively studied viscosifying agent discovered in 1961. Acetylation and pyruvylation have a major influence on its rheological properties and the effect of these groups on the conformation and rheological properties of xanthan have been studied for decades. However, these studies rely mainly on chemical modifications and therefore the degree of pyruvylation and acetylation as well as regioselectivity of deacetylation cannot be controlled. Here, we present an in-depth rheological characterization of natural xanthan and seven xanthan-variants, with defined acetylation and pyruvylation patterns created via genetic modification of Xanthomonas campestris LMG 8031. By that approach xanthan-variants with defined acetylation and pyruvylation patterns in their most natural state due to the mild production conditions were obtained. It was possible to link the defined substituent patterns to their corresponding rheological properties to give novel structure-function relationship insights of xanthan-variants in salt-free environments and in the presence of mono- and divalent cations.

1. Introduction

Xanthan, the exopolysaccharide produced by *Xanthomonas campestris* is one of the most commonly used microbial exopolysaccharides as a thickening agent for a wide range of industrial applications, due to its commercial availability (Becker, Katzen, Pühler, & Ielpi, 1998). Natural xanthan's field of application ranges from food, cosmetic and pharmaceutical products to construction and oil drilling industry (Palaniraj & Jayaraman, 2011). xanthan biosynthesis follows the Wzx/Wzy-pathway (Schmid, Sieber, & Rehm, 2015) and the 12 involved genes *gumB-gumH* are arranged in the 16 kilobasepairs (kbp) *gum*-cluster (Katzen, Becker, Zorreguieta, Pühler, & Ielpi, 1996). The genes *gumD, -M, -H, -K and -I* are involved in the synthesis of the pentasaccharide repeating unit (Becker et al., 1998; Ielpi, Couso, & Dankert, 1981; Vorhölter, Schneiker, Goesmann, Krause, & Bekel, 2008), while the genes *gumB, -C, -E* and *-J* are involved in polymerization and export of the polysaccharide (Becker et al., 1998; Galvan et al., 2013; Ielpi et al., 1981; Vorhölter et al., 2008). The repeating unit of xanthan consists of two ß-(1→4) linked ß-D-glucose (Glc) units as backbone and a trisaccharide side-chain, α-(1→3)-linked to every other glucose. The sidechain is composed of α-D-mannose (Man), ß-D-glucuronic acid (GlcA) and ß-D-mannose (Man), which are ß-(1→2) and ß-(1→4) linked to another, respectively (Jansson, Kenne, & Lindberg, 1975). In its natural state the α-D-Man is acetylated by the acetyltransferase GumF and the ß-D-Man is either acetylated or pyruvylated by the acetyltransferase GumG or pyruvate ketalase GumL, respectively (Jansson et al., 1975). The total amount of substituents highly depends on the used strain as well as culture conditions and can range from 6.5% to 13% for acetate and 2.8% to 14% for pyruvate (Abbazadeh et al., 2015; Garcia-Ochoa, Santos, Casas, & Gomez, 2000; Li & Feke, 2015). While xanthan exhibits excellent thickening properties over a wide range of pH and temperature (Garcia-Ochoa et al., 2000), the influence of salts on its rheological behavior is remarkable and has been widely studied (Bergmann, Furth, & Mayer, 2008; Callet, Milas, & Rinaudo, 1987; Dário, Hortêncio, Sierakowski, Neto, & Petri, 2011; Galván et al., 2018; Xu, Dong, Gong, Sun, & Li, 2015). Because of the regioselectivity of the transferases, it is possible, to create xanthan-variants with specific acetylation and pyruvylation-patterns by deletions of the genes *gumF, gumG* and *gumL* and combinations thereof. Although there have been recent studies about the impact of acetylation and pyruvylation of xanthan on its

---

* Corresponding author at: Chair of Chemistry of Biogenic Resources, Technical University of Munich, Schulgasse 16, 94315, Straubing, Germany.
  E-mail addresses: m.gansbiller@tum.de (M. Gansbiller), j.schmid@tum.de (J. Schmid), sieber@tum.de (V. Sieber).

physicochemical properties (Khouryieh, Herald, Aramouni, Bean, & Alavi, 2007; Kool, Gruppen, Sworn, & Schols, 2013a, Kool, Gruppen, Sworn, & Schols, 2014; Kool, Schols et al., 2013; Smith, Symes, Lawson, & Morris, 1981; Tako & Nakamura, 1984, 1988), these studies focus mainly on the conformational aspects. Moreover, these studies only characterize chemically modified xanthan, and processing often includes heating and cooling steps, which are known to alter the conformation and therefore its physicochemical properties (Bradshaw, Nisbet, Kerr, & Sutherland, 1983; Khouryieh et al., 2007). Some studies exist, which describe xanthan-variants produced by genetic modification of *X. campestris* (*Xcc*), however, they only describe the impact of substitution-pattern on the viscosity in dilute systems (Hassler & Doherty, 1990). While a recent study describes a genetically modified xanthan variant, the sole focus is on a maximum pyruvylated xanthan variant lacking acetylation of both mannose residues (Wu et al., 2018). The aim of this study is therefore to give an in-depth rheological characterization of xanthan-variants with defined acetylation and pyruvylation-patterns. These variants are produced by genetically modified *X. campestris* LMG 8031 strains, under mild conditions, to yield the most natural conformation of the modified polysaccharide variants. Another key aspect of this study is the investigation of the influence of cations on these variants. A comparison with most recent studies on xanthan's structure will give a revised insight on the structure-function-relationship of xanthan and elude how acetylation and pyruvylation influences its rheological properties in the absence and presence of salts. These variants are interesting for industrial application as they can be produced under identical established biotechnological production methods while having tailor-made properties like increased or decreased viscosity as well as altered impact of salt content or temperature on the rheological properties of the product. These properties can make the superior to the wild type concerning higher temperature stability or salt tolerance, as necessary for example in enhanced oil recovery or some cosmetic formulations.

2. Materials and methods

2.1. Fermentative cultivation of strains and production of xanthan

Xanthomonas campestris pv. campestris LMG 8031 (*Xcc*) (BCCM, Gent, Belgium) and deletion variants thereof were cultured at 30 °C in MM1 P100 as previously described (Rütering, Schmid, Rühmann, Schilling, & Sieber, 2016) containing 30 g L^{-1} glucose as carbon source. The fermentative production of xanthan and engineered variants thereof were carried out in a 2 L-benchtop fermenter (Biostat B plus, Sartorius AG, Germany) equipped with two 6 blade-stirrers over 48 h with a controlled pH of 6.8 and a pO$_2$ of 30% saturation. All fermentations were performed with a starting OD of 0.1 by inoculation with an appropriate volume of preculture. The precultures were grown in 50 ml of MM1 P100 Media containing 30 g L^{-1} glucose in 250 ml baffled Erlenmeyer-flasks over night at 250 rpm, 30 °C.

2.2. Preparation of competent cells

Electrocompetent *Xanthomonas* cells were produced by a method described by Wang, Zheng, and Liang (2016), with minor variations (Wang et al., 2016). In detail, 50 ml of cell cultures were grown to an OD$_{600}$ between 0.6 and 1.0, centrifuged (7500 g, 20 °C, 5 min) in a 50 ml conical tube, the pellet was washed in 20 ml 250 mM sucrose 3 times by resuspending and centrifugation (7500 g, 20 °C, 5 min) and finally resuspended in 1 ml of 250 mM sucrose. 100 µl aliquots were used right away for transformation or stored at −80 °C.

2.3. Creation of Xanthomonas deletion-mutants

For the creation of deletion mutants, homologous recombination with pK19Gm, a derivative of pK19mobsacB with the kanamycin

resistance exchanged with gentamicin resistance was applied. For the deletion of genes in *Xcc* two 500 base pair (bp)-fragments up- and downstream of the genes of interest were amplified via PCR, using isolated genomic DNA (gDNA) from *Xcc* as a template. Primers were designed based on the draft genome of *X. campestris* LMG 8031(Schmid, Huptas, & Wenning, 2016). The amplified fragments were fused via overlap extension PCR, gel-purified and digested with restriction enzymes according to the introduced restriction sites. The plasmid was digested with the same restriction enzymes as the fused flanks and dephosphorylated by adding 0.25 µl of alkaline phosphatase to the restriction digest 15 min before terminating the reaction, in order to prevent re-ligation. The digested plasmid was purified by agarose gel-extraction. Vector and insert were ligated using T4-ligase. 10 µl of the reaction were used to transform *E. coli* DH5α. The correctness of the constructs was validated by colony-PCR and sequencing. *X. campestris* cells were transformed by electroporation, using 600–1000 ng of pK19Gm plasmid carrying the respective fused flanks of the gene of interest. After electroporation, the cells were flushed with 1 ml of Super Optimal Broth with catabolite repression (SOC) media (20 g L^{-1} tryptone, 5 g L^{-1} yeast extract, 0.5 g L^{-1} NaCl, 10 mM MgSO$_4$, 10 mM MgCl$_2$, 2.5 mM KCl, 20 mM glucose) and agitated at 250 rpm for 2–3 h at 30 °C. After plating the cells on LB-Agar containing 30 µg ml^{-1} gentamicin, a single colony was subsequently cultivated in LB media without antibiotics for 24 h. The second homologous recombination event was triggered by plating dilution series onto LB-Agar containing 10% (w/v) sucrose. Gene deletions were verified by colony-PCR.

2.4. Recovery of xanthan-variants

For the recovery of the different xanthan-variants, the fermentation broth was diluted 1:10 and centrifuged (15,000 g, 20 min, 20 °C) to separate the cells from the xanthan containing aqueous phase. The supernatant was subsequently concentrated back to the initial volume by crossflow filtration using an ultrafiltration cassette (Hydrosart®, Sartorius AG, Germany) with a molecular weight cutoff of 100 kilodaltons (kDa). The concentrated supernatant was poured into 2 volumes of 2-propanol under stirring conditions (170 rpm). The precipitated xanthan was dried in a vacuum oven at 45 °C for 48 h and after the gravimetrical determination of the dry mass, it was milled into a fine powder in a ball mill (Mixer Mill MM 400, RETSCH GmbH, Germany) at 30 Hz for 30 s.

2.5. Rheology

2.5.1. Sample preparation

For the determination of rheological properties 1% (w/w) solutions of the xanthan-variants were prepared in a total amount of 200 g ddH$_2$O. The samples were prepared in a 1 l Erlenmeyer flask by shaking over night at 250 rpm at 50 °C. 50 g of the salt-free solution was used directly for all measurements. 49 g and 48 g of the sample were mixed with 1 ml of a 25% (4.28 M) NaCl-solution and 2 ml of a 23.5% (2.12 M) CaCl$_2$-solution, respectively, to obtain a total concentration of 85 mM for each approach. All samples were centrifuged (500 g, 2 min, 20 °C) in order to remove any air bubbles, which might occur during mixing and stored at 4 °C over night prior to measurements.

2.5.2. Rheological measurements

Rheological measurements were carried out with a stress-controlled MCR300 rotational rheometer (Anton Paar GmbH, Austria) equipped with a CP 50-1 cone-and-plate measuring system, 50 mm diameter, 1° cone angle and 50 µm cone truncation (Anton Paar GmbH, Austria) and a Peltier controlled TEK 150 P temperature unit (Anton Paar GmbH, Austria). All measurements, except the temperature sweeps, were carried out at 20 °C and all samples were incubated in the measuring system at 20 °C for 5 min prior to the measurement. All experiments were carried out in triplicates.

2.5.3. Flow curves

Determination of flow curves were carried out at a logarithmically increasing shear rate from 10^{-3}–10^3 s^{-1} by measuring 4 data points per decade with a decreasing measuring time of 100 - 5 s per data point.

2.5.4. Amplitude sweeps

Amplitude sweeps were performed at a logarithmically increasing shear stress amplitude from 10^{-1} - 10^2 Pa with a frequency of 1 Hz.

2.5.5. Frequency sweeps

Frequency sweeps were carried out in the linear viscoelastic region (LVE) at a logarithmically increasing frequency from 10^{-2} – 10^1 Hz.

2.5.6. Temperature sweeps

Temperature sweeps were preformed within the LVE at a frequency of 1 Hz A discrete temperature-ramp from 20 to 75 °C at a heating rate of 4 °C min^{-1} was applied. To prevent evaporation, the edge of the sample was covered with low viscosity paraffin oil (Carl Roth GmbH & Co. KG, Karlsruhe, Germany).

2.5.7. Thixotropy

Thixotropic behavior of the samples (salt free, 85 mM NaCl, 85 mM CaCl$_2$) was evaluated by a 3-stage oscillatory shear. During the first stage the sample was measured within the previously determined LVE-region followed by a high oscillatory shear of 10^2 Pa. The recovery of the structure was then measured over 10 min within the LVE region.

2.6. Analytical methods

2.6.1. Determination of monomer composition

Determination of the monomer composition was performed by the 1-phenyl-3-methyl-5-pyrazolone-high throughput method (HT-PMP) (Rühmann, Schmid, & Sieber, 2014). For this a 0.1% xanthan-solution was prepared by dissolving the powder in ultrapure water under stirring (250 rpm, room temperature). Samples were subsequently hydrolyzed by adding 20 µl of 4 M trifluoracetic acid (TFA) to 20 µl in a 96-well PCR plate, sealing with a rubber lid and sealing the plate in a custom made metal device. Hydrolysis was carried out at 121 °C over 90 min in a sand bath. After hydrolysis the samples were neutralized by the addition of 3.2% NH$_4$OH. The required volume was previously determined using 2 M TFA and phenol red as indicator. Derivatization was done by the addition of 75 µl PMP-mastermix to 25 µl of neutralized hydrolysate and incubation at 70 °C for 100 min in a thermal cycler. After derivatization 20 µl of the sample were mixed with 130 µl of 26-fold diluted 0.5 M acetic acid, mixed using the metal device and subsequently filtered through a 0.2 µm Filter plate (1000 g, 5 min, 20 °C). The 96-well microtiter plate was subsequently sealed with a silicone capmat and placed in the autosampler for HPLC-MS/MS measurements.

2.6.2. Determination of acetate and pyruvate content

For the determination of the acetyl- and pyruvyl-groups, 10 ml of 1% solution of the different xanthan-variants were prepared under the same conditions as described in 2.5.1, and hydrolyzed in 250 mM sulfuric acid for 5 h at 90 °C. After cooling the samples were centrifuged (21,000 g, 1 min) and filtered through a 0.22 µm PVDF syringe filter (Restek GmbH, Bad Homburg, Germany). The Samples were subsequently analyzed via HPLC on a Rezex ROA H$^+$-column (Phenomenex Inc, Torrance CA, USA) without further processing. For calibration a 5 mM pyruvate and 16.7 mM acetic acid standard was used.

2.6.3. Molecular weight determination

0.1% (w/v) of untreated EPS-powder was dissolved in 0.1 M LiNO$_3$ at 50 °C for 12 h under stirring (250 rpm). Treated samples (0.5% (w/v), 85 mM NaCl, pH 5.5) were diluted to a concentration of 0.1% (w/v) and no further treatment was applied prior to measurements. Determination

of molecular weight was carried out via size-exclusion chromatography (SECcurity GPC System, PSS Polymer Standards Service GmbH, Germany) with a SECcurity GPC1260 RI-Detector and a SECcurity SLD7000 7-angle light-scattering detector. Separation was performed by a Suprema 100 Å column coupled with two Suprema 10,000 Å columns and a Suprema guard column at 50 °C using 0.1 M LiNO$_3$ as eluent at a flow rate of 1 ml/min. 100 µl of sample was used for analysis.

3. Results and discussion

3.1. Creation of deletion variants

The knockout of the two acetyltransferases GumF and GumG was performed in one step using the upstream flank of *gumF* and the downstream flank of *gumG*, as these genes are directly adjacent to each other in the *gum*-cluster, creating the mutant *Xcc ΔgumFG*. The fused flanking regions were cloned into the pK19Gm plasmid and transferred to *X. campestris*. Using the up- and downstream flanks of the pyruvyl-transferase *gumL*, *Xcc ΔgumL* was created. The variant *ΔgumFGL* was designed by knocking out *gumL* in *Xcc ΔgumFG*. All knockouts have been verified via sequencing of the knock-out region on the chromosome. All knockout-variants did not grow on Gentamicin, indicating the markerless deletion of the genes. Additionally, the single knockout of the acetyltransferase *gumG* was achieved by using the same downstream flank as for creation of *Xcc ΔgumFG* and the upstream flanking region of *gumG*. As the double deletion mutant *Xcc ΔgumGL* was not successful, this variant was obtained by a plasmid-based re-establishment of the GumF acetyltransferases in the *ΔgumFGL* deletion mutant, using the IPTG-inducible pSRKGm broad host expression vector, harboring the *gumF* gene. Sequencing results of the deletion variants are given in Fig. S1.

3.2. EPS production and analysis

All xanthan-variants were produced in a 1.5 L-bioreactor scale within 48 h. As the strains *Xcc wt*, *Xcc ΔgumFG*, *Xcc ΔgumFGL*, *Xcc ΔgumL* and *Xcc ΔgumG* were markerless knock-out variants, they were cultivated without antibiotics. Since the strain *Xcc ΔgumGL* harbored the pSRKGm with *gumF*, the strain was cultivated using 30 mg ml^{-1} Gentamicin. The total product yields in dry mass of EPS before milling are given in Table 1.

For the analysis of the monomer-composition, a 0.1% solution of the dried powder of each cross-flow purified xanthan variant was hydrolyzed. Before hydrolyzation a part of the solution was used for the enzymatic detection of residual glucose or pyruvate in the xanthan solution. No significant amounts of glucose or pyruvate could be detected in the supernatant. After hydrolyzation a part of the neutralized solution was used to determine the pyruvate content of each xanthan variant. The calculated recovery ranged from 32.55% to 40%. All xanthan-variants had similar Glc:Man:GlcA ratios (Fig. S3) and the molecular weight of the variants were within the same order of magnitude (Table 2), indicating that the deletions of the pyruvyl- and acetyl-transferases had no effect on monomer composition or polymer chain length.

3.3. Effect of deletions of acyltransferases on acetylation and pyruvylation patterns

Acetate and pyruvate contents were determined by hydrolyzing a 1% solution of each xanthan variant and subsequent analysis of the supernatant of the hydrolysate via HPLC-UV. An overview of acetate and pyruvate content is given in Fig. 1.

Xanthan produced by the wildtype strain (wt) showed an acetate to pyruvate ratio of 1.5:1 and a calculated acetate and pyruvate amount of 2.5% and 3.5% respectively. However, due to the calculated recovery of 62.5% by the HT-PMP method (Fig. S3) acetate and pyruvate content

Table 1

Schematic representation of the acetylation and pyruvylation-patterns of the produced xanthan-variants. Production yields and productivity of the strain are given below each variant.

Strain	*Xcc wt*	*Xcc ΔgumF*	*Xcc ΔgumG*	*Xcc ΔgumFG*
Variant	Xanthan	XanΔF	XanΔG	XanΔFG
Repeating unit				
Yield [g/l]	18.03	11.30	10.91	16.87
Productivity [g l⁻¹ h⁻¹]	0.27	0.24*	0.15	0.23
Strain	*Xcc ΔgumL*	*Xcc ΔgumFL*	*Xcc ΔgumGL*	*Xcc ΔgumFGL*
Variant	XanΔL	XanΔFL	XanΔGL	XanΔFGL
Repeating unit				
Yield [g/l]	15.95	11.34	11.10	17.35
Productivity [g l⁻¹ h⁻¹]	0.24	0.45**	0.15	0.26

* Total reaction volume: 1 l

** Fermentation cancelled after 25 h

● Glc ● Man ● GlcA *Ac* Acetate *Pyr* Pyruvate

Table 2

Calculated M_w of xanthan variants. M_w was obtained by GPC-analysis of 0.1% xanthan in 0.1 M LiNO₃ using pullulan standards of different M_w (348 Da-2.35 MDa) for calibration.

Variant	M_w [Da]
Xan	$2,3 * 10^7$
XanΔF	$4,5 * 10^7$
XanΔG	$2,2 * 10^7$
XanΔFG	$2,5 * 10^7$
XanΔL	$1,8 * 10^7$
XanΔFL	$2,2 * 10^7$
XanΔGL	$1,6 * 10^7$
XanΔFGL	$1,8 * 10^7$
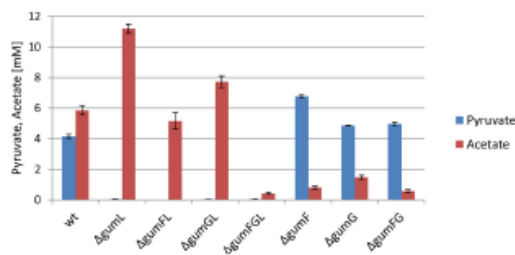
Fig. 1. Acetate and pyruvate content of the different xanthan-variants after hydrolysis with 0.25 M H₂SO₄. All samples were dissolved in ddH₂O at a concentration of 10 g l⁻¹ and 72% H₂SO₄ was added to a final concentration of 0.25 M. All samples were hydrolyzed in triplicates. The error bars show the standard deviation of triplicates.

accord to 4.0% and 5.6% respectively, which is well in the range of previously reported values (Candia & Deckwer, 1999; Kennedy & Bradshaw, 1984; Tako & Nakamura, 1988). The depyruvylated variants (XanΔL, XanΔFGL, XanΔFL and XanΔGL) showed no quantifiable amounts of pyruvate after hydrolysis, indicating the complete depyruvylation of the polysaccharide. The amount of acetate in these variants varied depending on the knockout of the acetyltransferases GumF and GumG. With both functional acetyltransferases present, the acetate content of XanΔL almost doubled compared to xanthan from the

wildtype, indicating a competition of pyruvate and acetate in respect to the outer mannose. We hypothesize that without the competing pyruvate, the available positions for acetylation by GumG increases and therefore, the overall acetate content rises. XanΔFL, lacking the acetyltransferase for the inner mannose showed considerably lower amounts of acetate compared to XanΔL, which were comparable to the unmodified xanthan. In contrast, XanΔGL lacking the outer acetate and pyruvate showed higher amounts of acetate compared to both XanΔFL and xanthan from the wildtype, indicating, that the inner mannose is more frequently acetylated than the outer mannose, when no pyruvate is present at the outer mannose. Previous studies report acetylation of 60–70% of the inner mannose, which is in good accordance with our findings in this variant (Abbaszadeh et al., 2015). XanΔFGL had no quantifiable amounts of pyruvate and the acetate content decreased 14-fold compared to the natural xanthan and lays within the detection limit of the analysis. Unexpectedly, the degree of pyruvylation was highest in XanΔF, which lacks acetylation of the inner mannose, rather than in XanΔG. This opposed our expectations, as the latter lacks acetylation of the outer mannose, which would result in more free positions for pyruvylation. Both XanΔG and XanΔFG showed very similar degrees of pyruvylation, which were comparable to native xanthan. XanΔF, XanΔG and XanΔFG exhibited a drastic decrease of acetylation compared to all other variants with a pyruvylation of the outer mannose. The higher pyruvate content of XanΔF compared to XanΔG can be explained by the competition for acetylation and pyruvylation of the outer mannose. While only the outer mannose can be acetylated in XanΔF, and the pyruvylation of outer mannose additionally reduces the positions for acetylation, this would explain the lower amount of acetate in this variant. On the other hand, the permanently available spot for acetylation of the inner mannose by GumF in XanΔG could explain the higher amounts of acetate of XanΔG. Overall acetate content of XanΔFL and XanΔGL indicates that without pyruvylation the inner mannose seems to be more frequently acetylated than the outer mannose, proved by the higher amount of acetate in XanΔGL compared to XanΔFL, which confirms previous reports of high degrees of acetylation of the inner mannose (Abbaszadeh et al., 2015; Hassler & Doherty, 1990). The acetate-concentrations in XanΔFL were also quite comparable to those reported by Hassler and Doherty (1990), who also report no pyruvate and a slightly decreased degree of acetylation compared to unmodified xanthan (Hassler & Doherty, 1990). On the other hand, acetate content of XanΔG, which is pyruvylated on the outer mannose, indicates a rare acetylation of the inner mannose in the

239

presence of pyruvate on the outer mannose. This is interesting, as this variant should theoretically have the same amount of acetate as XanΔGL. However, pyruvylation of the outer mannose seems to impact the acetylation of the inner mannose drastically. These findings contradict the data reported by Hassler and Doherty (1990), who reported a degree of acetylation of this variant similar to unmodified xanthan (Hassler & Doherty, 1990). As the degree of acetylation of XanΔF is as low as in XanΔFG, this gives further evidence for competition of acetylation and pyruvylation of the outer mannose and that the inner mannose is more often acetylated than the outer mannose.

3.4. Rheological characterization of the xanthan-variants

As the rheological properties of xanthan are quite dependent of ionic strength (Dário et al., 2011; Rochefort & Middleman, 1987), the scope of this work was to characterize the influence of defined acetylation and pyruvylation patterns of xanthan on its rheological properties including evaluation of the effect of cations on the variants. For rheological characterization, natural xanthan (Xan) as well as the seven different xanthan-variants (XanΔF, XanΔG, XanΔL; XanΔFG, XanΔFGL, XanΔFL, XanΔGL) produced by genetically modified *X. campestris*-strains, resulting in distinct acetylation and pyruvylation patterns have been thoroughly characterized in salt free solution as well as in presence of mono- and divalent cations, by the addition of NaCl and CaCl₂, respectively. For comparison of each xanthan variant and salt concentrations of 85 mM have been chosen, as these concentrations resulted in differences in rheological characteristics, which were optimal for describing the effects of modifications of the polysaccharide. For better comparability, the conductivities of all salt-free solutions and the ones of the solutions containing 85 mM NaCl or CaCl₂ were measured and are summarized in Table S2.

3.4.1. Effect of acetylation and pyruvylation patterns on viscosity

It has been widely accepted that depyruvylation of xanthan leads to a decrease of its viscosity (Callet et al., 1987; Cheetham & Norma, 1989; Erten, Adams, Foster, & Harding, 2014; Tako & Nakamura, 1988). Common theory is that pyruvate destabilizes the ordered structure of xanthan and by depyruvylation a more ordered structure is obtained (Sandford, Pittsley, Knutson, Watson, & Cadmus, 1977; Shatwell, Sutherland, Dea, & Ross-Murphy, 1990). Correlation with viscosity this in turn means, that the ordered structure of xanthan is responsible for a lower viscosity, especially at lower shear rates, as high viscosity at low shear rates can be explained by interactions of random coils of the exopolysaccharide, especially at high concentrations. This could be easily confirmed by our studies with the variant XanΔL, which showed a decreased viscosity by two orders of magnitude compared to unmodified xanthan (Fig. 2). The distinct η₀, which was absent in the xanthan produced by the wildtype further demonstrates the drastically decreased viscosity by depyruvylation. Furthermore, this variant showed increased degree of acetylation, which can be contributed to an increase of available position for acetylation of the outer mannose, as it cannot be pyruvylated anymore. The effects of different acetylation patterns and their combination with depyruvylation on the other hand were quite variable and to some extent puzzling. As described before, the degrees of acetylation in all variants lacking pyruvylation could be correlated with a higher degree of acetylation on the inner mannose as well as an increase of acetylation of the outer mannose in absence of the pyruvate-ketal. The degrees of acetylation and also pyruvylation of the xanthan-variants still having the pyruvate-ketal were against our expectations quite contradictory and so was their effect on the rheological properties. As the acetyl-groups in the sidechain are reported to stabilize the ordered structure of xanthan (Shatwell et al., 1990), a higher degree of acetylation would result in a decrease of viscosity and vice versa. Previous studies showed that while deacetylation leads to decreased viscosity in dilute concentrations, this effect is reversed at higher concentrations, which confirms the stabilizing effect of the

acetate groups (Khouryieh et al., 2007; Tako & Nakamura, 1984). However, most of the investigated variants were produced chemically, and therefore no reliable information of the acetylation-pattern could be concluded. One of the few rheological analyses of xanthan modified by genome editing of *X. campestris* by Hassler & Doherty (Hassler & Doherty, 1990) was carried out with xanthan concentrations below 0.2% and therefore the reported effects of acetylation are in the range of dilute solutions. The low viscosity of XanΔL compared to unmodified xanthan could therefore be both correlated with the absence of the pyruvate-ketal in combination with the higher degree of acetylation, which would further stabilize its ordered structure. As shown by the acetylation patterns of Xan, XanΔF and XanΔG the inner mannose is already highly acetylated. The high amount of acetate of XanΔL can therefore be explained by a higher degree of acetylation of the outer mannose due to absence of the pyruvate-ketal. Interestingly the deacetylated variants XanΔF and XanΔFG showed almost unaltered viscosity to unmodified xanthan. As both variants showed very low degrees of acetylation, which can be attributed to the missing acetylation of the inner mannose and a competing acetylation and pyruvylation of the outer mannose in XanΔF or a complete lack of acetylation in XanΔFG, there seems to be little effect of acetate on the viscosity of xanthan. As XanΔF shows higher degree of pyruvylation and by the ways of creating this variant, the deacetylation would only affect the inner mannose. As we suggest there is a competition for acetylation and pyruvylation, we predict a similar acetylation pattern in XanΔFG, however with an overall lower degree of pyruvylation. As these variants show very similar flow behavior compared to unmodified xanthan, this would contribute very little influence of deacetylation of xanthan on its rheological properties when the polysaccharide is pyruvylated. While XanΔG has an identical degree of pyruvylation as XanΔFG and only a very small, however considerably higher amount of acetylation compared to XanΔF and XanΔFG, it is the only deacetylated variant carrying the pyruvate ketal at the outer mannose. From the nature of creating the variant we predict that this small amount of acetate is bound to the inner mannose, contributing a highly stabilizing effect to the acetate group bound to the inner mannose. This becomes further evident by comparing XanΔFL, XanΔFGL and XanΔGL to XanΔL. While all four variants lack pyruvylation of the outer mannose, only XanΔGL and XanΔL are acetylated on the inner mannose, which results in a drastically reduced viscosity. The relative high amount of acetylation of the outer mannose in XanΔFL on the other hand has no further impact on the viscosity, which stays unaltered compared to XanΔF. This would mean that acetylation of the outer mannose in the absence of pyruvate and acetate on the inner mannose has a significantly smaller stabilizing effect compared to acetylation of the inner mannose compared in absence of the pyruvate ketal. The high viscosity of XanΔFGL compared to XanΔL can be explained by the lack of stabilizing acetyl-groups, somehow cancelling out the stabilizing effect of depyruvylation. While all xanthan-variants still containing the pyruvate-ketal showed increased viscosity after the addition of cations, the species (mono- or divalent cations) had no impact on the increase of viscosity. All variants lacking the pyruvate-ketal showed a decrease of viscosity in the presence of cations, while the effect of Ca²⁺-ions was slightly bigger compared to monovalent Na⁺-ions. These results are consistent with previous studies, which report the involvement of the pyruvyl-groups and the termini of the main chains in the interactions with cations (Bergmann et al., 2008). The influence of cations was generally higher at low shear rates, with diminishing effects towards higher shear rates. One exception was XanΔF, where the viscosity curves were higher throughout the investigated shear rates, resulting in a parallel trend of flow behavior in the presence and absence of cations. The diminishing effect of cations can be explained by high shear forces breaking up intermolecular cation mediated interactions, which are stable under low-shear conditions. The absence of this effect in XanΔF could be due the higher degree of pyruvylation, leading to increased intermolecular forces, which are more stable under high shear rates. While the addition
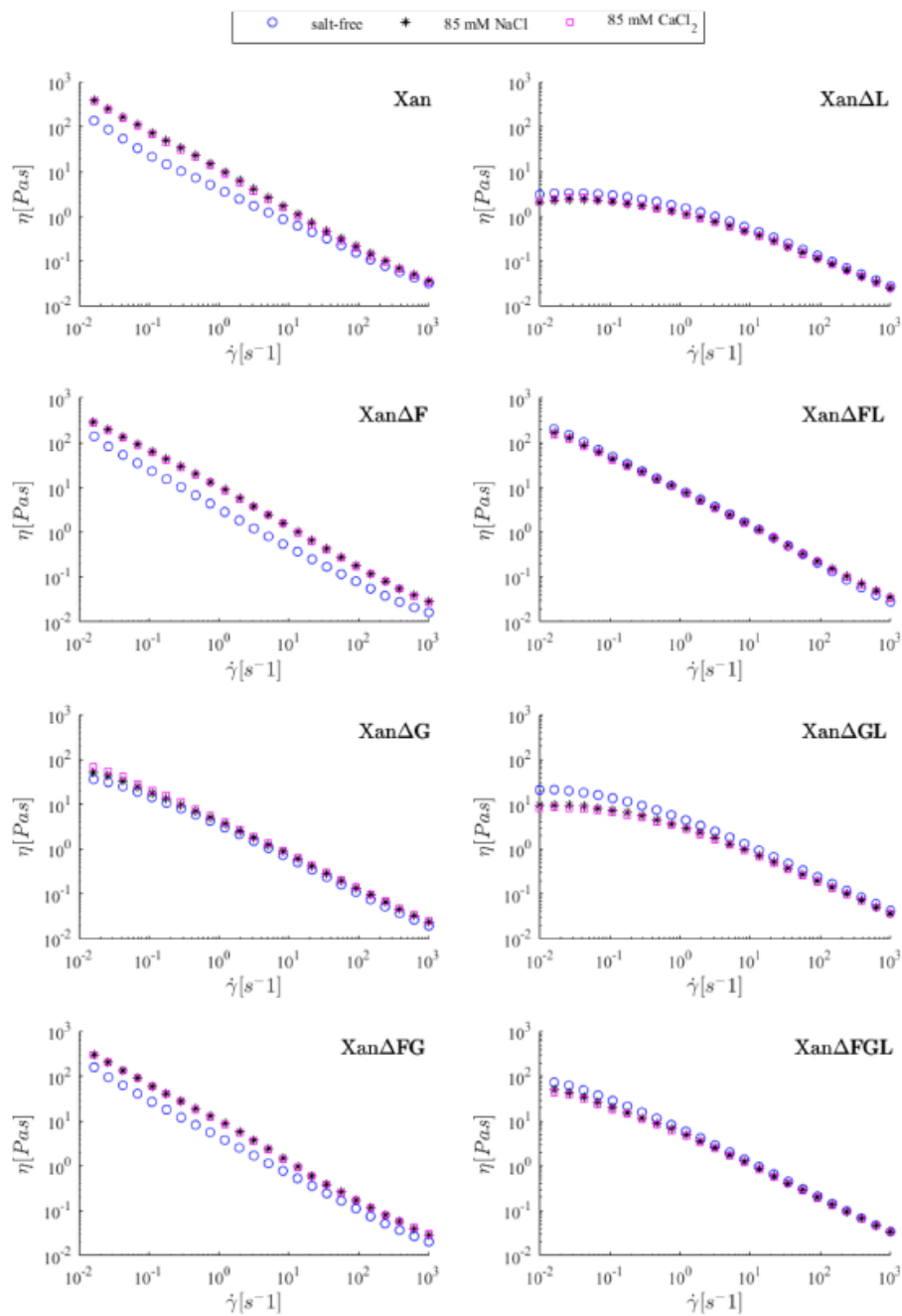
Fig. 2. Flow curves of 1% solutions of xanthan-variants, salt-free (O), 85 mM NaCl (*), 85 mM CaCl$_2$ (□) measurements were carried out in triplicates, from a shear rate from 10^{-2} to 10^3 s^{-1} at 20 °C. All samples rested for 5 min after application on the rheometer before measuring, to avoid shear-induced starting conditions.

of cations had a reduced effect on the viscosity of XanΔFG it showed almost no effect on the viscosity of XanΔG. As both of these variants show similar pyruvate levels, but XanΔG is still acetylated on the outer mannose, this raises the question if and how the ordered and unordered structure influence the intermolecular interactions mediated by cations. However, there might also be a synergistic effect between the decrease of viscosity by a higher degree of ordered structure and the interactions of cations. As all depyruvylated xanthan-variants showed decreased viscosity in the presence of cations, and in the case of XanΔFGL, where we assume a higher degree of unordered structure due to the lack of acetyl-groups this effect may only be attributed to the absence of pyruvyl-groups and does not correlate with the ordered or unordered structure.

3.4.2. Effect of acetylation and pyruvylation patterns on oscillatory shear behavior

While the flow curves already gave good and detailed impression about the properties of the different xanthan-variants, they inherit the problem giving information of a sample whose structure is irreversibly destroyed. In order to get more detailed information about the rheological properties, all variants were tested under oscillatory shear within the linear-viscoelastic (LVE) region. In order to determine the LVE for each sample an amplitude sweep was carried out (Fig. S4). Additionally, it was tested, if any structural destruction was reversible by performing a thixotropy test for each variant. Amplitude sweeps revealed, that at the chosen frequency of 1 Hz all xanthan-variants had gel character with G' > G" to a certain extent within the LVE. One exception was XanΔL, which showed liquid behavior (G' < G"). Unmodified xanthan showed gel strength of 14.4 Pa and a damping factor of 0.42. Upon the addition of cations, gel strength increased drastically from 14.4 Pa to 26.7 and 29.5 Pa for CaCl$_2$ and NaCl, respectively, while tanδ decreased towards 0.25 and 0.24 respectively, resulting in an overall stronger, elastic gel. Upon addition of cations, the gel structure also became more brittle as indicated by an increase of G" at the end of the LVE region. However, the LVE also increased towards higher deformation values and the gel-sol transition shifted considerably towards a higher strain. Variants XanΔF and XanΔFG showed similar behavior, however the addition of cations had less influence on the gel structure XanΔF and even less on XanΔFG. The lowest effect of cations was observed in XanΔG, which had overall weaker gel strength, and even with the addition of salts no increase of G" was observed, indicating a very weak gel structure. As observed in rotational shear experiments, the addition of salts had a contrary effect on the gel strength on all depyruvylated variants. As already mention XanΔL showed no gel character but liquid character. Depyruvylation in combination with deacetylation of the outer mannose (XanΔGL) lead to an increase in overall gel strength, however G" also increased, leading to an overall increase tanδ and therefore a very weak gel structure. The same effect was observed for XanΔFL and XanΔFGL, however not as prominent as in XanΔG and comparing all three variants this effect was least prominent in XanΔFL.

Frequency sweeps further supported our findings and showed a typical gel behavior for Xan, XanΔF and XanΔFG with a low frequency dependency of both G' and G". Across the investigated frequency range from 0.01 to 10 Hz no crossover of G' and G", was observed, indicating relaxation times > 100 s and an elastic gel structure, which would remain stable during long term storage of the samples (Fig. 3). For these three variants addition of cations resulted in a higher overall gel strength and the frequency dependency of G' and G" further decreased compared to the solutions without cations. XanΔG as the only deacetylated variant which still contains the pyruvate ketal on the other hand showed a relatively low relaxation time between 25 and 40 s (given by the inverse of a G' and G" crossover frequency between 0.025 Hz and 0.04 Hz) indicating a gel character with low elastic portion and a loss of a stable long term gel-character. The depyruvylated variants XanΔL, XanΔFL, XanΔGL and XanΔFGL all showed relatively short relaxation

times between 0.1 and 100 s. XanΔL shows the lowest one of 0.1 s and no gel character across a wide frequency region, demonstrating that depyruvylation leads to a complete loss of gel character in xanthan. The weak gel character at higher frequencies could be attributed to entanglements of the molecules, however it is still very weak and investigations at higher frequencies would be needed to confirm whether the weak gel character is stable at high frequencies. While XanΔFGL showed a relaxation time between 25 and 40 s, XanΔFL only indicated a transition point at frequencies below 0.01 Hz, resulting in a relaxation time > 100 s. The relatively low relaxation times of the depyruvylated xanthan variants confirm weak gel structures, which are attributed to the depyruvylation, resulting in a more ordered helical structure of the xanthan chains and thereby reducing the gel strength, which we propose to be due to random-coil entanglements, especially at low frequencies. This theory is further supported by the findings for XanΔL, which showed liquid character over a wide frequency with a relaxation time of 0.1 s, meaning than XanΔL showed weak gel properties at high frequencies. This is a typical behavior of a Maxwell fluid. The sol character of XanΔL over a wide frequency further backs the hypothesis of a highly ordered structure caused by depyruvylation combined with the increase of acetylation. At low frequencies these helical rods could flow easily past each other, while at high frequencies more entanglements would occur resulting in a slight gel character. Interestingly XanΔGL exhibited characteristics very similar to XanΔL. Comparing the acetate content of XanΔGL with XanΔL (Fig. 1), as XanΔGL has the second highest degree of acetylation after XanΔL we conclude that the high acetate content is due to acetylation of the inner mannose. From the rheological data we conclude, that the inner acetate is primarily responsible for the stabilization of the helical structure, leading to a decrease in viscosity and gel-strength. While XanΔF shows a degree of acetylation comparable to the native xanthan but exhibiting a sol-gel transition at low frequencies, we conclude, that acetylation of the outer mannose also affects the stability of the helical structure, but to a far less extent compared to acetylation of the inner mannose. XanΔFGL, which is completely deacetylated and depyruvylated still exhibits gel characteristics over a wide frequency range, which is slightly lower than XanΔFL. From a structural point of view and considering our previous conclusion that the ordered structure is responsible for higher viscosity and gel-strength, this would mean that the structure of xanthan is a more ordered one without any decoration compared to XanΔFL and XanΔGL, where the outer or inner mannose is still acetylated. From this data we can propose certain effects on how complete deacetylation and depyruvylation affects the structure of xanthan, however more information about its structure is necessary for a defined statement.

3.4.3. Effect of acetylation and pyruvylation patterns on temperature dependency of rheological properties

Next to mechanical stress, temperature plays an important role for the rheological properties of xanthan by its transition of the ordered-disordered structure (Matsuda, Biyajima, & Sato, 2009; Milas & Rinaudo, 1979). To investigate the effect of acetylation and pyruvylation patterns on the temperature induced effects, oscillatory shear in the LVE-region was carried out by heating the samples from 20 to 75 °C with subsequent cooling to 20 °C (Fig. 4). Table 3 gives an overview of all variants sorted by their temperature stability in the absence of cations based on the relative value of G' at 20 °C and 75 °C, as well as the influence of cations on the temperature stability. All variants showed a temperature dependency of their gel strength to different extents, while all effects were completely reversible. Unmodified xanthan showed high temperature stability and the addition of salts only lead to very slight increase of thermal stability. This may however be correlated to the increase of the gel strength upon addition of cations. The different deacetylation patterns lead to an evident decrease of gel strength upon heating. The effect was least evident in XanΔF, followed by the completely deacetylated XanΔFL and most pronounced in XanΔG. This
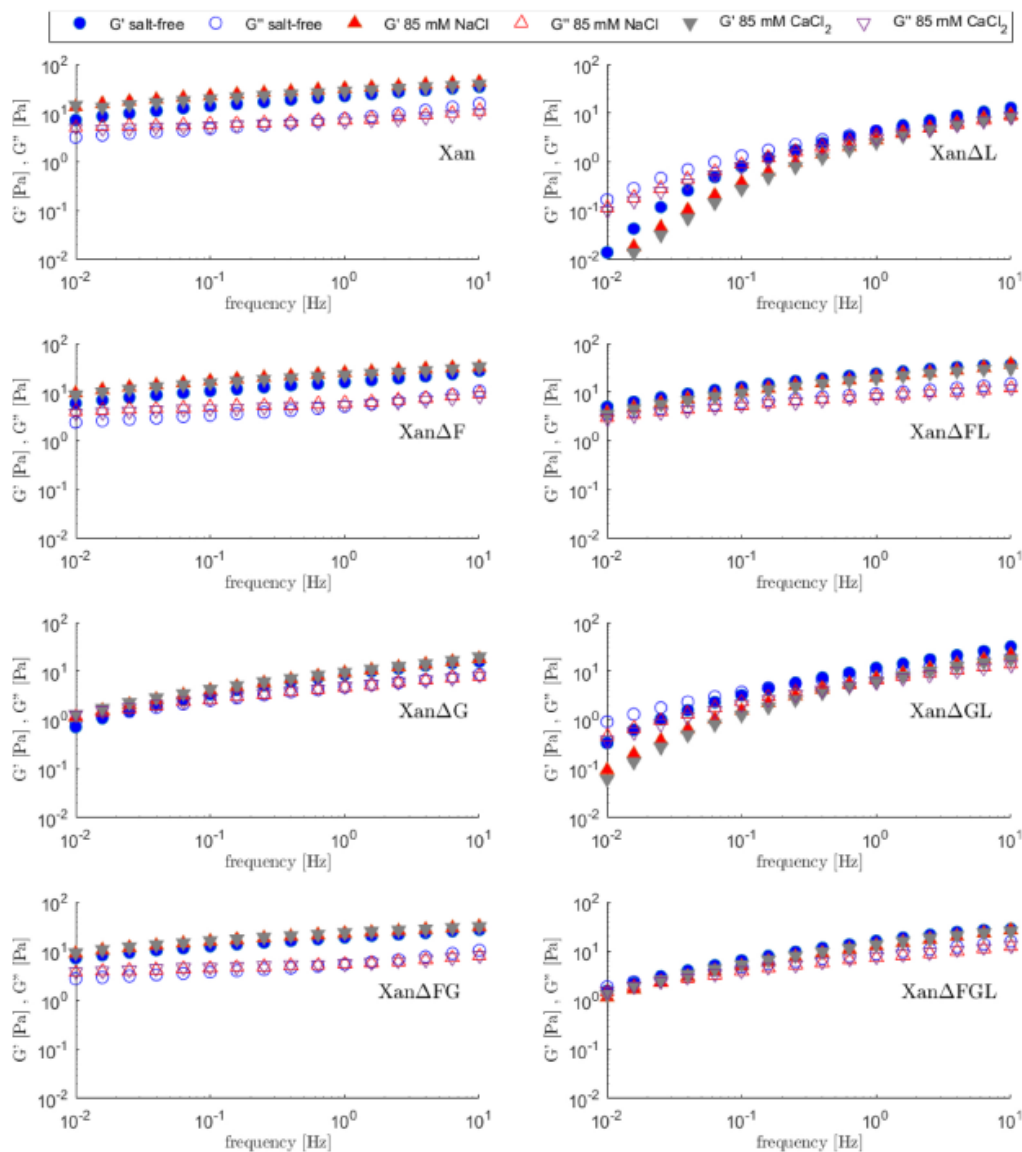
Fig. 3. Frequency sweeps of salt free 1% xanthan solutions and with 85 mM NaCl or 85 mM CaCl$_2$ Storage moduli G' (filled symbols) and loss moduli G"(empty symbols) are shown without salt ($\bullet$/$\circ$), with 85 mM NaCl ($\blacksquare$/$\square$) and 85 mM CaCl$_2$ ($\blacktriangle$/$\triangle$). All measurements were performed under a constant shear stress of 1 Pa and logarithmically increasing frequency amplitude from 0.01 to 10 Hz.

behavior could be attributed to the reduced gel strength of XanΔG by higher acetylation of the inner mannose. For all deacetylated variants addition of salts lead to a much higher stabilization compared to mechanical stress. As stated before, the $-COO^-$ residues of pyruvylated xanthan seem to play a major role in the interactions of cations and the polymer and these interactions seem to have higher temperature stability than mechanical stability. Addition of salts to the depyruvylated variants had, as described before an adverse effect on the gel strength of xanthan, however compared to the salt-free systems, cations seem to

somehow stabilize the structure during heating and cooling. This is especially evident by the missing sol-gel transition of XanΔFL/NaCl. A unique effect was observed for XanΔFL and XanΔFGL, by the distinct increase of both G' and G" upon heating, which then again decreased upon further heating, resulting in a peak of the moduli at a certain temperature. As the state changes from sol to gel and to sol again, this indicates a temperature transition of the secondary structure of xanthan. As this phenomenon only occurred in variants lacking acetylation of the inner mannose, the acetylation at this position also seems to play
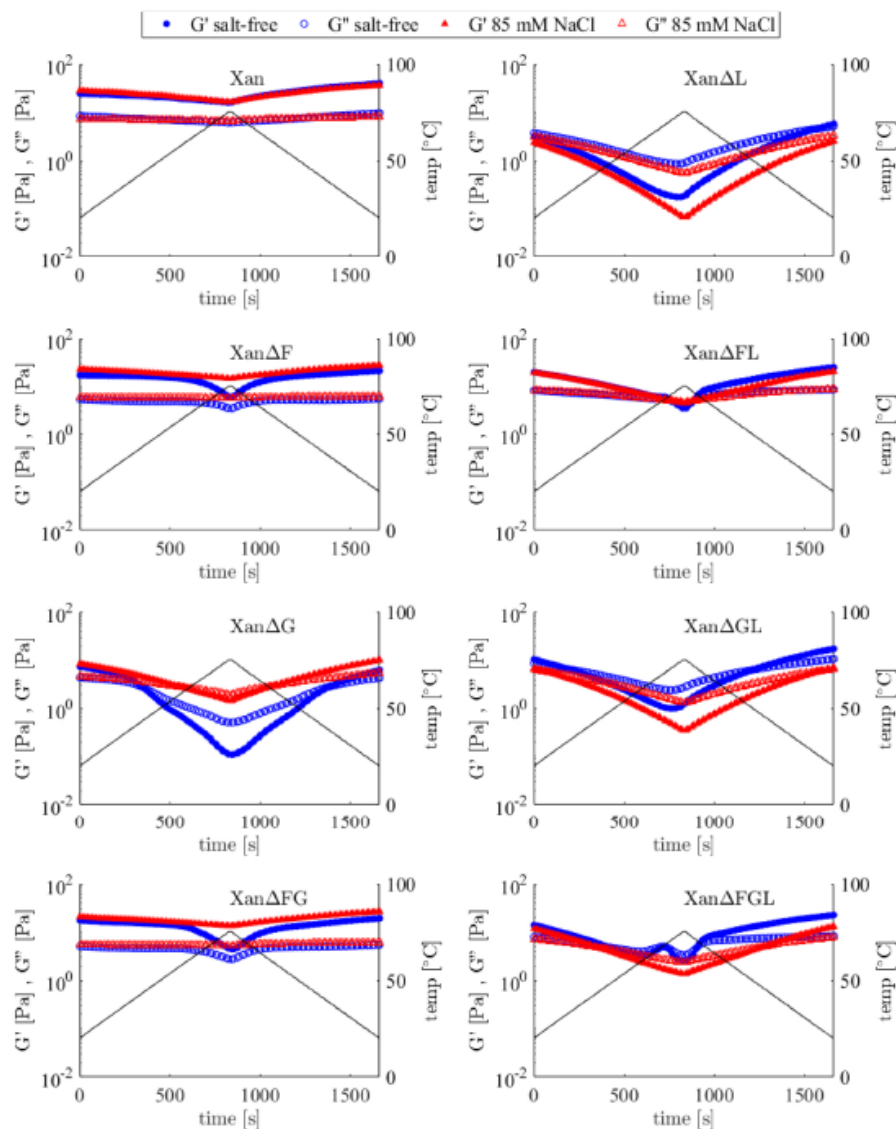
Fig. 4. Temperature sweeps of 1% xanthan solutions salt free and with 85 mM NaCl Storage moduli G' (filled symbols) and loss moduli G"(empty symbols) are shown without salt (●/○), with 85 mM NaCl (▲/△). For better visibility, xanthan with CaCl₂ is not shown. Temperature sweeps were carried out with a discrete temperature ramp at a heating rate of 4 °C per minute within the LVE at a shear stress of 1 Pa and a frequency of 1 Hz.

a major role in the temperature induced structural changes of xanthan. Interestingly this effect did not occur upon cooling and it was also absent after the addition of salts. As this "peak" was most evident in XanΔFGL which had no acetate at all but far less distinct in XanΔFL, which has a considerable degree of acetylation on the outer mannose, this effect could be due to masking effects of the outer acetate on the −COO- residue of the glucuronic acid. This could also explain why this effect is completely abrogated by the addition of cations. While under oscillatory measurements with varying mechanical stress, the addition of cations to the depyruvylated variants showed only minor effects, it

becomes evident that they play a stabilizing role in structural transition of xanthan under thermal treatment, especially in the absence of acetate.

4. Conclusion

The seven different xanthan-variants with unique, highly specific acetylation and pyruvylation patterns (XanΔF, XanΔG, XanΔFG, XanΔFL, XanΔGL and XanΔFGL) showed distinct rheological characteristics and specific interactions in presence of mono- and divalent

244

95

Table 3
Influence of temperature on the oscillatory shear behavior of the xanthan variants determined by the relative G' value at 20 °C and 75 °C. +/−: positive/ negative effect of cations on temperature stability.

Variant	G' 20 °C [Pa] (salt free/with salt)	G' 75 °C [Pa] (salt free/with salt)	Rel. gel strength at 75 °C [%]	Effect of salt on stability
Xan	24.7 / 28.1	15.7 / 16.1	63.6 / 57.4	−
XanΔF	17.1 / 22.8	6.1 / 14.5	35.7 / 63.6	+
XanΔFG	17.4 / 20.9	4.6 / 13.5	26.4 / 64.6	+
XanΔFGL	14 / 11.8	2.5 / 1.4	17.9 / 11.9	−
XanΔFL	19.9 / 19.3	3.5 / 4.5	17.6 / 23.3	+
XanΔGL	10.3 / 6.7	1.2 / 0.4	11.7 / 6.0	−
XanΔL	3.1 / 2.3	0.2 / 0.1	6.5 / 4.3	−
XanΔG	7.3 / 8.3	0.1 / 1.5	1.4 / 18.1	+

cations. From the depyruvylated variant XanΔL we conclude that the COO^--group of the terminal pyruvate ketal is mainly responsible for the increased viscosity and gel strength in presence of cations, while the combination of depyruvylation and higher degree of acetylation leads to dramatically decreased viscosity and gel strength. As pyruvate is known to decrease the ordered structural conformation of xanthan and a high degree of acetylation stabilizes the ordered structure, we conclude that the ordered, helical structure of xanthan results in a low viscosity and gel strength. XanΔL having the lowest viscosity and gel strength among all variants was therefore contributed to a synergistic effect of the absence of pyruvate and a higher degree of acetylation. By creating XanΔFL and XanΔGL with defined acetylation patterns in combination with the absence of the pyruvate ketal, it became evident that the inner mannose is more frequently acetylated than the outer mannose. While a higher degree of acetylation resulted in a decrease of viscosity, by linking the rheological properties of these variants to their acetylation pattern, we conclude that acetylation of the inner mannose is mainly responsible for stabilizing the ordered structure. Deacetylation at the specific mannose residues of XanΔF, XanΔG and XanΔFG led to a much lower degree of acetylation compared to the depyruvylated counterparts XanΔFL, XanΔGL and XanΔFGL and except for XanΔG their rheological properties were very similar to the unmodified xanthan. From the properties of XanΔG we concluded that only low degrees of acetylation of the inner mannose could stabilize ordered structure of xanthan enough to counter the destabilizing effect of the pyruvate ketal and therefore lead to an overall decreased viscosity. Effects of temperature on gel strength also showed that overall acetate content determines temperature stability, with higher acetate levels leading to a higher stability. Within this work, due to the nature of creating these xanthan-variants, we were able to directly link rheological properties to the distribution of acetate and pyruvate in the sidechain of xanthan to the rheological properties and gain several new insights on how these patterns affect the physicochemical behavior of xanthan. Additionally, this study shows that the rheological properties of the natural product xanthan can be specifically fine-tuned by modifying the acetylation and pyruvylation pattern on the genetic level towards defined and predictable properties for tailor-made applications. The question on how exactly the substitution patterns affect the conformation of the sidechains and thereby the overall secondary structure of xanthan has yet to be investigated in detail.

Acknowledgements

Appendix A. Supplementary data

Supplementary material related to this article can be found, in the online version, at doi:https://doi.org/10.1016/j.carbpol.2019.02.055.

References

Abbaszadeh, A., Lad, M., Janin, M., Morris, G., MacNaughtan, W., Sworn, G., et al. (2015). A novel approach to the determination of the pyruvate and acetate distribution in xanthan. *Food Hydrocolloids, 44*, 162–171.
Becker, A., Katzen, F., Pühler, A., & Ielpi, L. (1998). Xanthan gum biosynthesis and application: A biochemical/genetic perspective. *Applied Microbiology and Biotechnology, 50*(2), 145–152.
Bergmann, D., Furth, G., & Mayer, C. (2008). Binding of bivalent cations by xanthan in aqueous solution. *International Journal of Biological Macromolecules, 43*(3), 245–251.
Bradshaw, I. J., Nisbet, B. A., Kerr, M. H., & Sutherland, I. W. (1983). Modified xanthan—Its preparation and viscosity. *Carbohydrate Polymers, 3*(1), 23–38.
Callet, F., Milas, M., & Rinaudo, M. (1987). Influence of acetyl and pyruvate contents on rheological properties of xanthan in dilute solution. *International Journal of Biological Macromolecules, 9*(5), 291–293.
Candia, J. L. F., & Deckwer, W. D. (1999). Effect of the nitrogen source on pyruvate content and rheological properties of xanthan. *Biotechnology Progress, 15*(3), 446–452.
Cheetham, N. W., & Norma, N. N. (1989). The effect of pyruvate on viscosity properties of xanthan. *Carbohydrate Polymers, 10*(1), 55–60.
Dário, A. F., Hortêncio, L. M. A., Sierakowski, M. R., Neto, J. C. Q., & Petri, D. F. S. (2011). The effect of calcium salts on the viscosity and adsorption behavior of xanthan. *Carbohydrate Polymers, 84*(1), 669–676.
Erten, T., Adams, G. G., Foster, T. J., & Harding, S. E. (2014). Comparative heterogeneity, molecular weights and viscosities of xanthans of different pyruvate and acetate content. *Food Hydrocolloids, 42*, 335–341.
Galvan, E. M., Ielmini, M. V., Patel, Y. N., Bianco, M. I., Franceschini, E. A., Schneider, J. C., et al. (2013). Xanthan chain length is modulated by increasing the availability of the polysaccharide copolymerase protein GumC and the outer membrane polysaccharide export protein GumB. *Glycobiology, 23*(2), 259–272.
Galvín, Z. R. N., Soares, L.d. S., Medeiros, E. A. A., Soares, N.d. F. F., Ramos, A. M., Coimbra, J. S.d. R., et al. (2018). Rheological properties of aqueous dispersions of xanthan gum containing different chloride salts are impacted by both sizes and net electric charges of the cations. *Food Biophysics, 13*(2), 186–197.
García-Ochoa, F., Santos, V., Casas, J., & Gomez, E. (2000). Xanthan gum: Production, recovery, and properties. *Biotechnology Advances, 18*(7), 549–579.
Hassler, R. A., & Doherty, D. H. (1990). Genetic engineering of polysaccharide structure: Production of variants of xanthan gum in *Xanthomonas campestris. Biotechnology Progress, 6*(3), 182–187.
Ielpi, L., Couso, R., & Dankert, M. (1981). Lipid-linked intermediates in the biosynthesis of xanthan gum. *FEBS Letters, 130*(2), 253–256.
Jansson, P.-E., Kenne, L., & Lindberg, B. (1975). Structure of the extracellular polysaccharide from *Xanthomonas campestris. Carbohydrate Research, 45*(1), 275–282.
Katzen, F., Becker, A., Zorreguieta, A., Pühler, A., & Ielpi, L. (1996). Promoter analysis of the *Xanthomonas campestris* pv. *campestris* gum operon directing biosynthesis of the xanthan polysaccharide. *Journal of Bacteriology, 178*(14), 4313–4318.
Kennedy, J. F., & Bradshaw, I. J. (1984). Production, properties and applications of xanthan. *Progress in Industrial Microbiology, 19*, 319–371.
Khouryieh, H., Herald, T., Aramouni, F., Bean, S., & Alavi, S. (2007). Influence of deacetylation on the rheological properties of xanthan–guar interactions in dilute aqueous solutions. *Journal of Food Science, 72*(3).
Kool, M. M., Gruppen, H., Sworn, G., & Schols, H. A. (2014). The influence of the six constituent xanthan repeating units on the order–disorder transition of xanthan. *Carbohydrate Polymers, 104*, 94–100.
Kool, M. M., Gruppen, H., Sworn, G., & Schols, H. A. (2013). Comparison of xanthans by the relative abundance of its six constituent repeating units. *Carbohydrate Polymers, 98*(1), 914–921.
Kool, M. M., Schols, H. A., Delahaije, R. J. B. M., Sworn, G., Wierenga, P. A., & Gruppen, H. (2013). The influence of the primary and secondary xanthan structure on the enzymatic hydrolysis of the xanthan backbone. *Carbohydrate Polymers, 97*(2), 368–375.
Li, R., & Feke, D. L. (2015). Rheological and kinetic study of the ultrasonic degradation of xanthan gum in aqueous solution: Effects of pyruvate group. *Carbohydrate Polymers, 124*, 216–221.
Matsuda, Y., Biyajima, Y., & Sato, T. (2009). Thermal denaturation, renaturation, and aggregation of a double-helical polysaccharide xanthan in aqueous solution. *Polymer Journal, 41*, 526.
Milas, M., & Rinaudo, M. (1979). Conformational investigation on the bacterial polysaccharide xanthan. *Carbohydrate Research, 76*(1), 189–196.
Palaniraj, A., & Jayaraman, V. (2011). Production, recovery and applications of xanthan gum by *Xanthomonas campestris. Journal of Food Engineering, 106*(1), 1–12.
Rochefort, W. E., & Middleman, S. (1987). Rheology of xanthan gum: Salt, temperature, and strain effects in oscillatory and steady shear experiments. *Journal of Rheology, 31*(4), 337–369.
Rühmann, B., Schmid, J., & Sieber, V. (2014). Fast carbohydrate analysis via liquid chromatography coupled with ultra violet and electrospray ionization ion trap detection in 96-well format. *Journal of Chromatography A, 1350*, 44–50.
Rütering, M., Schmid, J., Rühmann, B., Schilling, M., & Sieber, V. (2016). Controlled production of polysaccharides–exploiting nutrient supply for levan and

heteropolysaccharide formation in Paenibacillus sp. *Carbohydrate Polymers, 148,* 326–334.

Sandford, P., Pittsley, J., Knutson, C., Watson, P., & Cadmus, M. (1977). *Variation in Xanthomonas campestris NRRL B-1459: Characterisation of xanthan products of differing pyruvic acid content.* USA: ACS Symposium Series-American Chemical Society.

Schmid, J., Huptas, C., & Wenning, M. (2016). Draft genome sequence of the xanthan producer *Xanthomonas campestris* LMG 8031. *Genome Announcements, 4*(5), e01069–01016.

Schmid, J., Sieber, V., & Rehm, B. (2015). Bacterial exopolysaccharides: Biosynthesis pathways and engineering strategies. *Frontiers in Microbiology, 6*(496).

Shatwell, K. P., Sutherland, I. W., Dea, I. C., & Ross-Murphy, S. B. (1990). The influence of acetyl and pyruvate substituents on the helix-coil transition behaviour of xanthan. *Carbohydrate Research, 206*(1), 87–103.

Smith, I., Symes, K., Lawson, C., & Morris, E. (1981). Influence of the pyruvate content of xanthan on macromolecular association in solution. *International Journal of Biological Macromolecules, 3*(2), 129–134.

Tako, M., & Nakamura, S. (1984). Rheological properties of deacetylated xanthan in aqueous media. *Agricultural and Biological Chemistry, 48*(12), 2987–2993.

Tako, M., & Nakamura, S. (1988). Rheological properties of depyruvated xanthan in aqueous media. *Agricultural and Biological Chemistry, 52*(6), 1585–1586.

Vorhölter, F. J., Schneiker, S., Goesmann, A., Krause, L., & Bekel, T. (2008). The genome of *Xanthomonas campestris pv. campestris* B100 and its use for the reconstruction of metabolic pathways involved in xanthan biosynthesis. *Journal of Biotechnology, 134*(1-2), 33–45.

Wang, X., Zheng, D., & Liang, R. (2016). An efficient electro-competent cells generation method of *Xanthomonas campestris pv. campestris*: Its application for plasmid transformation and gene replacement. *Advances in Microbiology, 6*(02), 79.

Wu, M., Qu, J., Shen, Y., Dai, X., Wei, W., Shi, Z., et al. (2018). Gel properties of xanthan containing a single repeating unit with saturated pyruvate produced by an engineered *Xanthomonas campestris* CGMCC 15155. *Food Hydrocolloids, 87,* 747–757.

Xu, L., Dong, M., Gong, H., Sun, M., & Li, Y. (2015). Effects of inorganic cations on the rheology of aqueous welan, xanthan, gellan solutions and their mixtures. *Carbohydrate Polymers, 121,* 147–154.

4.4 Engineering of the acetyltransferase GumG

The first step of engineering the cofactor spectrum of the transferase is to identify the cofactor binding site to target select motifs for mutation. As no crystal structure of the targeted transferase is available, an *ab-initio* modelling approach was used for a prediction of the structure of GumG. For modelling of GumG the translated amino acid sequence based on the draft genome sequence of *X. campestris* LMG 8031 (Schmid, Huptas, & Wenning, 2016) was used. Modelling was carried out on the Robetta server (University of Washington, http://robetta.bakerlab.org/) and resulted in 5 different predicted models, shown in Figure 4
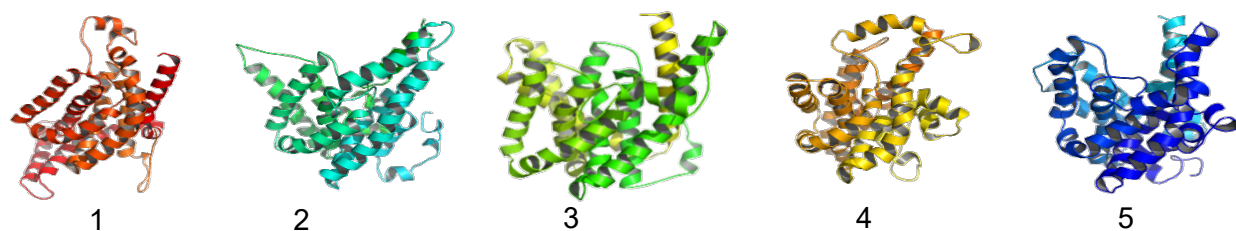
Figure 4. Predicted structures of acetyltransferase GumG obtained by *ab-initio* modelling based on the amino acid sequence of GumG of *X. campestris* LMG 8031

In the next step, highly conserved motifs were identified by multiple sequence alignment of all annotated acetyltransferases of *Xanthomonas sp.* (. Sequence alignment of annotated GumG proteins from *Xanthomonas sp.* (Uniprot, https://www.uniprot.org/; Clustal Omega, https://www.ebi.ac.uk/Tools/msa/clustalo/, EMBL-EBI, Heidelberg, Germany) as well as a 3D sequence alignment using the DALI server, (http://ekhidna2.biocenter.helsinki.fi/dali/index.html#tabs-2) . Sequence alignment showed high conservation of the amino acids histidine at positions 40 and 56, arginine at position 21, aspartic acid at position, phenylalanine at positions 55, 60, 61 and 144, Proline at positions 58 and 91, Glycine at position 65, threonine at positions 290 and 297, tyrosine at position 92, tryptophane at position 143 and leucine at positions 141 and 145.

Based on the five predicted models and the identified conserved amino acids, positions 21, 26, 29, 40, 56, 290 and 297 were chosen for an alanine scan. Each amino acid was mutated individually by QuikChange PCR of pSRKGm-*gumG*. Each variant was expressed in *X. campestris* Δ*gumFGL* for 48 h and produced xanthan was analyzed for acetylation to identify inactive GumG-variants Figure 5.
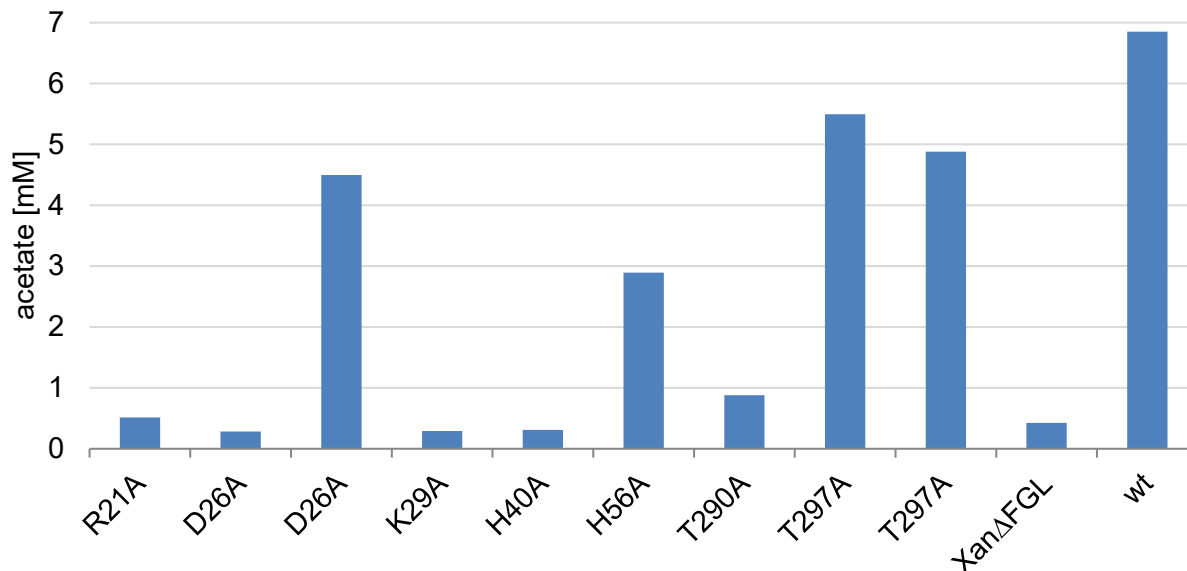
Figure 5. Acetate and pyruvate levels of xanthan produced by *X. campestris ΔgumFGL* pSRKGm-gumG with single amino acid mutations.

All values are normalized to 10 g L^{-1} hydrolyzed xanthan. All experiments were carried out using biological duplicates. *X. campestris* wt and Δ*gumFGL* with empty vector are shown as reference. D26A and T297A were screened twice due to ambiguous sequencing results.

Xanthan variants produced with the GumG variants R21A, K29A, H40A, T290A showed no acetylation, indicating a loss of function by the mutation at these positions. Variants D26A and T297A were screened twice due to ambiguous sequencing results. Re-sequencing of these variants showed no successful mutation of the second replicate of D26A, T297A showed successful mutation for both variants. With this confirmation, a re-screening of the inactive variants was carried out in biological triplicates, with the native GumG as reference. The results are shown in Figure 6. The positions of the amino acids, whose mutation to alanine led to a loss of functions were then cross-referenced in the respective ab-initio models of GumG. Cross-referencing with model 4 showed the closest proximity of the amino acids R21, D26, K29 and H40, indicating a binding-pocket-like structure. Cross-reference with the other models, showed positions of these amino acids along one helix extending through the enzyme's tertiary structure.
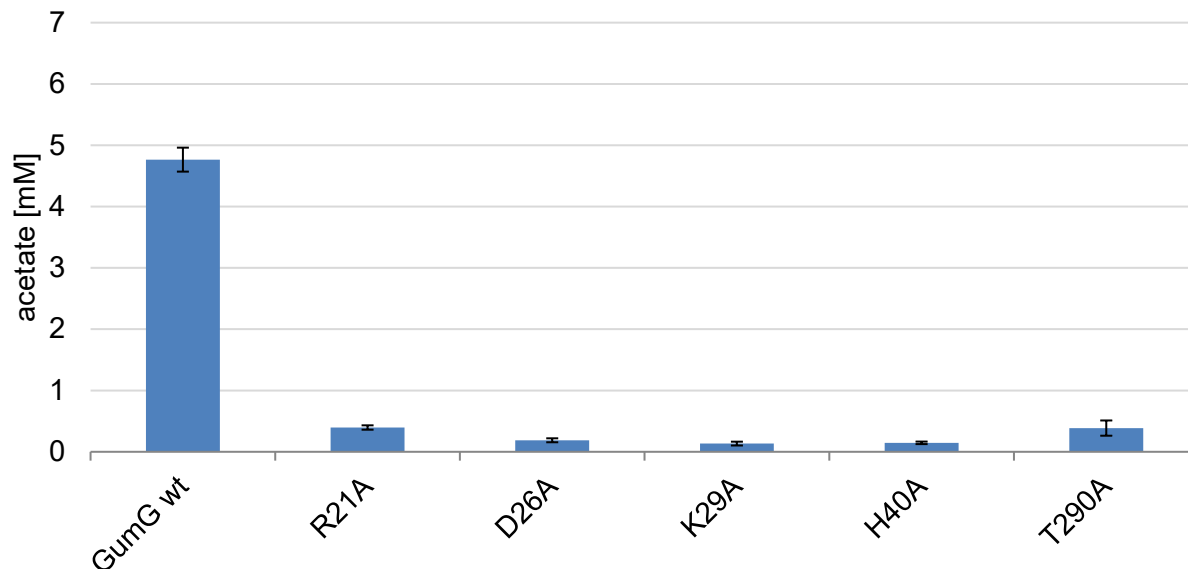
Figure 6. Re-screening of the inactive variants of GumG found in the first screening.

All variants, including the native enzyme (GumG wt) were constitutively expressed with the pHExXan-plasmid in *X. campestris* Δ*gumFGL*. All samples were tested in biological triplicates, shown values are normalized to 10 g L^{-1} of hydrolyzed xanthan.
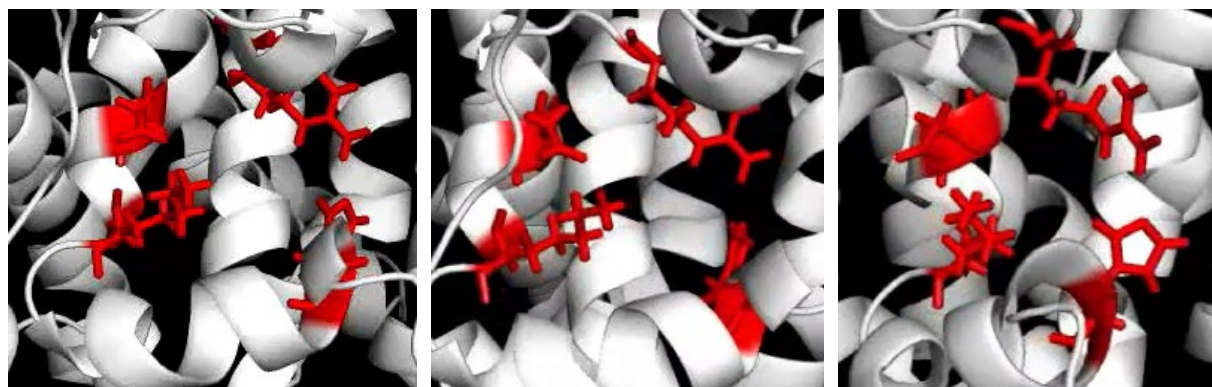
Figure 7. Front-, right-side and left-side view of the amino acids R21, D26, K29 and H40 (highlighted in red) in the predicted model number 4 of GumG.

Based on these results, further amino acids in close proximity to R21, D26, K29 and H40 in model 4 were selected for a second alanine scan. For this, amino acids S16, V18, F60, F61 and T87 were selected. For an easier expression, this mutagenesis and the first round of mutagenesis was carried out in the pHExXan plasmid with the *gum*-promoter for constitutive expression. The mutations of amino acids F61 and V18 showed significantly reduced activity. While mutation of F60 did not result in a loss of function it could actually partially reactivate the F61A variant. This might be due to a stabilization of F60 by F61, where the absence of F61 leads to major conformational changes, thereby inactivating the proposed active site. Interestingly, the mutation of D26 did not

show a loss of function this time. The plasmid from this variant was isolated and re-sequenced and showed the desired mutation, so the reason for the activity remained unclear. All other mutations showed the same results as in the first screening.
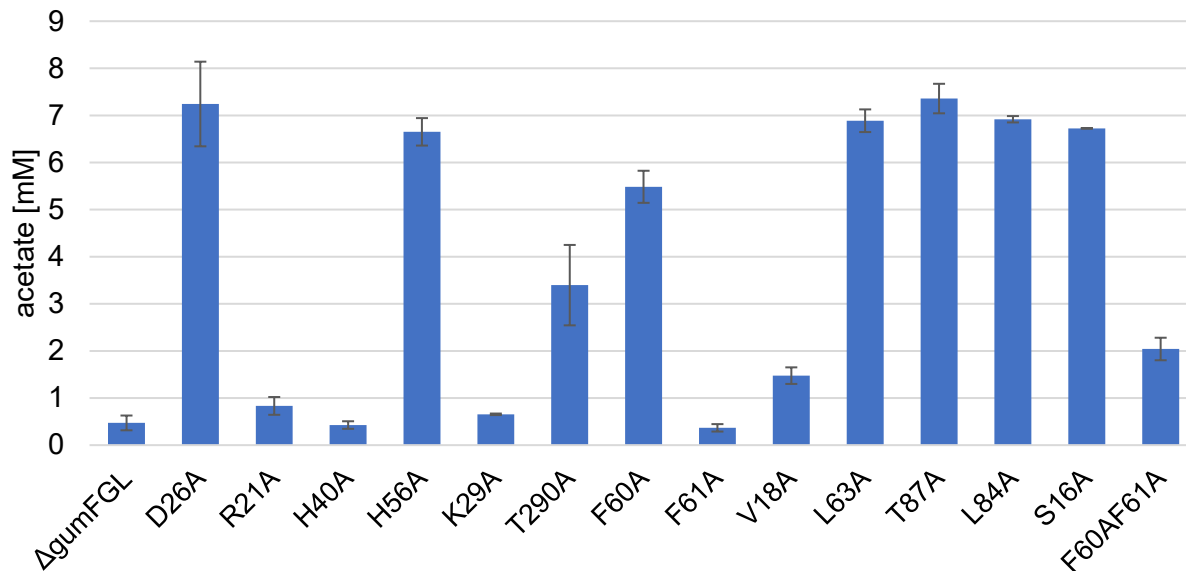
Figure 8. Final screening of the gumG variants constituively expressed in *Xcc* Δ*gumFGL* by the pHExXan plasmid.

All variants were constitutively expressed with the pHexXan-plasmid in *X. campestris* Δ*gumFGL*. All samples were tested in biological triplicates, shown values are normalized to 10 g L^{-1} of hydrolyzed xanthan.

As a last step of identifying a possible region for the mutagenesis towards the cofactor specificity, docking studies were carried out with both acetyl-CoA as well as the repeating unit of xanthan. In GumG model 1, one major and one smaller cluster was found for the docking of acetyl-CoA. In this model both of them were on the opposite site of the mutated regions in respect to the enzymes tertiary structure. In model 2, two major binding clusters, one minor cluster and one individual binding site were identified, were the single binding site had closest proximity to R21 and V18. The minor binding cluster was in close proximity to K29 and H40, however in this model, the ligand and the amino acids were on opposite sides of an α-helix. The Docking studies with model 3 showed two major binding clusters, one of them was directly adjacent to an α-helix with the amino acids V18, R21 and K29, whose mutations led to inactivity. For model 4, one major binding cluster and a small binding cluster with 2 ligand positions was identified, in the major binding cluster one position of the ligand was found in which the phosphopantetheine residue of Ac-CoA directly protrudes into the binding-pocket like structure described before. In model 5, two major clusters for binding of Ac-CoA were identified, where only one of them was in closer proximity to R21 and K29 with V18 being on the opposite side of the binding cluster, in a loop structure.

Docking studies with the pentasaccharide repeating unit of xanthan showed 3 major and one minor cluster in model 1, one major and three minor clusters for model 2, two major clusters in model 3, three major and one cluster containing only two possible ligand positions in model 4 and two clusters in model 5.

Comparing the binding clusters of acetyl-CoA and the xanthan repeating unit, for each model two adjacent acetyl-CoA and repeating unit binding clusters could be identified. While in model 1 these clusters had no proximity to the amino acids whose mutation led to a loss of function, the best alignment of AcCoA, repeating unit and these amino acids was found in model 2 and 4.

4.5 Pathway engineering and determination of intracellular CoA-levels

4.5.1   Pathway selection and design of expression plasmid

For the increase of intracellular levels of crotonyl-CoA (CrCoA), the introduction of a pathway from acetyl-CoA (AcCoA) to acetoacetyl-CoA (AcAcCoA) and from AcAcCoA to (R)-3-hydroxybutyryl-CoA (3-HBCoA), catalyzed by the thiolase PhaA and the (R)-3-hydroxybutyruyl-CoA-dehydrogenase PhaB from *Cupriavidus necator* and finally from (R)-3-HBCoA to CrCoA, catalyzed by the R-specific crotonase Crt from *Clostridium acetobutylicum*. As the genes *phaA* and *phaB* are clustered in the genome of *C. necator,* they were cloned together from *C. necator* gDNA. *Crt* was cloned from *C. acetobutylicum* gDNA, introdcuding a ribosome binding site and an overlap to the *phaAB* fragment with the forward-primer Forward primer of the *phaAB* fragment and reverse primer of the *crt* fragment were designed to overlap with the pGAKm backbone, creating the pCRT plasmid for IPTG inducible overexpression of *phaAB* and *crt*. The overexpressed pathway and the pCRT plasmid are shown in Figure 9. The genes were successfully amplified and pCRT was assembled by Gibson-Assembly. The insertion of the genes was confirmed by sequencing and *X. campestris* wt as well as *X. campestris* Δ*gumFGL* were transformed by electroporation.
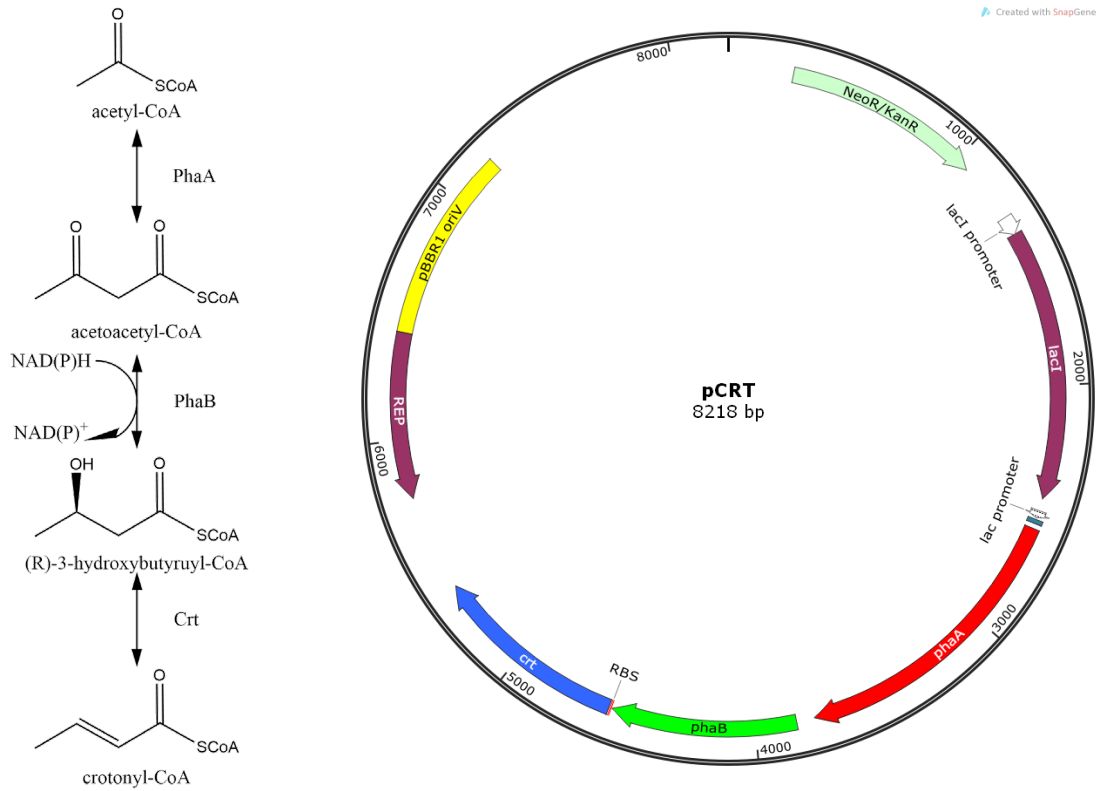
Figure 9. Pathway from acetyl-CoA to crotonyl-CoA, catalyzed by PhaA and PhaB from *C. necator* and Crt from *C. acetobutylicum* and the plasmid pCRT for the heterologous pathway expression in *X. campestris*.

4.5.2 Growth studies of *X. campestris* with expression-plasmid

Transformed *X. campestris* Δ*gumFGL* pCRT strains as designed production organisms were compared to *X. campestris* wt and *X- campestris* wt pCRT in a parallel-fermenter-system in order to validate its growth behavior. For a complete comparability, all reactos were inoculated to the same OD_{600} of 0.1 and 1 mM IPTG was added to all variants after 9.4 hours. While *Xcc* wt pCRT reached lower OD_{600} compared to *Xcc* wt, *Xcc* Δ*gumFGL* pCT reached higher OD, while all three variants had the same lag phase and reached log phase and stationary phase simultaneously. The maximum growth rate μ_{max} are shown in Table 8. The growth curves are shown in Figure 10, the glucose consumption and formation of EPS, measured by the viscosity of the fermentation broth are shown in Figure 11. Glucose consumption and increase of viscosity were highly comparable amongst the three variants and showed the same correlation between growth, glucose consumption and increase of viscosity. While the increased viscosity of *Xcc* wt pCRT correlated with a higher product yield, *Xcc* Δ*gumFGL* and *Xcc* wt had very similar product yields and the decreased viscosity of the fermentation broth of *Xcc* Δ*gumFGL* pCRT correlates with the decreased viscosity of this xanthan-variant (Gansbiller, Schmid, & Sieber, 2019). Concluding from this data, the growth behavior and xanthan production are not influenced by the overexpression of *phaA*, *phaB* and *crt* with the pCRT plasmid.

Table 8. Maximum growth rates μ_{max} of the different *Xcc* variants in parallel fermenter system

For calculation OD_{600} values were plotted semilogarithmic over time during exponential growth (0.35 h-11.5 h). μ_{max} is defined as exponent of the exponential fit.

Variant	*Xcc* wt	*Xcc* wt pCRT	*Xcc* Δ*gumFGL* pCRT
μ_{max} [h^{-1}]	0.32	0.25	0.23
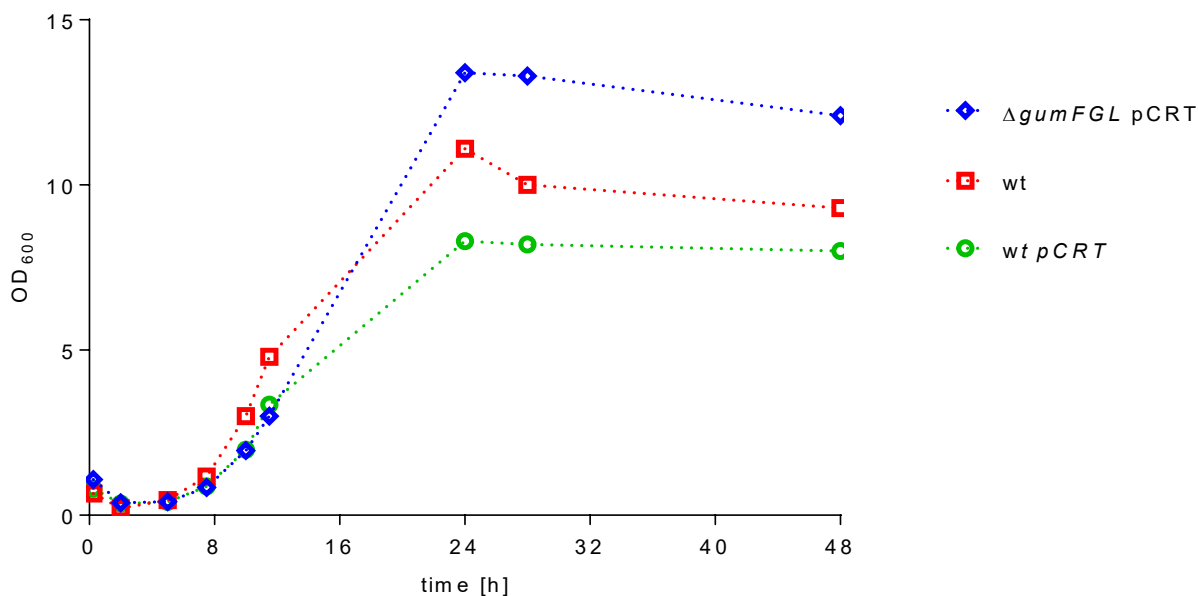
Figure 10. Growth curves of *X.campestris* variants in the parallel fermenter system.

OD$_{600}$ values were measured against the medium of each reactor and diluted to be measured within a range of 0.1-0.8
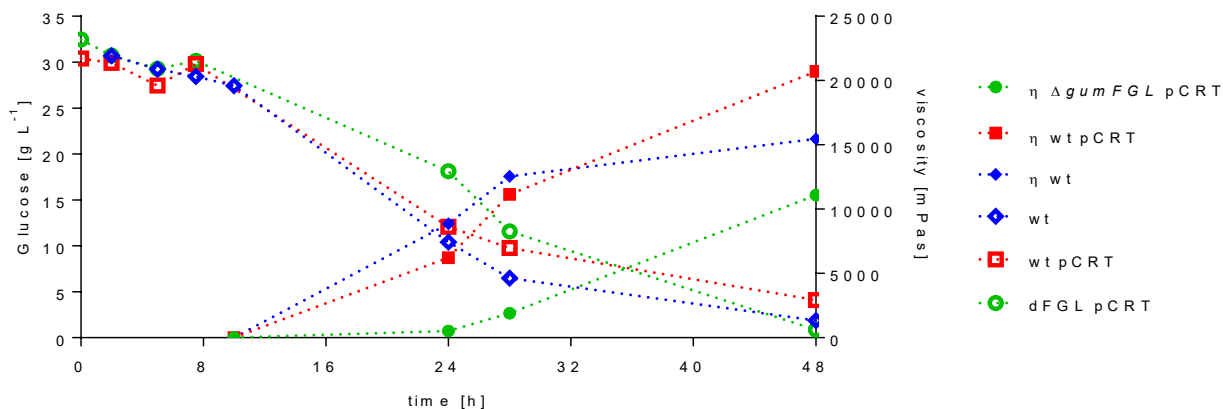

Figure 11. Glucose consumption and viscosity increase during fermentation of *X. campestris* variants in parallel fermenter system.

Glucose (empty symbols) was measured with an enzymatic assay by a 500-fold dilution the supernatant. Viscosity (filled symbols) was measured with the MCR 300 Rheometer and a cone-and-plate system at 30 °C at a constant shear rate of 1 s^{-1}. Viscosity values are averages of 20 data points, when viscosity reached steady state.

4.5.3 Incorporation of both pHExXan-*gumG* and pCRT plasmid in *Xcc* Δ*gumFGL*

It was not possible to achieve chromosomal integration of modified genes into *Xcc*, why a plasmid-based approach was used for the simultaneous overexpression of *phaA, phaB* and *crt* with pCRT and engineered *gumG* variants with pHExXan, using a kanamycin/gentamicin double selection. For this, electrocompetent *Xcc* Δ*gumFGL* pCRT were prepared under kanamycin selection and subsequently transformed with pHExXan-*gumG*. After transformation cells were grown with kanamycin/gentamicin double selection. Cells were grown on LB agar and single colonies were transferred into liquid culture and incubated over night at 30 °C. The culture volume was split, and one half was used to prepare cryo-stocks while the other half was used to isolate the plasmid DNA for quantification. Growth and plasmid isolation and quantification was then repeated using the cryo-cultures after several days of storage at -80 °C to test stability of the plasmids. The results indicated stability and replication of both plasmids in *Xcc* Δ*gumFGL*, which can be used as a strain for all further engineering studies.

4.6 Analysis of intracellular CoA and Cr-CoA levels

The analysis of intracellular CoA-levels of *Xcc* was carried out according to 3.3.3. Extraction was carried out at different $OD_{600.}$ The required OD_{600} was calculated based on literature values for *E. coli (Bennett et al., 2009)*. The cfu-OD correlation of *E. coli*, where OD 1 = $8\cdot10^8$ cfu mL^{-1} was assumed to calculate the required cfu mL^{-1} of *Xcc* (Watt, Wilke, Patschkowski, & Niehaus, 2005). Based on these values an OD_{600} of at least 1.0 was necessary to quantify CoA-levels in *Xcc* with the developed method.

For analytics, a formic acid/ ammonium formate/ ammonia buffer system at pH 4.5, 5.5, 6.5 and 8.5 were tested. Formic acid was used at a concentration of 0.1 % and pH was adjusted with ammonia. Ammonium formate was tested at concentrations of 10 mM and 26.5 mM, where the latter corresponded to the molarity of 0.1 % formic acid. The different buffers were compared at pH 8.5 and with 26.5 mM ammonium formate, the best combination of separation and signal intensity was achieved. With 26.5 mM ammonium formate a shift towards lower elution volumes was observed at increasing pH, while at pH 4.5 and 5.5 poor signal intensity and broad peaks were observed. Highest signal intensity was achieved at pH 6.5. The final used conditions resulted in a limit of detection (LOD) of 0.1 µM and a limit of quantification (LOQ) of 0.3 µM for both CoA and CrCoA.

As the initial extraction method of CoA and CoA-esters involved high solvent content (40 % acetonitrile, 40 % methanol) in the samples, the extraction matrix was spiked with CoA and CrCoA, respectively to a final concentration of 10 µM. The addition of solvents showed a strong peak shift of both CoA and CrCoA to the exclusion volume, hindering separation at these conditions. This effect increased with higher pH. Where at pH 4.5 only a small portion of the peak shifted to the exclusion volume, while at pH 8.5 > 95 % of the peak area shifted to the exclusion volume.

However, the poor peak quality at pH 4.5 did not allow for a sensitive quantification. To circumvent this problem, after extraction the solvent was removed by vacuum centrifugation at 65 °C for 1 h and the samples were subsequently dissolved in water. This method was validated by testing CoA and CrCoA standards with this method against untreated standards where a full recovery after this treatment was confirmed. When cell pellets of *Xcc* were treated with the extraction fluid and spiked with both CoA and CrCoA, a degradation of CrCoA was observed, but not for CoA. To further investigate this, spiking with 5 µM of CoA and CrCoA was carried out in two different ways.

1) during extraction, after centrifuging the sample and before vacuum centrifugation
2) after vacuum centrifugation during dissolving of the dried sample in water

These experiments showed a slightly lower yield of CoA with spiking method (1) compared to spiking method (2), however no significant degradation was observed, while CrCoA showed equally high degradation in both spiking experiments. Further analysis confirmed that the degradation of CrCoA only occurred when *Xcc* cells were involved in the extraction process and furthermore that the degradation occurred over time.
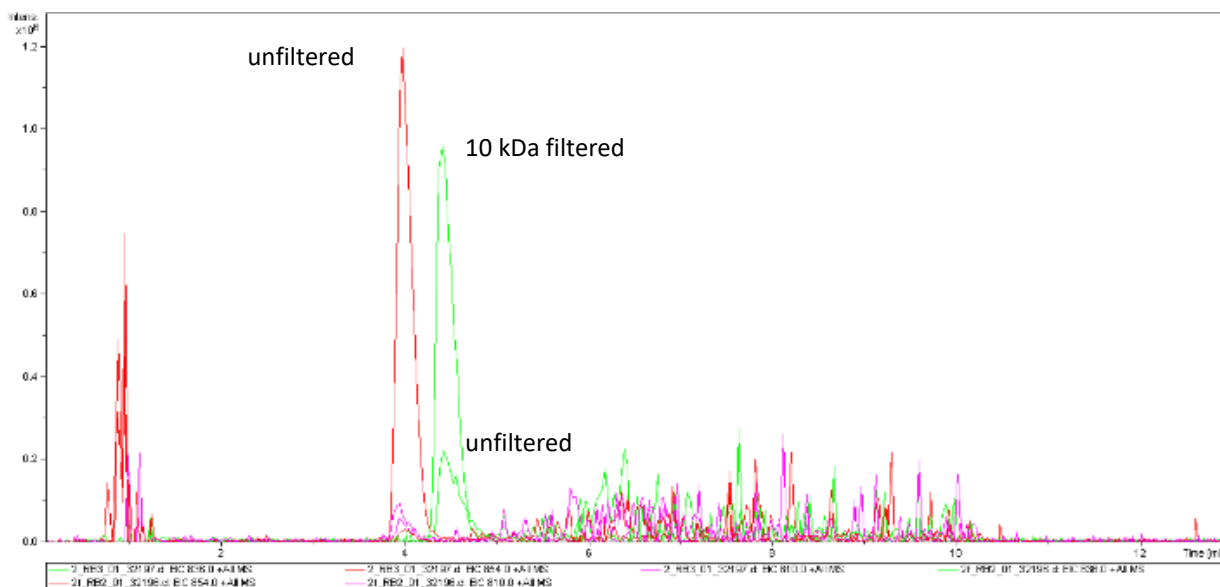
shows the extracted ion chromatogram of CrCoA (green peak, m/z 836 ([M+H]$^+$) at two different time points after extraction and spiking, showing a time sensitive degradation of CrCoA, and the time sensitive formation of a second peak (red peak, m/z 854 ([M+H]$^+$), which was analyzed for its MS/MS fragmentation pattern and could be identified as 3-hydroxybutyryl-CoA (3-HBCoA). In order to investigate, if the observed degradation could be due to remaining enzymatic activity, metabolite extraction was carried out as described above, and after evaporation of solvents and dissolving in water, the sample was filtered through a 10 kDa syringe filter prior to spiking with 5 µM CrCoA. The sample was then compared to an unfiltered spiked sample. The elution diagram (Figure 13) of both samples showed, that the conversion of CrCoA to 3-HBCoA did occur in the unfiltered sample, but not after filtration through a 10 kDa filter. Injection of the filtered sample at

different time points, up to 2 h after extraction, revealed, that the conversion from CrCoA to 3-HBCoA was completely inhibited in the filtered sample. Because of this conversion, a quantification of the intracellular CrCoA levels was not possible, however it was possible to quantify the intracellular CoA levels. It is also worth mentioning that the quantification of 3HBCoA together with CrCoA can be done to estimate the changes of the intracellular CrCoA levels after extraction. However, intracellular 3HBCoA will influence these results. As *Xcc* Δ*gumFGL* was designed as working strain, it has been tested in comparison to *Xcc* Δ*gumFGL pCRT*. For *Xcc* Δ*gumFGL* the total CoA-concentration were 3.35±0.07 µM, and 2.23±0.05 µM for *Xcc* Δ*gumFGL pCRT* induced with 1 mM IPTG, both concentrations were obtained from 10 ml culture volume at OD 2.1, indicating a decrease of CoA in *Xcc* pCRT. CrCoA could not be detected in any of the unspiked samples. Samples were spiked with 5 µM CoA and CrCoA directly during extraction and after dissolving the sample in water. The samples spiked during extraction showed recoveries of 7.43 ± 0.17 µM CoA/0.73 ± 0.02 µM CrCoA and 6.14 ± 0.14 µM CoA/0.92 ± 0.00 µM CrCoA for *Xcc* Δ*gumFGL* and *Xcc* Δ*gumFGL pCRT*, respectively. The samples spiked after the process showed concentrations of 8.59 ± 0.20 µM CoA/0.99 ± 0.02 µM CrCoA for *Xcc* Δ*gumFGL* and 6.95 ± 0.20 µM CoA/0.95 ± 0.02 µM CrCoA for *Xcc* Δ*gumFGL pCRT*.
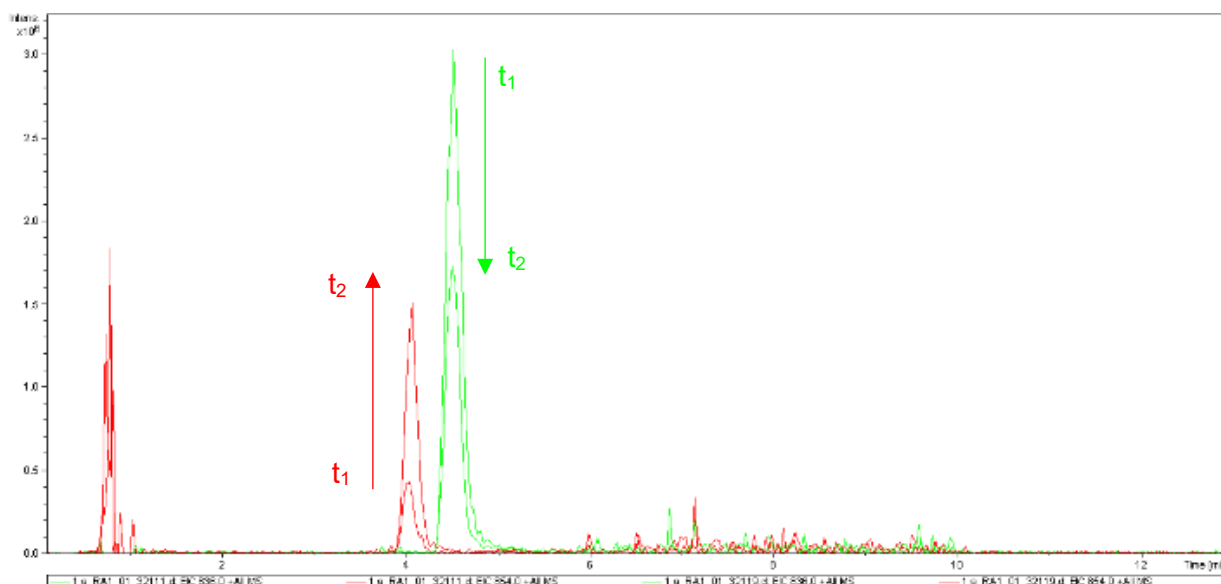
Figure 12. Conversion of CrCoA to 3-HBCoA over time monitored by HPLC-MS/MS.

EIC of the conversion of 5 µM CrCoA (green trace, m/z 836)) to 3-HBCoA (red trace, m/z 854) were measured at two different time points after spiking of the extraction mixture containing the extracted

metabolites of *Xcc* before further processing of the samples. Timepoint t_1 is measured directly after dissolving the dried sample in water, Timepoint t_2 was injected 1 hour after t_1 from the same sample vial.
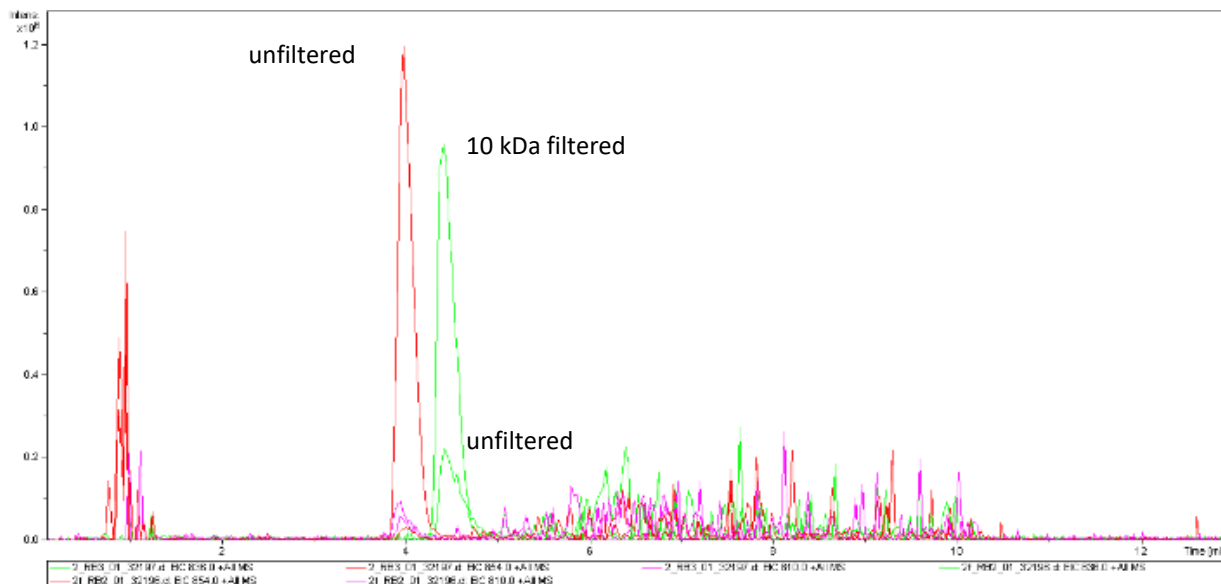

Figure 13. Conversion of CrCoA to 3-HBCoA with and without filtering of the cell extract

EIC showing CrCoA (green trance, m/z 836) and 3HBCoA (red trace, m/z 854) of samples with and without filtering of cell extract through a 10 kDa filter before spiking. The unfiltered sample was injected directly after dissolving of the dried sample in water, the filtered sample was injected directly after filtration and after 2h of incubation after filtration.

4.7 Production and properties of chemically crotonylated xanthan

To predict the properties of the modified xanthan created by an *in-vivo* design, an approach to create a chemically crotonylated xanthan variant. For this a solvent-free method was developed by suspending the acetyl- and pyruvyl-free xanthan variant XanΔFGL in a 2.6-fold excess of crotonic anhydride using 1.4 % sulfuric acid as a catalyst. The reaction was carried out at 60 °C over 16 h and resulted in a xanthan with low degrees of substitution of 0.2 - 0.4. The resulting variants therefore mirrored a degree of substitution, which was expected with the *in-vivo* approach and were still water soluble. First basic rheological characterizations showed a significant increase of the gel strength with higher brittleness compared to the unmodified variant, indicating a cross-linked structure caused by the C=C double bonds of the crotonic acid linked to the xanthan. However, while this method can describe the properties of a randomly crotonylated polysaccharide, the properties of a regiospecific crotonylation of mannose residues the sidechain might have different effects and as revealed by the studies of the genetically modified xanthan variants, individual site-specific substitutions of the mannose will have significant effect on the rheological properties.

Moritz Gansbiller and Sumanth Ranganathan were involved with the conceptualization, methodology, validation, formal analysis, investigation, data curation, writing and visualization of the original draft.

Volker Sieber was involved in conceptualization and supervision, reviewing and editing the original draft as well as resource provision, project administration and funding acquisition.

1   Communication

2   Solvent-free crotonylation of Xanthan

3   Moritz Gansbiller[a], Summanth Ranganathan[a] and Volker Sieber[a,b,c,*]

4   [a] Chair of Chemistry of Biogenic Resources, Technical University of Munich, Campus for
5   Biotechnology and Sustainability, Schulgasse 16, 94315, Straubing, Germany

6   [b] Fraunhofer IGB, Straubing Branch BioCat, Schulgasse 23, 94315, Straubing, Germany

7   [c] TUM Catalysis Research Center, Ernst-Otto-Fischer-Straße1, 85748, Garching,
8   Germany

9   * corresponding author

11   Abstract

12

13   Microbial exopolysaccharides offer a wide diversity of physicochemical properties

14   because of their structural diversity. These properties may be extended by chemical

15   modification to yield tailor-made polysaccharides. Till date, industrially relevant chemical

16   modification methods almost exclusively apply to non-microbial polysaccharides. The few

17   processes that exist for microbial polysaccharides are often limited to lab-scale and

18   represent energy- and material intensive procedures. Moreover, these studies often lack

19   the rheological characterization of the product, which is ultimately the sole purpose of the

20   produced substances. To tackle this issue, we developed an easy scalable, simple and

21   cost-efficient process for the crotonylation of xanthan using crotonic anhydride and sulfuric

22   acid as mediator in a solvent-free heterologous process, which introduces C=C double

23   bonds in the polysaccharide structure, thereby creating a water-soluble crosslinked

24   xanthan-variant with significantly higher gel strengths compared to natural xanthan.

25

26

27

28   1.1   Introduction

29

30   Polysaccharides offer structural variety along with a wide range of physicochemical

31   properties (Dumitriu, 2004). As polysaccharides are mostly used as so-called rheological

32   enhancers, thickening or gelling agents for instance, their diverse rheological properties

33   are the foundation of the various application in food, pharma, cosmetic or even

34   construction and oil drilling industry (Rehm, 2010). This variety primarily stems from the

35   diverse structures, such as glycosidic linkages, chain length or -branching (Wingender,

36   Neu, & Flemming, 2012). Another key factor affecting the physicochemical properties of

37   polysaccharides is the functionalization of these primary structures, for example acetyl-

38   glyceryl- esters or pyruvyl-ketals; the absence or presence of which, have a significant

39   impact on these properties (Gansbiller, Schmid, & Sieber, 2019; Tako et al., 2016;

40   Wingender et al., 2012). Modifying these functional groups by chemical (de-)acylation

41   processes (Xu et al., 2019), or enzymatic modifications (Karaki, Aljawish, Humeau,

42   Muniglia, & Jasniewski, 2016), and highly site-specific modifications by genetically

43   modifying the production organisms (Gansbiller et al., 2019; Wu et al., 2019), allows the

44   fine-tuning of their properties, and expansion of the field of application. As microbial EPS

45   show vast structural and functional varieties (Shukla, Mehta, Parmar, Pandya, & Saraf,

46   2019) along with the potential of modification via genetic engineering and cost-efficient

47   production processes, the benefits of fine-tuning the processes to industry scale is

48   undeniable. Despite this, the industrial applications are still almost exclusively applied to

49   non-microbial polysaccharides, such as starch, cellulose and other plant polysaccharides

50   (Cumpstey, 2013; Lapasin, 2012; Xu et al., 2019). Recently, chemical modifications of

51   microbial polysaccharides have emerged for alginate derivates and the chemically

52   deacylated sphingan Gellan with the promise of industrial significance (Pawar, 2017;

53   Shukla et al., 2019). Modifications of other microbial polysaccharides such as xanthan,

54   one of the most widely used and studied microbial EPS, have also been developed, but

55   these novel and interesting modifications are still limited to laboratory scale and high

56   material and/or energy cost hinder the scaling-up of these novel processes (Fantou et al.,

57   2017; Muljana et al., 2018). To expand these methods and show their potential for large-

58   scale applications, we developed a simple reaction setup for the esterification of a xanthan

59   variant with crotonic acid. Xanthan is widely used in various industrial applications. Its

60   primary structure consists of a cellulose (D-Glc$p$-(1→4)-ß-D-Glc$p$) backbone with an α-

61   (1→3) linked ß-D-Man$p$-(1→4)-ß-D-GlcA-(1→2)-α-D-Man$p$ sidechain. The inner Man$p$

62   can be O-acetylated at position 6, while the outer Man$p$ is either O-acetylated at position 6

63   or forms a pyruvyl-ketal at position 4 and 6. These decorations of the mannose residues

64   directly determine the rheological properties of Xanthan and the pattern of these functional

65   groups can be minutely governed by genetical modification of the production strain

66   (Gansbiller et al., 2019). For this work, a completely undecorated variant of Xanthan

67   (XanΔFGL) was used, as this variant has the highest possible number of free OH-Groups

68   for esterification and its modification by the developed method may expand the potential

69   of Xanthan in various industrial applications.

70

71 ## 2. Materials and Methods

72 ### 2.1 Materials

73

74 Crotonic anhydride, 95 % was purchased from Merck KGaA (Darmstadt, Germany.
75 Sulfuric acid, 96 % was purchased from Carl Roth GmbH + Co. KG (Karlsruhe, Germany).
76 MilliQ® Water (Merck KGaA, Darmstadt, Germany) was used for all experiments.

77

78 ### 2.2 Production and analysis of acetyl- and pyruvyl-free Xanthan

79

80 Acetyl- and pyruvyl-free Xanthan (XanΔFGL) was produced by fermentation of an
81 engineered *Xcc*-strain as described in a previous study. Acetate and Pyruvate content of
82 this variant was determined after hydrolysis via HPLC as described previously (Gansbiller
83 et al., 2019).

84

85 ### 2.3 Chemical crotonylation of xanthan

86

87 3.3 ml ($\hat{=}$22.82 mmol) crotonic anhydride containing 1.3 % sulfuric acid were heated up
88 to 60 °C in a 25 ml round bottom flask and 0.5 g XanΔFGL ($\hat{=}$0.61 mmol, calculated based
89 on the molecular mass of one repeating unit, 824 g mol^{-1}) were added as powder. The
90 reaction was stirred at 250 rpm to keep the Xanthan in suspension. After 16 h the reaction
91 was cooled to ambient temperature and subsequently washed with 45 ml water for
92 approximately 1 h in a 50 ml screw-cap tube and subsequently centrifuged (4000 *g*, 10
93 min, room temperature). Washing and centrifugation steps were repeated for 5 times total.
94 The water-soluble fractions after the washing steps were precipitated in 2 volumes
95 Isopropanol. The water insoluble fraction was separated by decanting the liquid phase
96 after centrifugation. The precipitated, water-soluble fractions and the water-insoluble
97 fraction were subsequently dried in a vacuum oven at 40 °C for at least 24 h.

98

99   2.4 Analysis of crotonylated Xanthan

100

101   5-10 mg of dried sample was suspended in 1 ml 250 mM sulfuric acid and hydrolyzed at

102   90 °C under vigorous shaking at 2000 rpm in 1.5 ml reaction tubes. As a control, 5-10 mg

103   of the same sample was treated likewise, except water was used instead of sulfuric acid.

104   After hydrolysis, samples were cooled to room temperature, centrifuged (21,000 g, 1 min,

105   RT) and supernatants were filtered through a 0.22 µm PVDF syringe filter (Restek GmbH,

106   Bad Homburg, Germany). Filtered supernatants were either used directly for HPLC-

107   analysis or diluted 10-fold prior to analysis. HPLC analyses were carried out on a Dionex

108   UlitMate 3000 (Thermo Fisher Scientific, Waltham, MA, USA) equipped with a Rezex ROA

109   H$^+$-column (Phenomenex Inc, Torrance CA, USA) at 70 °C with an isocratic flow rate of

110   0.5 ml min^{-1} using UV- and RI-detector (Shodex RI-101, Showa Denko K.K., Tokyo,

111   Japan). The quantified crotonic acid concentrations were normalized to 10 g l^{-1} sample

112   concentration and the (normalized) crotonic acid concentration from the respective

113   negative control was subtracted, as this was attributed to the amount of unbound crotonic

114   acid in the product.
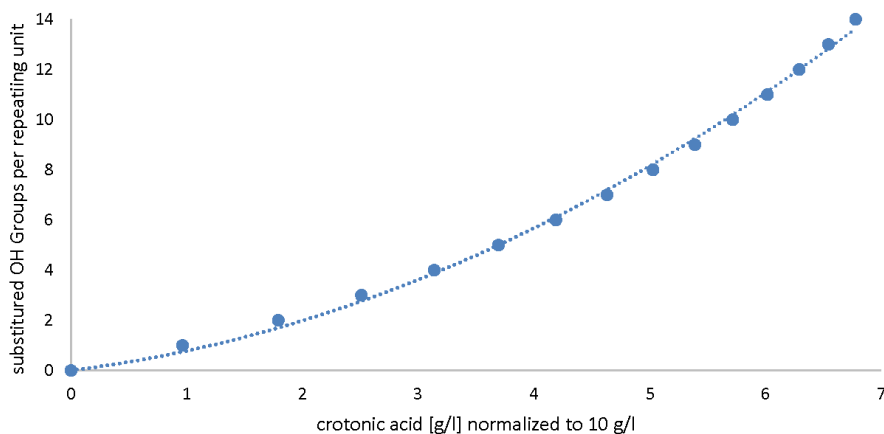
115

116   Fig. 1 calculated average number of substituted OH groups per repeating unit of XanΔgumFGL

117   A second-degree polynomial regression (dashed line) was applied and forced through the origin due to the
118   boundary conditions (R²=0.9978).

119 From the polynomial regression, substituted OH groups could be calculated from (I).

120 $$OH_{subs.} = (0.213\ c_{CA,norm.})^2 + 0.5655\ c_{CA,norm.} \tag{I}$$

121 OH_{subs}: substituted OH-groups per repeating unit

122 $c_{CA,\ norm}$: (corrected) concentration of crotonic acid after hydrolysis, normalized

123 2.5 Fourier-Transformation Infrared (FTIR) spectroscopy
124

125 FTIR spectroscopy was carried out on a Nicolet™ 380 (*Thermo Fisher Scientific Inc.*)
126 equipped with a Smart Orbit™ Diamond ATR (*Thermo Fisher Scientific Inc.*). Roughly 1 mg
127 of EPS powder was applied on the diamond and measured using the attenuated total
128 reflection (ATR). Each sample was blanked by a measurement with no sample on the
129 diamond. IR spectra were measured at wavenumbers 4,000-400 cm^{-1}.

130

131 # 3. Results

132

133 3.1 Analysis of XanΔFGL and determination molar excess of crotonic anhydride
134

135 HPLC analysis showed no detectable amounts of acetic and pyruvic acid after hydrolysis
136 of XanΔFGL, hence all OH groups of the repeating unit were free for chemical acylation,
137 resulting in a 2.68-fold molar excess of crotonic anhydride respective to free OH-Groups
138 in Xanthan, based on the molecular weight of 824 g mol^{-1} of the pentasaccharide repeating
139 unit.

140

141 3.2 Impact of the molar excess on the degree of crotonylation
142

143 The reaction with a 2.68-fold molar excess of crotonic anhydride resulted in two major
144 fractions of crotonylated Xanthan. The insoluble fraction with a substitution degree of
145 1.8±0.1, accounted for 14±1 % (w/w) of total product, while the remaining 86±1 % (w/w)
146 were found in the water-soluble fractions with a low degree of substitution of 0.41±0.03

147 and 0.23±0.05, respectively from wash fractions 1 and 2, respectively. Upscaling the
148 reaction by a factor of 10 resulted in only one wash fraction with a DS of 0.4, however, no
149 insoluble fraction with a higher DS was obtained. Further experiments with a higher molar
150 excess of crotonic anhydride of 4:1 and 10:1 was also tested, to investigate whether a
151 higher excess would result in higher degrees of substitutions. Like for a 2.68:1 molar
152 excess, with a 4:1 molar excess of crotonic anhydride two wash fractions and an insoluble
153 fraction was obtained, but unlike the 2.68:1 ratio, the first wash fraction had no quantifiable
154 DS, while the second wash fraction showed a higher degree of substitution of 0.6, which
155 was even higher to the DS of the insoluble fraction with a DS of 0.5. The 10:1 molar excess
156 resulted in three wash fractions, where the first two showed a DS below the limit of
157 quantification, while the third wash fraction had a DS of 0.6, which was identical to the DS
158 of the insoluble fraction. Additionally, crotonylation was monitored via FTIR spectroscopy.
159 Compared to the completely deacetylated and depyruvylated xanthan, crotonylated
160 xanthan showed emerging peaks at wavenumbers 960 cm^{-1} (disubstituted trans alkene
161 C=C bending), 1060 cm$^{-1,}$ 1150 cm^{-1} (C-O stretch) and the broad peak around 1600 cm^{-1}
162 shifted towards a narrower peak at 1580cm^{-1}. Also, a very weak peak was observed at
163 1725 cm^{-1} (ester bond C=O stretch), however it was very faint due to the low degree of
164 crotonylation. The distinctive double peak between wavenumbers 1700-1800 for the
165 symmetric and asymmetric C=O stretch of the crotonic anhydride , were not visible,
166 indicating the absence of this compound in the final product.

167

168 3.3 Viscoelastic properties of water-soluble low-crotonylated Xanthan
169

170 The water-insoluble fraction of crotonylated Xanthan exhibited rubber-like, sticky
171 properties and solubility test in different solvents (water, acetonitrile, DMSO, acetone and
172 hexane) did not result in proper solutions, event at very low concentrations of 0.1 % (w/w).
173 Low crotonylated Xanthan, however, was soluble in water at concentrations up to 1.0 %
174 (w/w) by stirring for 24 h at room temperature. Compared to XanΔFGL used for the starting
175 variant for crotonylation, the resulting solutions exhibited higher viscosity at equal
176 concentrations and a more pronounced gel-like character (Fig. 2.) Amplitude sweeps
177 showed that at both concentrations of 0.5 % (w/w) and 1.0 % (w/w) storage modulus G'

178 increased by a factor of 22 for the 0.5 % solution and a factor of 4 for the 1.0 % solution.
179 While the 0.5 % of unmodified xanthan showed predominant liquid character, the
180 crotonylated variant showed pronounced gel character at this concentration. The damping
181 factor decreased significantly compared to XanΔFGL for both concentrations. The
182 crotonylated variant showed highly increased gel strength and its viscoelastic properties
183 were also more brittle, indicated by a decreased yield and flow point. Additionally, a
184 significant increase of the los modulus G'' at the end of the LVE was evident, as often
185 seen in polymers with a strong network structure.
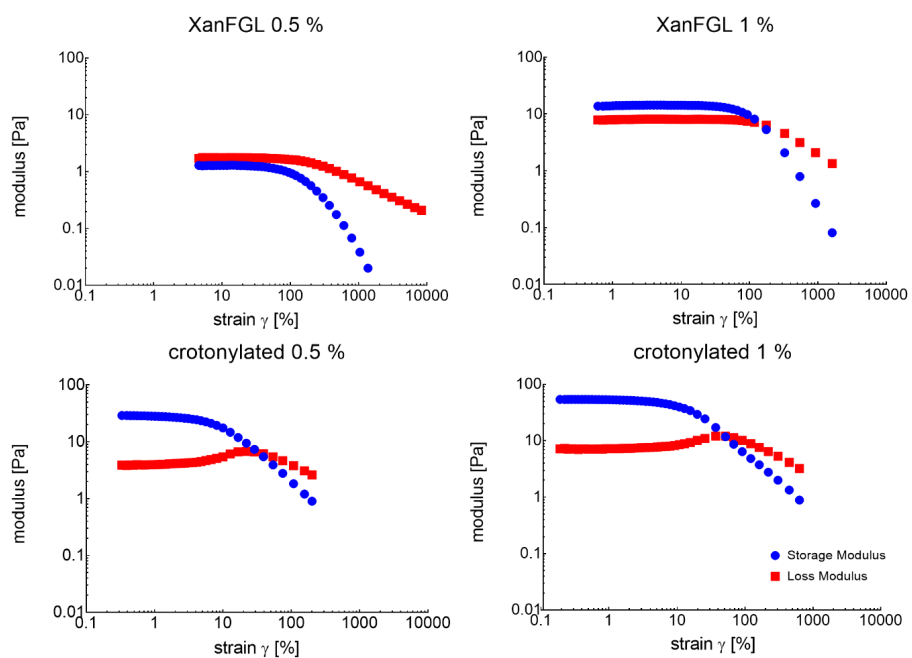
186

187 Fig. 2 Amplitude sweep of unmodified and low crotonylated XanFGL as 0.5 % (w/w) and 1.0 % (w/w)
188 aqueous solutions. Storage Modulus (blue dots) and Loss Modulus (red squares) are shown over the strain

189

4. Discussion

4.1 Degree of substitution

The developed method resulted in two major fractions of crotonylated xanthan. The highly crotonylated variant with a DS of about 2 OH-groups per repeating unit on average, accounted for about 15 % of the total yield. This water-insoluble fraction was also poorly soluble in a variety of organic solvents and is hence undesirable for further use as a rheological enhancer. The remaining 85 % of yield showed low levels of crotonylation with DS between 0.2-0.4. Previous studies described the acrylation of Xanthan, which also resulted in very low DS (Hamcerencu, Desbrieres, Popa, Khoukh, & Riess, 2007), similarly low DS were also achieved for the acrylation of Gellan, in both homo- and heterogenous reaction conditions, and independent of reaction temperature (Hamcerencu, Desbrieres, Khoukh, Popa, & Riess, 2008). In the same study with maleic acid, a significantly higher DS of 1 was achieved for xanthan under heterogenous conditions at 60 °C and 24 h. These studies, however, do not describe the physical properties or yields, impeding a good comparability. It seems, however, that the degree of substitution depends more on the chemical properties of the acid (activated or anhydride) and less on the reaction conditions. Preliminary experiments to this study with acetic anhydride confirmed these findings, as much higher degree of acetylation of xanthan was achieved compared to crotonylation using crotonic anhydride under identical reaction conditions. The increase of the molar excess of acid anhydride did not result in a significant increase of the DS and as an economically feasible process was targeted, this aspect was not investigated further, due to low efficiency of the synthesis (Cumpstey, 2013; do Nascimento Marques et al., 2020; Fantou et al., 2017; Pawar, 2017), (Fantou et al., 2017).

4.2 Effect of crotonylation on viscoelastic properties

Although the degree of crotonylation was very low, the rheological properties of xanthan changed drastically, shifting towards a strong gel character, indicated by both higher storage modulus G' and lower damping factor, combined with overall lower deformation. The strong gel character indicated a strong interaction between the polymer strands,

221 which may be due to crosslinking via the C=C double bonds of the crotonyl groups. The
222 viscoelastic properties were therefore significantly changed by the crotonylation and
223 increasing the concentration had very little effect on the rheological properties, compared
224 to the untreated xanthan. This might be due to an earlier saturation effect due to the limited
225 amount of available C=C bonds per repeating unit. On the other hand, this means that
226 similar properties can be achieved with less material input. This study and previous reports
227 (Hamcerencu et al., 2007) on acrylation or crotonylation of Xanthan suggest, that the
228 possible substitution of OH groups per repeating unit might be limited to a very low degree,
229 independent of the reaction parameters and it is therefore important to know that low DS
230 and low concentrations can be helpful in achieving the desired properties.

231 ## 5. Conclusion
232

233 This study reports the first ever chemical crotonylation method and the first rheological
234 investigation of xanthan possessing an introduced C=C double bond via an ester group.
235 It was possible to determine the degree of substitution by an HPLC method. The results
236 show that only a low degree of crotonylation can be achieved regardless of reaction
237 conditions, however this low degree of substitution is both necessary to allow proper water
238 solubility, but also sufficient to produce desired viscoelastic properties. As a water-soluble
239 polysaccharide, it remains advantageous as an environmentally friendly substance for
240 solvent-free applications coupled with a production process, that is both cost-effective and
241 easily scalable.

245

246   Cumpstey, I. (2013). Chemical modification of polysaccharides. *ISRN organic chemistry, 2013*.
247   do Nascimento Marques, N., dos Santos Alves, K., Vidal, R. R. L., da Silva Maia, A. M., Madruga, L. Y. C.,
248   Curti, P. S., & de Carvalho Balaban, R. (2020). *Chemical Modification of Polysaccharides and*
249   *Applications in Strategic Areas*. In *Emerging Research in Science and Engineering Based on*
250   *Advanced Experimental and Computational Strategies* (pp. 433-472): Springer
251   Dumitriu, S. (2004). *Polysaccharides: structural diversity and functional versatility*: CRC press.
252   Fantou, C., Roy, A. N., Dé, E., Comesse, S., Grisel, M., & Renou, F. (2017). Chemical modification of
253   xanthan in the ordered and disordered states: An open route for tuning the physico-chemical
254   properties. *Carbohydr Polym, 178*(Supplement C), 115-122.
255   Gansbiller, M., Schmid, J., & Sieber, V. (2019). In-depth rheological characterization of genetically
256   modified xanthan-variants. *Carbohydr Polym, 213*, 236-246.
257   Hamcerencu, M., Desbrieres, J., Khoukh, A., Popa, M., & Riess, G. (2008). Synthesis and characterization
258   of new unsaturated esters of Gellan Gum. *Carbohydr Polym, 71*(1), 92-100.
259   Hamcerencu, M., Desbrieres, J., Popa, M., Khoukh, A., & Riess, G. (2007). New unsaturated derivatives of
260   Xanthan gum: Synthesis and characterization. *Polymer, 48*(7), 1921-1929.
261   Karaki, N., Aljawish, A., Humeau, C., Muniglia, L., & Jasniewski, J. (2016). Enzymatic modification of
262   polysaccharides: Mechanisms, properties, and potential applications: A review. *Enzyme and*
263   *Microbial Technology, 90*, 1-18.
264   Lapasin, R. (2012). *Rheology of industrial polysaccharides: theory and applications*: Springer Science &
265   Business Media.
266   Muljana, H., Sugih, A. K., Kristijarti, A. P., Karlus, R., Kurnia, R., Evan, C., & Picchioni, F. (2018). Acetylation
267   of xanthan gum in densified carbon dioxide (CO_2). *Materials Today: Proceedings, 5*(10), 21551-
268   21558.
269   Pawar, S. N. (2017). *Chemical modification of alginate*. In *Seaweed Polysaccharides* (pp. 111-155):
270   Elsevier
271   Rehm, B. H. A. (2010). Bacterial polymers: biosynthesis, modifications and applications. *Nat Rev*
272   *Microbiol, 8*.
273   Shukla, A., Mehta, K., Parmar, J., Pandya, J., & Saraf, M. (2019). Depicting the exemplary knowledge of
274   microbial exopolysaccharides in a nutshell. *European Polymer Journal, 119*, 298-310.
275   Tako, M., Yogi, T., Uechi, K., Onaga, M., Tamaki, Y., & Uechi, S. (2016). Structure-Function Relationship of
276   a Gellan Family of Polysaccharide, S-198 Gum, Produced by Alcaligenes ATCC31853. *Advances in*
277   *Biological Chemistry, 6*(03), 55.
278   Wingender, J., Neu, T. R., & Flemming, H.-C. (2012). *Microbial extracellular polymeric substances:*
279   *characterization, structure and function*: Springer Science & Business Media.
280   Wu, M., Qu, J., Tian, X., Zhao, X., Shen, Y., Shi, Z., . . . Ma, T. (2019). Tailor-made polysaccharides
281   containing uniformly distributed repeating units based on the xanthan gum skeleton. *Int J Biol*
282   *Macromol, 131*, 646-653.
283   Xu, Y., Wu, Y.-j., Sun, P.-l., Zhang, F.-m., Linhardt, R. J., & Zhang, A.-q. (2019). Chemically modified
284   polysaccharides: Synthesis, characterization, structure activity relationships of action. *Int J Biol*
285   *Macromol, 132*, 970-977.

286

5 Discussion

5.1 Structure function relationship of sphingans and paenan

The first part of this work was the investigation of the rheological properties of different groups of heteropolysaccharides in regard of their monomeric sequence, and, if available, their spatial structures. For this, xanthan, a branched heteropolysaccharide, the sphingans, a group of structurally highly similar polysaccharides with differences in branching and branched chain composition as well as paenan, a distinct combination of three simultaneously produced exopolysaccharides, were investigated. The obtained data is important towards understanding effects of (unnatural) modifications of the polysaccharides on the resulting physicochemical properties. The sphingans were investigated in an application-oriented manner, by their interactions with surfactants, as both polysaccharides and surfactants share common application in the cosmetic and personal care sector. The recent establishment of diutan as ingredient for personal care and cosmetic products as the second sphingan next to gellan, reinforces their significance in this sector (Cebrian et al., 2019). Minor differences between the branched sphingans diutan, welan and S-88 could be observed by the differences in the mechanical modeling of their rheological behavior. Diutan was most different from welan and S-88, which also showed in differences in the rheological properties of the mixtures with surfactants. These differences, however small, could be attributed to the disaccharide sidechain of diutan compared to the monosaccharide sidechains of welan and S-88 (Jansson, Savitri Kumar, & Lindberg, 1986; Jansson & Widmalm, 1994; Lee & Chandrasekaran, 1991; E. R. Morris et al., 1996; M Tako, 1992; M. Tako & Kiriaki, 1990; Masakuni Tako & Tamaki, 2005), which may cause different spatial orientations of the polymer chains. The largest differences could be observed with gellan, an unbranched sphingan, which, in this study is also deacylated . Its strong gel properties in the presence of cations in solution are caused by strong intermolecular interactions between the negatively charged uronic acids in the main chain (Mazen, Milas, & Rinaudo, 1999; Paulsson, Hagerstrom, & Edsman, 1999; Masakuni Tako, Sakae, & Nakamura, 1989; Tang, Mao, Tung, & Swanson, 2001), which is prohibited by the presence of sidechains and acyl-residues in diutan, welan and S-88.

Rheological studies of paenan in respect to the different ratios of the naturally produced polysaccharide mixture showed a similar effect of the pyruvyl-group as in xanthan (Callet, Milas, & Rinaudo, 1987; Cheetham & Norma, 1989; Shatwell, Sutherland, Dea, & Ross-Murphy, 1990; Smith, Symes, Lawson, & Morris, 1981; Masakuni Tako & Nakamura, 1988; Wu, Qu, Shen, et al., 2019). However, the data strongly suggests, that the interaction is not caused between two pyruvyl-groups of the same type of molecule, but rather by the interaction with a glucuronic residue of paenan III and the pyruvyl-group of paenan I. This became evident from the highly similar rheological properties of paenan I & II compared to the wildtype paenan I, II & III, showing high gel strength and flow viscosity. Paean I & II and all individual paenan polymers showed low viscosity, Newtonian flow behavior and no elastic portion, which indicates absence of significant intermolecular interactions. Interestingly, the addition of paenan II to paenan I & III causes an increase

changes in the temperature stability, caused by additional intermolecular interactions, however the mechanism is yet to be clarified. Compared to the properties of xanthan, the molecular mechanism seems very similar, however caused by interaction of superstructures, like helices formed by the different paeans or by the interaction of these structures formed by the individual paenan types(Edwin R Morris, 2019; Shatwell et al., 1990). The nature of these superstructures and their precise interactions need yet to be clarified. While the monomer composition and primary structure of paenan has been mostly clarified (ref. paenan I-III) and it has been found that paenan is most likely a mixture of three different polymers produced naturally by *P. polymyxa* DSM 365, the secondary and tertiary structures of these exopolysaccharides have not been investigated yet. This lack of information complicates the approach of a direct structure function relationship. The approaches and data from xanthan and the sphingans however, enabled to link the rheological properties to possible structural conformations and interactions given just information the monomeric composition and their glycosidic linkages. Finally, deeper structural elucidations giving information about the tertiary structures, as they have been described for other polysaccharides are necessary to confirm these conclusions (Bian, Chandrasekaran, & Rinaudo, 2002; Lee & Chandrasekaran, 1991; Mazen et al., 1999; E. R. Morris et al., 1996).

5.2 Structure function relationship of xanthan and effects of decoration (pattern) on rheological properties

Investigation of the structure function relationships of the structurally similar sphingan group of EPS showed, that the absence or presence of a side chain is one of the main influencing factors regarding the rheological properties of EPS. But minor differences in rheological properties, visible by the variations of the mechanical models, revealed, that minor differences in the side-chain composition (c.f. monomeric and dimeric sidechains of the sphingan EPS) affect the tertiary spatial orientation of the EPS and thereby influence the rheological behavior of EPS (Chandrasekaran, Radha, & Lee, 1994; Mazen et al., 1999; E. R. Morris et al., 1996; Xu, Gong, Dong, & Li, 2015). In case of xanthan on the other hand, it was shown, that by systematically altering single acetylation and pyruvylation at defined positions, it is not only possible to tailor the rheological properties of the EPS (Betlach et al., 1987; Callet et al., 1987; Cheetham & Norma, 1989; Hassler & Doherty, 1990; Khouryieh, Herald, Aramouni, Bean, & Alavi, 2007; Smith et al., 1981; Masakuni Tako, 1992; Masakuni Tako & Nakamura, 1984, 1988; Wu, Qu, Tian, et al., 2019), but also draw precise conclusions for the structure function relationship of the decoration pattern on xanthan. The production under controlled conditions in the bioreactor combined with a uniform downstream processing allowed the first characterization of these xanthan-variants in their most naturally occurring state, resulting in a high comparability of these variants. Furthermore, it was first proven, from a mainly rheology-based study, that the acetylation of the inner mannose plays a major role in the thermostability of rheological properties of xanthan, which were later confirmed by different studies (Bercea & Morariu, 2020; Wu, Qu, Tian, et al., 2019). One important conclusion from this study

concerning the production of engineered variants was, that xanthan production is not affected by the degree of acetylation or pyruvylation of the polysaccharide, which is an essential basis for an efficient production of a modified xanthan-variant. Contrary to that, modifications of the sidechain, drastically influences the productivity, and a clear trend is shown, that the shorter the sidechain, the lower the productivity will be (Hassler & Doherty, 1990; Wu, Qu, Tian, et al., 2019). The low productivity of xanthan variants with truncated sidechains represents the high specificity of the enzymes involved in the polymerization & export of the protein, but it is not completely clarified, which enzymes (flippase/polymerase/PCP/OPX) are most limiting in the production of modified variants. Thereby the modification of the natural xanthan would hold the most promising results. Based on the results of the rheological study of the xanthan-variants, an effect of the rheological properties of a crotonylated xanthan-variant was expected, on the one hand due to the altered substitution of the sidechain. The crotonyl-group might, like pyruvate or acetate groups, alter the orientation of the sidechain, on the other hand a cross-linking of terminal crotonyl-groups would result in an increased gel-strength and gel behavior (Bejenariu et al., 2010; Ghorpade, 2020; Matricardi, Cencetti, Ria, Alhaique, & Coviello, 2009). As natural xanthan forms non-crosslinked gel structures, the gel structure is rather soft and elastic, while crosslinked polysaccharide net-works, show stronger and more brittle gel properties.

The chemical modification of the undecorated xanthan allowed for a crotonylation of xanthan with-out any other substituents or the addition of chemical crosslinkers. This approach allowed for a maximum availability of OH-groups available for derivatization. As result the produced xanthan showed drastically altered properties regarding water-solubility, but also possessed a much stronger and more brittle gel character, indicating a crosslinked structure without the addition of a mediator, as it is often found in previous approaches (Bejenariu, Popa, Dulong, Picton, & Le Cerf, 2009; Bueno, Bentini, Catalani, & Petri, 2013; Elella, Sabaa, Abd ElHafeez, & Mohamed, 2019; Guo, Ge, Li, Mu, & Li, 2014; Tao et al., 2016) . Because of the unspecific derivatization of xanthan by the chemical modification, these results are limited in predicting the properties of a site-specific crotonylation of xanthan but based on the results the evidence of the crosslinkability of crotonyl-ated xanthan is given (Tao et al., 2016). As the presence of acetylation on the inner mannose further determines temperature stability of the rheological properties, most likely by stabilizing the orientation of the side-chain, a crotonylation of this variant might lead to a higher crosslinkabilty due to better sterically accessibility in an ordered structure (Marijn M. Kool, Gruppen, Sworn, & Schols, 2014).

5.3 Engineering *Xanthomonas* towards increased CrCoA-levels and engineering GumG towards acceptance of CrCoA as a substrate

5.3.1 Engineering of the acetyltransferase GumG and development of screening methods

Two important steps for the creation of an engineered xanthan variant are the increase of the intracellular Crotonyl-CoA (CrCoA) levels and the engineering of a transferase, which would decorate xanthan with crotonic acid using the increased intracellular CrCoA as the substrate. As confirmed by the study on the modification of the acetylation and pyruvylation patterns of xanthan, these transferases are highly site-specific. This specificity and their structurally similar natural substrate CoA is why the approach of engineering the acetyltransferases GumF or GumG of Xanthomonas towards CrCoA was chosen over the screening for CrCoA accepting transferases and their modification towards accepting the pentasaccharide as a substrate. Due to the lack of structural information on both membrane-bound transferases GumF and GumG, a rational design approach was not possible and gaining these structural information of membrane proteins via crystallography would have been a too tedious process, given the uncertainty of the outcome. After these facts, the acetyltransferase GumG for the outer mannose of the pentasaccharide repeating unit was chosen, as the crotonylation of the outer mannose would lead to a higher accessibility for crosslinking, due to the better steric accessibility, with the possibility on transferring gained knowledge towards engineering of the acetyltransferase for the inner mannose GumF. Due to the lack of structural information, a bioinformatics-assisted approach combined with a systematic alanine scan was chosen to identify a possible active site of the protein as the target for further mutagenesis studies. The system was based on the *de-novo* modelling of the GumG protein and conserved amino-acid motifs were identified via sequence alignments of all annotated acetyltransferases from the Xanthomonas genus. Highly conserved residues could be systematically exchanged with Alanine and the expression of these variants could be successfully achieved with the pHExXan plasmid, a derivative of pSRKGm, carrying the *gum*-promoter from *Xcc.* for a regulated, induction-free expression in Xanthomonas. The system was validated by expression of the initial glycosyltransferase GumD in the *gumD*-deletion mutant. Production showed highly comparable xanthan productivity compared to the wildtype, validating sufficient expression levels for the plasmid-based screening of engineered transferases. The xanthan variants used for screening were produced by the *Xcc ΔgumFGL* strain, lacking any acetylation or pyruvylation, facilitating the screening effort by analyzing the product for the absence or presence of acetate via HPLC analysis after production and hydrolysis. The screening system could be successfully transferred into a 5 ml production scale, allowing the simultaneous production of 24 variants per plate, and easily scalable by increasing the number of plates. For the hydrolysis of xanthan and the subsequent analysis of the supernatant, it was shown that a 10% xanthan solution was necessary. Rühmann et al. showed a production of approximately 1.6 g L^{-1} produced by *Xcc* in the 96 well scale (Broder Rühmann, 2015), while in the 24 well scale, on average 7.5 g L^{-1} could be produced from 3 ml

supernatant, with a total yield of 23 mg xanthan. For a sufficient quantification of acetylation an amount of 10 mg in 1 mL 250 mM sulfuric acid was required, and therefore upscaling has to be carried out by increasing the numbers of 24 well plates rather than switching to cultivation in 96 well plates. For the recovery of the EPS, the supernatant was precipitated manually and dried in a 24 well plate, where it was also re-dissolved in water by shaking at 1000 rpm for 24 h, using the resulting 10 % solution for hydrolysis. This process may also be modified for a higher throughput, by dissolving the supernatant after production directly and quantifying the concentration by the phenol-sulfuric acid method, adapting the automated screening platform by Rühmann et al. (B. Rühmann, Schmid, & Sieber, 2015). The upscale to a 96 well plate format would also be feasible by switching from the HPLC analysis of acetate to an enzymatic assay (Clarke & Payton, 1983), which would in term further increase the throughput by reducing the analysis time from 30 min per sample few minutes for up to 96 samples simultaneously. As a drawback compared to HPLC analysis a precise adjustment of the pH of the hydrolysate is required, introducing another critical step in the process. However, as the targets for an alanine scan in the protein are limited none-theless and can be further reduced by information gained from bioinformatics methods like se-quence alignment, the effort of optimizing this method has to be carefully evaluated. Within this study, four promising mutations which lead to inactivity of GumG could be united with one of the *de-novo* structural models, giving a first hint on an active site and thereby a possible region for mutagenesis. These results have to be interpreted very cautiously, however, because other fac-tors as changes in expression levels or misfolding caused by the mutagenesis may also be the reason for inactivation of the enzyme. Therefore, for a more reliable mutagenesis, eventually the determination of the crystal structure will be necessary. However, these mutagenesis studies paved the way to the engineering of the transferase by creating a plasmid-based expression and subsequent analysis of the produced xanthan variant.

Considering the screening for crotonylation of xanthan, the much higher absorbance of crotonic acid compared to acetic acid could also allow the production in the 96 well scale, and even allow direct photometric measurements of the hydrolysis. First preliminary studies showed a significant higher absorbance of xanthan hydrolysate containing even small amounts of crotonic acid, and a linear calibration curve between 0.1 and 10 mg/L crotonic acid could be achieved with 250 mM, 25 mM and 2.5 mM sulfuric acid as a background (R^2 0.9995, 0.9999 and 0.98, respectively), allowing for respective dilutions after hydrolysis, based on the amount of crotonic acid. The major drawback is the measurement at 210 nm, requiring specialized equipment. Additionally, the anal-ysis of xanthan hydrolysate also showed relatively high absorption levels at 210 nm (A=0.56+-0.07), however 1 mg/L crotonic acid already shows an absorption of A=0.4 at 210 nm in 250 mM sulfuric acid, which could make this method a viable pre-screening at appropriate dilutions. To further increase specificity and sensitivity of the screening the bathochromic shift of crotonic acid to 260 nm could be used, known from the hydrolysis of PHB, however, at least 72 % sulfuric acid is required for this shift which would in turn require the separation of the hydrolyzed polysaccharide before adding the sulfuric acid (Slepecky & Law, 1960). The separation could be done by gel

filtration in a MTP scale, as described by Rühmann et al. (Broder Rühmann, 2015). These preliminary studies provide helpful data and show, that an efficient screening might be possible by adapting the high throughput screening method by Rühmann et al. (B. Rühmann et al., 2015) and adapting the necessary steps. Additionally, a property-based screening (e.g. viscoelastic behavior) was considered, however the chemical crotonylation of xanthan revealed, that these differences of the properties might be too small to screen at this scale to provide reliable results.

5.3.2 Engineering of *Xanthomonas campestris* towards higher intracellular crotonyl-CoA-levels

For the engineering of the intracellular CrCoA levels, the integration of a pathway from acetyl-CoA (AcCoA) to acetoacetyl-CoA (AcAcCoA) to CrCoA was targeted. Initially it was planned to integrate the pathway into the genome of *Xcc* via the pK19mobsacB suicide plasmid, however preliminary tests on integration by the integration of *gumD* in the Δ*gumD* variant were not successful, so a plasmid-based expression of the pathway was prioritized. For this the enzymes PhaA (acetyl-CoA acetyltransferase) and PhaB (acetoacetyl-CoA reductase) from *Cupriavidus necator* (H16) and the Crotonase Crt from *Clostridium acetobutylicum* (ATCC 824) were cloned into the pSRKGm plasmid, with an inducible lac-promoter, resulting in the plasmid named pCRT. While direct expression studies were not carried out for the enzymes, the pSRKGm plasmid was shown to be functional in *Xanthomonas campestris* for multiple homologous and heterologous gene expressions and these genes were successfully expressed in Gram-negative bacteria before (Atsumi et al., 2008; Boynton, Bennet, & Rudolph, 1996; Inui et al., 2008; Lin, Lee, Sue, Liu, & Li, 2017; Srirangan et al., 2016; Tseng, Martin, Nielsen, & Prather, 2009). Growth studies also showed, that, while the maximum growth rate of the targeted production organism *Xcc* Δ*gumFGL* showed lower maximum growth rates (μ_{max}=0.23) compared to the wildtype (μ_{max}=0.32), it was highly comparable to the wildtype (μ_{max}=0.25) with the same plasmid, and even achieved higher cell densities compared to both *Xcc* wt and *Xcc* wt pCRT. The values of growth rates were well within or above previously recorded values in own and other studies (Garcia-Ochoa, Gomez, Alcon, & Santos, 2013; Lo, Yang, & Min, 1997; Shu & Yang, 1990) All three variants showed extremely similar growth behavior at the lag to early exponential phases, with larger differences concerning OD in the late exponential and stationary phase. As 1 mM IPTG was added to all variants, no increased stress on cell growth could be observed. Both *Xcc* wt/*Xcc* wt pCRT and *Xcc* Δ*gumFGL* pCRT showed very similar behavior compared to the fermentations of *Xcc* wt and *Xcc* Δ*gumFGL* in the 1.5 L scale for the xanthan production carried out for the rheological study. The high similarity of both *Xcc* wt and *Xcc* Δ*gumFGL* with and without the plasmid concerning cell growth and viscosity of the fermentation media indicates, that the plasmid does not impact growth and thereby productivity. It is therefore able to be used for the introduction of the new pathway in this strain, without affecting productivity. However, it is important to mention, that different pathways other than the one tested in this study might still affect growth and productivity.

It was further shown, that although both the pCRT for the introduction of the pathway and the pHExXan-plasmid for the expression of engineered GumG-variants have the same origin of replication (Nordström & Austin, 1989; Novick, 1987), it was possible to bring them stably into *Xcc ΔgumFGL* using double antibiotics selection, as proven by plasmid specific PCR amplicons. Although this method carries the risks of plasmid competition and the loss of one of the plasmids (Velappan, Sblattero, Chasteen, Pavlik, & Bradbury, 2007), and therefore has to be regularly retested, it proves to be a viable solution for testing different pathway expressions in combination with an engineered transferase, and it is worth mentioning, that this system could be also extended to further studies.

As a higher priority, for the resulting increase of intracellular levels of CrCoA a highly sensitive analytical method had to be developed. To ensure highest sensitivity a HPLC-MS based system was targeted. The screening of different buffers and buffer concentrations at different pH values showed that 26.5 mM ammonium formate buffer at pH 6.5 delivered the best results with a LOD of 0.1 µM and a LOQ of 0.3 µM for both CoA and CrCoA, making this method sensitive enough to determine intracellular CoA-concentrations (Abrankó, Williamson, Gardner, & Kerimi, 2018; Bennett et al., 2009; Bennett, Yuan, Kimball, & Rabinowitz, 2008; Neubauer et al., 2015; Petzold, Chan, Nhan, & Adams, 2015; Shimazu, Vetcher, Galazzo, Licari, & Santi, 2004; Shurubor et al., 2017). For the extraction of metabolites, a quenching of the metabolism is essential, in order to ensure a "snapshot" of the current metabolic state. For this an extraction with an aqueous solution of 40 % acetonitrile and 40 % methanol at -20 °C was chosen for a combined quenching and extraction of metabolites, adapted by Bennett et al. (Bennett et al., 2008), who successfully showed this method for the metabolite analysis in *E. coli* (Bennett et al., 2009). As CoA and CrCoA elute at 20-40 % Acetonitrile, it was necessary to remove any solvents from the extracted samples. For this spiking of CoA and CrCoA standards at 10 µM a 10-fold dilution of the samples, resulting in 8 % solvent concentration would not have been sufficient, and furthermore decreased sensitivity. For the final method, 10 ml of cell culture was used and with a 10-fold dilution in mind, a minimum of 500 ml cell suspension would have been required to achieve a sufficient quantification, severely impeding handling, and scalability of the process. The chosen alternative by evaporating the solvent by vacuum centrifugation showed high stability of both CoA and CrCoA with 100 % recovery when spiking the standards before the entire process, including adding them to the 40 %/40 % acetonitrile/methanol mixture at -20 °C and no difference to the spiking after the whole process. The major advantage of this method is the possibility of a concentration of up to 50-fold, or higher if the initial cell volume is increased. However, these high concentrations were not necessary, given the observed CoA concentrations from the total 5-fold concentration of the sample during the extraction step. Analyzation of *Xcc ΔgumFGL* and *Xcc ΔgumFGL* pCRT showed CoA concentrations of 3.35±0.07 µM and 2.23±0.05 µM and although no CrCoA could be detected, the lower CoA levels of *Xcc ΔgumFGL* pCRT indicated a depletion of the CoA pool, which could be due to the activity of PhaA from AcCoA to AcAc-CoA. However, in the MS no AcAcCoA or CrCoA could be detected, and thereby the establishment of the pathway could not be confirmed. 3-HB-

CoA could be detected only after the spiking with CrCoA and in the presence of cell extracts from *Xcc*. It was confirmed that the reaction was occurring over time after the addition of CrCoA when added to the analyte and the reaction could be prevented by filtering the extract through a 10 kDa filter, however not by a 0.2 µm filter. This arises the question, whether this reaction is catalyzed enzymatically. This reaction could be catalyzed by the crotonase, which catalyzes the reaction from 3-HB-CoA to CrCoA, however the reaction equilibrium is on the side of the 3-HB-CoA with a K_{eq} of 10^{-1} (Bond-Watts, Bellerose, & Chang, 2011), however these values represent in-vitro studies and other metabolic pathways might also influence the equilibrium. More importantly, as this reaction also occurred in *Xcc* without the pCRT plasmid, it indicates an involvement of an enzyme from *Xcc,* which might catalyze this reaction. One possibility might be EC 4.2.1.17, an enoyl-CoA hydratase, which could be identified in the sequenced genome of *Xcc* LMG 8031, catalyzing the reaction from CrCoA to (S)-3-HB-CoA, which in term might me metabolized by a 3-hydroxyacyl-CoA dehydrogenase (EC 5.1.2.3) into (R)-3-HB-CoA. This would, in turn feed (R)-3HB-CoA back into the introduced pathway, and an equilibrium might be reached, if CrCoA is not used as a substrate for xanthan acylation. Although the prevention of the reaction by filtering through a 10 kDa filter could be explained by the removal of the 27.6 kDa enzyme, this would mean that the enzyme will survive the harsh treatment of 80 % solvent in combination with sub-zero temperatures as well as the following treatment at 65 °C for approximately 1 h. This might be plausible, as there is a number of reported organic solvent tolerant or stable enzymes, including proteases, lipases, esterases and other enzyme classes with solvent tolerances up to 90 % (Ogino & Ishikawa, 2001). On the other hand, the concentrations used for spiking do not exceed 10 µM of substrate and as the process was observed to take several minutes up to 1 hour, it might just be very little residual activity. However, to confirm residual enzymatic activity further studies are necessary, for example enzymes from *Xcc* with the annotated activity in question could be deleted by gene editing or even be produced and purified with an *E. coli* expression system and investigated for their solvent and temperature stability.

6 Conclusion and outlook

Based on the comprehensive sets of data on two groups of polysaccharides, xanthan and the sphingan groups it was possible to expand on known information about the correlation of the structural conformation of exopolysaccharides and their rheological properties. With these correlations, it was possible to suggest structural conformations and intermolecular interactions of a previously unknown polysaccharide, paenan based on its rheological properties. This shows, that given a required set of minimum data, i.e. monomeric composition and glycosidic linkage data, it is possible to predict interactions of these polymers based on the rheological properties. However, further studies on molecular interactions by electron microscopy, NMR, x-ray diffraction are required to confirm these findings, as rheological data might explain general structure function relationships by comparing them to highly structurally clarified EPS groups but is unable to precisely explain these structural conformations as a stand-alone method.

For the modification of xanthan towards an *in-vivo* crotonylation, two main goals were targeted: First, increase of the intracellular crotonyl-CoA levels in *X. campestris* by metabolic engineering and secondly, the engineering of an acyltransferase for the acceptor of crotonyl-CoA as substrate. As a production strain, the triple deletion mutant *X. campestris ΔgumFGL,* lacking both acetyltransferases GumF and GumG as well as the Pyruvyltransferase GumL was successfully created with the pK19mobsacB suicide plasmid, enabling production and modification of a completely undecorated xanthan-variant. For the increase of intracellular CrCoA, the pathway from AcCoA to CrCoA with PhaA and PhaB from *C. necator* as well as Crt from *C. acetobutylicum* based on the pRSKGm-expression plasmid was expressed in *Xcc ΔgumFGL* and growth studies in the bioreactor showed no negative impact on growth or xanthan production in the desired production strain *Xcc ΔgumFGL*. While based on expression tests via SDS, no significant amount of these proteins could be detected. Analysis based on metabolite extraction and quantification via LCMS showed a decrease in AcCoA compared to the variant without the expressed pathway, which could be due to the reaction (and following reactions) catalyzed by PhaA. However, no crotonyl-CoA could be detected in the analyses, which was found to be due to a residual activity in the *Xanthomonas* metabolite extract, and while this reaction, however unlikely due to the harsh treatment of the sample, is indicated to be enzymatically catalyzed, this has still to be proven. While the increase of the intracellular CrCoA pool still requires further experiments, including screening for alternative pathway, the established extraction method and the highly sensitive HPLC-MS-analytics provide a solid foundation for future investigations.

For the engineering of an acyltransferase for the substrate acceptance of CrCoA, the acetyltransferase GumG of *X. campestris* itself was targeted for mutagenesis studies, as the engineering of the substrate binding pocket promised higher chances for success than engineering of the carbohydrate binding domain (cbd). The engineering itself proofed to be highly complex, as there is lacking information of almost all acetyltransferases active on exopolysaccharides. One major impediment is the lack of structural information, as most members of this protein family are

membrane bound and difficult to extract and crystalize for structural elucidation. The chosen, bio-informatics assisted approach based on the identification of conserved motifs and *de-novo* modelling, combined with alanine scans in order to identify possible substrate binding pockets as target for mutagenesis was therefore highly indirect, as these mutations could also lead to misfolding causing the loss of activity. For further approaches, some promising regions have been identified for the actual mutagenesis studies towards the cofactor, however only a structural elucidation of the target protein will allow an efficient and direct engineering of the transferase.

Considering the screening methods following an increment of the intracellular CrCoA levels and the engineering of GumG in order to obtain a crotonylated xanthan-variant, the creation of a chemically modified crotonylated xanthan showed distinct alterations of its rheological properties, but larger amounts for testing would be required and the process would take several days for screening of a low number of variants. An alternative which was investigated was the hydrolysis of the product with sulfuric acid, which can be automated based on the established HT-PMP screening, following HPLC analysis of the free crotonic acid after hydrolysis. However, the HPLC analysis will form the bottleneck, requiring an additional 48 h for the screening of one 96-well plate following hydrolysis. A photometric detection of the samples at 210 nm was tested to circumvent this problem and first tests showed promising results with a LOD of 0.1 mg L^{-1} of free crotonic acid. While this method showed a high background with the hydrolysate of the polysaccharide, in the required 250 mM of sulfuric acid for hydrolysis, this method could be viable as a pre-screening option followed by HPLC analysis.

The final step to combine all methods and integrate a selected pathway and re-integrate the engineered acetyltransferase into the chromosomal DNA, rather than plasmid-based expression, is yet to be achieved, however integration studies with the pK19mobsacB for the re-integration of the 1.5 kb *gumD* were not successful. To achieve this step, different genome editing tools like the CRISPR/Cas-System might be necessary, which have yet to be established in this strain. Finally, it is worth mentioning, that while these studies have been carried out in *X. campestris* LMG 8031, the methods might also be transferred to other xanthan-producing strains, e.g. *X. campestris* DSM 3586, which share high sequence homology with LMG 8031 concerning the *gum*-operon and therefore a very high similarity of the acetyltransferases (>99 %), while the developed or future genome editing tools might be more efficient in different strains.

7   List of figures

8   List of tables

9   List of formulas

10 List of abbreviations

(U)HPLC	(ultra) high performance liquid chromatography
µ	micro (10-3)
3HBCoA	3-hydroxybutyryl-Coenzyme A
ac	acetate/acetyl
AcAcCoA	acetoacetyl-Coenzyme A
AcCoA	acetyl-Coenzyme A
BMIMCl	1-Butyl-3-methyl-imidazolium-chloride
bp	basepair
CALB	Candida antarctica Lipase B
cbd	carbohydrate binding domain
Cel	cellubiose
Cl	Chloride
CoA	coenzyme A
cpCR	colony polymerase chain reaction
CPS	capsular polysaccharide(s)
CrCoA	crotonyl-Coenzyme A
CRISPR	Clustered Regularly Interspaced Short Palindromic Repeats
Da	dalton
DH	dehydrogenase
DMF	dimethyl formamide
DMSO	dimethyl sulfoxide

DNA	desoxyribonucleic acid
dNTP	deoxyribonucleotide triphosphate
DS	degree of substitiution
DWP	deep well plate
EC	Enzyme Commission
EFSA	European Food Safety Authority
EPS	exopolysaccharide(s)
FDA	Food and Drug Administration
FT	fourier transformation
Fuc	fucose
GDP	Guanosine diphosphate
GK	glucokinase
Glc	glucose
GlcA	glucouronic acid
Glc*p*	gulucopyranose
HT	high throughput
IR	infra-red
k	kilo (10^3)
kbp	kilobasepair
KOAc	potassium acetetae
KOH	potassium hydroxide
LB	lysogeny broth
LOD	limit of detection

LOQ	limit of quantification
LVE	linear viscoelastic (region)
M	mega (10^6)
m	milli(10^{-3})
MALS	multi-angle light scattering
Man	mannose
Man*p*	mannopyranose
MS	mass spectrometry/mass spectrometer
mt	metric tons
n	nano(10^{-9})
n.a.	not available/ not applicable
Na	sodium
OD_{600}	optical density at 600 nm
OE	overlap extension
OH	hydroxy/hydroxyl
OPX	outer membrane polysaccharide export protein
PCP	polymer co-polymerase
PCR	polymerase chain reaction
PEP	phosphoenol-pyruvate
PMP	1-Phenyl-3-methyl-5-pyrazolon
pO_2	partial oxygen saturation
PP	polyprenol
pv.	pathovar

PVDF	polyvinylidene fluoride
pyr	pyruvate/pyruvyl
Rha	rhamnose
Rha*p*	rhamnopryanose
rpm	revolutions per minute
SEC	size exclusion chromatography
SOB	super optimal broth
SOC	super optimal broth with catabolite repression
TFA	trifluoroacetic acid
TFB	transformation buffer
UDP	uridine diphosphate
urf	unknown reading frame
v/v	volume per volume
w/v	weight per volume
X.	*Xanthomonas*
Xcc	*Xanhtomonas campestris* pv. *campestris*

12 Supplemental data

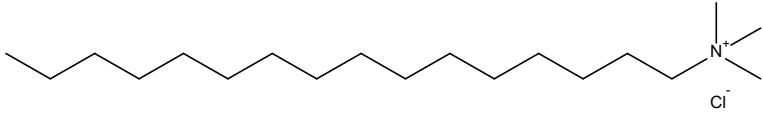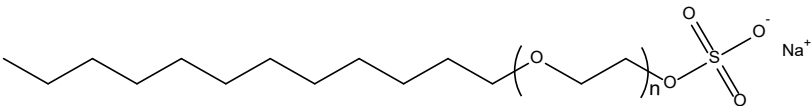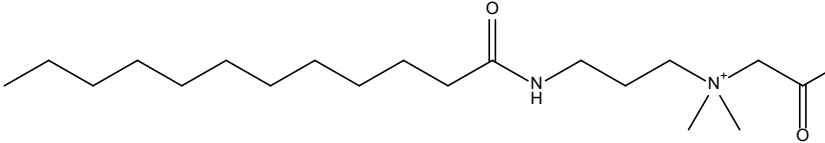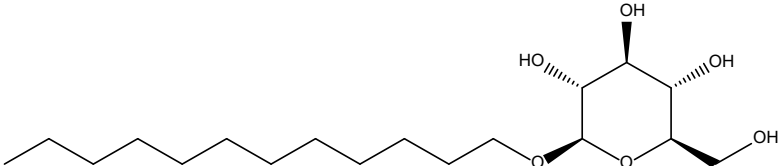## 12.1 Supplemental data rheology of sphingans in EPS-surfactant systems

surfactant	Head charge	Structure
CTAC	Cationic	
SLES	Anionic	
CAPB	Zwitterionic	
PC	Uncharged	

Figure S1. Chemical structure of the four investigated surfactants.

CTAC cetrimonium chloride; SLES sodium laureth sulfate; CAPB Cocamidopropyl betaine; PC Plantacare® (lauryl glucoside)
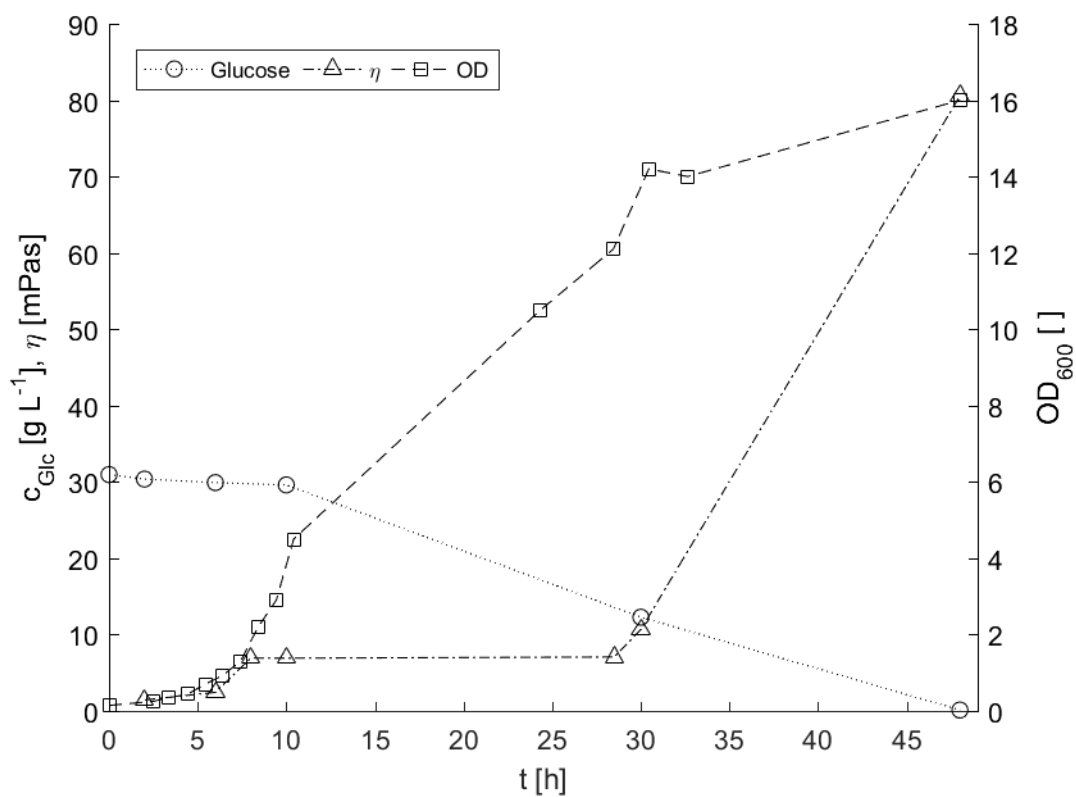
Figure S2. Process parameters of the S-88 fermentation

Glucose levels were checked by an enzymatic assay after proper dilution and filtration of the cells. Viscosity was checked at a constant shear rate of 10 s^{-1}. The increase of viscosity was used to qualitatively monitor EPS-production
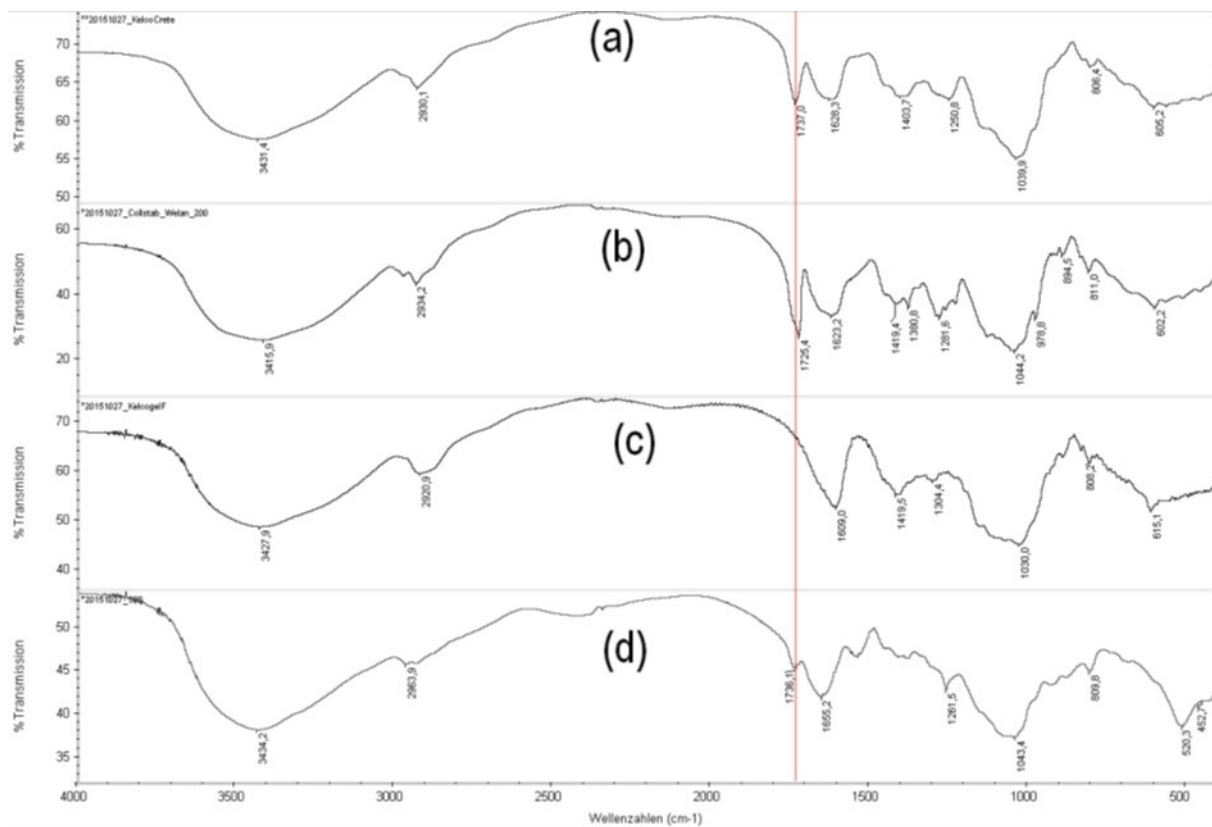
Figure S3. IR-Spectra of the sphingans

(a) Diutan, (b) Welan, (c)Gellan and (d) S-88. For IR spectra about 10 mg of EPS were mixed with 90 mg KBr and pressed to a pellet. The red line highlights the C=O stretch at wavenumber 1725-1737 of carbonyl esters. A distinct peak can be detected if the polysaccharide is acetylated.

Table S1. Overview of theoretical and calculated monomer distributions and acetylation of sphingans.

The monomer distribution was calculated after the TFA hydrolysis and derivatization with PMP and the subsequent HPLC-UV-MS/MS analysis, using rhamnose as a stable reference.

Ratio Rha : Glc : GlcA : Man

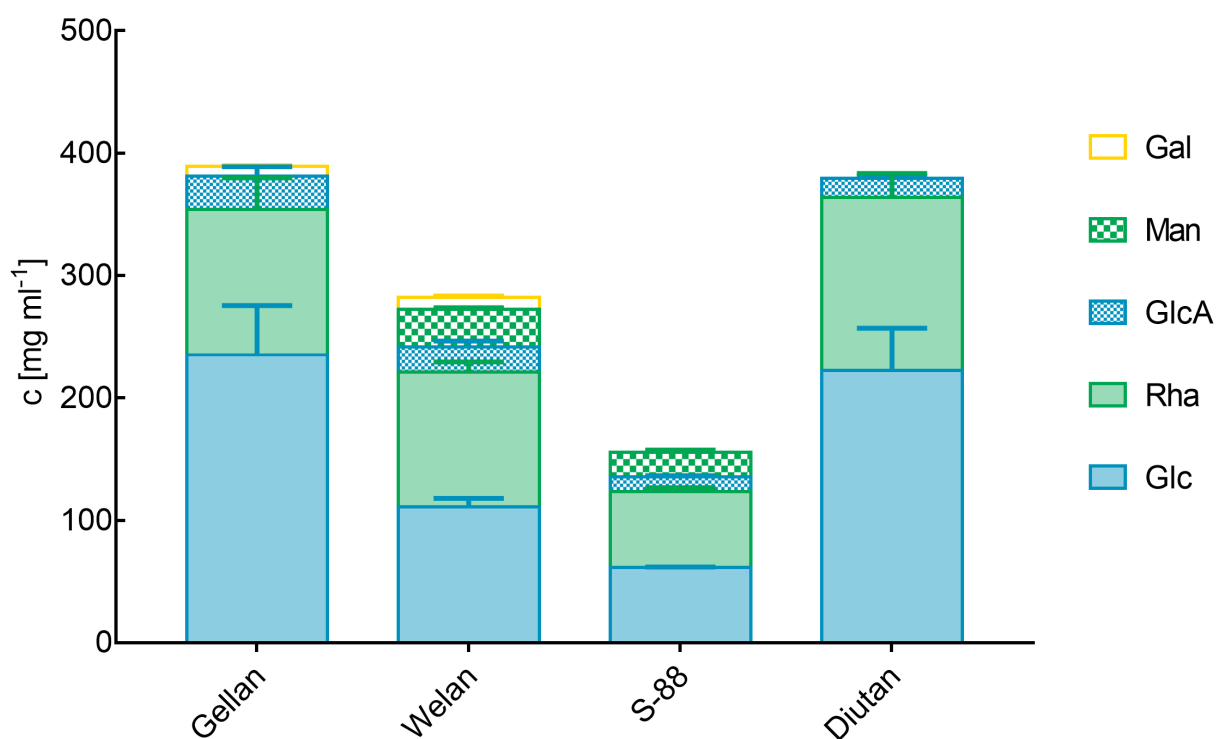| Sphingan	Theoretical	Analyzed	Acetylated
Gellan	1 : 2 : 1 : 0	1 : 1.98 : 0.23 : 0	no
Welan	1 : 1.33 : 0.67 : 0.33	1 : 1.05 : 0.18 : 0.33	yes
Diutan	1 : 0.67 : 0.33 : 0	1 : 0.99 : 0.11 : 0	yes
S-88	1 : 1.33 : 0.67 : 0.33	1 : 1.57 : 0.19 : 0.32	yes

Figure S4. monomer recovery after hydrolysis and HT-PMP analysis of the sphingans.

For analysis the polysaccharides were dissolved in water at a concentration of 1 g L^{-1}. Error bars show the standard deviation of technical triplicates. Galactose might represent impurities from cell debris.
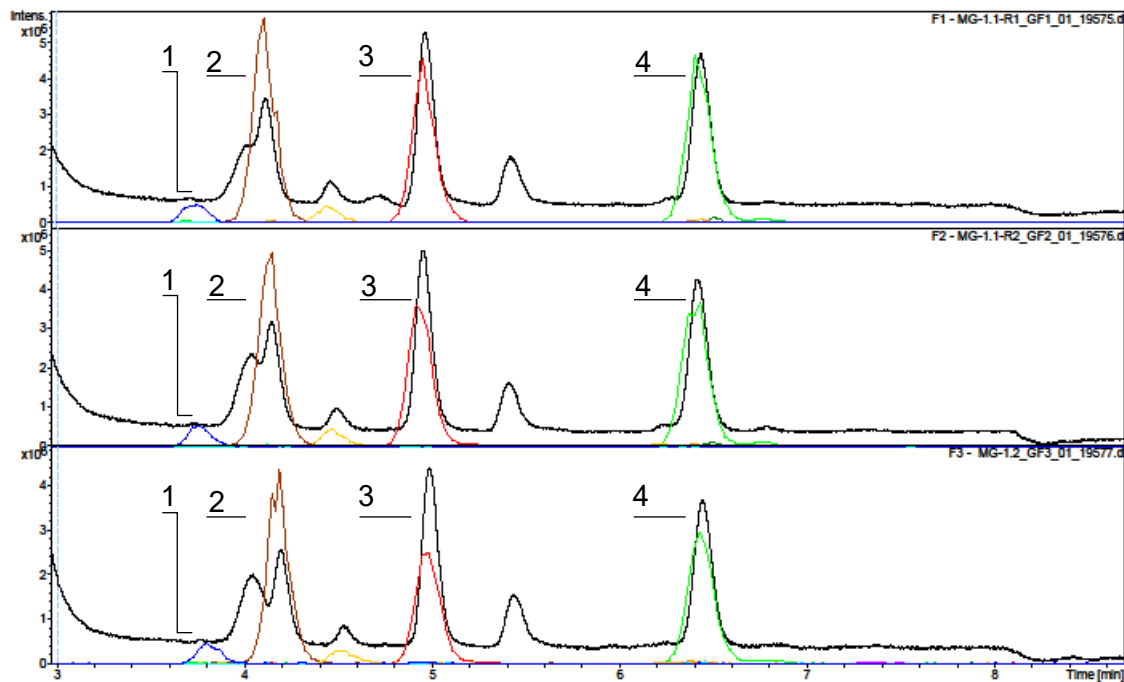
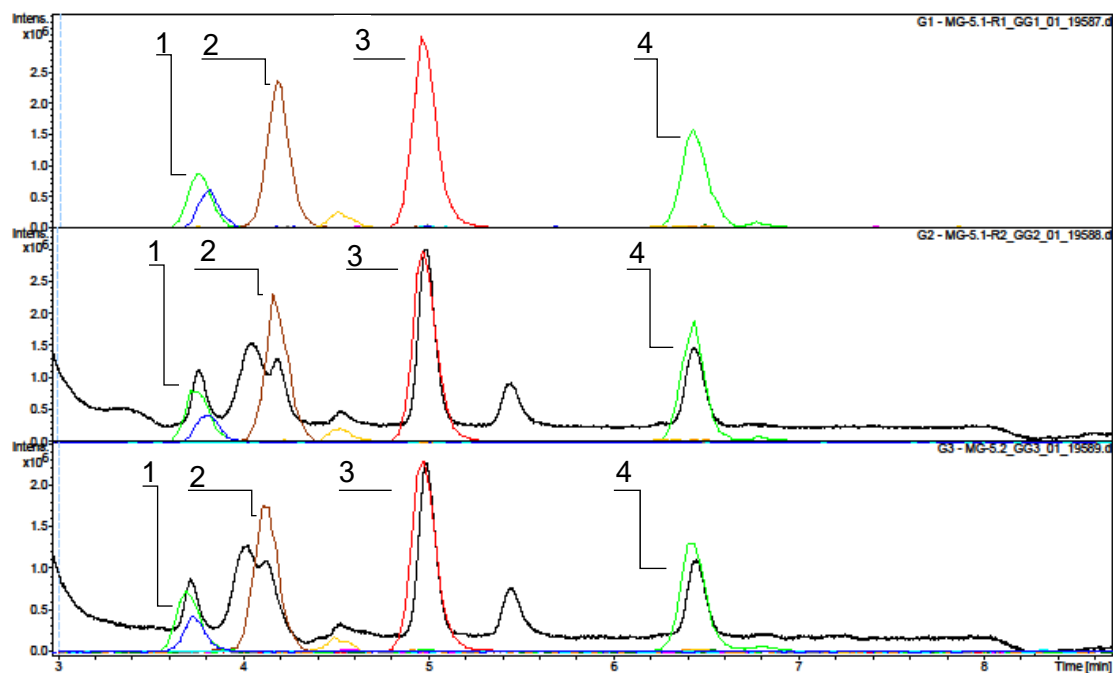**Figure S5.** Overlay of UV- and XIC signals of monomer analysis of gellan

Figure S6. Overlay of UV- and EIC signals of monomer analysis of welan
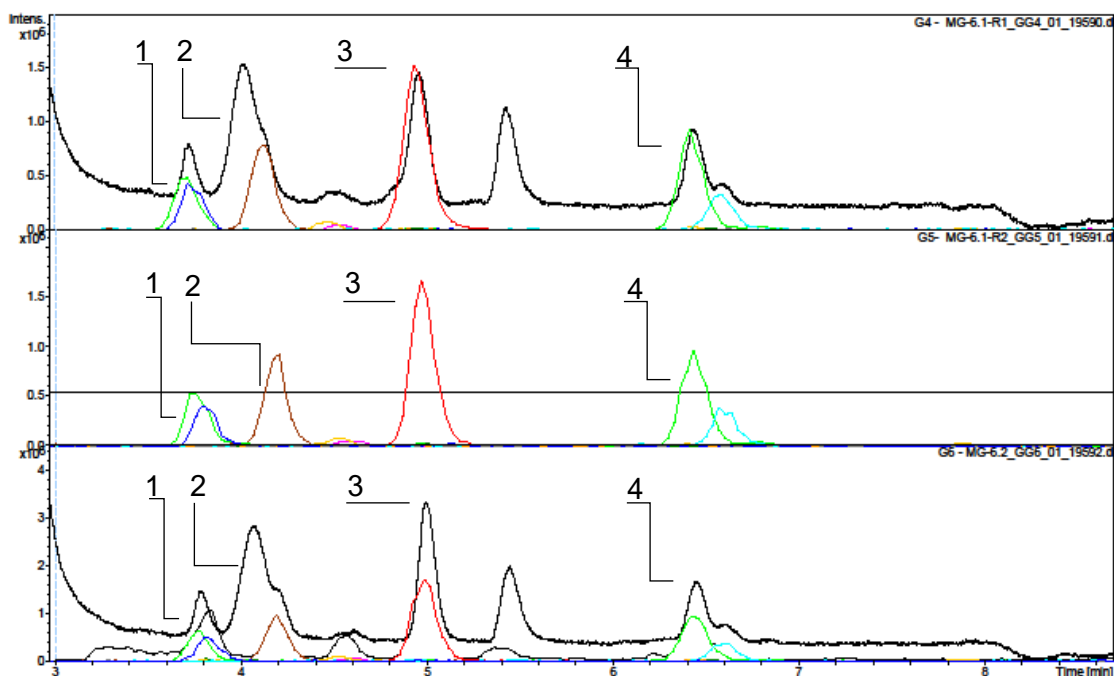
Figure S7. Overlay of UV- and EIC signals of monomer analysis of S-88
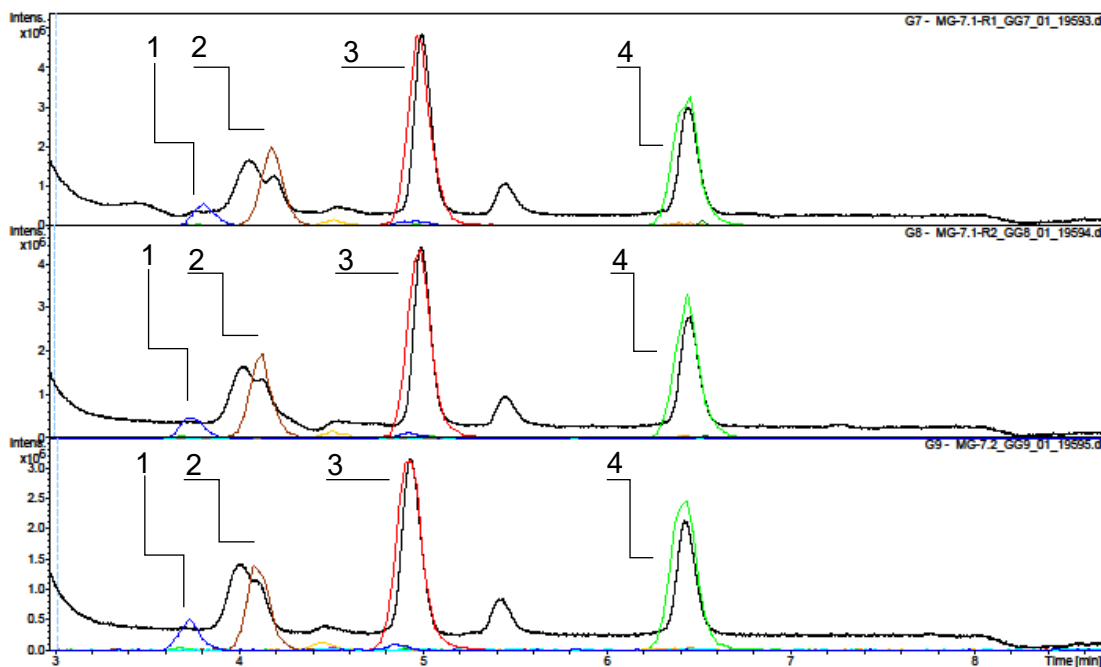
Figure S8. Overlay of UV- and EIC signals of monomer analysis of diutan

Figure S5-S8 show the 235 nm UV and extracted ion chromatogram (EIC) traces (in triplicates) of the monomer analysis of the sphingans after hydrolysis and derivatization of the sphingans (1 g L^{-1}) with PMP according to Rühmann et al. (B. Rühmann et al., 2014). 1) mannose m/z 511. 2) glucuronic acid m/z 525. 3) rhamnose m/z 495. 4) glucose m/z 511
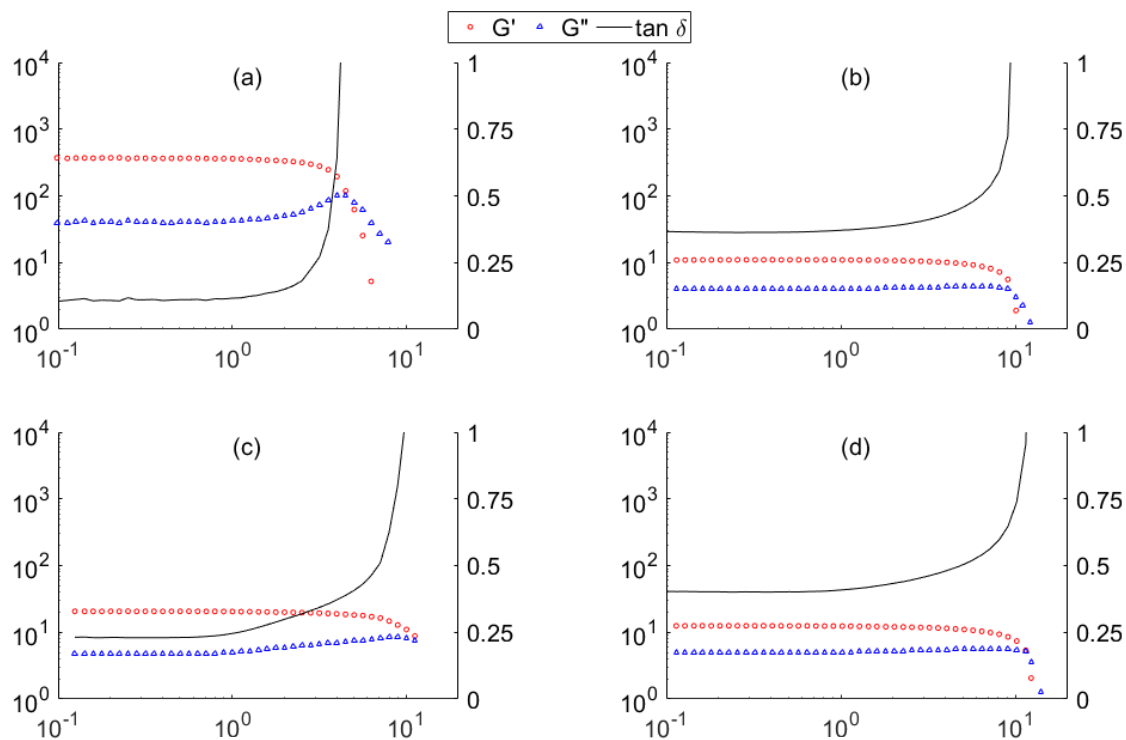
Figure S9. Amplitude test of pure sphingan solutions

(a) Gellan, (b) Welan, (c) Diutan and (d) S-88 showing the storage modulus G' (○), loss modulus G'' (Δ) and damping factor (-) depending on shear stress. The yield point, which marks the end of the linear viscoelastic (LVE) region was defined at an aberration of either G' or G'' of 5% of the plateau value. The flow point is defined at the intersect of G' and G''.
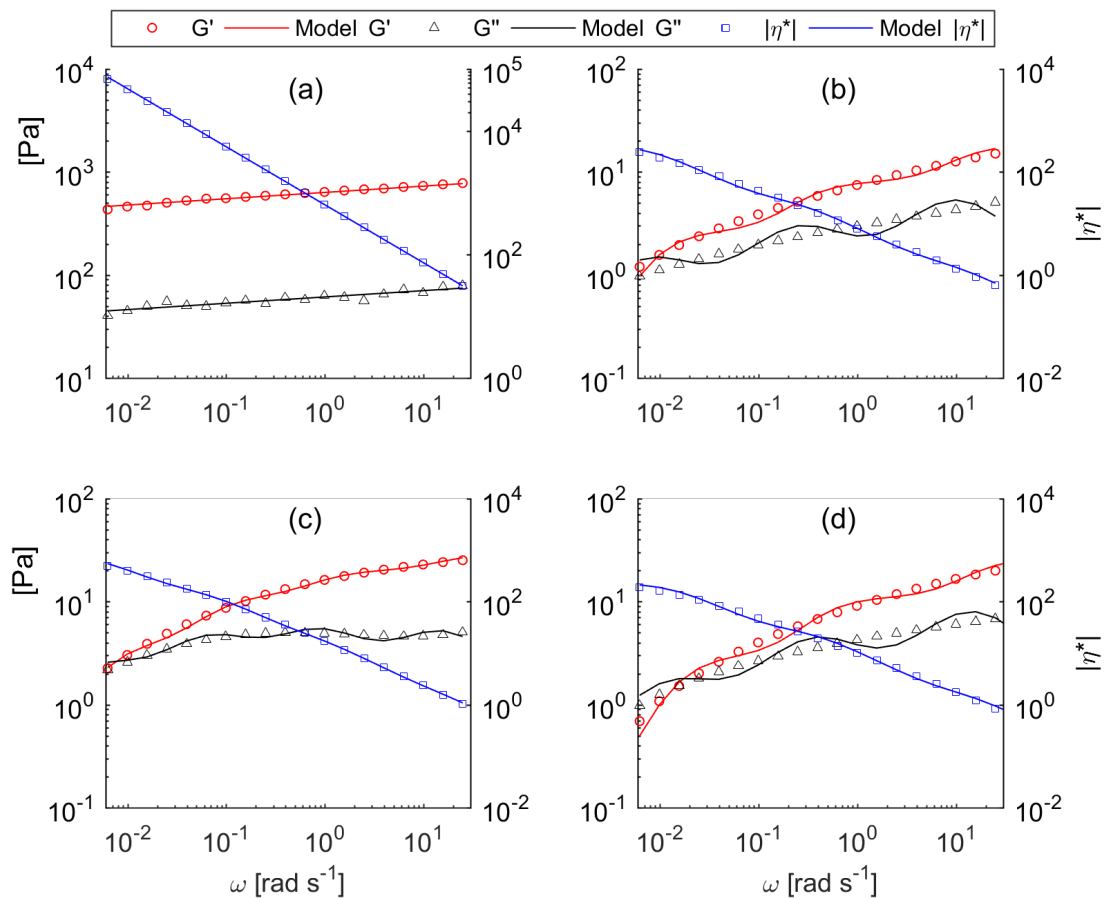
Figure S10. Frequency sweeps and modeling of pure sphingan solutions

(a) Gellan (b) Welan (c) Diutan and (d) S-88. Applied models were the Power-law (a), 3-element Maxwell model (b), (d), and 4-element Maxwell model (c). The fitting of the models was done using MATLAB.
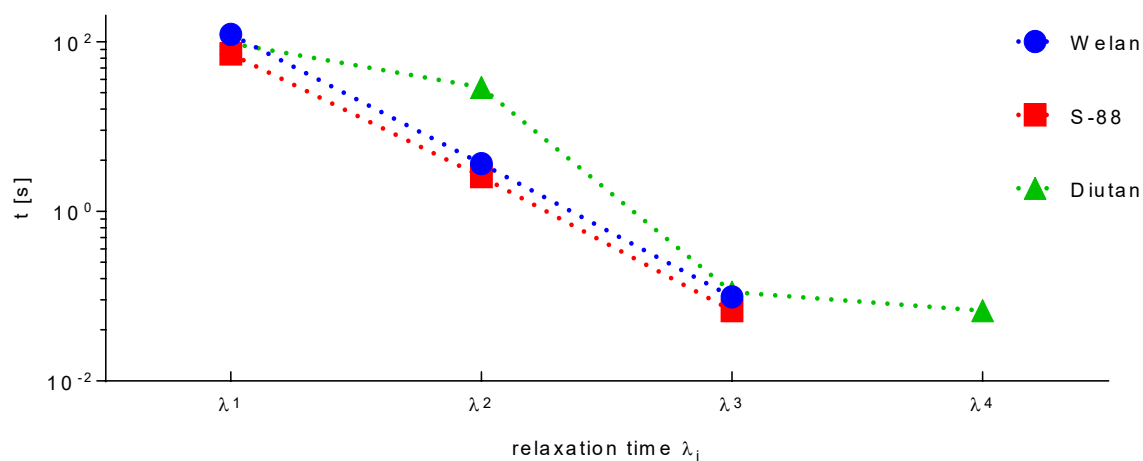
Figure S11 Relaxation time spectra of pure sphingan solutions

(a) Diutan, (b) Welan, and (c) S-88 obtained from the Maxwell models of the frequency sweeps
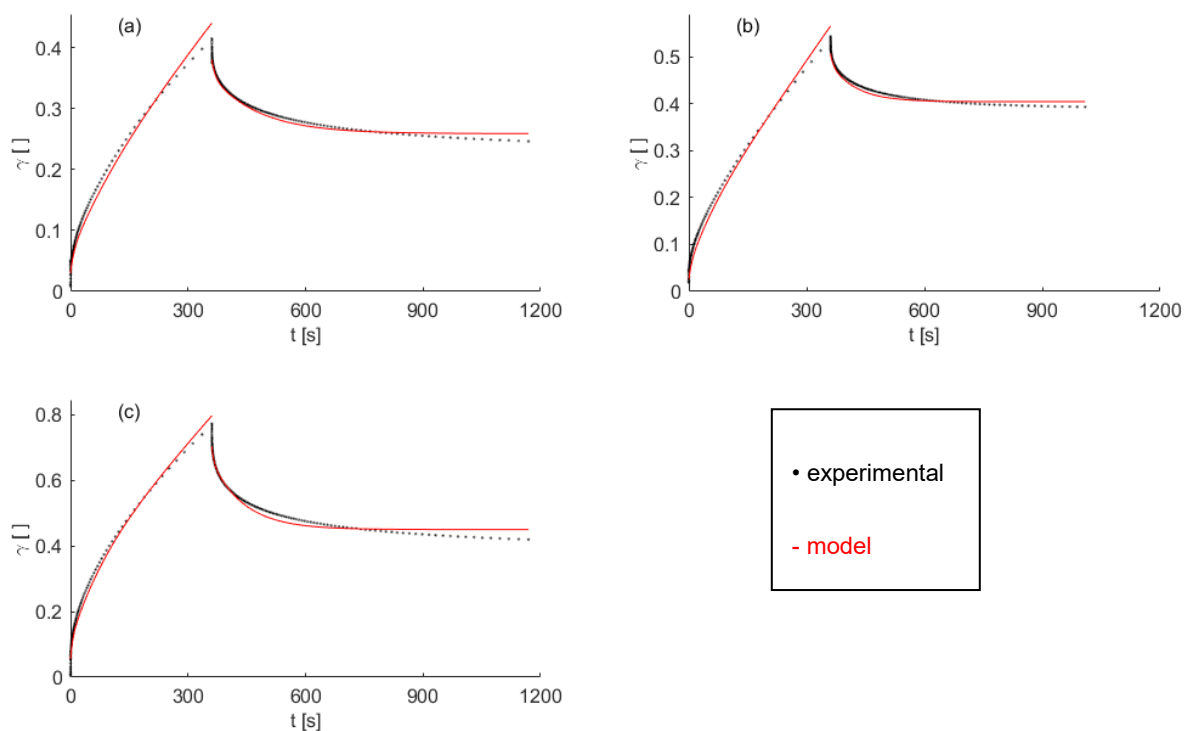
Figure S12. Creep and creep recovery of pure sphingan solutions

(a) Welan, (b) S-88, and (c) Diutan and the respective fitting with the Burgers model (red line)
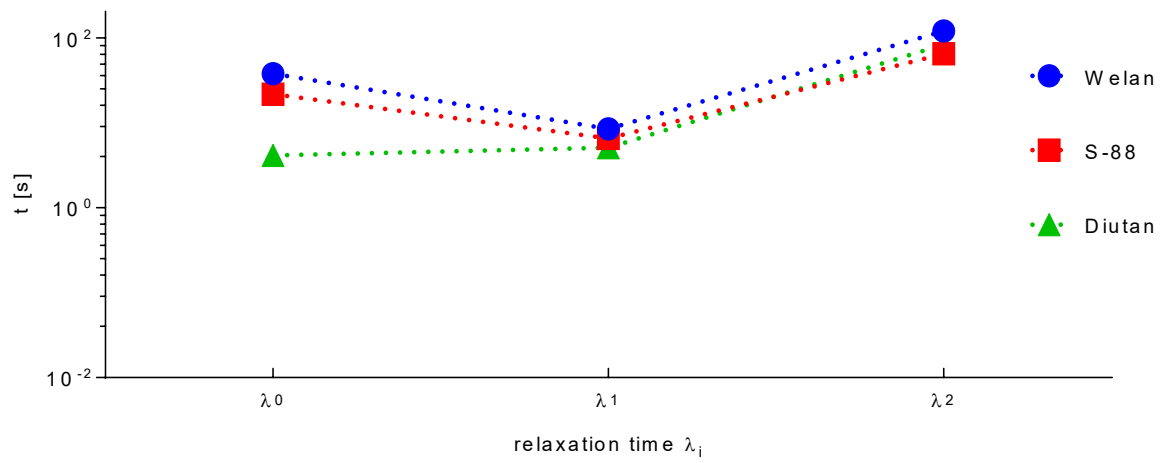
Figure S13. Relaxation times of welan, diutan, and S-88 calculated from the Burgers model of creep and creep-recovery test
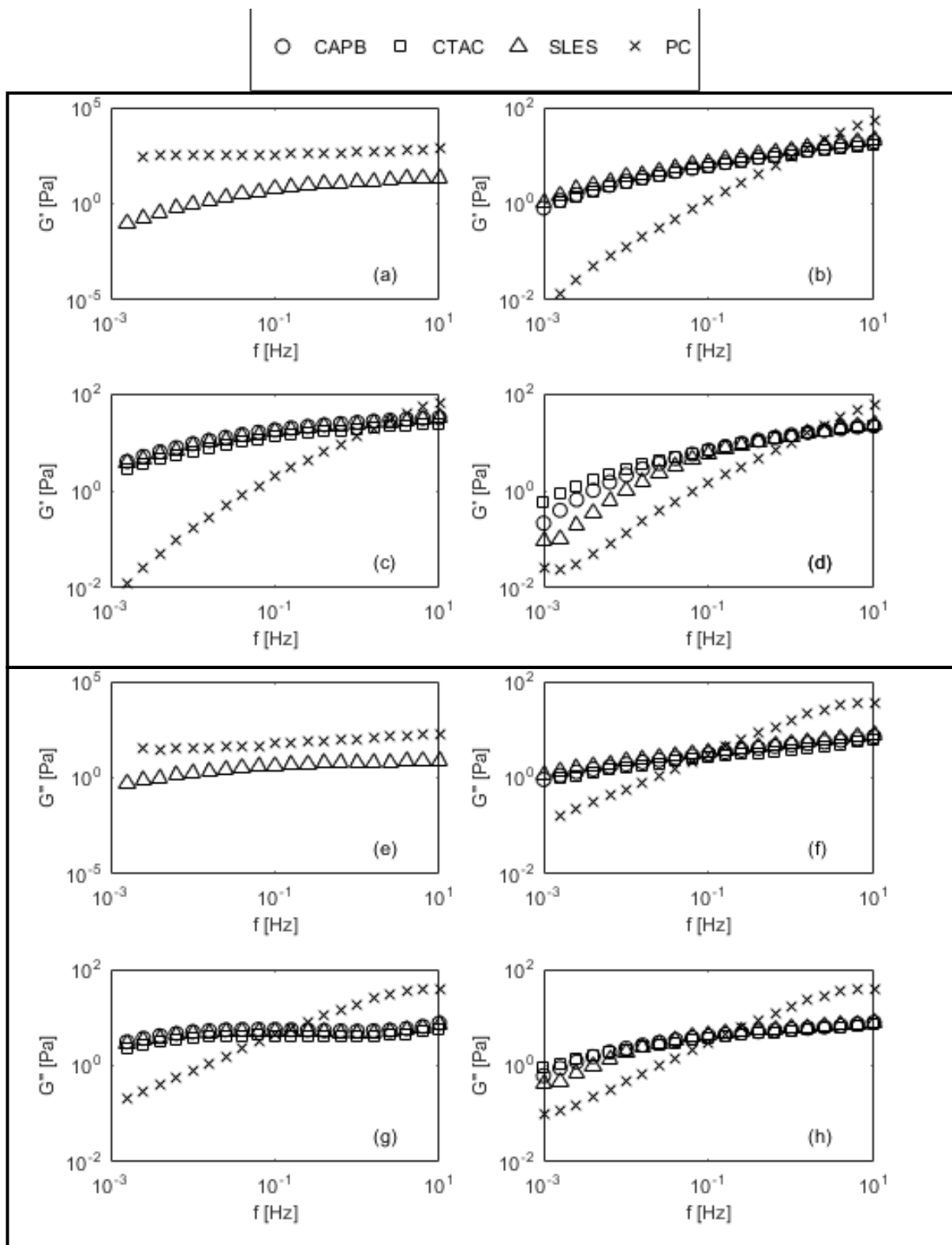
Figure S14. Frequency sweeps of the sphingan-surfactant systems.

Storage modus G' (top box) and loss modulus G'' (bottom box) shown individually. (a) (e) Gellan. (b) (f) Welan. (c) (g) Diutan and (d) (h) S-88

Table S2. Model parameters of the mechanical modelling of the frequency sweeps of the sphingan-surfactant systems

	Model/parameter						
System	**Generalized Maxwell model (3 elements)**						
Plantacare®	**G_1 [Pa]**	**G_2 [Pa]**	**G_3 [Pa]**	**λ_1 [s]**	**λ_2 [s]**	**λ_3 [s]**	**R^2**
Gellan	400.57	313.10	126.42	0.03	330.26	1.28	0.9952
Diutan	84.52	10.25	0.74	0.03	0.51	9.34	0.9975
Welan	73.03	6.46	0.40	0.03	0.54	13.10	0.9965
S-88	75.99	4.55	0.25	0.03	0.84	19.51	0.9962
SLES							
Gellan	16.02	9.78	2.37	0.04	1.05	15.7	0.9934
Diutan*	16.51	14.10	7.71	0.03	2.30	89.02	0.9895
Welan*	17.61	8.25	3.55	0.03	1.59	77.47	0.9885
S-88	16.31	9.73	1.96	0.04	1.23	19.26	0.9933
CTAC							
S-88	17.5	8.9	2.9	0.03	1.6	61.4	0.9884

Table S2. (continued) Model parameters of the mechanical modelling of the frequency sweeps of the sphingan-surfactant systems

	Model/parameter								
System	**Generalized Maxwell model (4 elements)**								

SLES	G_1	G_2	G_3	G_4	λ_1	λ_2	λ_3	λ_4	R^2
Diutan	15.1	9.8	9.6	5.1	0.02	0.53	9.43	161	0.9980
Welan	16.0	8.40	4.48	2.50	0.02	0.35	6.91	119	0.9976

CTAC									
Diutan	12.4	7.9	7.8	4.0	0.02	0.5	8.9	146	0.9979
Welan	19.3	7.1	4.1	2.0	0.01	0.2	4.8	106	0.9960

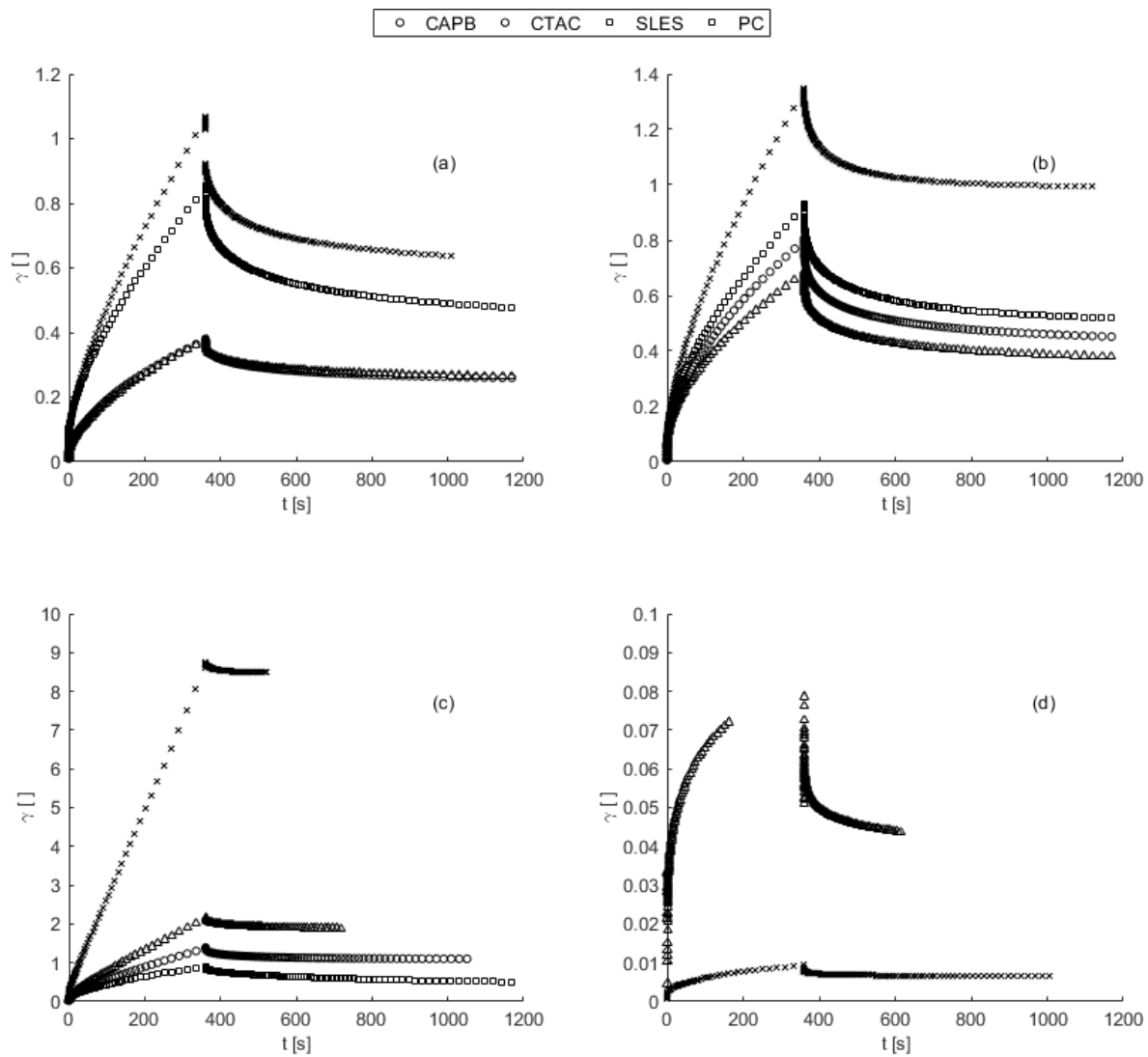| **CAPB**									
Diutan	15.7	10.6	10.7	5.6	0.02	0.5	9.5	161	0.9975
Welan	14.8	7.7	4.0	2.0	0.02	0.4	7.0	118	0.9976
S-88	15.9	9.6	5.5	1.5	0.01	0.3	5.1	58.3	0.9974

Figure S15. Creep and creep recovery test of the sphingan-surfactant systems.

Strain during creep and recovery during creep recovery phase of (a) Diutan (b) Welan (c) S-88 and (d) Gellan in combination with different surfactants.

Table S3. Model parameters of the Burgers model of the creep- and creep recovery test of the sphingan-surfactant systems

	Model/parameter						
System	**Burgers model (6 parameters)**						

Plantacare®	**η_0 [Pa·s]**	**η_1 [Pa·s]**	**η_2 [Pa·s]**	**G_0 [Pa]**	**G_1 [Pa]**	**G_2 [Pa]**	**R^2**
Diutan	141.90	69.63	30.06	3.30	0.27	1.04	0.9483
Welan	164.30	12.57	84.28	17.73	2.56	2.00	0.9819
S-88	12.44	0.22	0.01	9.67	0.01	17.92	0.9962
SLES							
Diutan	401.97	0.59	592.55	16.74	0.07	6.07	0.9690
Welan	408.22	16.15	237.81	9.93	3.00	2.84	0.9789
S-88	33.76	14.42	74.13	47.01	0.05	2.25	0.9939
CTAC							
Diutan	659.17	1.63	247.65	13.83	0.05	5.06	0.9788
Welan	310.07	29.77	174.96	8.23	5.53	2.02	0.9838
S-88	261.69	28.19	476.37	9.30	2.62	1.88	0.9672
CAPB	**η_0 [Pa·s]**	**η_1 [Pa·s]**	**η_2 [Pa·s]**	**G_0 [Pa]**	**G_1 [Pa]**	**G_2 [Pa]**	**R^2**
Diutan	456.98	22.13	226.04	16.31	0.06	6.64	0.9677
Welan	347.08	21.25	197.54	9.55	4.16	2.37	0.9834
S-88	154.61	16.53	175.68	12.17	3.05	2.96	0.9875

12.2 Supplemental data In-depth rheological characterization of genetically engineered Xanthan-variants

Table S4. List of oligonucleotides used in this work. Introduced restriction sites are <u>underlined</u>, overlap extension (OE) primers were designed as complete reverse complements to each other.

| Oligo	Sequence 5'→3'
gumFG_check_fw	CATGATTGTGGCATCCGACG
gumFG_check_rev	TGCCCTGCATACTTCTCCAC
gumFG_fld_fw_OE	ATACGGTGACAGGGGCATCGCAGAATCATCAGTCGATGTG
gumFG_fld_rev_BamHI	TATATA<u>GGATCC</u>CGAACAGATCGCCGTCATTC
gumFG_flu_fw_XbaI	TATATA<u>TCTAGA</u>GCCGTTATTGAAACGGATGG
gumFG_flu_rev_OE	CACATCGACTGATGATTCTGCGATGCCCCTGTCACCGTAT
gumL_check_fw	ACGTCTTCCATGTAGGTCAC
gumL_check_rev	CGGAGAGAAATCCAGCAAG
gumL_fld_fw_OE	GTTTGAAGGAGGATCCCTGTAACGACAATGCATGGCCAGC
gumL_fld_rev_HindIII	TATATA<u>AAGCTT</u>GTTGCCGAAGGCCACCAAC
gumL_flu_fw_XbaI	TATATA<u>TCTAGA</u>GTATGCCGAAGGCATCCATG
gumL_flu_rev_OE	GCTGGCCATGCATTGTCGTTACAGGGATCCTCCTTCAAAC
gumF_fld_fw_OE	ATACGGTGACAGGGGCATCGATGACGACGGCTGCGATC
gumF_fld_rev_NheI	TATATA<u>GCTAGC</u>CAACCAGCAAACTGCAGACC
gumF_flu_rev_OE	GATCGCAGCCGTCGTCATCGATGCCCCTGTCACCGTAT
gumG_fld_fw_OE	CCTCAACTGTCGCGGAGCGCCAGAATCATCAGTCGATGTG
gumG_flu_fw_XbaI	TATATA<u>TCTAGA</u>ATTGTTCTGGGGCCTGGATG
gumG_flu_rev_OE	CACATCGACTGATGATTCTGGCGCTCCGCGACAGTTGAG
gumF_gDNA_check_rev	GCAGCACATCCAGTGCAAAC
gumG_gDNA_check_fw	GGCTGTCGCAGTTGTTCTC
gumF_GA_fw	CACACAGGAAACAGCAGGTGAATACGGTGACAGGGGC
gumF_GA_rev	TCGAATTTGCTTTCGAATTGTCATGCCGACACCGGACGTG
pSRK_check_fw	TGCTTCCGGCTCGTATGTTG
pSRK_check_rev	TTAACGACCCTGCCCTGAAC
pSRK_BamHI_fw	TATATAT<u>GGATCC</u>AATTCGAAAGCAAATTCGAA
pSRK_BamHI_rev	TATATA<u>GGATCC</u>TGCTGTTTCCTGTGTGAAA
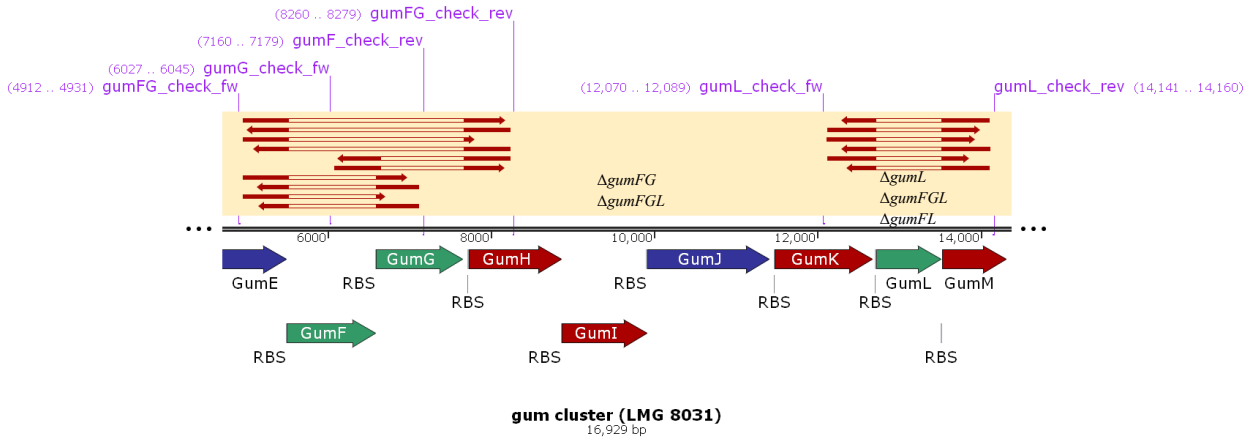
Figure S14. visualization of the sequence-alignments of the different knockout-strains.

The red regions symbolize the aligned sequence, the empty spaced indicate the deleted regions. For Sequencing, the genomic DNA was isolated, after the knockout was confirmed via colony-PCR. The DNA region of interest was amplified via PCR with the appropriate primers outside the homology regions. The amplified DNA-fragments were sequenced and the knockouts were confirmed by alignment of the ab1 files with the original sequence. For double-knockouts, both regions were amplified and sequenced using the isolated gDNA of the double mutant as template.
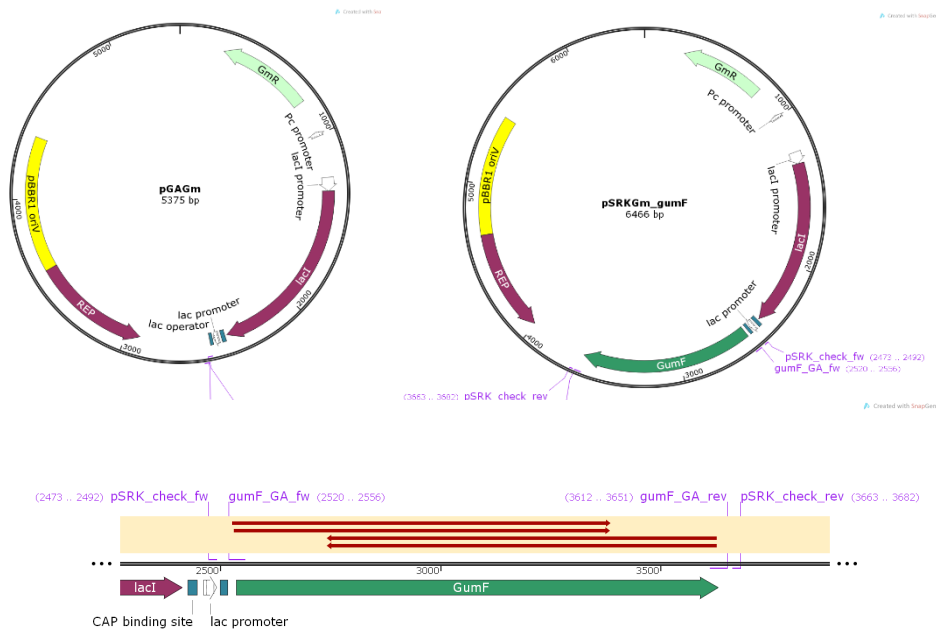
Figure S15. Maps of (a) pSRKGm-derived expression plasmid pGAGm, (b) pSRKGm_*gumF*, (c) visualization the sequenced region of pSRKGm_*gumF*.

pGAGm was created for Gibson-Assembly by amplifying pSRKGm (Khan, Gaines, Roop, & Farrand, 2008) with pSRK_BamHI_fw and pSRK_BamHI_rev, subsequent digestion with BamHI. The gel-purified linearized plasmid was then religated using T4 DNA Ligase. For pSRKGm_*gumF*, *gumF* was amplified with primers gumF_GA_fw and gumF_GA_rev using *Xcc* LMG 8031 wt gDNA as template and subsequently cloned into linearized pGAGm (BamHI) via Gibson ssembly.The insert was verified by sequencing the purified plasmid using primers pSRK_check_fw and pSRK_check rev.
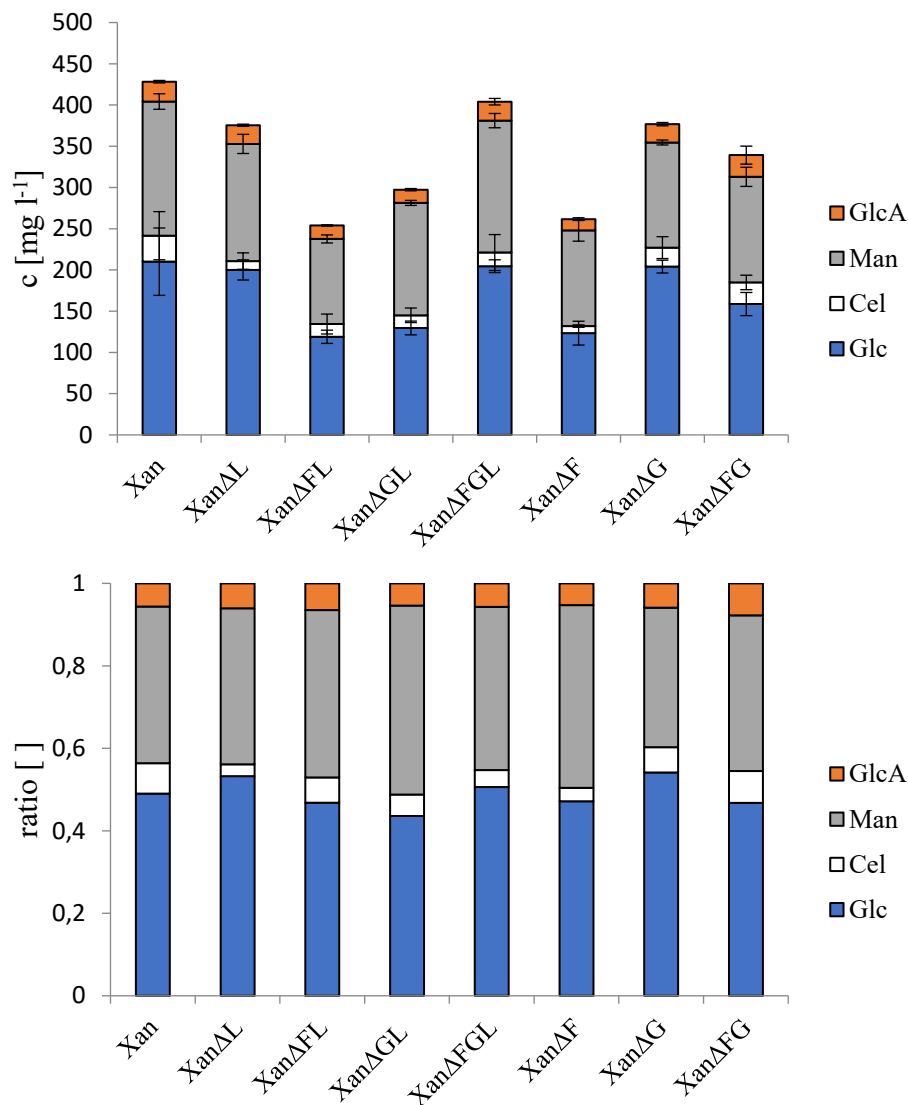
Figure S 16. Monomer composition of xanthan-variants after TFA-hydrolysis and quantification via HPLC-MS/MS.

For hydrolysis 10 mg of xanthan (powder) were dissolved in 10 ml H_2O and 20 µl were used for hydrolysis and subsequent derivatization. (a) total amount of monomers recovered, error bars indicate standard deviation of triplicates (b) relative monomer distribution. Note that part of mannose and glucuronic acid is bound in a non-quantifiable Man-GlcA dimer and most of the GlcA is degraded during hydrolysis, leading to the deviation of reported Glc:Man:GlcA ratio of 2:2:1

Table S5. Conductivity values of the characterized xanthan-variants.

For determination of conductivity the same samples used for rheological characterization were measured at room temperature

	Conductivity [mS cm^{-1}]		
Variant	Salt-free	85 mM NaCl	85 mM CaCl$_2$
Xan	0.61	10.52	14.70
XanΔL	0.97	11.53	15.50
XanΔF	0.54	12.45	14.31
XanΔFL	0.78	11.43	14.49
XanΔG	0.92	11.81	15.50
XanΔGL	0.75	11.34	14.45
XanΔFG	0.32	11.56	15.18
XanΔFGL	0.68	11.39	15.51
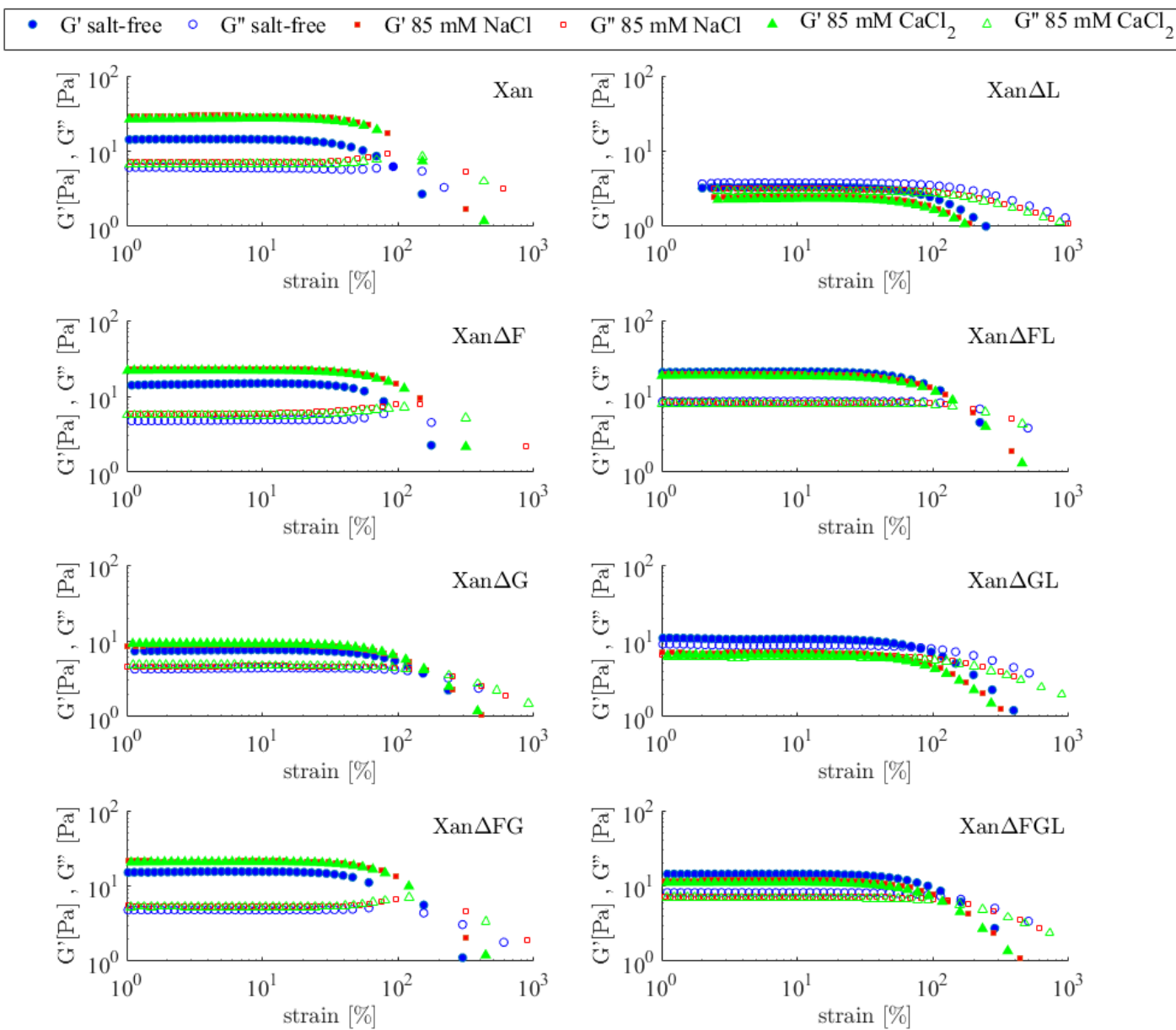
Figure S17. Amplitude sweeps of 1 % xanthan solutions salt free and with 85 mM NaCl or 85 mM CaCl$_2$

Storage moduli G' (filled symbols) and loss moduli G''(empty symbols) are shown without salt (●/○), with 85 mM NaCl (■/□) and 85 mM CaCl$_2$ (▲/Δ). All measurements were performed in triplicates under a constant frequency of 1 Hz with a logarithmically increasing shear stress amplitude from 0.1 to 1,000 Pa. For better comparability, the correlating strain of the samples is shown in the diagrams.
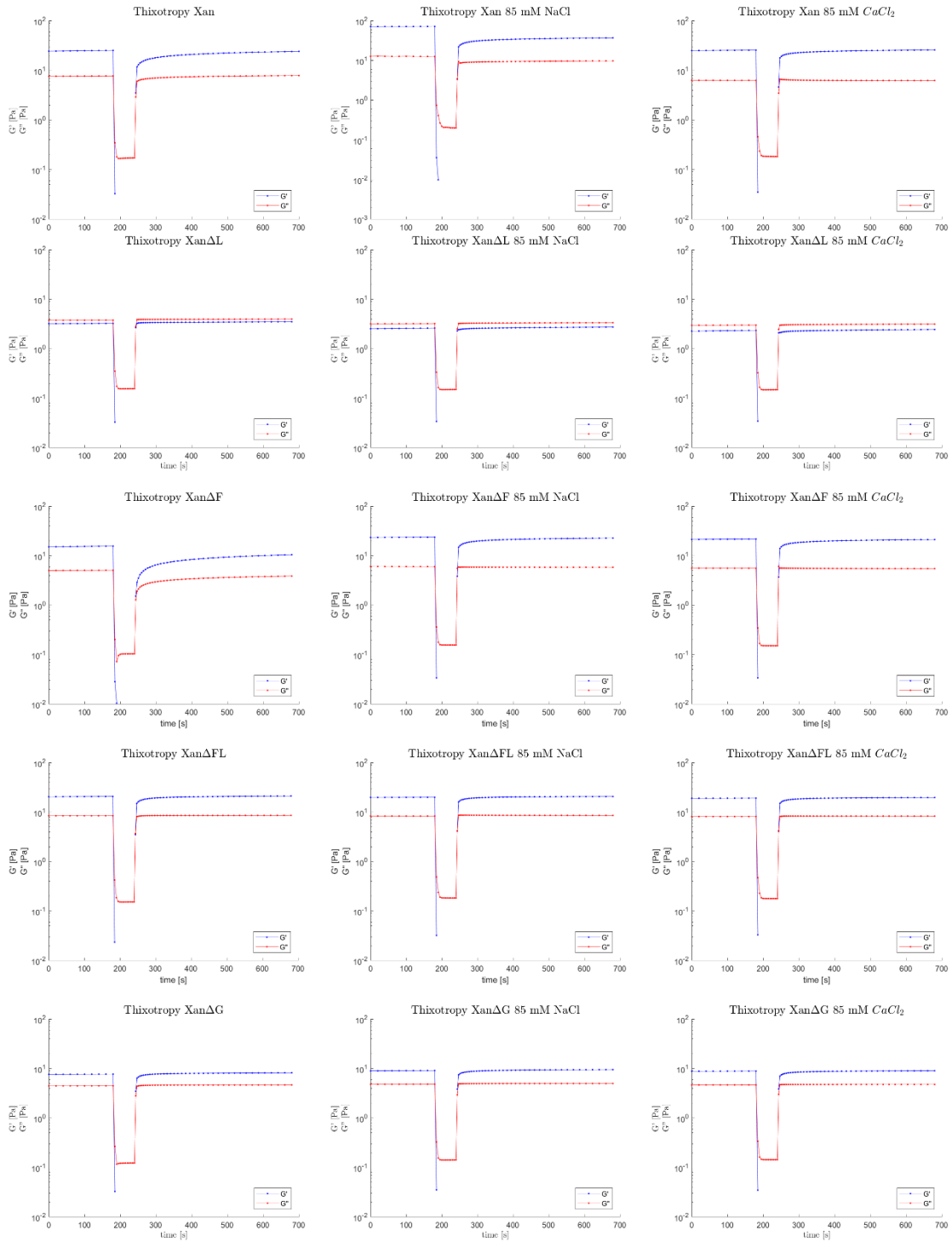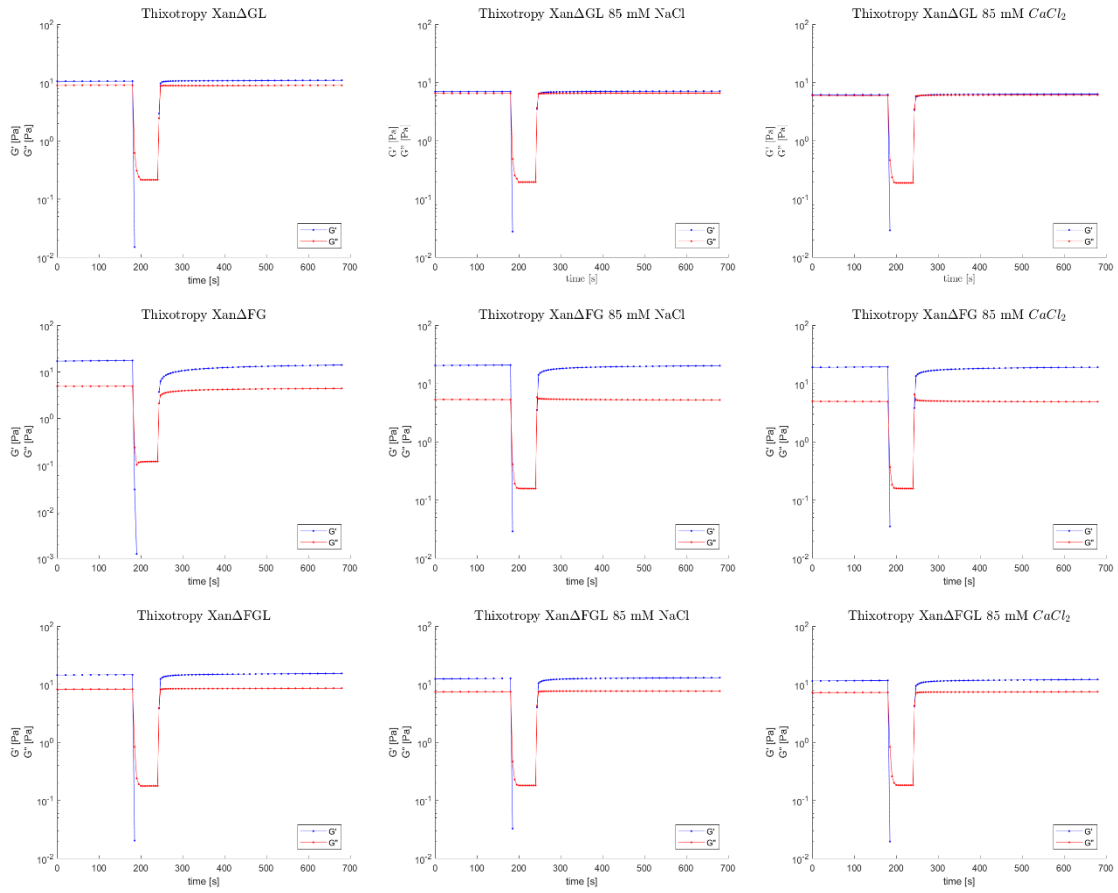
Figure S 18. Thixotropic behavior of xanthan-variants.

Storage and loss modulus were measured within the LVE-region at 1 Pa and 1 Hz in section 1 and 3. For destruction of the samples the shear stress was increased to 100 Pa. Structural recovery was monitored for 10 min after destruction.
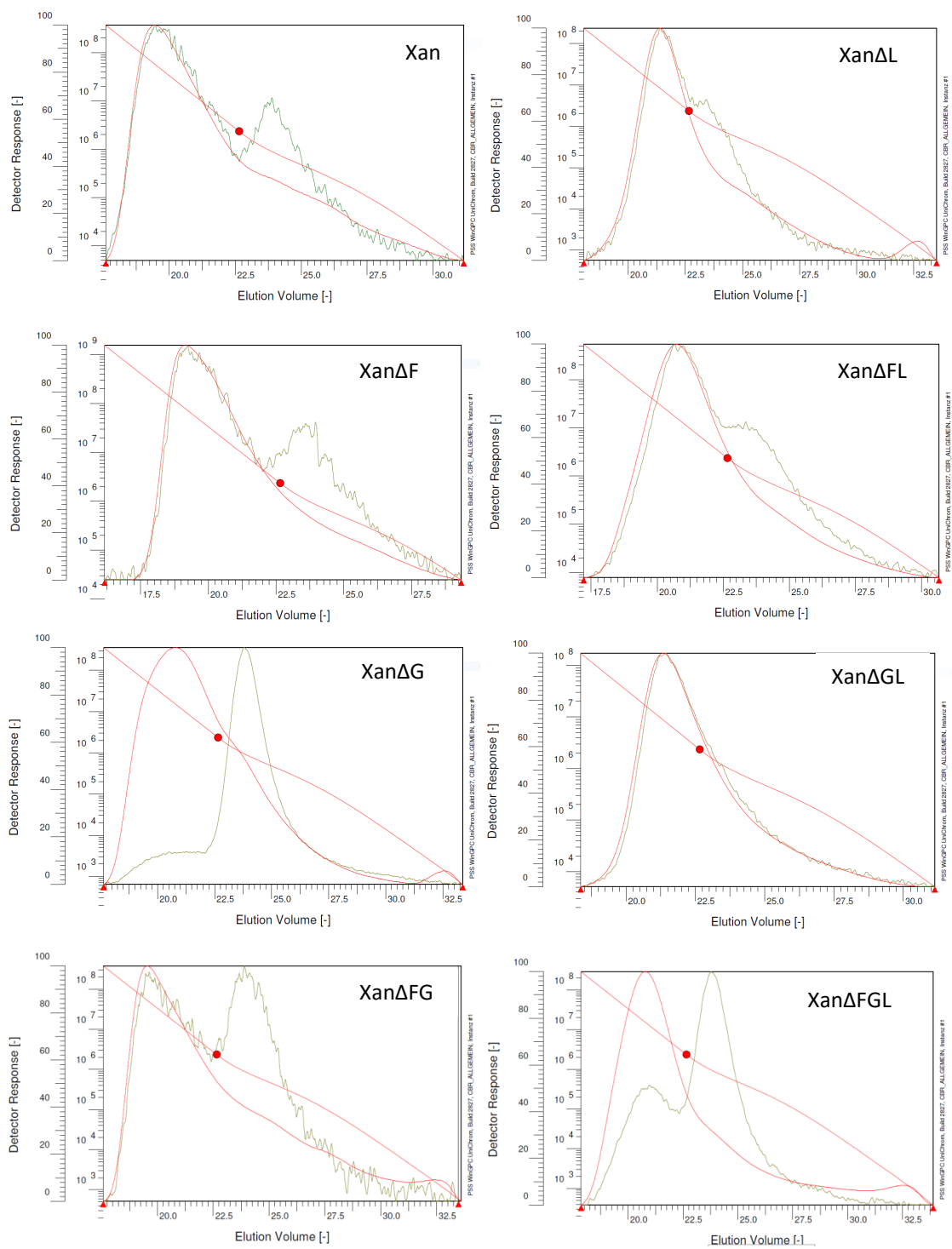
Figure S 19. GPC elution profiles of xanthan variants.

0.1 % xanthan solutions in 0.1 M LiNO₃ were prepared for analysis, eluent was 0.1 M LiNO₃ at a flow rate of 1 ml min⁻¹. Analysis was done as previously described. The red line indicates the calibration curve, the

red dot is the peak mass of the 2.35 MDa pullulan standard. For calibration the RI signal (red line) was used.

12.3 Sequence alignment of all annotated GumG porteins of Xanthomonas

Figure S 20. Sequence alignment of annotated GumG proteins from *Xanthomonas sp.*
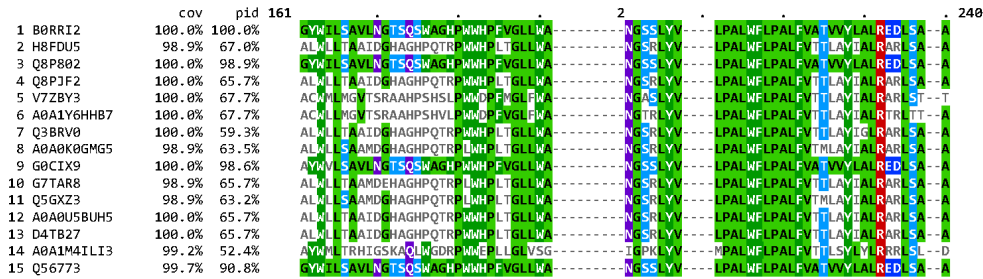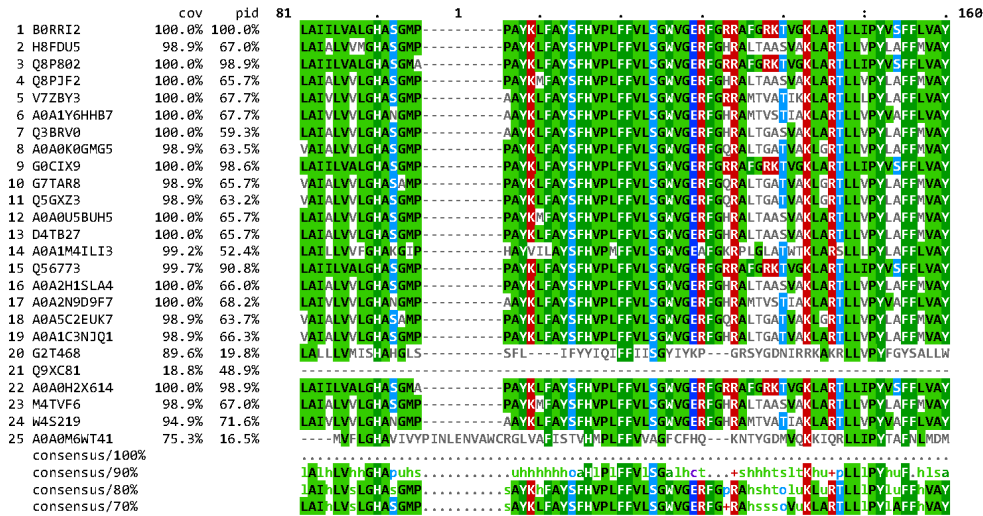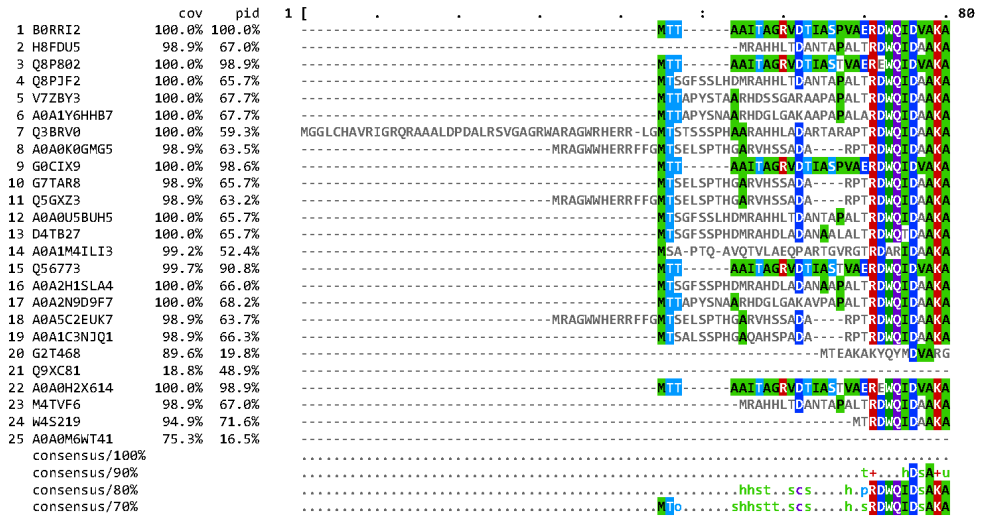
Figure S20. (cont.) Sequence alignment of annotated GumG proteins from *Xanthomonas sp.*

```
    7 Q3BRV0        100.0%  59.3%    ---------VARTGLIARSAIGTPAMALGLSAFAIAVSVPMRAVLVPIAPWMLGLKRK---------------------
    8 A0A0K0GMG5     98.9%  63.5%    ---------VARTGLIARSAIGTPAMALGLSAFAITMSVPMRAVLVRGAPWMLGLKRK---------------------
    9 G0CIX9        100.0%  98.6%    ---------VVRTGVIDRKLIGTPVMALALCAFAIAACIPMRAVLVRAAPWMLGLKRK---------------------
   10 G7TAR8         98.9%  65.7%    ---------VARTGLIARSAIGTPAMALGLSAFAIAMSVPMRAVLVRGAPWMLGLKRK---------------------
   11 Q5GXZ3         98.9%  63.2%    ---------VARTGLIARSAIGTLAMALGLSAFAITMSVPMRAVLVRGAPWMLGLKRK---------------------
   12 A0A0U5BUH5    100.0%  65.7%    ---------VARTGLIARSAIGTPAMALGLSAFAIAASVPMRAVLVPIAPWMLGLKRK---------------------
   13 D4TB27        100.0%  65.7%    ---------VARTGLIARSAIGTPAMALGLSAFAIAASVPMRAVLVPMAPWMLGLKRK---------------------
   14 A0A1M4ILI3     99.2%  52.4%    ---------ASRTGLVHGDAWG-PAMAVSVSVFAVLASVPMRAVIRRVAPWMIGVRR----------------------
   15 Q56773         99.7%  90.8%    ---------VVRTGVIDRKLIGTPVMALALCAFAIAACIPMRAVLVRRALD-VGIETQVRHFQNHQSMWRVRVSHRQRRS
   16 A0A2H1SLA4    100.0%  66.0%    ---------VARTGLIARSAIGTPAMALGLSAFAIAASVPMRAVLVPMAPWMLGLKRK---------------------
   17 A0A2N9D9F7    100.0%  68.2%    ---------VARTGVIARSLIGTPAMAMGLSAFAVAVSVPMRAVLVRVAPWMLGLKRK---------------------
   18 A0A5C2EUK7     98.9%  63.7%    ---------VARTGVIARSAIGTPAMALGLSAFAIAMSVPMRAVLVRGAPWMLGLKRK---------------------
   19 A0A1C3NJQ1     98.9%  66.3%    ---------VARTGVIARSAIGTPAMALGLSVFAIATSVPMRAVLVRVAPWMLGLKRK---------------------
   20 G2T468         89.6%  19.8%    ---------IASHVIPVQELTGVAEMIYVAVRVGAAVCGS--LLFGVGVSMVKKKRGR---------------------
   21 Q9XC81         18.8%  48.9%    ---------VARTGLIARSAIGTPAMALGLSAFAITMSVPMRAVLVRGAMD-VGIETQMTSFQNHQPSQKLDARRWQRRL
   22 A0A0H2X614    100.0%  98.9%    ---------VVRTGVIDRKLIGTPVMALALCAFAIAACIPMRAVLVRAAPWMLGLKRK---------------------
   23 M4TVF6         98.9%  67.0%    ---------VARTGLIARSAIGTPAMALGLSAFAIAASVPMRAVLVPIAPWMLGLKRK---------------------
   24 W4S219         94.9%  71.6%    ---------VARTGVIARSLIGTPAMAMGLSAFAVAVSVPMRAVLVRVAPWMLGLKRK---------------------
   25 A0A0M6WT41     75.3%  16.5%    ACTNPLVIVAGNTLFDLAGAFGTAKYVLMKAKVLRVLCGEK-------------------------------------
      consensus/100%                ..........hspphh...thhG....ahh.hshhhhhhsh..............................
      consensus/90%                 ..........lsRTGllstphhGTssMAhulsshAlshs1PMRAVlV.hA...1Glctp............
      consensus/80%                 ..........VARTGlIsRphIGTPsMAluLsAFAlshs1PMRAVLV.hAPWMLGLKRK............
      consensus/70%                 ..........VARTGlIsRuhIGTPsMALuLuAFAIAsSVPMRAVLV.hAPWMLGLKRK............
```

```
                        cov      pid   481  ] 482
    1 B0RRI2        100.0% 100.0%        --
    2 H8FDU5         98.9%  67.0%        --
    3 Q8P802        100.0%  98.9%        --
    4 Q8PJF2        100.0%  65.7%        --
    5 V7ZBY3        100.0%  67.7%        --
    6 A0A1Y6HHB7    100.0%  67.7%        --
    7 Q3BRV0        100.0%  59.3%        --
    8 A0A0K0GMG5     98.9%  63.5%        --
    9 G0CIX9        100.0%  98.6%        --
   10 G7TAR8         98.9%  65.7%        --
   11 Q5GXZ3         98.9%  63.2%        --
   12 A0A0U5BUH5    100.0%  65.7%        --
   13 D4TB27        100.0%  65.7%        --
   14 A0A1M4ILI3     99.2%  52.4%        --
   15 Q56773         99.7%  90.8%        AQ
   16 A0A2H1SLA4    100.0%  66.0%        --
   17 A0A2N9D9F7    100.0%  68.2%        --
   18 A0A5C2EUK7     98.9%  63.7%        --
   19 A0A1C3NJQ1     98.9%  66.3%        --
   20 G2T468         89.6%  19.8%        --
   21 Q9XC81         18.8%  48.9%        AQ
   22 A0A0H2X614    100.0%  98.9%        --
   23 M4TVF6         98.9%  67.0%        --
   24 W4S219         94.9%  71.6%        --
   25 A0A0M6WT41     75.3%  16.5%        --
      consensus/100%                    ..
      consensus/90%                     ..
      consensus/80%                     ..
      consensus/70%                     ..
```

MView 1.63, Copyright © 1997-2018 Nigel P. Brown

Figure S20. (cont.) Sequence alignment of annotated GumG proteins from *Xanthomonas sp.*

13 References

Bond-Watts, B. B., Bellerose, R. J., & Chang, M. C. (2011). Enzyme mechanism as a kinetic control element for designing synthetic biofuel pathways. *Nature chemical biology,* 7(4), 222-227.

Abrankó, L., Williamson, G., Gardner, S., & Kerimi, A. (2018). Comprehensive quantitative analysis of fatty-acyl-Coenzyme A species in biological samples by ultra-high performance liquid chromatography–tandem mass spectrometry harmonizing hydrophilic interaction and reversed phase chromatography. *Journal of Chromatography A,* 1534, 111-122.

Amanullah, A., Satti, S., & Nienow, A. (1998). Enhancing xanthan fermentations by different modes of glucose feeding. *Biotechnology Progress,* 14(2), 265-269.

Atsumi, S., Cann, A. F., Connor, M. R., Shen, C. R., Smith, K. M., Brynildsen, M. P., . . . Liao, J. C. (2008). Metabolic engineering of Escherichia coli for 1-butanol production. *Metabolic engineering,* 10(6), 305-311.

Bajaj, I. B., Survase, S. A., Saudagar, P. S., & Singhal, R. S. (2007). Gellan gum: fermentative production, downstream processing and applications. *Food Technology and Biotechnology,* 45(4), 341-354.

Becker, A., Katzen, F., Pühler, A., & Ielpi, L. (1998). Xanthan gum biosynthesis and application: a biochemical/genetic perspective. *Applied Microbiology and Biotechnology,* 50.

Bejenariu, A., Popa, M., Dulong, V., Picton, L., & Le Cerf, D. (2009). Trisodium trimetaphosphate crosslinked xanthan networks: synthesis, swelling, loading and releasing behaviour. *Polymer Bulletin,* 62(4), 525-538.

Bejenariu, A., Popa, M., Picton, L., & Le Cerf, D. (2010). Effect of concentration, pH and temperature on xanthan conformation: A preliminary study before crosslinking. *Revue Roumaine de Chimie,* 55(2), 147-152.

Bennett, B. D., Kimball, E. H., Gao, M., Osterhout, R., Van Dien, S. J., & Rabinowitz, J. D. (2009). Absolute metabolite concentrations and implied enzyme active site occupancy in Escherichia coli. *Nature chemical biology,* 5(8), 593.

Bennett, B. D., Yuan, J., Kimball, E. H., & Rabinowitz, J. D. (2008). Absolute quantitation of intracellular metabolite concentrations by an isotope ratio-based approach. *Nature protocols,* 3(8), 1299.

Bercea, M., & Morariu, S. (2020). Real-time monitoring of the order-disorder conformational transition of xanthan gum. *Journal of Molecular Liquids*, 113168.

Betlach, M., Capage, M., Doherty, D., Hassler, R., Henderson, N., Vanderslice, R., . . . Ward, M. (1987). Genetically engineered polymers: manipulation of xanthan biosynthesis. *Progress in biotechnology*.

Bian, W., Chandrasekaran, R., & Rinaudo, M. (2002). Molecular structure of the rhamsan-like exocellular polysaccharide RMDP17 from Sphingomonas paucimobilis. *Carbohydrate Research,* 337(1), 45-56.

Blekas, G. A. (2016). *Food Additives: Classification, Uses and Regulation*. In B. Caballero, P. M. Finglas & F. Toldrá (Eds.), *Encyclopedia of Food and Health* (pp. 731-736). Oxford: Academic Press

Bond-Watts, B. B., Bellerose, R. J., & Chang, M. C. (2011). Enzyme mechanism as a kinetic control element for designing synthetic biofuel pathways. *Nature chemical biology,* 7(4), 222-227.

Boynton, Z. L., Bennet, G., & Rudolph, F. B. (1996). Cloning, sequencing, and expression of clustered genes encoding beta-hydroxybutyryl-coenzyme A (CoA) dehydrogenase, crotonase, and butyryl-CoA dehydrogenase from Clostridium acetobutylicum ATCC 824. *Journal of Bacteriology,* 178(11), 3015-3024.

Bueno, V. B., Bentini, R., Catalani, L. H., & Petri, D. F. S. (2013). Synthesis and swelling behavior of xanthan-based hydrogels. *Carbohydr Polym,* 92(2), 1091-1099.

Callet, F., Milas, M., & Rinaudo, M. (1987). Influence of acetyl and pyruvate contents on rheological properties of xanthan in dilute solution. *Int J Biol Macromol,* 9(5), 291-293.

Cebrian, J., Tan, G., Martin, M., Dupin, L., Wetzel, T., Moran, B., & Blasco, L. (2019). Kelco Care™ Diutan Gum (Sphingomonas Ferment Extract) as a thickener in cosmetic formulations. IP.com PAD: Lubrizol Advanced Materials, Inc. .

Chandrasekaran, R., Radha, A., & Lee, E. J. (1994). Structural roles of calcium ions and side chains in welan: an X-ray study. *Carbohydr Res,* 252, 183-207.

Cheetham, N. W., & Norma, N. N. (1989). The effect of pyruvate on viscosity properties of xanthan. *Carbohydr Polym,* 10(1), 55-60.

Clarke, P. M., & Payton, M. A. (1983). An enzymatic assay for acetate in spent bacterial culture supernatants. *Analytical Biochemistry,* 130(2), 402-405.

Coleman, R. J., Patel, Y. N., & Harding, N. E. (2008). Identification and organization of genes for diutan polysaccharide synthesis from Sphingomonas sp. ATCC 53159. *Journal of Industrial Microbiology & Biotechnology,* 35(4), 263-274.

Coplin, D., & Cook, D. (1990). Molecular genetics of extracellular polysaccharide biosynthesis in vascular phytopathogenic bacteria. *Mol. Plant-Microbe Interact,* 3(5), 271-279.

Cumpstey, I. (2013). Chemical modification of polysaccharides. *ISRN organic chemistry,* 2013.

Ding, J., Li, C., Liu, J., Lu, Y., Qin, G., Gan, L., & Long, M. (2017). Time and energy-efficient homogeneous transesterification of cellulose under mild reaction conditions. *Carbohydr Polym,* 157, 1785-1793.

Dumitriu, S. (2004). *Polysaccharides: structural diversity and functional versatility*: CRC press.

EFSA Panel on Food Additives Nutrient Sources added to Food. (2017). Re-evaluation of xanthan gum (E 415) as a food additive. *EFSA Journal,* 15(7), e04909.

Elella, M. H. A., Sabaa, M. W., Abd ElHafeez, E., & Mohamed, R. R. (2019). Crystal violet dye removal using crosslinked grafted xanthan gum. *Int J Biol Macromol,* 137, 1086-1101.

Esgalhado, M. E., Roseiro, J. C., & Collaço, M. A. (1995). Interactive effects of pH and temperature on cell growth and polymer production by Xanthomonas campestris. *Process Biochemistry,* 30(7), 667-671.

Fry, S. C. (1995). Polysaccharide-modifying enzymes in the plant cell wall. *Annual review of plant biology,* 46(1), 497-520.

Gansbiller, M., Schmid, J., & Sieber, V. (2019). In-depth rheological characterization of genetically modified xanthan-variants. *Carbohydr Polym,* 213, 236-246.

Garcia-Ochoa, F., Gomez, E., Alcon, A., & Santos, V. (2013). The effect of hydrodynamic stress on the growth of Xanthomonas campestris cultures in a stirred and sparged tank bioreactor. *Bioprocess and biosystems engineering,* 36(7), 911-925.

García-Ochoa, F., Santos, V., Casas, J., & Gomez, E. (2000). Xanthan gum: production, recovery, and properties. *Biotechnology advances,* 18(7), 549-579.

Ghorpade, V. S. (2020). *Chapter 4 - Preparation of hydrogels based on natural polymers via chemical reaction and cross-Linking*. In Y. Chen (Ed.), *Hydrogels Based on Natural Polymers* (pp. 91-118): Elsevier

Guo, J., Ge, L., Li, X., Mu, C., & Li, D. (2014). Periodate oxidation of xanthan gum and its crosslinking effects on gelatin-based edible films. *Food Hydrocolloids,* 39, 243-250.

Hashimoto, W., Inose, T., Nakajima, H., Sato, N., Kimura, S., & Murata, K. (1996). Purification and characterization of microbial gellan lyase. *Applied and Environmental Microbiology,* 62(4), 1475-1477.

Hashimoto, W., Nankai, H., Mikami, B., & Murata, K. (2003). Crystal structure of Bacillus sp. GL1 xanthan lyase, which acts on the side chains of xanthan. *Journal of Biological Chemistry,* 278(9), 7663-7673.

Hashimoto, W., Sato, N., Kimura, S., & Murata, K. (1998). Polysaccharide lyase: Molecular cloning of gellan lyase gene and formation of the lyase from a huge precursor protein in Bacillus sp. GL1. *Archives of Biochemistry and Biophysics,* 354(1), 31-39.

Hassler, R. A., & Doherty, D. H. (1990). Genetic engineering of polysaccharide structure: production of variants of xanthan gum in Xanthomonas campestris. *Biotechnology Progress,* 6(3), 182-187.

Ielpi, L., Couso, R., & Dankert, M. (1981). Lipid-linked intermediates in the biosynthesis of xanthan gum. *FEBS letters,* 130(2), 253-256.

Ielpi, L., Couso, R. O., & Dankert, M. A. (1981). Xanthan gum biosynthesis pyruvic acid acetal residues are transferred from phosphoenolpyruvate to the pentasaccharide-PP-lipid. *Biochemical and biophysical research communications,* 102(4), 1400-1408.

Inui, M., Suda, M., Kimura, S., Yasuda, K., Suzuki, H., Toda, H., . . . Yukawa, H. (2008). Expression of Clostridium acetobutylicum butanol synthetic genes in Escherichia coli. *Applied Microbiology and Biotechnology,* 77(6), 1305-1316.

Jansson, P.-e., Kenne, L., & Lindberg, B. (1975). Structure of the extracellular polysaccharide from xanthomonas campestris. *Carbohydrate Research,* 45(1), 275-282.

Jansson, P.-E., Savitri Kumar, N., & Lindberg, B. (1986). Structural studies of a polysaccharide (S-88) elaborated by Pseudomonas ATCC 31554. *Carbohydrate Research,* 156, 165-172.

Jansson, P.-E., & Widmalm, G. (1994). Welan gum (S-130) contains repeating units with randomly distributed L-mannosyl and L-rhamnosyl terminal groups, as determined by FABMS. *Carbohydrate Research,* 256(2), 327-330.

Jeanes, A., Pittsley, J. E., & Senti, F. R. (1961). Polysaccharide B-1459: A new hydrocolloid polyelectrolyte produced from glucose by bacterial fermentation. *Journal of Applied Polymer Science,* 5(17), 519-526.

Joersbo, M., Marcussen, J., & Brunstedt, J. (2001). In vivo modification of the cell wall polysaccharide galactomannan of guar transformed with a α-galactosidase gene cloned from senna. *Molecular Breeding,* 7(3), 211-219.

Kang, K., & Pettitt, D. (1993). *Xanthan, gellan, welan, and rhamsan*. In *Industrial Gums (Third Edition)* (pp. 341-397): Elsevier

Katzen, F., Ferreiro, D. U., Oddo, C. G., Ielmini, M. V., Becker, A., Pühler, A., & Ielpi, L. (1998). Xanthomonas campestris pv. campestris gum Mutants: Effects on Xanthan Biosynthesis and Plant Virulence. *Journal of Bacteriology,* 180(7), 1607-1617.

Kaur, V., Bera, M. B., Panesar, P. S., Kumar, H., & Kennedy, J. F. (2014). Welan gum: Microbial production, characterization, and applications. *Int J Biol Macromol,* 65, 454-461.

Kelco, C. (2008). *KELTROL® / KELZAN® xanthan gum book*. (8 ed.). CPKelco.com: CP Kelco.

Kelco, C. CP Kelco Announces Global Collaboration with Lubrizol.(2019). **https://www.cpkelco.com/cp-kelco-announces-global-collaboration-with-lubrizol/** Accessed 20 Jul.2020.

Kennedy, L., & Sutherland, I. W. (1994). Gellan Lyases - Novel Polysaccharide Lyases. *Microbiology-Uk,* 140, 3007-3013.

Khan, S. R., Gaines, J., Roop, R. M., & Farrand, S. K. (2008). Broad-Host-Range Expression Vectors with Tightly Regulated Promoters and Their Use To Examine the Influence of TraR and TraM Expression on Ti Plasmid Quorum Sensing. *Applied and Environmental Microbiology,* 74(16), 5053-5062.

Khouryieh, H., Herald, T., Aramouni, F., Bean, S., & Alavi, S. (2007). Influence of deacetylation on the rheological properties of xanthan–guar interactions in dilute aqueous solutions. *Journal of Food Science,* 72(3).

Kool, M. M. (2014). Enzymatic modification and characterization of xanthan. Wageningen University.

Kool, M. M., Gruppen, H., Sworn, G., & Schols, H. A. (2014). The influence of the six constituent xanthan repeating units on the order–disorder transition of xanthan. *Carbohydr Polym,* 104, 94-100.

Lee, E. J., & Chandrasekaran, R. (1991). X-Ray and computer modeling studies on gellan-related polymers: Molecular structures of welan, S-657, and rhamsan. *Carbohydrate Research,* 214(1), 11-24.

Li, H., Zhu, H., Sun, S., Feng, Z., Sun, Y., & Zhou, W. (2016). Biological production of welan gum. *Physical Sciences Reviews,* 1(10), 20160049.

Lin, J.-H., Lee, M.-C., Sue, Y.-S., Liu, Y.-C., & Li, S.-Y. (2017). Cloning of phaCAB genes from thermophilic Caldimonas manganoxidans in Escherichia coli for poly (3-hydroxybutyrate)(PHB) production. *Applied Microbiology and Biotechnology,* 101(16), 6419-6430.

Lo, Y.-M., Yang, S.-T., & Min, D. B. (1997). Effects of yeast extract and glucose on xanthan production and cell growth in batch culture of Xanthomonas campestris. *Applied Microbiology and Biotechnology,* 47(6), 689-694.

Matricardi, P., Cencetti, C., Ria, R., Alhaique, F., & Coviello, T. (2009). Preparation and characterization of novel gellan gum hydrogels suitable for modified drug release. *Molecules,* 14(9), 3376-3391.

Mazen, F., Milas, M., & Rinaudo, M. (1999). Conformational transition of native and modified gellan. *Int J Biol Macromol,* 26(2-3), 109-118.

Misailidis, N., & Petrides, D. (2020). Xanthan Gum Production via Fermentation - Process Modeling and Techno-Economic Assessment (TEA) using SuperPro Designer.

Morris, E. R. (2019). Ordered conformation of xanthan in solutions and "weak gels": Single helix, double helix–or both? *Food Hydrocolloids,* 86, 18-25.

Morris, E. R., Gothard, M. G. E., Hember, M. W. N., Manning, C. E., & Robinson, G. (1996). Conformational and rheological transitions of welan, rhamsan and acylated gellan. *Carbohydr Polym,* 30(2), 165-175.

Neubauer, S., Chu, D. B., Marx, H., Sauer, M., Hann, S., & Koellensperger, G. (2015). LC-MS/MS-based analysis of coenzyme A and short-chain acyl-coenzyme A thioesters. *Analytical and Bioanalytical Chemistry,* 407(22), 6681-6688.

Nordström, K., & Austin, S. J. (1989). Mechanisms That Contribute To The Stable Segregation Of Plasmids. *Annual Review of Genetics,* 23(1), 37-69.

Novick, R. P. (1987). Plasmid incompatibility. *Microbiological reviews,* 51(4), 381.

Ogino, H., & Ishikawa, H. (2001). Enzymes which are stable in the presence of organic solvents. *Journal of Bioscience and Bioengineering,* 91(2), 109-116.

Palaniraj, A., & Jayaraman, V. (2011). Production, recovery and applications of xanthan gum by Xanthomonas campestris. *Journal of Food Engineering,* 106(1), 1-12.

Paulsson, M., Hagerstrom, H., & Edsman, K. (1999). Rheological studies of the gelation of deacetylated gellan gum (Gelrite) in physiological conditions. *Eur J Pharm Sci,* 9(1), 99-105.

Petri, D. F. S. (2015). Xanthan gum: A versatile biopolymer for biomedical and technological applications. *Journal of Applied Polymer Science,* 132(23).

Petzold, C. J., Chan, L. J. G., Nhan, M., & Adams, P. D. (2015). Analytics for metabolic engineering. *Frontiers in bioengineering and biotechnology,* 3, 135.

Phillips, G. O. (2016). Food polysaccharides and their applications.

Pinto, E. P., Furlan, L., & Vendruscolo, C. T. (2011). Chemical deacetylation natural xanthan (Jungbunzlauer®). *Polímeros,* 21(1), 47-52.

Poli, A., Di Donato, P., Abbamondi, G. R., & Nicolaus, B. (2011). Synthesis, production, and biotechnological applications of exopolysaccharides and polyhydroxyalkanoates by archaea. *Archaea,* 2011.

Pollock, T. J. (2005). *Sphingan Group of Exopolysaccharides (EPS).* In *Biopolymers Online*: Wiley-VCH Verlag GmbH & Co. KGaA

Psomas, S. K., Liakopoulou-Kyriakides, M., & Kyriakidis, D. A. (2007). Optimization study of xanthan gum production using response surface methodology. *Biochemical Engineering Journal,* 35(3), 273-280.

R Sharma, B., C Dhuldhoya, N., U Merchant, S., & C Merchant, U. (2006). *Xanthan Gum-A Boon to Food Industry*.

Ranganathan, S., Zeitlhofer, S., & Sieber, V. (2017). Development of a lipase-mediated epoxidation process for monoterpenes in choline chloride-based deep eutectic solvents. *Green Chemistry,* 19(11), 2576-2586.

Razeq, F. M., Jurak, E., Stogios, P. J., Yan, R., Tenkanen, M., Kabel, M. A., . . . Master, E. R. (2018). A novel acetyl xylan esterase enabling complete deacetylation of substituted xylans. *Biotechnology for Biofuels,* 11(1), 74.

Rosales-Calderon, O., & Arantes, V. (2019). A review on commercial-scale high-value products that can be produced alongside cellulosic ethanol. *Biotechnology for Biofuels,* 12(1), 240.

Rühmann, B. (2015). Development of a Modular High Throughput Screening Platform for Microbial Exopolysaccharide Producers. Technische Universität München.

Rühmann, B., Schmid, J., & Sieber, V. (2014). Fast carbohydrate analysis via liquid chromatography coupled with ultra violet and electrospray ionization ion trap detection in 96-well format. *J Chromatogr A,* 1350, 44-50.

Rühmann, B., Schmid, J., & Sieber, V. (2015). High throughput exopolysaccharide screening platform: from strain cultivation to monosaccharide composition and carbohydrate fingerprinting in one day. *Carbohydr Polym,* 122, 212-220.

Rütering, M., Cress, B. F., Schilling, M., Rühmann, B., Koffas, M. A., Sieber, V., & Schmid, J. (2017). Tailor-made exopolysaccharides—CRISPR-Cas9 mediated genome editing in Paenibacillus polymyxa. *Synthetic Biology,* 2(1), ysx007.

Rütering, M., Schmid, J., Gansbiller, M., Braun, A., Kleinen, J., Schilling, M., & Sieber, V. (2018). Rheological characterization of the exopolysaccharide Paenan in surfactant systems. *Carbohydr Polym,* 181, 719-726.

Rütering, M., Schmid, J., Rühmann, B., Schilling, M., & Sieber, V. (2016). Controlled production of polysaccharides–exploiting nutrient supply for levan and heteropolysaccharide formation in Paenibacillus sp. *Carbohydr Polym,* 148, 326-334.

Schilling, C., Klau, L. J., Aachmann, F. L., Rühmann, B., Schmid, J., & Sieber, V. (2022). Structural elucidation of the fucose containing polysaccharide of Paenibacillus polymyxa DSM 365. *Carbohydr Polym,* 278, 118951.

Schilling, C., Klau, L. J., Rühmann, B., Aachmann, F. L., Schmid, J., & Sieber, V. (2022). CRISPR-Cas9 driven structural elucidation of the heteroexopolysaccharides from *Paenibacillus polymyxa* DSM 365. *Prepared Manuscript*.

Schmid, J., Huptas, C., & Wenning, M. (2016). Draft Genome Sequence of the Xanthan Producer Xanthomonas campestris LMG 8031. *Genome Announcements, 4*(5).

Schmid, J., Sieber, V., & Rehm, B. (2015). Bacterial exopolysaccharides: biosynthesis pathways and engineering strategies. *Frontiers in Microbiology, 6*(496).

Schmid, J., Sperl, N., & Sieber, V. (2014). A comparison of genes involved in sphingan biosynthesis brought up to date. *Applied Microbiology and Biotechnology, 98*(18), 7719-7733.

Shatwell, K. P., Sutherland, I. W., Dea, I. C., & Ross-Murphy, S. B. (1990). The influence of acetyl and pyruvate substituents on the helix-coil transition behaviour of xanthan. *Carbohydrate Research, 206*(1), 87-103.

Shimazu, M., Vetcher, L., Galazzo, J. L., Licari, P., & Santi, D. V. (2004). A sensitive and robust method for quantification of intracellular short-chain coenzyme A esters. *Analytical Biochemistry, 328*(1), 51-59.

Shu, C. H., & Yang, S. T. (1990). Effects of temperature on cell growth and xanthan production in batch cultures of Xanthomonas campestris. *Biotechnology and bioengineering, 35*(5), 454-468.

Shurubor, Y., D'Aurelio, M., Clark-Matott, J., Isakova, E., Deryabina, Y., Beal, M., . . . Krasnikov, B. (2017). Determination of coenzyme A and acetyl-coenzyme A in biological samples using HPLC with UV detection. *Molecules, 22*(9), 1388.

Slepecky, R. A., & Law, J. H. (1960). A rapid spectrophotometric assay of alpha, beta-unsaturated acids and beta-hydroxy acids. *Analytical chemistry, 32*(12), 1697-1699.

Smith, I., Symes, K., Lawson, C., & Morris, E. (1981). Influence of the pyruvate content of xanthan on macromolecular association in solution. *Int J Biol Macromol, 3*(2), 129-134.

Srirangan, K., Liu, X., Tran, T. T., Charles, T. C., Moo-Young, M., & Chou, C. P. (2016). Engineering of Escherichia coli for direct and modulated biosynthesis of poly (3-hydroxybutyrate-co-3-hydroxyvalerate) copolymer using unrelated carbon sources. *Scientific reports, 6*(1), 1-11.

Stankowski, J. D., Mueller, B. E., & Zeller, S. G. (1993). Location of a second O-acetyl group in xanthan gum by the reductive-cleavage method. *Carbohydrate Research, 241*, 321-326.

Stephen, A. M. (1995). *Food polysaccharides and their applications*: CRC press.

Sutherland, I. W., & Kennedy, L. (1996). Polysaccharide lyases from gellan-producing Sphingomonas spp. *Microbiology-Uk,* 142, 867-872.

Sworn, G. (2009). *Gellan gum*. In *Handbook of hydrocolloids* (pp. 204-227): Elsevier

Tako, M. (1992). MOLECULAR-ORIGIN FOR THERMAL-STABILITY OF WELAN AND RHAMSAN GUM. *ABSTRACTS OF PAPERS OF THE AMERICAN CHEMICAL SOCIETY* (Vol. 204, pp. 38-CARB): AMER CHEMICAL SOC 1155 16TH ST, NW, WASHINGTON, DC 20036.

Tako, M. (1992). *Molecular origin for rheological characteristics of xanthan gum*. In: ACS Publications

Tako, M. (1993). Molecular Origin of Thermal Stability of Rhamsan Gum in Aqueous Media. *Bioscience, Biotechnology, and Biochemistry,* 57(7), 1182-1184.

Tako, M. (1994). Molecular origin for the thermal stability of S-657 polysaccharide produced by Xanthomonas ATCC 53159. *Polymer Gels and Networks,* 2(2), 91-104.

Tako, M., & Kiriaki, M. (1990). Rheological Properties of Welan Gum in Aqueous-Media. *Agricultural and Biological Chemistry,* 54(12), 3079-3084.

Tako, M., & Nakamura, S. (1984). Rheological Properties of Deacetylated Xanthan in Aqueous Media. *Agricultural and Biological Chemistry,* 48(12), 2987-2993.

Tako, M., & Nakamura, S. (1988). *Rheological Properties of Depyruvated Xanthan in Aqueous Media*.

Tako, M., Sakae, A., & Nakamura, S. (1989). Rheological properties of gellan gum in aqueous media. *Agricultural and Biological Chemistry,* 53(3), 771-776.

Tako, M., & Tamaki, H. (2005). Molecular Origin for the Thermal Stability of S-88 Gum Produced by Pseudomonas ATCC 31554. *Polym J,* 37(7), 498-505.

Tang, J., Mao, R., Tung, M., & Swanson, B. (2001). Gelling temperature, gel clarity and texture of gellan gels containing fructose or sucrose. *Carbohydr Polym,* 44(3), 197-209.

Tao, Y., Zhang, R., Xu, W., Bai, Z., Zhou, Y., Zhao, S., . . . Yu, D. (2016). Rheological behavior and microstructure of release-controlled hydrogels based on xanthan gum crosslinked with sodium trimetaphosphate. *Food Hydrocolloids,* 52, 923-933.

Tseng, H.-C., Martin, C. H., Nielsen, D. R., & Prather, K. L. J. (2009). Metabolic engineering of Escherichia coli for enhanced production of (R)-and (S)-3-hydroxybutyrate. *Applied and Environmental Microbiology,* 75(10), 3137-3145.

Valli, R., & Clark, R. (2009). 8 Gellan Gum. *Food stabilisers, thickeners and gelling agents*, 145.

Velappan, N., Sblattero, D., Chasteen, L., Pavlik, P., & Bradbury, A. R. M. (2007). Plasmid incompatibility: more compatible than previously thought? *Protein Engineering, Design and Selection,* 20(7), 309-313.

Wang, X., Zheng, D., & Liang, R. (2016). An Efficient Electro-Competent Cells Generation Method of Xanthomonas campestris pv. campestris: Its Application for Plasmid Transformation and Gene Replacement. *Advances in Microbiology,* 6(02), 79.

Watt, S. A., Wilke, A., Patschkowski, T., & Niehaus, K. (2005). Comprehensive analysis of the extracellular proteins from Xanthomonas campestris pv. campestris B100. *Proteomics,* 5(1), 153-167.

Wilson, D. B., Sahm, H., Stahmann, K.-P., & Koffas, M. (2019). *Industrial Microbiology*: John Wiley & Sons.

Wu, M., Qu, J., Shen, Y., Dai, X., Wei, W., Shi, Z., . . . Ma, T. (2019). Gel properties of xanthan containing a single repeating unit with saturated pyruvate produced by an engineered Xanthomonas campestris CGMCC 15155. *Food Hydrocolloids,* 87, 747-757.

Wu, M., Qu, J., Tian, X., Zhao, X., Shen, Y., Shi, Z., . . . Ma, T. (2019). Tailor-made polysaccharides containing uniformly distributed repeating units based on the xanthan gum skeleton. *Int J Biol Macromol,* 131, 646-653.

Xu, L., Gong, H., Dong, M., & Li, Y. (2015). Rheological properties and thickening mechanism of aqueous diutan gum solution: Effects of temperature and salts. *Carbohydr Polym,* 132, 620-629.

Yamazaki, M., Thorne, L., Mikolajczak, M., Armentrout, R. W., & Pollock, T. J. (1996). Linkage of genes essential for synthesis of a polysaccharide capsule in Sphingomonas strain S88. *Journal of Bacteriology,* 178(9), 2676-2687.

Curriculum vitae

Persönliche Angaben

Name:	Moritz Gansbiller
Geburtsdatum:	01. August 1988
Geburtsort:	Regensburg
Familienstand:	verheiratet

Beruflich Werdegang

08/2020-heute	wissenschaftlicher Mitarbeiter am Institut für Molekulare Mikrobiologie und Biotechnologie der Westfälischen Wilhelms-Universität Münster
09/2015-12/2019	wissenschaftlicher Mitarbeiter am Lehrstuhl für Chemie Biogener Rohstoffe am TUM Campus

Studium

10/2010 - 03/2014	Technische Universität München, B.Sc. Bioprozesstechnik, Abschlussnote 2,3 Abschlussarbeit „Identifizierung und Charakterisierung von Dehydrogenasen für den Einsatz in zellfreien Syntheserouten" am WZ Straubing, Note 1,0
04/2014-09/2015	Technische Universität München, M.Sc. Pharmazeutische Bioprozesstechnik, Abschlussnote 1,8 Abschlussarbeit „Struktur-Funktions-Beziehung von Sphinganen und deren Wechselwirkungen mit Tensiden - Eine rheologische Studie -" am WZ Straubing, Note 1,0

Praktische Erfahrung

2010-06 - 2019-07	Forschungspraktikum Geneart AG, Regensburg, Deutschland Produktion synthetischer Oligonukleotide
2011-08 - 2011-09	Forschungspraktikum Krones AG, Regensburg, Germany Forschung und Entwicklung, Abteilung Aseptik und Verfahrenstechnik

Zivildienst

09/09 – 05/10	Zivildienst bei Medicus Rehaklinik Regensburg

Schulbildung

09/99 – 07/10	Goethe Gymnasium Regensburg, Abschluss: Abitur

1. Edilberto Vicente Medina-Cabrera, Moritz Gansbiller, Broder Rühmann, Jochen Schmid, Volker Sieber (2021) Rheological characterization of *Porphyridium sordidum* and *Porphyridium purpureum* exopolysaccharides Carbohydrate Polymers, 253,117237

2. Moritz Gansbiller, Jochen Schmid, Volker Sieber (2020)
Rheology of sphingans in EPS–surfactant systems
Carbohydrate Polymers, 248, 2020, 116778

3. Moritz Gansbiller, Jochen Schmid, Volker Sieber (2019) In-depth rheological characterization of genetically modified xanthan-variants
Carbohydrate Polymers, 213, 2019, pp 236-246

4. Marius Rütering, Jochen Schmid, Moritz Gansbiller, André Braun,
Jochen Kleinen, Martin Schilling, Volker Sieber (2018) Rheological characterization of the exopolysaccharide Paenan in surfactant systems
Carbohydrate Polymers, 181, pp 719-726